



**HAL**  
open science

## Wirelessbox- Multifunctional road monitoring system

Natasha Bahrani

► **To cite this version:**

Natasha Bahrani. Wirelessbox- Multifunctional road monitoring system. Civil Engineering. École centrale de Nantes, 2021. English. NNT : 2021ECDN0003 . tel-03377332

**HAL Id: tel-03377332**

**<https://theses.hal.science/tel-03377332>**

Submitted on 14 Oct 2021

**HAL** is a multi-disciplinary open access archive for the deposit and dissemination of scientific research documents, whether they are published or not. The documents may come from teaching and research institutions in France or abroad, or from public or private research centers.

L'archive ouverte pluridisciplinaire **HAL**, est destinée au dépôt et à la diffusion de documents scientifiques de niveau recherche, publiés ou non, émanant des établissements d'enseignement et de recherche français ou étrangers, des laboratoires publics ou privés.

# THESE DE DOCTORAT DE

L'ÉCOLE CENTRALE DE NANTES

ÉCOLE DOCTORALE N° 602  
*Sciences pour l'Ingénieur*  
Spécialité : Génie Civil

Par

**Natasha BAHRANI**

***Wirelessbox- Multifunctional road monitoring system***

Thèse présentée et soutenue à l'Université Gustave Eiffel le 19 janvier 2021

Unité de recherche : Département Matériaux et Structures (MAST), laboratoire LAMES,  
Université Gustave Eiffel

## **Rapporteurs avant soutenance :**

Christophe PETIT, Professeur des universités, Université Limoges, Egletons

Sigurdur ERLINGSSON, Professeur, VTI, Sweden an Uol, Iceland

## **Composition du Jury :**

Président : Frédéric GRONDIN, Professeur des universités, École Centrale de Nantes

Examineurs : Eyal LEVENBERG, Professeur associé, Technical University of Denmark

Dir. de thèse : Pierre HORNYCH, Ingénieur des TPE HDR, Université Gustave Eiffel, Bouguenais

Co-directrice de thèse : Juliette BLANC, Ingénieure des TPE HDR, Université Gustave Eiffel, Bouguenais



## **ACKNOWLEDGEMENT**

First of all, I would like to thank Professors Christophe Petit and Sigurdur Erlingsson for agreeing to be reviewers for this thesis and also express my gratitude to Professors, Eyal Levenberg and Frédéric Grondin for the time they devoted to reading and commenting on this manuscript. I would like to extend my sincere thanks to SMARTI, Marie Curie European Project, who funded this project. This thesis would not have been possible without the trust, direction and follow-up carried out by my supervisors: Mr. Pierre Hornyh and Ms. Juliette Blanc, whom I would like to express my sincere thanks. Their knowledge and encouragement allow me to overcome difficulties and always gave me motivation for my work. I will keep their advice for my future endeavors. I would also like to thank Mr. Fabien Menant for sharing his expertise and knowledge during this work. I would like to convey my sincere gratitude to Professor Eyal Levenberg who assisted my work during my secondment at DTU and whose insight and knowledge was very useful for the completion of this thesis. My thanks also go to all my colleagues at IFSTTAR (Diana Khairallah, Benjamin Shiferaw, Domenico Vizzari, Rodrigo Siroma, Marie Antoinette ALHAJJ, Jean-Luc Geffard, Jacques Kerveillant, and others) for the fruitful discussions and especially the doctoral students with whom I had unforgettable moments and who encouraged me a lot during this thesis. I would also like to thank my friends Anum Talpur and Faryal Fatima for being by my side and for their help during these years of PhD. Finally, I would like to thank all my family who have given me so much support during this period of my life. Their encouragement helped me a lot to complete this project.

## Table of Contents

|  |           |
|--|-----------|
| <b>General Introduction .....</b>  | <b>7</b>  |
| <b>Chapter 1 Literature Review .....</b>                                       | <b>13</b> |
| 1.1 Objectives of pavement monitoring.....                                     | 15        |
| 1.2 Pavement Structures .....  | 15        |
| 1.2.1. Different types of pavements.....                                       | 16        |
| 1.2.2. Factors affecting pavement performance .....                            | 17        |
| 1.3 Pavement Design method.....  | 18        |
| 1.3.1. Empirical method.....   | 19        |
| 1.3.2. Mechanical empirical method .....                                       | 19        |
| 1.3.3. French pavement design method .....                                     | 20        |
| 1.4 Mechanical pavement models.....  | 23        |
| 1.4.1. Burmister model (Burmister, 1943).....                                  | 23        |
| 1.4.2. Huet-Sayegh viscoelastic model (Huet, 1965) (Sayegh, 1966).....         | 25        |
| 1.5 Computer programs for pavement modelling .....                             | 27        |
| 1.5.1. Alize LCPC.....   | 27        |
| 1.5.1.1. Defining the pavement structure and responses .....                   | 28        |
| 1.5.1.2. Special load module .....   | 30        |
| 1.5.1.3. Back-calculation module .....   | 31        |
| 1.5.2. Visco-route .....   | 33        |
| 1.5.2.1. Defining the pavement structure.....                                  | 33        |
| 1.5.3. Ellea software.....   | 35        |
| 1.5.3.1. Defining pavement structure and retrieving mechanical responses ..... | 35        |
| 1.5.3.2. Back-calculation using Ellea .....                                    | 36        |
| 1.6 Sensors used for instrumentation .....                                     | 37        |
| 1.6.1. Deflectometer .....   | 38        |
| 1.6.1.1. Types: Single Layer Deflectometer .....                               | 38        |
| 1.6.1.2. Types: Multidepth deflectometer .....                                 | 39        |
| 1.6.1.3. Application .....   | 39        |
| 1.6.2. Geophones .....   | 40        |
| 1.6.2.1. Working principle.....  | 40        |
| 1.6.2.2. Application .....   | 41        |
| 1.6.3. Accelerometers .....  | 42        |

|  |  |           |
|--|--|-----------|
| 1.6.3.1.   | Working principle.....   | 42        |
| 1.6.3.2.   | Capacitive accelerometers.....   | 42        |
| 1.6.3.3.   | Piezo electric accelerometers.....   | 43        |
| 1.6.3.4.   | Piezo resistive accelerometers.....  | 43        |
| 1.6.3.5.   | Applications.....  | 44        |
| 1.6.4.   | Strain gauges.....   | 44        |
| 1.6.4.1.   | Horizontal strain gauges.....  | 44        |
| 1.6.4.2.   | Vertical strain gauges.....  | 45        |
| 1.6.4.3.   | Types of strain gauges.....  | 46        |
| 1.6.5.   | Temperature probes.....  | 47        |
| 1.6.5.1.   | Resistance temperature detectors.....  | 48        |
| 1.6.5.2.   | Thermistor sensors.....  | 48        |
| 1.6.5.3.   | Thermocouples.....   | 48        |
| 1.6.6.   | Pressure cells.....  | 48        |
| 1.6.7.   | Installation of the sensors.....   | 49        |
| 1.7  | Case studies.....  | 50        |
| 1.7.1.   | Short term monitoring.....   | 50        |
| 1.7.2.   | Long term monitoring.....  | 58        |
| 1.8  | Conclusion.....  | 73        |
| <b>Chapter 2 Laboratory testing of sensors (Geophones &amp; Accelerometers).....</b> |  | <b>75</b> |
| 2.1  | Introduction – Objectives of the preliminary instrumentation tests.....                            | 77        |
| 2.2  | Selecting the sensors to measure pavement deflections.....   | 78        |
| 2.3  | Experimental Protocol.....   | 79        |
| 2.3.1.   | Objectives of the laboratory tests.....  | 79        |
| 2.3.2.   | Modelling of pavement deflections with the Alize software.....                                     | 80        |
| 2.3.3.   | Test Program.....  | 81        |
| 2.3.4.   | Determination of transfer functions.....   | 82        |
| 2.4  | Sensor Responses: untreated sensor signals.....  | 83        |
| 2.4.1.   | Results from the geophones.....  | 84        |
| 2.4.2.   | Results from accelerometers.....   | 85        |
| 2.5  | Processing and improving the geophone Signal measurements.....                                     | 85        |
| 2.6  | Method for filtering and converting the vertical velocity signals into vertical displacements..... | 87        |
| 2.6.1.   | Step1: Filtering the signals.....  | 87        |
| 2.6.2.   | Step 2: Amplification of the signal with respect to the reference signal amplitude.....            | 88        |

|  |   |            |
|--|---|------------|
| 2.6.3.   | Step 3: Integration and detrending to remove the continuous part of the signal .....    | 88         |
| 2.6.4.   | Step 4: Application of the Hilbert transform .....                                      | 89         |
| <b>2.7 Method for filtering and converting the vertical acceleration signals into vertical displacements .....</b> |   |            |
| <b>91</b>  |   |            |
| 2.7.1.   | Step1: Filtering the signals .....  | 91         |
| 2.7.2.   | Step 2: Amplification of the signal with respect to the reference signal amplitude..... | 92         |
| 2.7.3.   | Step 3: Integration and detrending to remove the continuous part of the signal .....    | 93         |
| 2.7.4.   | Step 4: Application of the Hilbert transform .....                                      | 94         |
| <b>2.8 Comparison of the treated geophone and accelerometer measurements with the reference laser sensor .....</b> |   |            |
| <b>95</b>  |   |            |
| <b>2.9 Results obtained with the treated sensor signals.....</b>   |   |            |
| <b>96</b>  |   |            |
| 2.9.1.   | Pulse signals.....  | 96         |
| 2.9.2.   | Truck signals .....   | 101        |
| <b>2.10 Conclusion .....</b>   |   |            |
| <b>106</b>   |   |            |
| <b>Chapter 3 Accelerated pavement tests .....</b>  |   | <b>109</b> |
| <b>3.1 Introduction .....</b>  |   |            |
| <b>110</b>   |   |            |
| <b>3.2 Instrumentation of the pavement structure .....</b>   |   |            |
| <b>110</b>   |   |            |
| 3.2.1.   | Objectives of the Full scale testing.....   | 110        |
| 3.2.2.   | The Fatigue carousel .....  | 111        |
| 3.2.3.   | The pavement structure .....  | 111        |
| 3.2.4.   | Loading configuration .....   | 112        |
| 3.2.5.   | Instrumented section .....  | 113        |
| 3.2.6.   | Sensor Arrangement .....  | 115        |
| <b>3.3 Test program.....</b>   |   |            |
| <b>116</b>   |   |            |
| 3.3.1.   | Test scheme.....  | 116        |
| <b>3.4 Data processing of the signals .....</b>  |   |            |
| <b>117</b>   |   |            |
| 3.4.1.   | Validation of correction method on the APT data .....                                   | 117        |
| 3.4.2.   | Methodology .....   | 118        |
| <b>3.5 Tests Results.....</b>  |   |            |
| <b>118</b>   |   |            |
| 3.5.1.   | Deflection values at different speeds .....   | 119        |
| 3.5.2.   | Deflection values at different wheel positions .....                                    | 126        |
| <b>3.6 Comparison between accelerometers, geophones, and deflectometer sensor .....</b>                            |   |            |
| <b>129</b>   |   |            |

|   |            |
|---|------------|
| 3.7 Conclusion.....   | 130        |
| <b>Chapter 4 Calculation of pavement layer moduli .....</b>   | <b>132</b> |
| 4.1 Introduction .....  | 133        |
| 4.2 Pavement material and properties.....   | 134        |
| 4.3 Methodology of back-calculation of the mechanical properties of the pavement .....              | 135        |
| 4.4 Modelling and back calculation with Alize .....   | 135        |
| 4.4.1. Calculation scenario .....   | 135        |
| 4.4.2. Estimation of Pavement layer moduli .....  | 136        |
| 4.5 Modelling and back-calculation with Ellea .....   | 141        |
| 4.5.1. Calculation scenario .....   | 141        |
| 4.5.2. Optimization of layer moduli with ELLEA .....  | 142        |
| 4.5.3. Comparison of measurements and model prediction and estimation of pavement layer moduli .... | 142        |
| 4.6 Comparison of the two back-calculation approaches.....  | 148        |
| 4.7 Conclusion.....   | 150        |
| <b>Chapter 5 Test site experiment and results .....</b>   | <b>152</b> |
| 5.1 Introduction .....  | 153        |
| 5.2 Presentation of the instrumented site of motorway Ax .....                                      | 153        |
| 5.2.1. Test site experimentation.....   | 153        |
| 5.2.2. Pavement structure .....   | 154        |
| 5.2.3. Instrumentation .....  | 154        |
| 5.2.4. Presentation of the data acquisition system.....   | 155        |
| 5.2.5. Application to the instrumented site.....  | 156        |
| 5.3 Geophone Measurements .....   | 157        |
| 5.3.1. Geophones data recording .....   | 157        |
| 5.3.2. Calculation of Deflections .....   | 159        |
| 5.3.3. Examples of integrated signals.....  | 160        |
| 5.3.4. Characterisation of heavy vehicle silhouettes .....  | 161        |
| 5.3.5. Examples of truck signal with different load values .....                                    | 166        |
| 5.3.6. Calculation of vehicle speeds .....  | 167        |
| 5.3.7. Selection of T2S3 truck signals .....  | 169        |
| 5.3.8. Effect of geophone position on measured vertical displacements.....                          | 170        |
| 5.4 Analysis of the influence of temperature on deflections .....                                   | 174        |

|  |   |            |
|--|---|------------|
| 5.4.1.                                       | Temperature variations in the experimental section .....              | 174        |
| 5.4.2.                                       | Temperature correction.....   | 176        |
| 5.5  | Comparison of measured deflections with pavement modelling.....       | 179        |
| 5.5.1.                                       | Objectives of the comparisons .....                                   | 179        |
| 5.5.2.                                       | Initial back-calculation of pavement layer moduli.....                | 179        |
| 5.5.3.                                       | Determination of mean deflection basins.....                          | 180        |
| 5.5.4.                                       | Modelling of the deflection basins with ALIZE .....                   | 181        |
| 5.5.5.                                       | Evaluation of heavy vehicle loads using deflection measurements ..... | 187        |
| 5.6  | Conclusion.....   | 194        |
| <b>General conclusion .....</b>              |   | <b>197</b> |
| <b>conclusion Générale (Française) .....</b> |   | <b>201</b> |
| <b>perspectives.....</b>                     |   | <b>206</b> |
| <b>References .....</b>                      |   | <b>207</b> |
| <b>Annex .....</b>                           |   | <b>213</b> |
| Annex A.....                                 |   | 213        |
| Annex B.....                                 |   | 217        |
| Annex C.....                                 |   | 219        |
| Annex D .....                                |   | 220        |



## GENERAL INTRODUCTION

For any flourishing society having better roads and transport infrastructure is essential not only for the mobility of people and goods but also for the economic growth and better quality of life. It therefore is important to have better road conditions and maintain a high level of service. Millions of euros are spent each year on the monitoring and maintenance of roads. Regular and preventive maintenance is essential to ensure a better performance of pavement structures. This maintenance must be based on reliable data characterising pavement performance. For this reason, there has been a growing interest in long term monitoring of roads by using non-destructive techniques in order to study the effect of traffic and changing environmental conditions on the pavement.

Several non-destructive testing methods have been developed to measure the surface deflection and to assess the structural capacity of asphalt pavements. The most commonly used are static measurement methods like the Benkelman beam and impulse loading methods like the FWD. These methods present the advantage of reproducing closely the loading conditions and the stress state in the pavement. However, these techniques can only measure the deflection at discrete locations, and require interrupting the traffic. Also, these techniques are costly and the measurements are recorded infrequently, i.e., only once per year or two years. There is a need to develop solutions for monitoring road condition in a remote and continuous manner, without the need of road closures.

For this purpose, instrumentation using different sensing technologies is the approach used to measure the mechanical response of the pavement. The concept of remote continuous monitoring is to analyse the changes with the course of time and with the ease of collecting the data remotely. This data can then be used to determine different indicators of pavement performance, which allow to monitor the road condition, and to plan maintenance operations.

Instrumentation with adequate technology for characterising the conditions and deterioration caused due to heavy traffic is an active topic of research among the pavement-engineering field. The type of suitable instrumentation depends on the type of road structure and traffic. Ease of installation and durability of the sensors, measurement frequency and instrumentation cost are also very important factors.

The work presented in this thesis concerns methods of pavement instrumentation and remote monitoring, which can be used to monitor pavement performance on a long-term basis, under normal traffic. One of the preferred methods of instrumentation for such application is the use of strain gauges, measuring horizontal or vertical strains in the different pavement layers. This type of

instrumentation gives very accurate local information, on the behaviour of a given layer, but because this information is very local, sensors must be installed in all pavement layers, to measure the global response of the pavement structure, which increases the cost. Because the information is very local, the measurements also become more and more scattered as the pavement starts to crack and deteriorate. Another disadvantage is that the gauges must be installed during construction, to ensure a good bond with the materials.

For this reason, in this thesis, focus is set on the measurement of pavement deflections (vertical displacements), which appears as an interesting alternative or complementary solution to strain gauges: deflection is a more global parameter, which allows to characterise, with only one sensor, the overall response of the pavement, and can also be used to back-calculate pavement layer properties, if sufficient information about the pavement structure is known. In addition, the deflection can be measured at the pavement surface (or very close to the surface), which makes installation of sensors on existing, in service pavements more easy.

The search for appropriate solutions for measuring pavement deflections has led to study two types of sensors: geophones and accelerometers. These sensors measure respectively the displacement velocity and acceleration, and by integrating their measurements, it is possible to determine the corresponding displacement. An important advantage of these sensors, compared for instance with displacement sensors, is that they do not require a fixed reference point to measure the displacement.

The first step of the study consisted in selecting geophones and accelerometers of suitable characteristics, and to evaluate their response and accuracy in the laboratory, under loadings representative of the field conditions. During this stage, signal processing techniques were developed to enhance the signals received from the sensors. This step was very useful to further interpret the data from the sensors.

In a second step, the sensors were evaluated in full scale, but under controlled conditions, on the IFSTTAR fatigue carousel, a large scale accelerated pavement testing facility. These tests helped in understanding the responses under real wheel loading and under different controlled load levels and loading speeds, and different environmental conditions. The controlled tests condition were useful to understand the effect of each parameter on the responses. Because the characteristics of the pavement structure were well known, the tests were also used to evaluate back-calculation procedures, for calculating pavement layer moduli from the measured deflection basins.

Finally, the last part of the study concerned the evaluation of these measurement methods in real field conditions, on a road section open to traffic. IFSTTAR has several motorway sites

instrumented with the partnership of the motorway agencies. These experimental sections are mostly instrumented with strain gauges and temperature probes, but also with geophones, for more research purposes. These sensors are attached to a data acquisition system that is transmitting the information to a remote server. The data from one of the instrumented sites, on the Ax motorway (the name is not cited for confidentiality reasons) is studied. The objectives of the study were to evaluate the sensor accuracy to measure the vertical deflections, in real field conditions, and also to explore different possibilities of interpretation of the sensor measurements, not only to measure the deflection, and its evolution with time, but also to characterise the heavy vehicle traffic.

From the analysis of this instrumented site, the main advantages of this monitoring solution are the following:

- The small size, ease of installation and accuracy of the embedded sensors
- The real-time data processing capacities, which allow to perform continuous monitoring, under a heavy motorway traffic and the wireless data transmission possibilities.
- The good reliability of the system, over relatively long periods of time (approximately two years of monitoring).
- The very detailed information available due to the continuous monitoring, and the different possibilities of interpretation of the data.

This study demonstrates different possibilities of using geophones and accelerometers to analyse pavement performance and shows promising perspectives for the future of remote monitoring systems.

The layout of the work of this thesis is described more in detail below:

### **First chapter:**

This chapter presents a literature review about different methods of pavement instrumentation and analysis. A detailed evaluation of different types of sensors used for the applications of instrumentation and monitoring of pavements is carried out. Studied sensors include geophones, accelerometers, strain gauges, temperature probes and pressure probes. Case studies regarding the short term monitoring and long term monitoring of pavements are also discussed in this chapter, emphasizing on the instrumentation type, data acquisition methods, and methods of analysis of the sensor measurements

### **Second chapter:**

This chapter describes the selection of appropriate sensors for measuring pavement deflections, and the testing of these sensors in a laboratory setting. Two types of accelerometers and geophones

are tested using a hydraulic vibrating table, to understand their performance at different frequencies and displacement amplitudes. Data processing techniques are also developed at this stage to treat the data from the sensors to improve the accuracy of the deflection measurements. Finally, the results are validated by comparing the measurements with a displacement sensor, used as reference

### **Third chapter:**

In this part, the selected sensors have been installed in an experimental pavement tested on the IFSTTAR fatigue carousel and subjected to accelerated pavement tests. These tests have been conducted at different speeds, load levels, and different transversal positions of the wheels. This was an important aspect to validate the response of the sensors embedded in the pavement, under heavy loads and different loading speeds. The same data processing methods were used for the treatment of the sensor signals as in the laboratory, and validation of the measurements was done using two methods: comparison with results obtained with a pavement modelling software, and with measurements obtained with an anchored deflectometer, which is considered as a reference method for the measurement of vertical deflections.

### **Fourth chapter:**

After validating the approaches for the measurement of pavement deflections, using APT tests, these responses were used for the back-calculation of pavement layer moduli. Two different methodologies of back-calculation were used to estimate the layer moduli. The first method, based on the use of the ALIZE software, is based on the modelling of the deflection basins. The second method uses the Ellea software, and is based on the direct modelling of the velocity or acceleration measurements. This second approach allows to use directly the sensor signals, without previous processing and integration of the measurements. In both cases, an iterative approach is used to determine the pavement layer moduli leading to the best fit between the measured and calculated response (in terms of vertical deflection, velocity or acceleration).

### **Fifth chapter:**

This last chapter presents the analysis of the data received from the instrumented site of the Ax motorway, in France. The experimental section was instrumented with geophones, strain gauges and temperature probes and the data was recorded for a period of 22 months. The focus in this chapter was on analysis of the geophone data and the deflections obtained with these. After appropriate signal treatment, different methods of analysis of the deflection measurements were proposed, including the analysis of seasonal variations of deflections, but also the identification of vehicle types, calculation of vehicle speeds and estimation of vehicle loads. This study was important to validate the effectiveness of the use of the sensors for monitoring deflections and to

analyse the pavement behaviour under real motorway traffic and different environmental conditions.



# CHAPTER 1 LITERATURE REVIEW

|  |    |
|--|----|
| 1.1 Objectives of pavement monitoring.....                                     | 15 |
| 1.2 Pavement Structures .....  | 15 |
| 1.2.1. Different types of pavements.....                                       | 16 |
| 1.2.2. Factors affecting pavement performance .....                            | 17 |
| 1.3 Pavement Design method.....  | 18 |
| 1.3.1. Empirical method.....   | 19 |
| 1.3.2. Mechanical empirical method .....                                       | 19 |
| 1.3.3. French pavement design method.....                                      | 20 |
| 1.4 Mechanical pavement models.....  | 23 |
| 1.4.1. Burmister model (Burmister, 1943).....                                  | 23 |
| 1.4.2. Huet-Sayegh viscoelastic model (Huet, 1965) (Sayegh, 1966).....         | 25 |
| 1.5 Computer programs for pavement modelling .....                             | 27 |
| 1.5.1. Alize LCPC.....   | 27 |
| 1.5.1.1. Defining the pavement structure and responses .....                   | 28 |
| 1.5.1.2. Special load module .....   | 30 |
| 1.5.1.3. Back-calculation module .....   | 31 |
| 1.5.2. Visco-route .....   | 33 |
| 1.5.2.1. Defining the pavement structure.....                                  | 33 |
| 1.5.3. Ellea software.....   | 35 |
| 1.5.3.1. Defining pavement structure and retrieving mechanical responses ..... | 35 |
| 1.5.3.2. Back-calculation using Ellea .....                                    | 36 |
| 1.6 Sensors used for instrumentation .....                                     | 37 |
| 1.6.1. Deflectometer .....   | 38 |
| 1.6.1.1. Types: Single Layer Deflectometer .....                               | 38 |
| 1.6.1.2. Types: Multidepth deflectometer .....                                 | 39 |
| 1.6.1.3. Application .....   | 39 |
| 1.6.2. Geophones .....   | 40 |
| 1.6.2.1. Working principle.....  | 40 |
| 1.6.2.2. Application .....   | 41 |
| 1.6.3. Accelerometers .....  | 42 |
| 1.6.3.1. Working principle.....  | 42 |
| 1.6.3.2. Capacitive accelerometers.....  | 42 |
| 1.6.3.3. Piezo electric accelerometers.....                                    | 43 |
| 1.6.3.4. Piezo resistive accelerometers .....                                  | 43 |
| 1.6.3.5. Applications.....   | 44 |

|          |  |    |
|----------|--|----|
| 1.6.4.   | Strain gauges.....                     | 44 |
| 1.6.4.1. | Horizontal strain gauges.....          | 44 |
| 1.6.4.2. | Vertical strain gauges .....           | 45 |
| 1.6.4.3. | Types of strain gauges .....           | 46 |
| 1.6.5.   | Temperature probes.....                | 47 |
| 1.6.5.1. | Resistance temperature detectors ..... | 48 |
| 1.6.5.2. | Thermistor sensors.....                | 48 |
| 1.6.5.3. | Thermocouples .....                    | 48 |
| 1.6.6.   | Pressure cells .....                   | 48 |
| 1.6.7.   | Installation of the sensors .....      | 49 |
| 1.7      | Case studies .....                     | 50 |
| 1.7.1.   | Short term monitoring.....             | 50 |
| 1.7.2.   | Long term monitoring.....              | 58 |
| 1.8      | Conclusion.....                        | 73 |

## **1.1 Objectives of pavement monitoring**

In pavement engineering, measurement of in situ pavement structural properties is an important issue, both for control after construction, and for evaluation of pavement condition, after several years of service, for evaluating the residual service life, and defining maintenance needs. Monitoring of mechanical properties of in situ pavements can be done using non-destructive test methods. These methods are most often based on the measurement of pavement deflections under static, dynamic or moving wheel loads. Deflection measuring equipment include the FWD, deflectograph, or more recent high speed deflection measurement vehicles like the Traffic Speed Deflectometer (TSD). These methods, which use dedicated measurement vehicles, can be used to survey a whole network, but only at relatively large time intervals. Typically, measurements are made once every one or two years.

Alternatively, the measurement of structural properties of pavements can be done using sensors placed in the pavement layers. This type of solution offers the possibility to measure several response parameters (deflections, strains, temperatures) and also to perform continuous measurements, under traffic, and thus to monitor continuously the variations of the pavement layer properties. The disadvantage of instrumentation is that it can be used only to make local measurements.

The objective of this work is to develop effective instrumentation methods to monitor and analyse the pavement response, using mainly geophones and accelerometers. This chapter presents a literature review on pavement instrumentation methods, to better position the problems that are focused in this work. The literature review covers the following subjects:

- Characteristics of pavement structures
- Mechanical response of pavement structures and factors affecting this response
- Sensors used for pavement instrumentation and their working principles
- Modelling of pavement structures and back-calculation of layer properties
- Different case studies on short term and long term monitoring of pavements using different sensor technologies

## **1.2 Pavement Structures**

A pavement structure can be defined as the superposition of layers of different materials and thickness that enable to distribute traffic loads on the subgrade. The different layers forming the pavement structure are shown in Figure 1-1. They are designed to allow the movement of traffic,

and to ensure the safety and comfort of road users (SETRA et LCPC, 1994) (Technique et Regionaux, 2003).



Figure 1-1. Composition of a pavement structure

The different layers and their composition are described below:

**Surface course:** It is the uppermost layer of the pavement structure. It may consist of two layers: the wearing course and the binder course. The first layer is designed to resist to the effects of climate and traffic. The second layer of the pavement helps transfer the loads and resist to rutting. It is the interface between the surface and base layers, and also helps to delay reflective cracking from base layers treated with hydraulic binders.

**Road base:** The road base generally consists of two layers, the base course and the subbase. They provide the mechanical resistance to the vertical loads induced by traffic. They distribute the stresses on the subgrade to keep the deformation in permissible limits.

**Capping layer:** This layer ensures the transition between the subgrade and the road base layers. During construction, it protects the subgrade and offers a level surface of good quality for the construction of the pavement layers. It also improves the homogeneity of the natural soil, and contributes to protect it from water and frost.

**Subgrade:** The lowest layer in the pavement structure. It is the compacted natural soil immediately below the pavement layers and acts as a foundation for the highway.

### 1.2.1. Different types of pavements

There are six main types of pavement structures in France (SETRA et Lcpc, 1998) (Goacolou, 2003) which are described below:

**Flexible pavements:** These structures consist of a thin bituminous surface course of less than 15 cm, resting on one or more layers of unbound granular materials. Commonly, the thickness of the

structure is between 30 and 60 cm. These structures are used for low traffic roads, which constitute a large part of the French road network.

**Thick bituminous pavements:** These structures consist of a bituminous wearing course, resting on one or two bituminous layers, constituting the base and sub-base layers. The thickness of the base layers is typically between 15 and 40 cm. these structures are suitable for any type of traffic, and mostly used on the French motorways and main national roads.

**Semi rigid pavements:** these structures consist of a bituminous surface course and a base of materials treated with hydraulic binders. The thickness of the base layers is typically between 20 and 50 cm. These structures are able to withstand heavy traffic due to the high stiffness of materials treated with hydraulic binders. These material are susceptible to drying shrinkage and thermal shrinkage phenomena, which can lead to transverse cracking of the layers.

**Rigid (or cement concrete) pavements:** In this type of pavements the wearing course is a thin bituminous layer, covering a cement concrete base layer of 15 to 40 cm. The concrete slabs lie on a foundation layer, generally consisting of materials treated with hydraulic binders, or directly on the subgrade.

**Mixed structure pavements:** These structures consist of a wearing course and base course of bituminous materials, with a typical thickness of 10 to 20 cm. the sub-base consists of materials treated with hydraulic binders, with a typical thickness of 20 to 40 cm. The thickness of bituminous and cement-treated layers is often of the same order (ratio 1/1). These structures offer a better resistance to the propagation of cracks initiated in the layers treated with hydraulic binders. The bituminous layers also protect the foundation against water infiltration and thermal variations.

**Inverted pavement structures:** These structures consist of a bituminous surface course of approximately 15 cm, resting on a layer of unbound granular material (about 12 cm thick), in turn resting on a base layer treated with hydraulic binders. The total thickness is around 60 to 80 cm. The unbound granular layer helps to prevent the propagation of cracks from the materials treated with hydraulic binders. These structures are less and less used, because the granular layer can sometimes act as a trap for infiltrated water, which leads to a reduction of its modulus, and a premature deterioration of the surface course.

### **1.2.2.Factors affecting pavement performance**

The most common types of damage affecting pavement layers (LCPC-SETRA, 1994), are presented below:

**Stresses due to traffic:**

In flexible pavements, the bituminous layers are thin and so the vertical stresses due to the traffic are transmitted to the subgrade with little lateral spreading. The repeated high vertical stresses lead to the deformation of the ground or of the granular materials resulting in permanent deformations.

In thick bituminous or rigid pavements, the stiffness of the treated layers reduces the vertical stresses transmitted to the subgrade. However, the traffic loads lead to bending of the treated layers, and development of high tensile stresses and strains at the base of these treated layers. The most common damage mechanism of the treated layers is fatigue, due to these repeated tensile stresses.

#### **Influence of the environment conditions:**

In flexible pavements, the low structural stiffness renders the pavements particularly sensitive to variations in the moisture conditions of the pavement foundation. Reduced bearing capacity during the wet seasons leads to increased permanent deformations, and sometimes to subsidence at the road edges and shrinkage due to drying out later in dry periods.

In thick bituminous pavements, high moisture conditions can also induce permanent deformations. High temperatures can also induce rutting of the surface layers, due to creep of the bituminous materials.

#### **Evolution of damage:**

On flexible pavements the most frequent evolution is first of all the appearance of permanent deformation like wide radius rutting and subsidence, which degrade the cross section and longitudinal profile. More traffic causes more deformation both in extent and gravity depending on the quality of the structure and variability of the mechanical characteristics of the pavement. Repeated bending stresses also lead to deterioration due to fatigue in the form of cracks. This allows water to penetrate in the structure, which accelerates crack deterioration and permanent deformations.

In thick bituminous pavements, high tensile stresses lead to the development of longitudinal fatigue cracks, which can then evolve into alligator cracking. As the cracks deteriorate, the damage process accelerates due to the infiltration of water in the pavement structure.

### **1.3 Pavement Design method**

Pavement design methods generally consist in determining the mechanical response of the pavement structure under traffic loads, and comparing values of stresses or strains, calculated at some critical locations with maximum permissible values. These permissible values are defined by

deterioration models, defining the relationship between the number of traffic loads and the level of damage, often based on laboratory test results.

Mostly, these approaches are based on the multilayer linear elastic model for the calculation of the response of pavement structures and usually require ad hoc software for the calculations.

### **1.3.1. Empirical method**

These methods, still used in many countries, represent a simple method to define standard pavement structure, with well-known materials. They define the thickness of the pavement layers based on simple equations, or nomograms. They are generally based on experimental observations of pavement performance. However, such approaches limit the possibilities of optimization of the pavement structure, and innovative materials, presenting a different behaviour cannot be evaluated. Some of the well-known empirical methods are given below:

- AASHTO design equation (AASHTO, 1986)
- CBR method (California bearing ratio)(AASHTO, 2000)
- Group index method

### **1.3.2. Mechanical empirical method**

The Mechanistic Empirical Pavement Design Guide (MEPDG)(AASHTO, 2008) and the associated software were developed under the NCHRP 1-37A in 1993 to update the empirical AASHTO method, which was strictly based on empirical observations. This method aims to take into account a mechanistic approach associated with empirical elements, based on experimental feedback, for predicting the performance of the pavement. The mechanistic-empirical design method is based on linear elastic calculations, and takes into account the precise composition of traffic, climate conditions and mechanical properties of materials.

The MEPDG design method involves:

- Use of the multi-layer linear elastic model of Burmister for the calculation of the stress and strain response of the pavement. The response is calculated under variable traffic loads and climatic conditions.
- Material characterization procedures which are used to define the different material properties necessary for the calculations.

- Distress models, which define relationships between the critical pavement responses and the distresses generated on the pavement. Several types of distresses are taken into account: fatigue cracking, top down cracking, thermal cracking, rutting.

The method takes into account in detail the traffic, the composition of traffic, in terms of types of vehicles, vehicle loads and traffic speeds, as well as the daily and annual traffic distributions are taken into account. Climatic variations (temperature moisture) in the pavement are predicted using a climatic model, based on meteorological data.

Depending on the level of detail of the input data available for the calculations, the MEPDG method proposes three levels of accuracy:

- Level 1 requires a large amount of data and has the highest level of accuracy
- Level 2 requires a more limited amount of data has an intermediate level of accuracy
- Level 3 is largely based on the use of default data sets and has the lowest level of accuracy

### 1.3.3. French pavement design method

This method is described in the Pavement Design Technical Guide (SETRA-LCPC, 1994). It is based on a multi-layer linear elastic model, and the adjustment of the calculated design lives on experimental observations from real roads.

The traffic loading is defined by the cumulative number of standard axle loads (NE) during the period of design (20 or 30 years). In France, the reference standard axle is a single axle with dual wheels, loaded at 130 kN, and applying a constant vertical pressure of 662 kPa. The geometry of the load considered in the calculations is described in Figure 1-2.

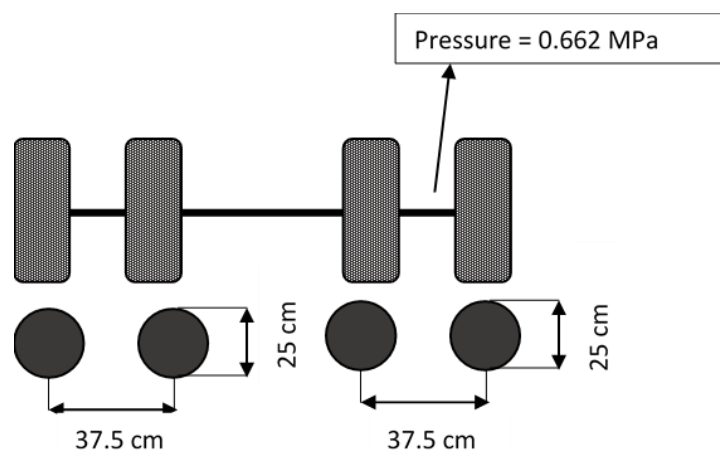


Figure 1-2. Geometry of the standard 130 kN dual wheel axle load

The heavy vehicle traffic on the roadway is converted into an equivalent number NE of passage of the reference 130 kN axle, using the following formula:

$$NE = N * CAM \quad (1.1)$$

With:

N = Total number of heavy goods vehicles (with a total weight > 35 kN) traveling on the roadway

CAM = Average coefficient of aggressiveness

For each type of axle (single, tandem, tridem, etc.), the aggressiveness A is given by:

$$A = k * \left( \frac{P}{P_0} \right)^\alpha \quad (1.2)$$

With:

P = the axle load for which the aggressiveness is calculated

P<sub>0</sub> = the load of the standard equivalent axle (130 kN)

K = coefficient depending on the type of axle (single, tandem or tridem)

The CAM coefficient is therefore defined as the average of the different aggressiveness values A, of all the vehicles composing the traffic.

The speed of the vehicles and the temperature conditions are taken into account through the mechanical characteristic (elastic moduli) of the materials. The French pavement design method considers a unique equivalent temperature for the design. This temperature is equal to 15°C for France.

The pavement structure is characterised by the thickness, elastic modulus, and Poisson ratio of each material, at the design conditions (by default a temperature of 15 °C and a frequency of 10 Hz).

The pavement model is used to calculate the stresses and strains in the different layers of the pavement under the reference axle loading. To determine the maximum number of load cycles that the structure can withstand, these computed stresses and strains are compared with maximum permissible stresses or strains defined by fatigue laws.

The failure mode of each layer is determined based on the following critical strain or stress values:

- For bituminous layers, the maximum tensile strain  $\epsilon_t$  at the bottom of the bituminous layers
- For cement treated layers, the maximum tensile stress  $\sigma_t$  at the bottom of these layers

- For granular layers, the maximum vertical strain  $\epsilon_z$  at the top of the granular layers
- For the subgrade, the maximum vertical strain  $\epsilon_z$  at the top of the subgrade

The bituminous materials are characterised by laboratory complex modulus tests and fatigue tests. The complex modulus is determined at 15 °C and 10 Hz, and fatigue tests are performed at 10 °C and 25 Hz, in two point bending mode.

The maximum permissible tensile strain for the bituminous materials, at the equivalent temperature of 15 °C, is defined in equation (1.3):

$$\epsilon_{t,adm} = \epsilon_6(10^\circ C, 25Hz) \sqrt{\frac{E(10^\circ C)}{E(15^\circ C)}} \left(\frac{NE}{10^6}\right)^b k_r k_s k_c \quad (1.3)$$

Where

- $\epsilon_6(10^\circ C, 25Hz)$  is the failure strain level obtained in lab for 1 million load cycles
- The ratio  $E(10^\circ C)/E(15^\circ C)$  is the correction of the lab fatigue result to standard temperature condition
- NE is the number of equivalent standard axle loads
- $1/b$  is the slope of the Wohler curve, as determined by the fatigue tests
- $k_r$  is a reliability coefficient, which takes into account the variability of pavement construction and material characteristics.
- $k_s$  is a subgrade coefficient, which take into account the homogeneity of the subgrade
- $k_c$  is a calibration coefficient, determined from the comparison between model predictions and field results

The maximum permissible tensile stress for materials treated with hydraulic binders and cement concrete is defined by the following equation (1.4):

$$\sigma_{t,adm} = \sigma_6 * \left(\frac{NE}{10^6}\right)^b * k_c * k_r * k_s * k_d \quad (1.4)$$

With:

$\sigma_6$  is the stress leading to a failure for  $10^6$  cycles in fatigue tests on specimens cured for 360 days (standard NF P 98-233-1).

b is the slope of the material fatigue law ( $-1 < b < 0$ ).

NE is the number of equivalent standard axle loads.

kc, kr, ks, kd are adjustment coefficients.

For unbound materials and for the subgrade, the permissible vertical deformation at the surface of these layer is defined by following equation (1.5):

$$\varepsilon_{z,adm} = A * (NE)^b \quad (1.5)$$

With:

A, b parameters depending on the level of traffic ( $-1 < b < 0$ ).

NE The number of equivalent standard axle loads.

## 1.4 Mechanical pavement models

This part presents some numerical and analytical models used for pavement design calculations and for structural analysis of pavements.

### 1.4.1. Burmister model (Burmister, 1943)

As the flexible pavement is made of layers, (Burmister, 1943) developed a multi-layer linear elastic model for pavement structures. The model allows to calculate the stresses and displacements in a multilayer pavement system (n layers) under the effect of a circular load, considering axisymmetric conditions. The structure is described as follows: The pavement consists of n layers, which are supposed to be homogenous, elastic linear and isotropic. The upper layers are of finite thickness but the thickness of the lowest layer (soil) is infinite. All the interfaces can be bonded or unbonded.

The load is described by a uniform pressure applied on a circular surface of radius a. Each layer is characterised by its thickness, elastic modulus  $E_i$  and Poisson ratio  $\nu_i$ . The stresses and displacements in this model are determined from the following function (Burmister, 1943) (Van Cauwelaert, 1995).

$$\varphi_i = pa \int_0^{\infty} \frac{J_0(mr)J_1(ma)}{m} [A_i e^{mz} - B_i e^{-mz} + zC_i e^{mz} - zD_i e^{-mz}] dm \quad (1.6)$$

The results for the stresses and displacements are as follows where  $\sigma_z$  = vertical stress,  $\sigma_r$  = radial stress,  $\sigma_\theta$  = circumferential stress,  $\tau_z$  = vertical shear stress,  $w$  = vertical displacement and  $u$  = radial displacement

$$\sigma_z = pa \int_0^\infty J_0(mr)J_1(ma)[A_i m^2 e^{mz} + B_i m^2 e^{-mz} + C_i m(1 - 2v_i + mz)e^{mz} + D_i m(1 - 2v_i - mz)e^{-mz}] dm \quad (1.7)$$

$$\begin{aligned} \sigma_r = & -pa \int_0^\infty J_0(mr)J_1(ma)[A_i m^2 e^{mz} + B_i m^2 e^{-mz} \\ & + C_i m(1 - 2v_i + mz)e^{mz} \\ & - D_i m(1 - 2v_i - mz)e^{-mz}] dm \\ & + pa \int_0^\infty \frac{J_1(mr)J_1(ma)}{mr}[A_i m^2 e^{mz} + B_i m^2 e^{-mz} \\ & + C_i m(1 + mz)e^{mz} - D_i m(1 - mz)e^{-mz}] dm \end{aligned} \quad (1.8)$$

$$\begin{aligned} \sigma_\theta = & -pa \int_0^\infty J_0(mr)J_1(ma)[C_i m e^{mz} - D_i m e^{-mz}] 2v_i dm \\ & - pa \int_0^\infty \frac{J_1(mr)J_1(ma)}{mr}[A_i m^2 e^{mz} + B_i m^2 e^{-mz} \\ & + C_i m(1 + mz)e^{mz} - D_i m(1 - mz)e^{-mz}] dm \end{aligned} \quad (1.9)$$

$$\begin{aligned} \tau_{rz} = & -pa \int_0^\infty J_1(mr)J_1(ma)[A_i m^2 e^{mz} - B_i m^2 e^{-mz} \\ & + C_i m(2v_i + mz)e^{mz} + D_i m(2v_i - mz)e^{-mz}] dm \end{aligned} \quad (1.10)$$

$$\begin{aligned} w = & \frac{1 + v_i}{E_i} pa \int_0^\infty \frac{J_0(mr)J_1(ma)}{mr}[A_i m^2 e^{mz} - B_i m^2 e^{-mz} \\ & + zC_i m(2 - 4v_i - mz)e^{mz} \\ & - zD_i m(2 - 4v_i - mz)e^{-mz}] dm \end{aligned} \quad (1.11)$$

$$u = -\frac{1 + \nu_i}{E_i} pa \int_0^\infty \frac{J_0(mr)J_1(ma)}{mr} [A_i m^2 e^{mz} + B_i m^2 e^{-mz} + C_i m(1 + mz)e^{mz} - D_i m(1 - mz)e^{-mz}] dm \quad (1.12)$$

With:

a = Radius of the circular loading surface

p =Loading pressure (evenly distributed)

r =Radial distance in cylindrical coordinates

z =Depth

E<sub>i</sub> =Young's modulus of the with layer

ν<sub>i</sub> =Poisson's ratio of the with layer

A<sub>i</sub>, B<sub>i</sub>, C<sub>i</sub>, D<sub>i</sub> Unknown parameters, determined by the boundary conditions

J<sub>0</sub> =Bessel function of the first kind of order 0

J<sub>1</sub> =Bessel function of the first kind of order 1

m =Integration parameter

This model is commonly used in pavement design methods, and in particular in the French design method.

#### **1.4.2.Huet-Sayegh viscoelastic model (Huet, 1965) (Sayegh, 1966)**

Bituminous materials present a thermo-viscoelastic behaviour, which is strongly dependent on temperature and loading frequency. Huet model (1963) proposed a visco-elastic model which consists of a stiff spring E and two parabolic dampers. This model was found to give unrealistic results at low frequencies and high temperatures, where the complex modulus tends to zero. Hence Sayegh (Sayegh, 1966)(Sayegh, 1965) introduced a model with a spring in parallel to the huet model as shown in Figure 1-3 which proved to describe particularly well the behaviour of bituminous mixes.

The Huet-sayegh model is an analogue model, which consists of a combination of an elastic spring E<sub>0</sub> and two parabolic dampers attached in series with an elastic spring ( E<sub>inf</sub>-E<sub>0</sub>). (Chupin et al., 2010) (Chabot et al., 2006).

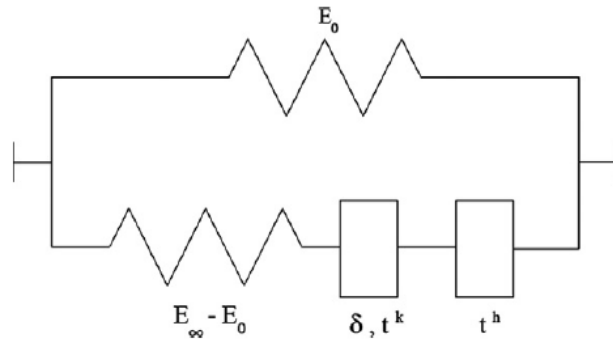


Figure 1-3. Huet-Sayegh (1965) model

In the frequency domain the complex modulus of the model is given by the following equation:

$$E^*(\omega, \theta) = E_0 + \frac{E_\infty - E_0}{1 + \delta(i\omega\tau(\theta))^{-k} + (i\omega\tau(\theta))^{-h}} \quad (1.13)$$

Where:

$E_0$  is the static elastic modulus,

$E_\infty$  is the instantaneous elastic modulus,

$E_0, E_\infty$  are the limits of the complex modulus for  $\omega = 0$  or  $\omega = \infty$

$h$  and  $k$  are exponents of the parabolic dampers ( $1 > h > k > 0$ )

$\delta$  is a dimensionless coefficient which is balancing the contribution of the first damper in the global behaviour

$\theta$  denotes temperature

$\tau(\theta)$  is a response time parameter which accounts for the equivalence principle between frequency and temperature.

$\tau(\theta)$  is governed by equation (1.14):

$$\tau(\theta) = \exp(A_0 + A_1\theta + A_2\theta^2) \quad (1.14)$$

Where  $A_0, A_1$  and  $A_2$  are constant parameters.

The Huet-Sayegh model has been subjected to several validations, which have shown that it describes very realistically the thermo visco-elastic behaviour of bituminous mixes in the frequency and temperature ranges encountered in pavements.

## 1.5 Computer programs for pavement modelling

### 1.5.1. Alize LCPC

Alize is a standard software that is used for pavement modelling in France since its first version developed in the sixties. It is based on the linear elastic isotropic homogenous multilayer model of Burmister. It implements the French pavement design method, developed by LCPC and SETRA, which principles are defined in the French pavement design guide (SETRA et al., 1994), which was recently updated and converted into a design standard (AFNOR, 2018). This software was also used to develop the French pavement structure catalog (SETRA et Lcpc, 1998).

This is a powerful software used for pavement projects and it integrates a calculation tool with admissible values (stress and strains) depending on the traffic context and materials. It can be used for any type of pavement (flexible, rigid, concrete etc). This software also has a back-calculation tool for determining the pavement layer moduli. This option is useful for road managers for condition assessments of pavements. The different modules of the software (Figure 1-4) are the following:

**Basic Road module** through which we can model different pavement systems and analyse their mechanical responses like stresses, strains and deflections, and compare them with design criteria.

**Frost thaw module** is used for checking the frost protection of the subgrade, and is based on a thermal calculation.

**Special loads module** is used to calculate pavement response under non-standard wheel or vehicle loads (specific vehicles, with multiple wheels, etc).

**Back-calculation module** aids to carry out back-calculations, based on deflection basin measurements, to determine the pavement layer moduli.

**Airfield pavement module** is created in partnership with the STAC (service Technique de l'aviation civile – French Aviation Administration and is dedicated to the design of airfield pavements under aircraft loads.

For the calculations carried out in this project, we focus on the basic road module, special loads module and the back-calculation module.

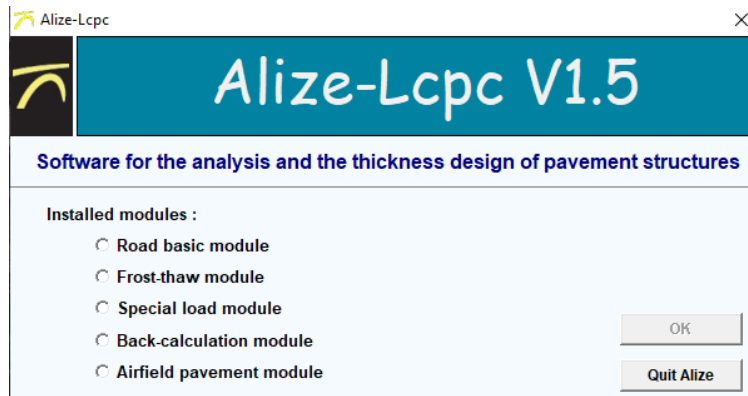


Figure 1-4. Alize modules

### 1.5.1.1. Defining the pavement structure and responses

The basic road module is used in Alize to calculate the stress and strain fields in pavement structures. Each layer of the pavement is defined by a thickness, elastic modulus, Poisson's ratio and material type. A material library as shown in Figure 1-5, proposing a list of standard materials, which characteristics are defined by the the NF P98-086 standard at 15 °C and 10 Hz is available in ALIZE. This library includes five major types of materials: Bituminous materials, materials treated with the hydraulic binders, cement concrete, unbound granular materials and subgrade soils.

| status | name     | E (MPa) | Nu   | Epsi6 (10°C) | -1/b | SN   | Sh (m) | Kc  | Variations $E(10Hz) = f(temperature)$ |        |         |         |         |         |
|--------|----------|---------|------|--------------|------|------|--------|-----|---------------------------------------|--------|---------|---------|---------|---------|
|        |          |         |      |              |      |      |        |     | T -10                                 | T 0 °C | T 10 °C | T 20 °C | T 30 °C | T 40 °C |
| system | eb-bba1  | 5500    | 0,35 | 130          | 5    | 0,25 | stdard | 1,1 | 14800                                 | 12000  | 7315    | 3685    | 1300    | 1000    |
| system | eb-bba2  | 5500    | 0,35 | 100          | 5    | 0,25 | stdard | 1,1 | 14800                                 | 12000  | 7315    | 3685    | 1300    | 1000    |
| system | eb-bba3  | 7000    | 0,35 | 100          | 5    | 0,25 | stdard | 1,1 | 16000                                 | 13500  | 9310    | 4690    | 1800    | 1000    |
| system | eb-bbsg1 | 5500    | 0,35 | 100          | 5    | 0,25 | stdard | 1,1 | 14800                                 | 12000  | 7315    | 3685    | 1300    | 1000    |
| system | eb-bbsg2 | 7000    | 0,35 | 100          | 5    | 0,25 | stdard | 1,1 | 16000                                 | 13500  | 9310    | 4690    | 1800    | 1000    |
| system | eb-bbsg3 | 7000    | 0,35 | 100          | 5    | 0,25 | stdard | 1,1 | 16000                                 | 13500  | 9310    | 4690    | 1800    | 1000    |
| system | eb-bbme1 | 9000    | 0,35 | 100          | 5    | 0,25 | stdard | 1,1 | 17300                                 | 15400  | 11970   | 6030    | 3000    | 1900    |
| system | eb-bbme2 | 11000   | 0,35 | 100          | 5    | 0,25 | stdard | 1,1 | 19500                                 | 18200  | 14630   | 7370    | 3800    | 2300    |
| system | eb-bbme3 | 11000   | 0,35 | 100          | 5    | 0,25 | stdard | 1,1 | 19500                                 | 18200  | 14630   | 7370    | 3800    | 2300    |
| system | bbm      | 5500    | 0,35 | /            | /    | /    | stdard | 1,1 | 14800                                 | 12000  | 7315    | 3685    | 1300    | 1000    |
| system | bbtm     | 3000    | 0,35 | /            | /    | /    | stdard | 1,1 | 8500                                  | 7000   | 4200    | 1800    | 1000    | 800     |
| system | bbdr     | 3000    | 0,35 | /            | /    | /    | stdard | 1,1 | 8500                                  | 7000   | 4200    | 1800    | 1000    | 800     |
| system | acr      | 5500    | 0,35 | /            | /    | /    | stdard | 1,1 | 14800                                 | 12000  | 7315    | 3685    | 1300    | 1000    |
| system | eb-gb2   | 9000    | 0,35 | 80           | 5    | 0,3  | stdard | 1,3 | 22800                                 | 18300  | 11880   | 6120    | 2700    | 1000    |
| system | eb-gb3   | 9000    | 0,35 | 90           | 5    | 0,3  | stdard | 1,3 | 22800                                 | 18300  | 11880   | 6120    | 2700    | 1000    |
| system | eb-gb4   | 11000   | 0,35 | 100          | 5    | 0,3  | stdard | 1,3 | 25000                                 | 20000  | 14300   | 7700    | 3500    | 1200    |
| system | eb-eme1  | 14000   | 0,35 | 100          | 5    | 0,3  | stdard | 1   | 30000                                 | 24000  | 16940   | 11060   | 6000    | 3000    |
| system | eb-eme2  | 14000   | 0,35 | 130          | 5    | 0,25 | stdard | 1   | 30000                                 | 24000  | 16940   | 11060   | 6000    | 3000    |

Figure 1-5. Alize material library

The interfaces of the layers can be defined as bonded or unbonded/sliding or semi-bonded, one of the assumptions of the French design method. The semi-bonded condition corresponds to the half sum of the results obtained with the bonded and unbonded interfaces. Figure 1-6 shows the layout of the basic road module.

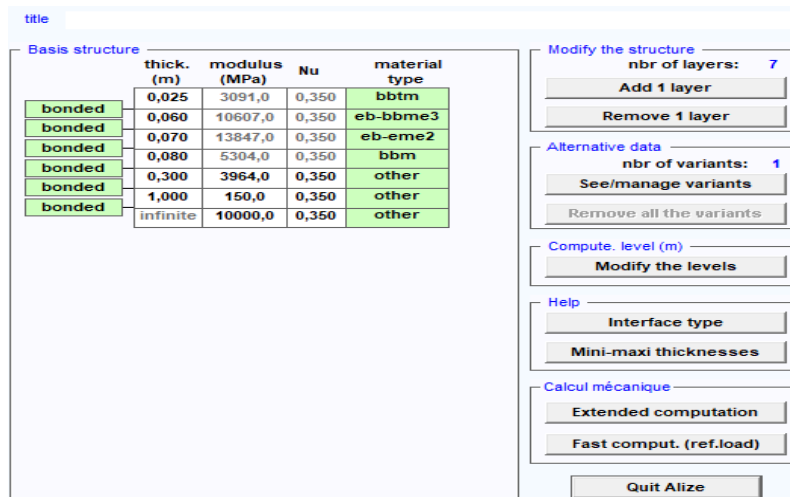


Figure 1-6. Basic road module interface

The reference load used for the calculation is the French Equivalent Standard Axle Load, defined as a half-axle with dual wheels, loaded at 65 kN. This load is described by two circles, as shown on Figure 1-7. Other types of loads, including more complex loads, corresponding to multiple-axle vehicles, can be defined in the “special load module”.

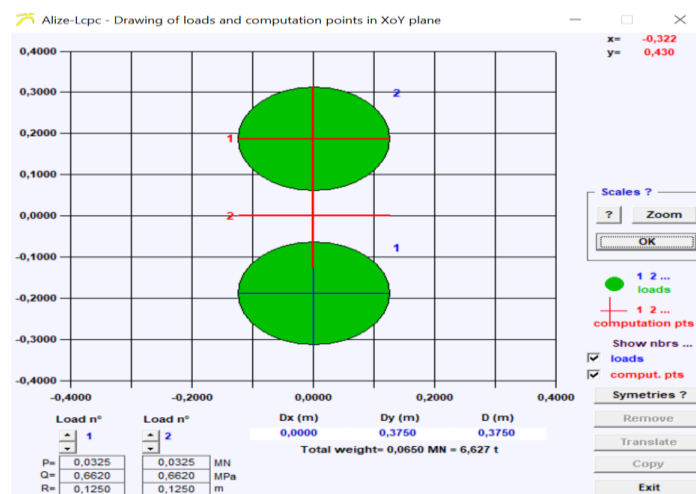


Figure 1-7. Reference load dimensions in Alize

The responses under load in the basic road module can be calculated by two methods:

- Fast computations
- Extended computations

The fast computations are made under the reference load (standard half-axle load of 65kN), and only the maximum stresses and strains are calculated for each layer of the pavement, at the most critical locations in the structure as shown in Figure 1-8(a). The extended computations allow to calculate the stresses and strains in the whole structure, at a large number of points, defined by a

3D mesh. With this second option, it is possible to plot stress and strain contours (in 2D), or horizontal stress and strain profiles, at different depths, in the x and y direction. Figure 1-8(b) shows a surface deflection profile in the x direction, calculated under the loading of a 5-axle semi-trailer truck.

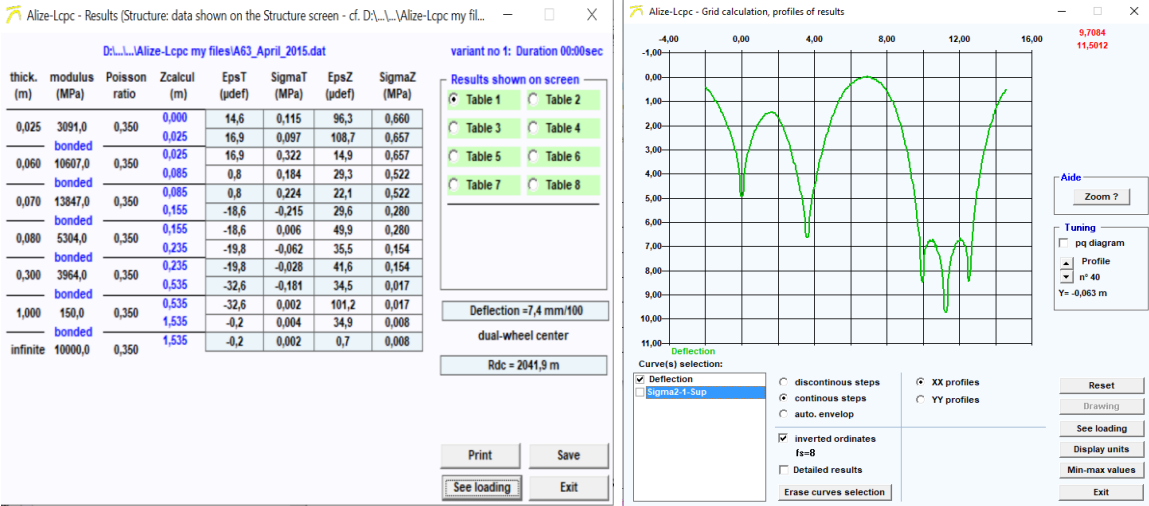


Figure 1-8 (a). Example of fast computations (b). Extended computation of deflections

### 1.5.1.2. Special load module

This module is used for the calculation of the pavement response under specific load types, defined by the user. Each load can be circular or pseudo rectangular and is defined by its radius R (m) (or length and width for the rectangle), the contact pressure of the wheel (MPa) or the total load applied on the wheel (MN). Each wheel is defined by the x,y coordinates of its center, and several wheel loads can be superimposed, to describe a complete vehicle as shown in Figure 1-9. The special load module has been used in this work to calculate the response of the pavements under the loading of the specific heavy vehicles which have been studied.

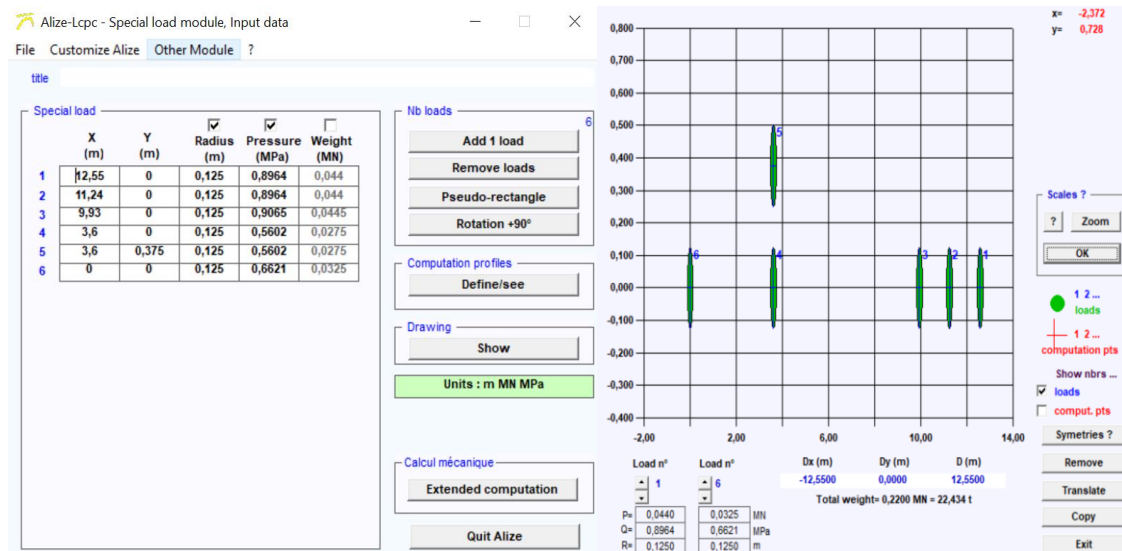


Figure 1-9. Special load module interface

### 1.5.1.3. Back-calculation module

For estimating pavement layer moduli, a common approach is to use the back-calculation technique, applied to deflection basin measurements. The back-calculation module of Alize LCPC requires as inputs:

- The pavement structure, defined by the pavement layer thicknesses, Poisson ratios, and initial moduli (Figure 1-10)
- The applied load (Figure 1-10)
- The measured deflection basin of the pavement (Figure 1-11)

The deflection basins can be measured using deflectometers, vertical displacement sensors, but the most common practice is to use the Falling weight deflectometer (FWD) to measure the deflections.

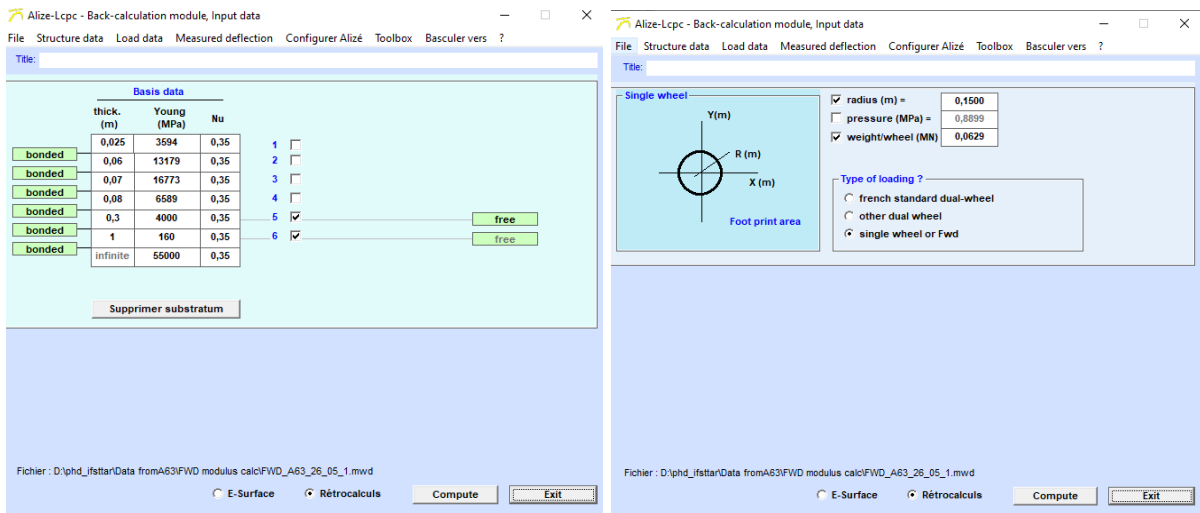


Figure 1-10. Back-calculation module interface

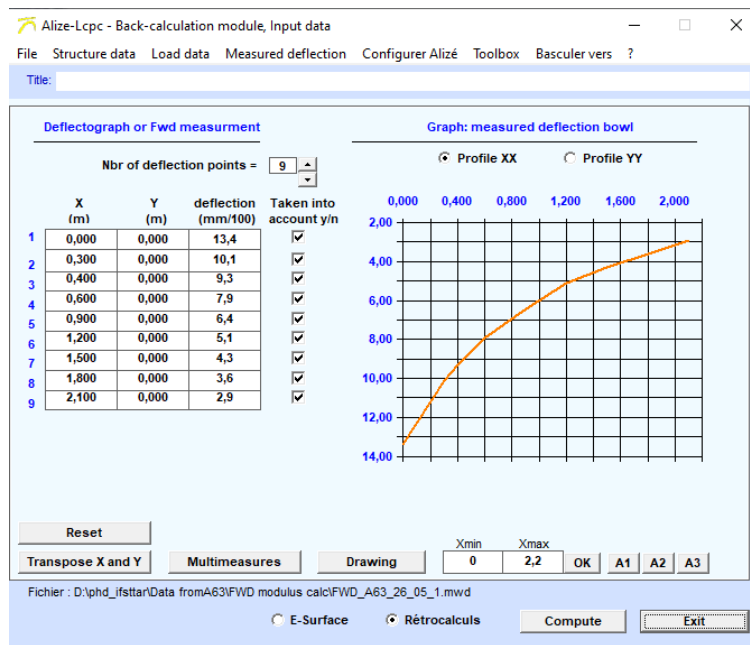


Figure 1-11. Interface for the input deflection data retrieved from sensors

After defining the initial data corresponding to the tests, the program uses an iterative procedure to adjust the pavement layer moduli, to obtain the best match between the measured deflections and those calculated with the linear elastic model, as shown in Figure 1-12. The final moduli obtained using this procedure correspond to the back-calculated moduli of the pavement layers, as shown in Figure 1-12.

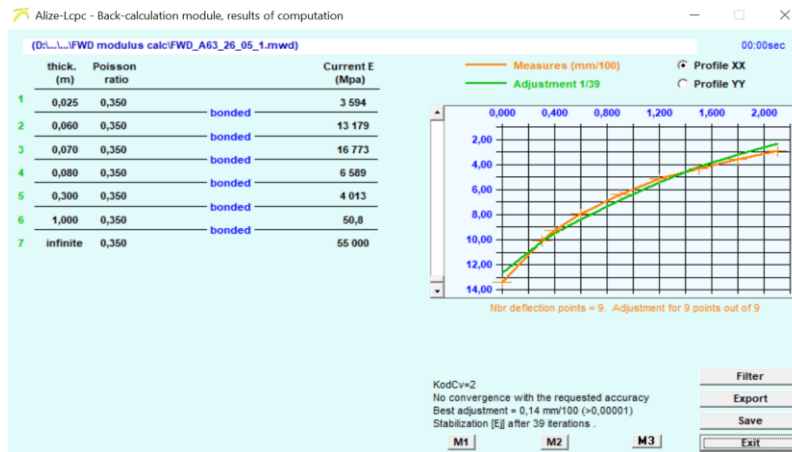


Figure 1-12. Back-calculated modulus values obtained by fitting the deflection curves

## 1.5.2. Visco-route

Viscoroute is a semi-analytical software, for the calculation of pavement response under moving wheel loads (Chabot et al., 2010). Viscoroute considers a multi-layer structure, with layers of infinite extension in the horizontal plane. The behaviour of the pavement layers can be considered linear elastic, or thermo-visco-elastic, described by the Huet-Sayegh model (Huet-Sayegh 1966). The Huet Sayegh model is described in section 1.4.2.

### 1.5.2.1. Defining the pavement structure

The structure section of Viscoroute is used to define the pavement structure. Each pavement layer is characterized by its thickness, its mechanical properties and its density. The materials can be either linear elastic or viscoelastic. An elastic material is defined by its modulus and Poisson ratio. A viscoelastic material is characterized by its density, Poisson's ratio and by the parameters of the Huet-Sayegh model ( $E^\infty$ ,  $E_0$ ,  $k$ ,  $h$ ,  $\delta$ ,  $A_0$ ,  $A_1$ ,  $A_2$ ). These parameters are obtained from a complex modulus test at different frequencies and temperatures. The interfaces of the pavement layers can be considered bonded or unbonded. Figure 1-13 shows the basic arrangement of Viscoroute.

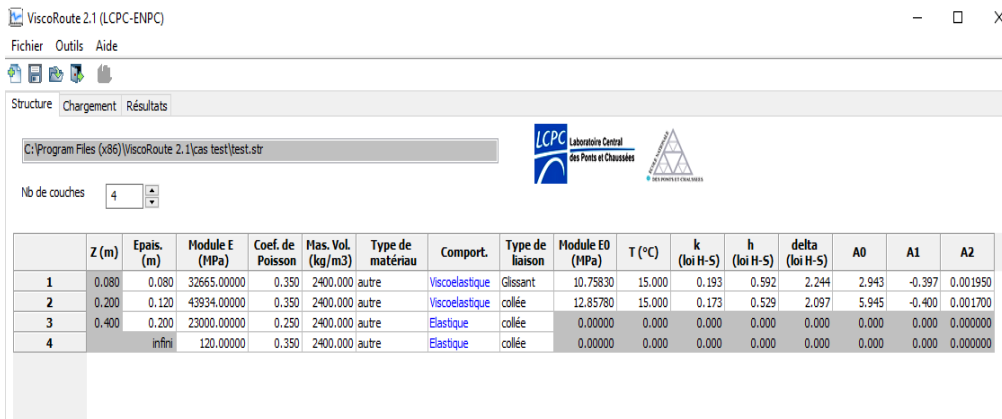


Figure 1-13. Defining the structure in Viscoroute

The loading is defined by the number of wheel loads and the loading speed. Each wheel load can be defined as a point load, or a load distributed over a rectangular, or elliptical surface (Figure 1-14). This surface is defined by the (x, y) coordinates of its center, and its dimensions a and b along the x and y axis respectively, as shown on Figure 1-15. The load is described by its components  $f_x$ ,  $f_y$  and  $f_z$  in the 3 directions. The forces are converted into uniform stresses distributed over the contact surface of the load.

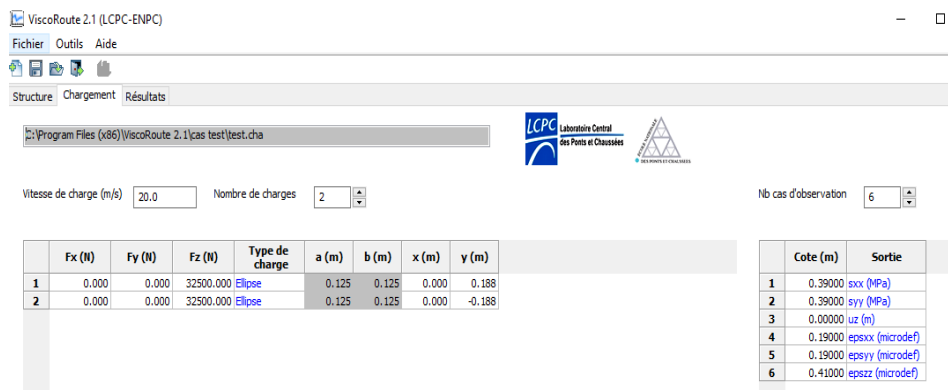


Figure 1-14. Defining the load in Viscoroute

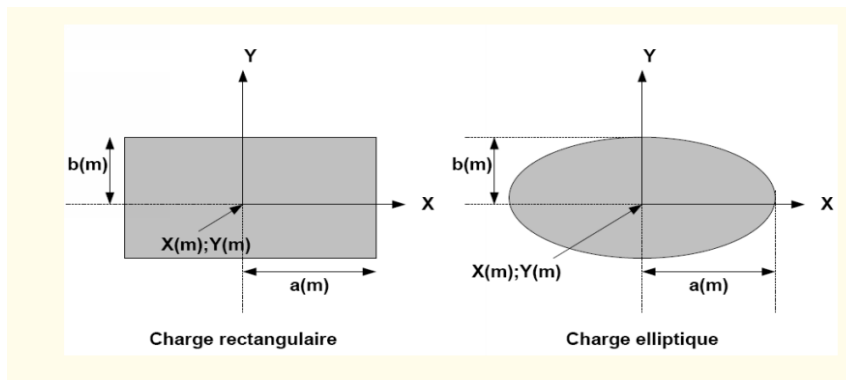


Figure 1-15. Load types and dimensions in Viscoroute

The Figure 1-16 shows an example of results, of variation of the deflection calculated with Viscoroute at the bottom of the base layer under the passage of the wheels of a dual wheel heavy vehicle. Due to the viscoelastic behaviour of the pavement, the response does not have symmetry on the right and left side.

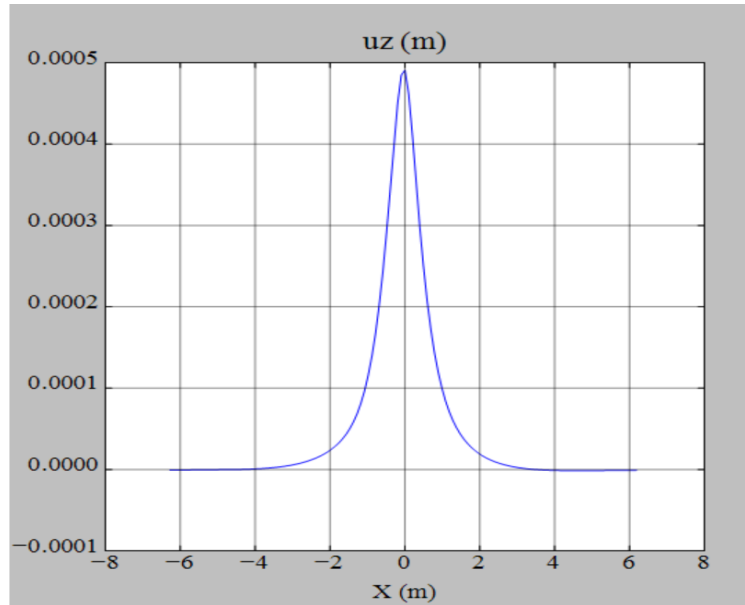


Figure 1-16. Deflection obtained with Viscoroute

### 1.5.3.Ellea software

The software ELLEA1(ver0.96), (E. Levenberg, 2009) is based on a multilayer isotropic linear elastic model. The equations are implemented into an Excel based tool, which calculates the stresses, strains and vertical displacements due to two circular loads, with a uniform vertical pressure. Five homogeneous fully bonded and isotropic layers are considered. The stress, strains and displacements are calculated according to the isotropic LET principles; the velocity and acceleration are calculated using the numerical derivatives of the displacement values. It is a flexible tool which gives the response at one point, which can then be applied to calculate the complete deflection basin, or stress or strain variations in a given direction.

Ella is used in this thesis to model the measurements obtained with deflection sensors, geophones and accelerometers. The velocities and accelerations used for comparison with the geophone and accelerometer signals are obtained by numerical derivation of the displacements.

#### 1.5.3.1. Defining pavement structure and retrieving mechanical responses

The ELLEA tool is used for the calculating the mechanical properties of the pavement. The Input parameters of ELLEA are:

- The thicknesses of each pavement layer and the layers are considered bonded
- The elastic parameters of each pavement layer : elastic modulus, Poisson's ratio
- The load characteristics. ELLEA considers two loads, defined as two circular areas, loaded by a uniform vertical stress. The loads are defined by the position of their center (x,y), their radius r and the vertical stress; the two loads can be different.
- The coordinates (x,y,z) of the points where the response is calculated, z representing the depth under the pavement surface.

The effect of the two loads is superimposed and the axially symmetric results under each circular load are converted to a Cartesian coordinate system. The stresses, strains and displacements are calculated at a specific point of coordinates (x,y,z) ( see Figure 1-17).

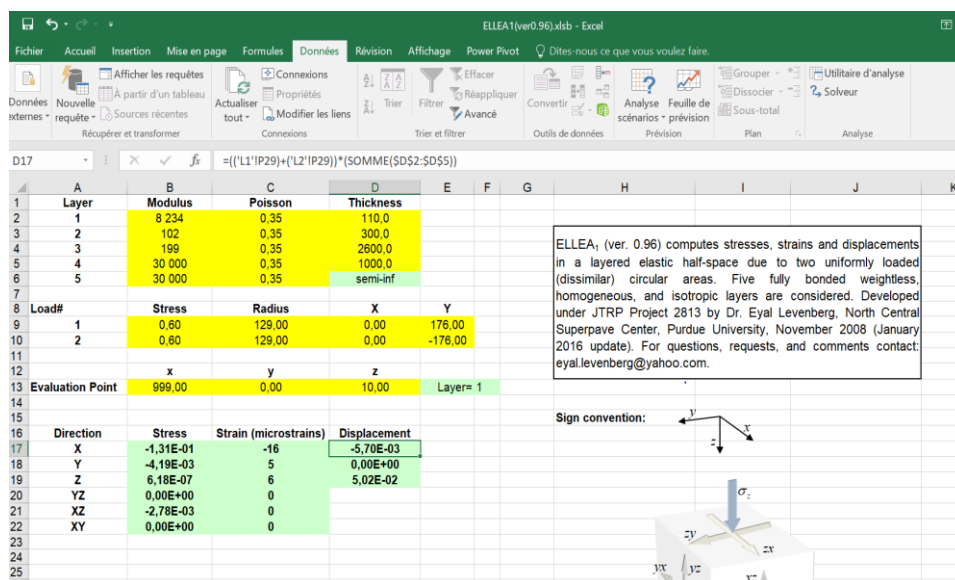


Figure 1-17. Ellea file interface

### 1.5.3.2. Back-calculation using Ellea

ELLEA can also be used for back-calculation of pavement layer moduli. The procedure consists in comparing the calculated stresses, strains, vertical displacements, vertical velocities or vertical accelerations with the measured response of the corresponding sensor, and adjusting the pavement layer moduli until the model predictions match the sensor measurements. The difference between the calculated and measured values is termed as the error and the objective is to minimize this error. For that purpose, an iterative procedure based on the EXCEL Solver tool is used, to adjust the model parameters (the pavement layer moduli), until the minimum error and the best match between the calculated responses and the measurements are obtained.

Figure 1-18 shows an example of back calculation using displacement values. To determine the deflection basin produced by the passage of a moving wheel, ELLEA is used to calculate the vertical displacements at different points on the surface of the pavement along the x axis, using initial values of the pavement layer moduli. The displacement values measured by a deflection sensor are then compared with the calculated response, and the difference between the measured and calculated response is determined. Using the EXCEL Solver tool, this difference is minimized, and the best match between the calculated and measured responses is found, by changing the pavement layer moduli.

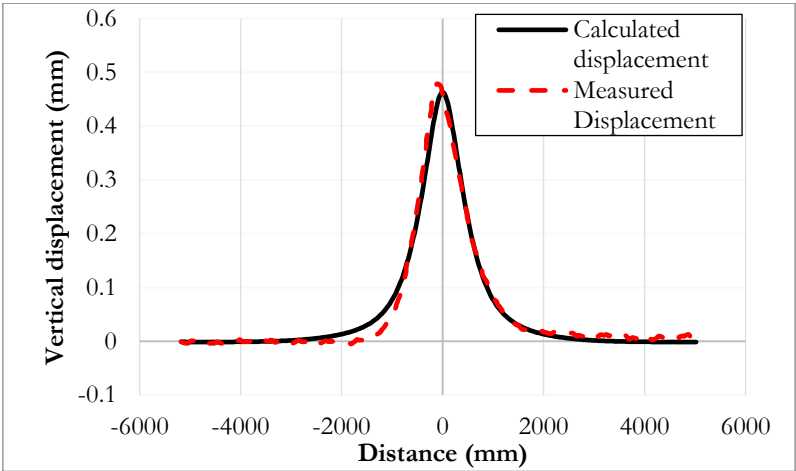


Figure 1-18. Results obtained with Ellea

**1.6 Sensors used for instrumentation**

Pavement instrumentation has received more attention in recent years, in order to improve the monitoring of the condition of new or aging pavements. Recent technological advances have also led to the development of new sensor and data acquisition technologies, and to a significant reduction of costs, thus opening new possible applications of pavement instrumentation (Lajnef et al., 2011).

In general, instrumentation can be used only on a local basis, and remains mainly based on wired sensors; Wireless sensors still do not present a sufficient autonomy for long-term measurements. Despite these limitations, an important advantage of embedded sensors is the possibility to measure directly the response of the different pavement layers, and to perform continuous monitoring, over long periods.

Analysis of instrumentation measurements requires precise information about the characteristics of the pavement structure (layers, materials), the loading conditions and the environmental conditions (temperature, rainfall) on the site. Depending on the objectives of the instrumentation

(evaluation of overall pavement performance, monitoring of specific pavement layers), different measurement methods can be selected. Generally, information needed to correctly estimate the response of the pavement, includes:

- Displacements
- Stress and strain in the pavement layers
- Environmental parameters (temperature, moisture)
- Traffic loads (types of loads, load levels, speeds, positions)

The following sections describe different types of sensors used for pavement monitoring, and examples of their application.

### **1.6.1. Deflectometer**

These sensors measure the vertical deflection (displacement) of the pavement under loading, either at the pavement surface, or at various depths. Commonly these devices use LVDT (Linear Variable Differential Transformer) sensors which measure the deflection with respect to a fixed reference point (Montalv, 2015). They can be used to measure the displacement under the passage of a single load, or the cumulative displacement (permanent deformation) after several load applications. The measured deflection basins can be used to back-calculate pavement layer moduli. These devices allow to measure accurately the pavement deflections, but they are relatively difficult to install, because the sensor must be connected with a rod anchored at a significant depth, typically about 4 meters below the pavement surface.

#### **1.6.1.1. Types: Single Layer Deflectometer**

This SLD consists of an LVDT, or strain gauges, fixed at one end to a layer of the pavement, and with the other end connected with a reference rod, as described in Figure 1-19. (Tabatabaee et Sebaaly, 1990). The rod is 2.5 to 3 m long, and is anchored in the soil at a sufficient depth, so that the end of the rod can be considered as fixed. During a displacement of the pavement, the upper end will move with the pavement, while the reference rod will remain fixed, and the relative displacement of the upper part will correspond to the vertical displacement of the pavement. The SLD can measure both static and dynamic deflections.

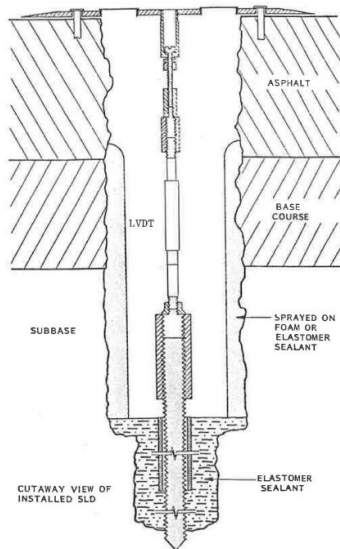


Figure 1-19. Single layer Deflectometer (Tabatabaee et al., 1990)

### 1.6.1.2. Types: Multidepth deflectometer

The Multi-depth deflectometer (MDD) is an LVDT based device used to measure the elastic and permanent deformation in the pavement. Each LVDT is mounted in a module that laterally expands to lock onto the sides of hole. Six MDD modules can be installed on the rod, at a distance of 6 inches from each other, as shown in Figure 1-20. By installing multiple MDD modules in a single hole, it is possible to measure the vertical strains of the different layers of the pavement. The end of the rod is anchored about 2.5 to 3 m below the pavement surface.

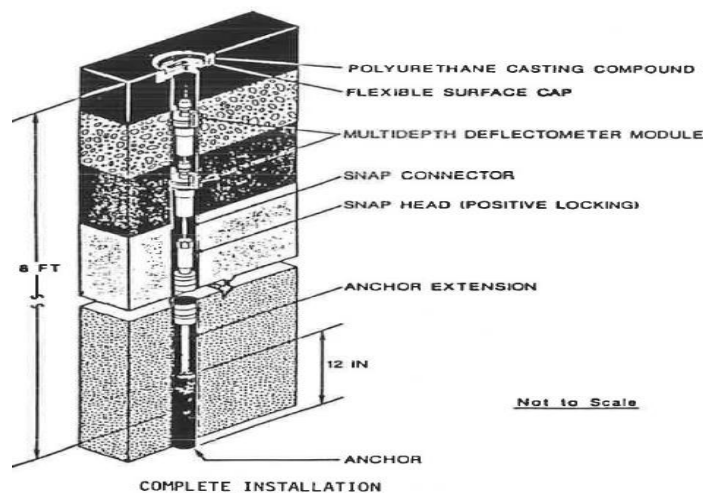


Figure 1-20. Multidepth Deflectometer (Tabatabaee et al., 1990)

### 1.6.1.3. Application

Saevarsdottir et al., (2016) present an application of displacement sensors in an accelerated pavement test performed at VTI in Sweden. The test section is a thin flexible pavement with

unbound aggregate base and subbase layers and the loads were applied using a heavy vehicle simulator. The aim of the project was to study the behaviour of the flexible pavement and validate its mechanical performance. Different sensors, including LVDT displacement sensor were installed at various depths to measure the layer properties. The displacement sensors were used to measure the deflection basins and the deformations in the pavement layers as a function of the number of load repetitions. The environmental effects and the bearing capacity of the pavement were analysed. The results showed that during the whole period the deformation increased with the level of moisture. It was estimated that there was a drop in the stiffness of the subgrade and of the granular subbase due to the increase of the water content. Tao et al., (2008) used the MDD deflectometer to study the behaviour of a full scale test section built with recycled asphalt materials.

**1.6.2. Geophones**

**1.6.2.1. Working principle**

Geophones are lightweight sensors that are able to detect small ground displacements in terms of velocity. Most geophones are based on the principle of a suspended mass, which oscillations record the ground motions, at a frequency lower than their resonant frequency. The magnetic mass is placed inside a coil. The relative movement between the mass and the coil induces an electric current in the coil. The output voltage of the geophone is proportional to the displacement velocity. This vertical velocity can then be converted into a displacement to quantify the deflection caused by the moving vehicle.

Figure 1-21 shows the working principle of the electromagnetic geophones, using a magnetic mass and a coil. There are two possible designs: moving coil where the magnet is stationary or moving magnet where the coil is stationary.

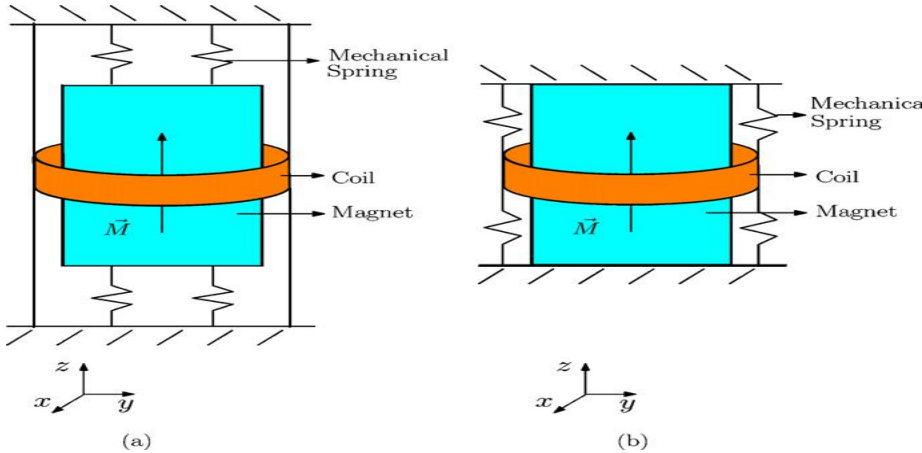


Figure 1-21. Operating principle of a geophone (Oome et al., 2009)

The general working principle of electromagnetic geophones is based on Faraday's law, which defines that the voltage across the coil is proportional to the change in magnetic flux with respect to time (Oome et al., 2009).

$$emf = -N \frac{\partial \phi}{\partial t} \quad (1.15)$$

Where N is the number of turns of the coil and  $\phi$  is the magnetic flux density through a single loop. The movement of the magnet causes a change in magnetic flux which induces an emf in the coil, which depends on the velocity of the magnetic mass. When the change in flux is constant, the voltage through the coil is directly proportional to the velocity and is termed as the sensitivity of the geophone in equation (1.16):

$$S = \frac{U(s)}{v(s)} \quad (1.16)$$

Where: U is the voltage and v is the geophone velocity.

The geophone is characterised by its resonance frequency, its damping coefficient and its bandwidth. The bandwidth is the interval between the natural frequency and the spurious frequency; in this range the sensitivity of the geophone is constant.

The natural frequency is defined by:

$$f_r = \frac{1}{2\pi} \sqrt{\frac{k}{m}} \quad (1.17)$$

Where: K is the stiffness of the spring and m is the suspended mass

Geophones do not require an electrical power to operate and are effective in detecting small ground displacements. Their performance depends on their natural frequency, which has to be as low as possible, for measuring low frequency signals and their bandwidth, which should be as large as possible, to measure high frequency signals.

The most common type of geophones or velocity sensors are electromagnetic geophones, which have been described above. Other types of velocity transducer are the piezo-electric velocity transducers (PVT's), which have an internal integration circuit, which produces velocity signals.

#### 1.6.2.2. Application

Most applications of geophones are in the field of seismic vibrations recording, and mostly to detect earthquake vibrations in mines and gas fields (Chang et Cui, 2013). In (Zan et al., 2002) a

system for detecting ground vibrations due to landslides was developed using geophones, which were used to produce a warning alert. Similarly, Arattano and Marchi (2008) used geophones to record vibrations, and detect early signs of landslides.

Duong et al., (2020) used geophones to measure the response to traffic of a flexible pavement. The velocity signals were integrated into vertical displacements, but with the applied treatment method, the shape of the deflection basins was not very realistic.

### **1.6.3. Accelerometers**

#### **1.6.3.1. Working principle**

Accelerometers are inertial sensor that measure accelerations in 1 direction (1D) or in 3 directions (3D). Most often, accelerations are measured indirectly, by measuring the force induced by the acceleration on a spring-suspended mass. The system is damped so that oscillations of the mass and spring do not affect the needed measurements. Because of the damping, accelerometers always respond in different ways to different frequencies of acceleration and this is called the "frequency response".

Accelerometers are characterised by their sensing range ( $R$ ), resolution  $\delta$ , sensing frequency, and number of axis of measurement, which are important to determine the performance of the accelerometer and its suitability for certain applications. The measurements are generally expressed in units of  $g$  with respect to the earth's gravity  $9.81 \text{ m/s}^2$ .

The operating regime of the sensor is based on the limit defined by the sensing range and the resolution. The sensitivity defines the ability to measure the amount of the vibrations needed to be measured.

#### **1.6.3.2. Capacitive accelerometers**

This type of accelerometer measures the acceleration by measuring the change in capacitance; it has a mass attached to a spring which is confined to move along one direction, and fixed outer plates as shown in Figure 1-22. . When the acceleration in a particular direction is applied, the mass will then move and the capacitance between the mass and plates will change. This change in capacitance induces the displacement of the inertial mass and this corresponds to the vertical accelerations. (D'Alessandro et al., 2019)

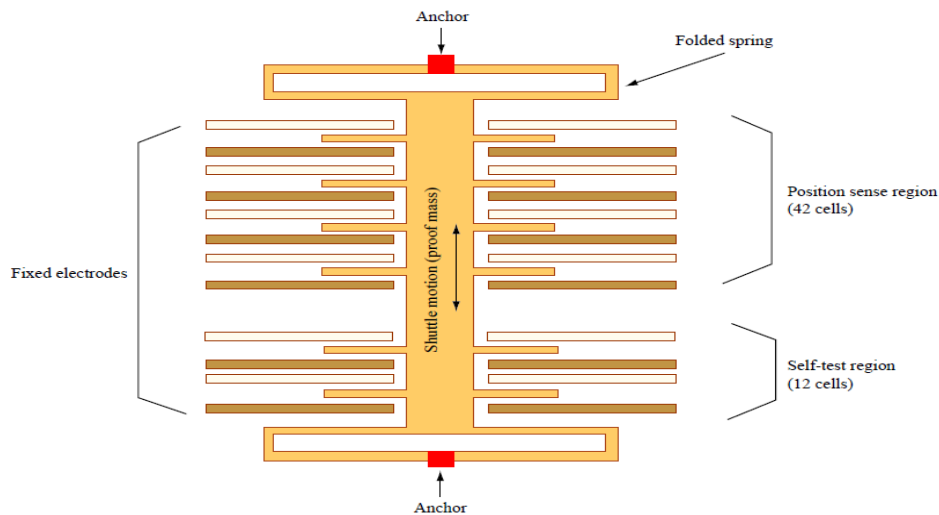


Figure 1-22. Capacitive accelerometer (Voldman et al., 2007)

### 1.6.3.3. Piezo electric accelerometers

This type of accelerometer contains a piezo-electric crystal and uses the properties of the crystal to generate electrical charges when it is submitted to a load. When an acceleration is applied, the crystal is submitted to a force which is proportional to the input acceleration following the newton law  $F=ma$ . Electrical charges appear on the opposite sides of the crystal, and this generates a voltage which is measured (Montalv, 2015).

### 1.6.3.4. Piezo resistive accelerometers

Piezo resistive accelerometer consists of a seismic mass  $M$  and elastic blade equipped with 2 or 4 piezo resistive gauges mounted in a Wheatstone bridge. These gauges measure strain caused by the deflection of the blade, by the variations of the resistance of the piezo resistors which are measured as an electrical signal. They measure the variations directly in the case of low frequency accelerations, or indirectly with a mechanical amplifier, in the case of medium frequency accelerations or shock accelerometers(Tran, 2012). The Table 1.1 summarizes some characteristics of the different types of accelerometers:

Table 1.1 Characteristics of different types of accelerometer (Aszkler, 2005)

| Accelerometer type                 | Advantages                         | Sensitivity        | Frequency range    | Size                  |
|------------------------------------|------------------------------------|--------------------|--------------------|-----------------------|
| <b>Piezoelectric accelerometer</b> | Wide frequency range<br>Small size | 0.5 mv/g to 10 V/g | 0.5 Hz to 50000 Hz | 2 gram to 200 grams   |
| <b>Capacitive accelerometer</b>    | DC response<br>Good resolution     | 10 mv/g to 1 V/g   | 0 to 1000 Hz       | 10 grams to 100 grams |

|                                      |                           |                           |               |                     |
|--------------------------------------|---------------------------|---------------------------|---------------|---------------------|
| <b>Piezo-resistive Accelerometer</b> | Dc response<br>Small size | 0.0001 mV/g<br>to 10 mV/g | 0 to 10000 Hz | 1 gram to 100 grams |
|--------------------------------------|---------------------------|---------------------------|---------------|---------------------|

### 1.6.3.5. Applications

Accelerometers are used in the fields of seismology, machinery, automotive, electronics. They can be used to measure shocks, vibrations, accelerations, velocities (by integration), and displacements (by double integration). In the field of seismic vibration detection, Micro-Electro Mechanical Systems (MEMS) accelerometers have gained a lot of popularity. In the paper of Mougenot et Thorburn, 2004), it is explained that accelerometers using this technology have the capacity to measure both at low and high frequencies, their response being linear in acceleration from 0 Hz to several hundred Hz. The power, reliability, weight and deployment issues are discussed.

Up to now, the use of accelerometers in the field of pavement monitoring is limited. The work done by (Arraigada et al., 2009) consisted in measuring pavement deflections using accelerometers and deflectometers. They also used a visco-elastic pavement model to fit the measurements obtained. The work done by (Levenberg, 2012) describes the use of accelerometers and utilization of the data to model the pavement.

### 1.6.4. Strain gauges

Strain gauges are the most conventional sensors used to measure pavement response, by measuring strains in pavement layers during the passage of the load. Measured strains can be used to estimate pavement layer moduli. Most often, strain gages are placed at the bottom of asphalt layers, and used to measure the high horizontal tensile strains generated at this location by traffic loads. These tensile stresses are used to estimate the risk of fatigue and the fatigue life of the pavement.

#### 1.6.4.1. Horizontal strain gauges

These gauges are placed in the treated layers and are used to measure the horizontal (longitudinal and transverse) deformations in these layers. These gauges are placed in the wheel path to measure the deformations under the passage of the heavy vehicles.

These sensors consist of a central rod, which is the sensitive part which contains one to four strain gauges, and two metal bars at both ends of the rod, which give to the sensor an H shape, as shown in Figure 1-23. This H shape helps to anchor the gauges in pavement materials.

When the sensor is subjected to an elongation, the resistance variation of the strain gauges can be converted into strain measurement by means of the gauge factor. (Barriera et al., 2020)

$$GF = (\Delta R/R) / \Delta L/L \quad (1.18)$$

With:

$$\epsilon = \text{strain} = \Delta L/L$$

$\Delta L$  = absolute change in length

$L$  = original length

$\Delta R$  = change in strain gauge resistance due to axial strain and lateral strain

$R$  = unstrained resistance of strain gauge

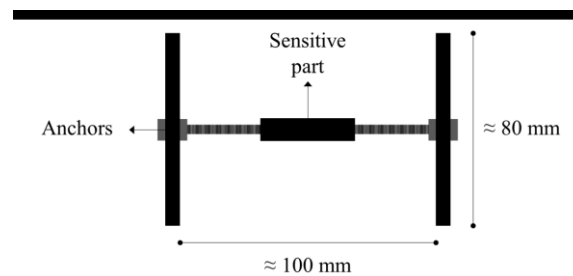


Figure 1-23. Horizontal strain gauge (Barriera et al., 2020)

#### 1.6.4.2. Vertical strain gauges

These gauges are placed in layers of unbound granular materials, to measure the vertical deformations of these layers. The vertical gauges often consist of a central sensing part, and two circular plates at both ends. The circular plates allow to keep the sensor in vertical position, and to anchor it in the granular material. Some of these sensors are equipped with a stake under the bottom plate, which facilitates insertion in the pavement layer, as shown in Figure 1-24.

The measurement principle is the same as for the horizontal gauges (see equation (1.4)).

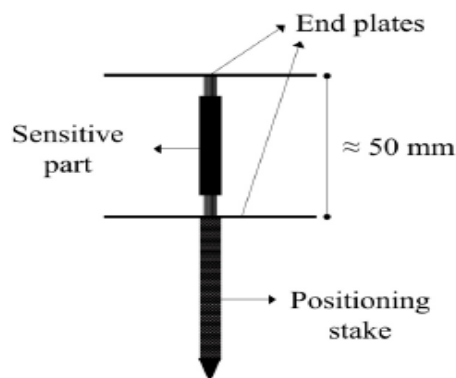


Figure 1-24. Vertical strain gauge (Barriera et al., 2020)

### 1.6.4.3. Types of strain gauges

Different types of strain gauges used for pavement applications are presented below:

Kyowa KM-120-120-H211W1M3 type 120 ohm gauges consist of a resin strip equipped with gauges. They have a range of  $\pm 2000 \mu\text{def}$ . In order to create an anchoring system for fixing the gauges in the asphalt layers, two aluminum bars are added at each end of the gauge (see Figure 1-25).



Figure 1-25. KM-120-120-H211W1M3 type strain gauge

A similar type of gauges consist of an aluminum support, equipped with HBM type gauges (20 or 50 mm long). As for the Kyowa gauges, aluminum bars are fixed at each end of the sensor, to ensure good anchoring in the asphalt material (see Figure 1-26). Both of these gauges are wired and protected with resin to be resistant to high temperature.



Figure 1-26. Aluminum support strain gauge

These two types of strain gauges have been tested at IFSTTAR, but it was found that they tend to underestimate strains of asphalt materials at high temperatures, due to the relatively high stiffness of these gauges. These gauges also tend to get damaged during compaction of the pavement layers; sometimes, damage rates as high as 50 % of installed gauges have been observed.

To overcome these limitations, IFSTTAR has started to use another type of sensors, KM-100HAS gauges from TML (Tokyo Sokki Kenkyujo) with 350 ohm resistance. These sensors consist of strain gauges, glued on a thin metal blade, protected by a metal tube and strips of Teflon type material, as shown in Figure 1-27. Two metal bars are attached at each end to form an H-shaped anchoring system. These sensors have a good resistance to temperature and compaction loading, and a very low stiffness (around 40 MPa), ensuring reliable measurements at all temperatures.

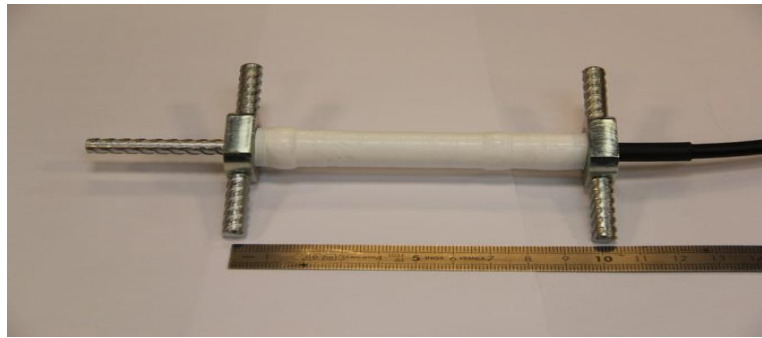


Figure 1-27. TML strain gauge

Finally, another type of strain gauges is manufactured by CTL (Construction Technology Laboratories). They consist of a vinyl rod with gauges glued to it and covered with a protective material which provides a good mechanical resistance as shown in Figure 1-28. Two metal bars are positioned at the end of the gauges. CTL proposes two types of gauges, for the measurement of horizontal and vertical strains. The range of measurement is around  $\pm 1500 \mu\text{def}$ .



Figure 1-28. Horizontal and vertical CTL gauges

### 1.6.5. Temperature probes

Bituminous pavements are highly depended on temperature variations. They mainly affect the stiffness of asphalt mixtures, and it is therefore important to analyse temperatures of pavement layers (Swett and al. 2008). Deformation measurements together with temperature measurements allow to the seasonal variations of pavement response.

There are three main types of temperature sensors, described in the next section.

#### **1.6.5.1. Resistance temperature detectors**

RTD sensors are based on the change of resistance of a metal resistor with temperature. The most popular ones are the PT100 sensors, (see Figure 1-29), which are also used in this work. This type of sensor uses a ceramic or glass core, with a platinum wire around, and has a 100 ohm resistance. These sensors have a high accuracy of about 0.1 °C. They are also immune to electrical noise and deliver stable measurements.

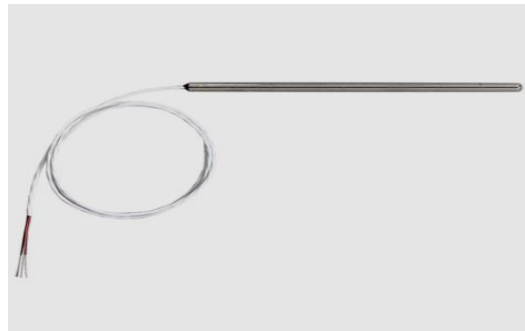


Figure 1-29. RTD sensor

#### **1.6.5.2. Thermistor sensors**

Thermistor sensors contain a ceramic or polymer or semiconductor resistor core, instead of metal. Their resistance is dependent upon the material it is composed, and they present large changes in resistance with temperature. They are highly accurate, between  $\pm 0.05$  to  $\pm 1.5^\circ\text{C}$ , and limited over the range within  $50^\circ\text{C}$  of the base temperature. The working range is limited around  $0^\circ\text{C}$  to  $100^\circ\text{C}$ . These have been used for the thermal analysis of the asphalt concrete caused due to the experimental heating device installed in the pavement (Sangiorgi et al., 2018).

#### **1.6.5.3. Thermocouples**

This type of sensors consist of different metal wires connected through a junction. When this junction is submitted to a temperature variation, it produces a voltage that is correlated to the temperature at the junction. There are several types of thermocouples, depending on the different metals used. These sensors are robust and cost effective, but less accurate, around 0.5 to 5 °C. (Dessouky et al., 2014).

### **1.6.6. Pressure cells**

The main function of pressure cells is to measure the stress without changing the state of the stress in the pavement. However, they are not 100 percent accurate as the measuring instrument always causes a stress redistribution. This redistribution is depended on the stiffness of the cell diaphragm,

and the thickness of the cell. The ratio of the diameter and thickness of the cell diaphragm is termed as aspect ratio. There are two type of pressure cells, diaphragm and hydraulic cells (Tabatabaee and Sebaaly, 1990).

The diaphragm cell consists of a stiff circular plate. With the soil pressure the diaphragm is deflected and the gauges bonded to the interior of the face of the diaphragm measure the pressure. The hydraulic cell consist of two circular steel plates welded together on the outside to form a cavity. The space between the plates is filled with a liquid and the liquid is connected to a pressure sensor by a tube.



Figure 1-30. Hydraulic pressure cell

In (Dessouky et al., 2014; Swett et al., 2008, Al-Qadi, et al., 2004), pressure sensors are used to measure vertical stresses in unbound granular pavement layers. Mostly hydraulic type pressure cells are used in these projects.

### **1.6.7. Installation of the sensors**

Installation of the sensors are also another aspect that need to keep in mind when using strain gauges, geophones and accelerometers.

Elseifi (2009) indicates that the gauges can be subjected to deformations during the construction and compaction phase hence it is advised to place gauges out of the passage areas of the paver tracks. It is also recommended to apply the first passes of the compactor without vibrating, to limit the risk of damaging the gauges.

And by manual sieving and compaction of the materials placed around them expand and adjust with time. But this step could increase the deformations in the pavements and measurements if the pavement structure is thin and the modulus of the layers is low (Leiva-Villacorta, 2012).

Strain gauges need to be installed during construction, and so they need to resist to the construction temperature and to the compaction stresses.

An advantage of using geophones and accelerometers is that they can be installed more easily after the construction, because they can be placed close to the pavement surface. Using small size sensor further reduces the impact of installation on the pavement.

## 1.7 Case studies

### 1.7.1. Short term monitoring

In many applications of pavement instrumentation found in the literature, pavement monitoring is performed on a short-term basis. This section presents work focusing on instrumentation and data collection of the pavements in a limited time. These studies elaborate methods to evaluate the pavement structure with the aid of data collected from the instrumented test sections. These represent the measured responses from the different in situ layers of the pavement.

#### *Inferring pavement properties using an embedded accelerometer* (Eyal Levenberg, 2012)

In this work, a single axis piezoelectric accelerometer KB12VD was used to record the mechanical response of the pavement layers.

The paper shows the approach of using the inertial sensor for measuring the pavement response while the traffic is lightweight and slow in speed. The experiment is performed on a flexible pavement structure, with 100mm asphalt concrete and a 120mm aggregate base course layer. The accelerometer was installed by drilling, at a depth of 80 mm, and was connected via a DAQ module with a portable computer. Also a Tekscan pressure sensor was placed near the accelerometer to measure the load distribution in the tire footprint. The tires 1 and 2 drove over the Tekscan map, passing near the accelerometer. Figure 1-31 shows the experimental setup for the measurements. Several passes of the vehicle were performed, however the data presented relates to a single pass performed at a temperature of 23 degrees and a speed of 21km/h.

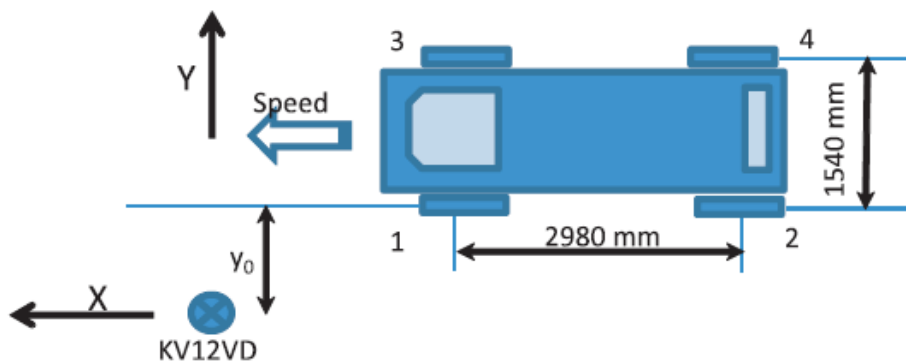


Figure 1-31. Experimental setup (Levenberg, 2012)

One of the distinctive objectives was to analyse directly the measured accelerations and not to integrate them into displacements, as this would induce a lot of errors.

The transducers used are single axis inertial sensors (accelerometers) recording the vertical acceleration. The pavement model is a two-layer elastic half space and back calculation of layer properties is carried out using directly the recorded accelerations by the means of a nonlinear optimization algorithm. These measurements went through smoothing procedures to reduce the vibration sources. An iterative algorithm is used, each iteration consists in applying linear interpolation between the measurement points and then selecting the center of each segment as new point of the signal. By performing several iterations the noise is progressively reduced and a smoother signal is obtained. A fitting error is calculated which defines the difference between the set of raw accelerations and the smoothed accelerations. As the number of smoothing iterations increases, the fitting error increases, while the roughness level in the data decreases as shown Figure 1-32.

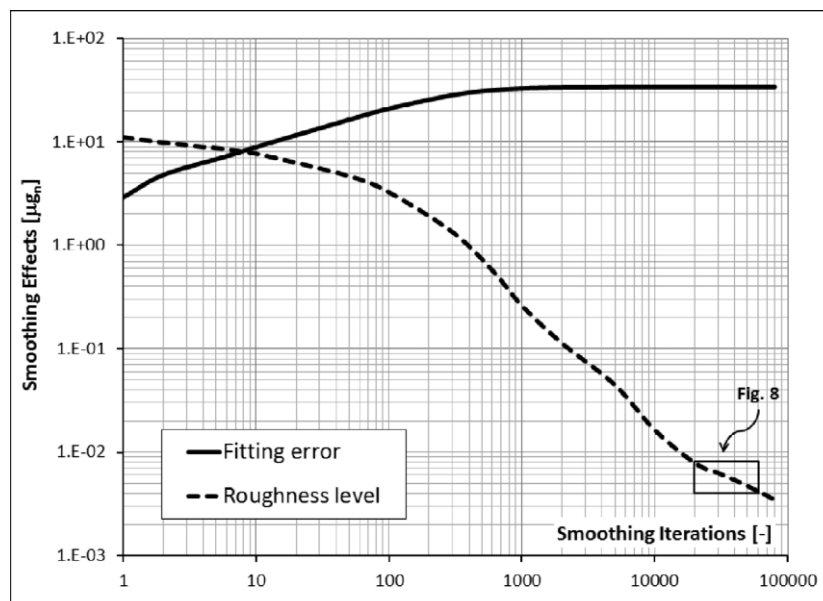


Figure 1-32. Example of iterative smoothing of the signals. Increase of the fitting error and reduction of the roughness level with the number of iterations (Levenberg, 2012)

The ELLEA tool is used to model the acceleration, using the characteristics of the pavement structure (layer moduli and thicknesses), and of the vehicle (speed, vehicle dimensions, load on each axle). Figure 1-33 shows the comparison of the sensor measurements with the modelled accelerations.

The sensor data indicated an even weight distribution, with 50% of the load applied on the front and rear axles. The Tekscan map showed that 52% of the load was applied on the front axle and

48 % on the rear axle. The back-calculation was done through the ELLEA tool, and the modelled accelerations were compared with the measured signals of the accelerometers. The analysis leads to modulus values  $E_1=260$  MPa for the top layer and  $E_2=70$ MPa for the bottom layer, for the simplified two layer pavement model, which were considered adequate in terms of magnitude.

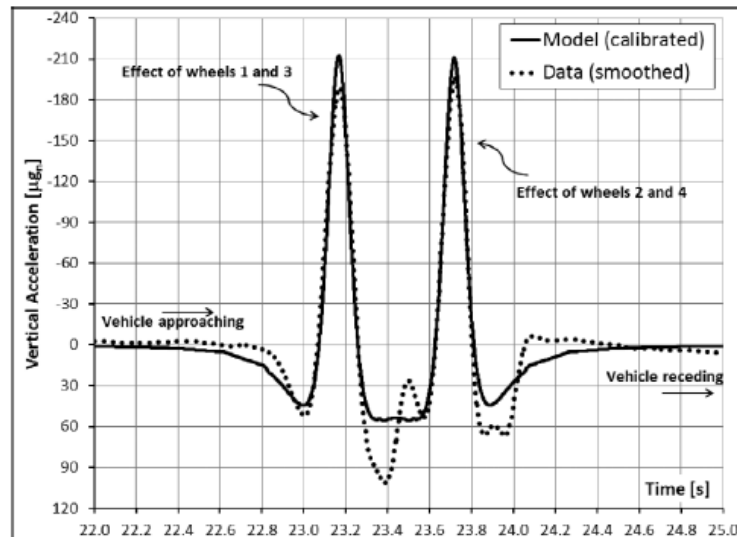


Figure 1-33. Comparison of sensor measurements and calibrated model accelerations (Eyal Levenberg, 2012)

***Measurement and evaluation on deterioration of asphalt pavements by geophones*** (P. Liu et al., 2017)

The experiment was carried out to determine the possibility of assessing the analytical pavement design method using in-situ monitoring of in service asphalt pavements. A non-destructive method of determining asphalt pavement deteriorations was set up, using geophones and a mobile load simulator in order to determine the layer moduli by back-calculation. The experiment was conducted on a test section in the German Federal Highway Research Institute (BAST). Twelve geophones were setup on the test track equidistantly over a length of 3.30 m in the direction of traffic as shown in Figure 1-34. The accelerated loading facility MLS30 was used to simulate the loading of the heavy vehicle and induce vertical displacements in the pavement. Then after different numbers of load cycles, the pavement response was measured with a truck of known geometry and known speed. The position of the axles could be determined by post processing techniques.

Two parameters were changed to analyse their effect:

- 1) The average vehicle speed (7.5, 15 and 30 km/h)
- 2) The lateral distance (30, 60 and 90 cm) between the tire axis and the vehicle driver side

The recorded data was then converted from vertical displacement velocities into deflections in longitudinal and transverse directions using integration. No information on the integration process is given in the paper.



Figure 1-34. Geophone experimental setup on the test section and test vehicle (Liu et al., 2017)

To study the effect of the deterioration on the test track, three service life states of track were considered

- State 1 : initial state before loading by the MLS30
- State 2: the state after 1.5 million loading cycles
- State 3: the state after 3.0 million loading cycles

The back-calculation tool was developed using a semi analytical finite element calculation method (SAFEM) and artificial neural networks (ANN). With the combination of these two methodologies, the fatigue of the test track after the given numbers of load cycles could be analysed. The analysis method is described in the flow chart presented in Figure 1-35.

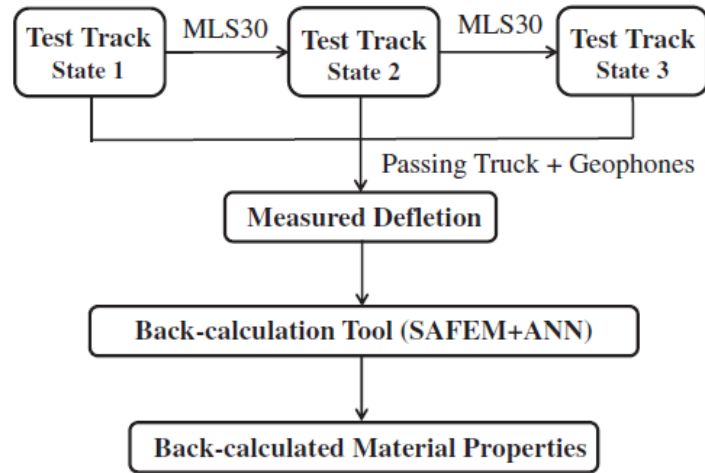


Figure 1-35. Flow chart of the analysis of the deflections measured by the geophones(P. Liu et al., 2017)

Figure 1-36 shows measurements obtained with the 12 geophones, at state 1 (before loading). All the geophones give a very similar response, with a slight time lag due to the distance between them and the constant speed of the moving vehicle.

To compare the results at different states, the deflection bowl obtained when the second truck axle was passing at a speed of 30km/h, over the fourth geophone, was selected. The deflection bowls obtained with this geophone (and the corresponding standard deviations), for the three states of the pavement, are shown on figure 1-34.

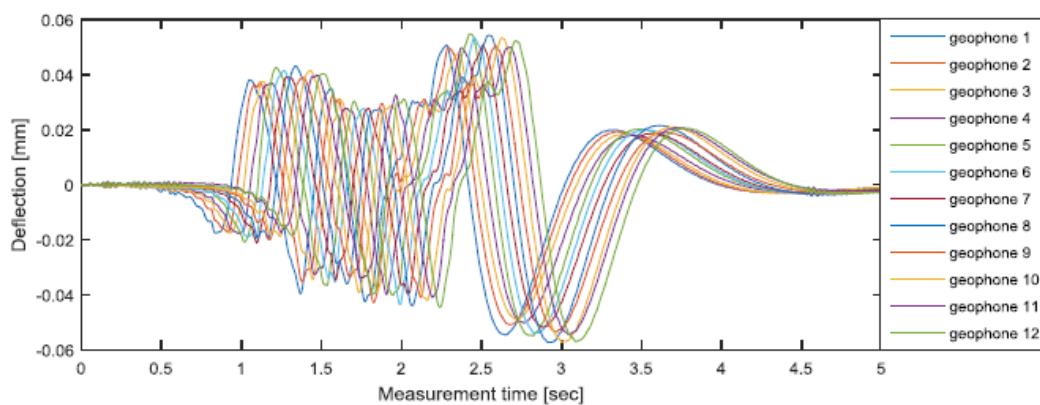


Figure 1-36. Surface deflections measured by all the geophones at state 1 (P. Liu et al., 2017)

With the help of artificial neural networks (ANN), back-calculations were conducted for the three states of the pavement. The back-calculation shows that the modulus of the asphalt layer decreased from state 1 to state 3 as shown in Figure 1-37. On the contrary the modulus of the unbound layer was the highest at state three due to the progressive compaction of the unbound layer, explaining the irregular changes in the deflection as shown in Figure 1-38. This system has been validated to

efficiently measure and analyse the evolution of the moduli and the deterioration of the asphalt pavement under moving loads.

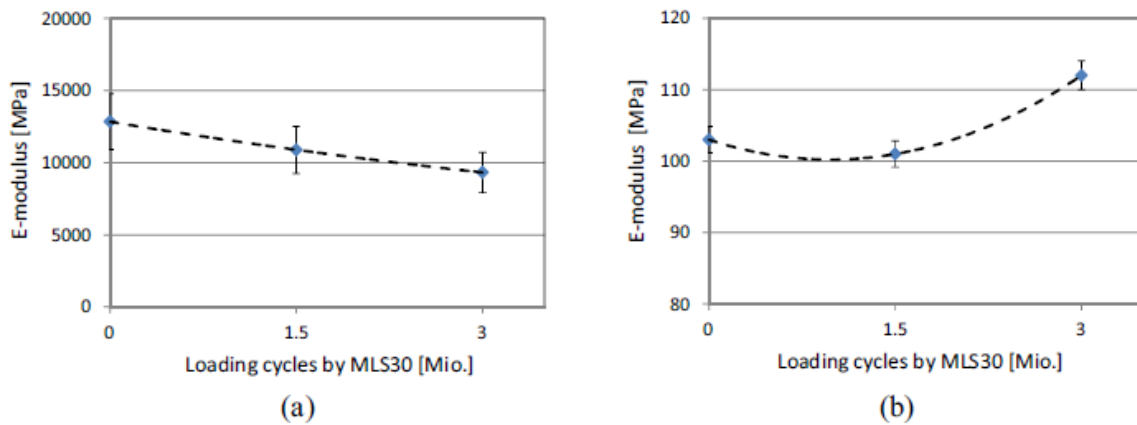


Figure 1-37. (a) Modulus for asphalt concrete values with respect to loading cycles (b) Modulus for unbound layer with respect to loading cycles (P. Liu et al., 2017)

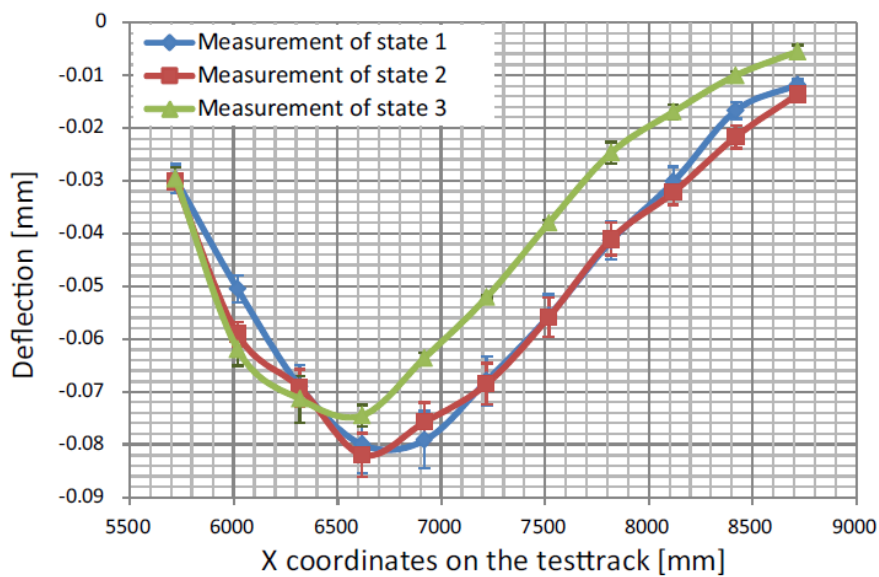


Figure 1-38. Deflection of the test tracks after 3 levels of loading (P. Liu et al., 2017)

***The use of accelerometers in the pavement performance monitoring and analysis***

(Ryynänen et al., 2014)

This study was conducted to study the application of sensor technology for monitoring of highway infrastructure. It was carried out by three universities: Helsinki University of Technology, Tampere

University of Technology and University of Oulu. The experiment was laid out on the highway infrastructure of Finland, for improving its management.

A test road was instrumented in the northern part of Finland at Taivalkoski. The pavement consisted of a 50 mm asphalt concrete surface course, a crushed aggregate base layer and a 300 mm thick subgrade. Several temperature and moisture probes, 7 accelerometers (A1 to A 7), 3 pressure cells (P1, P2 and P3) and displacement transducers were installed to measure environmental and load response of the pavement. Accelerometers were installed in the top layer, 20 mm below the pavement surface, whereas the pressure cells were installed at different depths. Pressure cell P1 was placed in the subbase layer, at a depth of 0.13m from the surface layer, P2 at a depth of 0.29 m and P3 at the bottom of the gravel layer, at a depth of 0.54 m. A four axle truck, with a total weigh of 32000 Kg was used to apply loads on the pavement. A lateral wander of 1.2 meter was introduced, to study lateral wander effects. The pressures measured by the cell P1 were compared with the model signal generated using a simplified analytical model (with a non-linear gauss equation).

The accelerations recorded from the sensors were double integrated into deflection of the pavement. A single deflection bowl of the pavement was defined using the maximum accelerometer readings of several accelerometers placed at different transverse positions, as shown in Figure 1-39. When the load increases, the magnitude of the acceleration increases and the deflection increases.

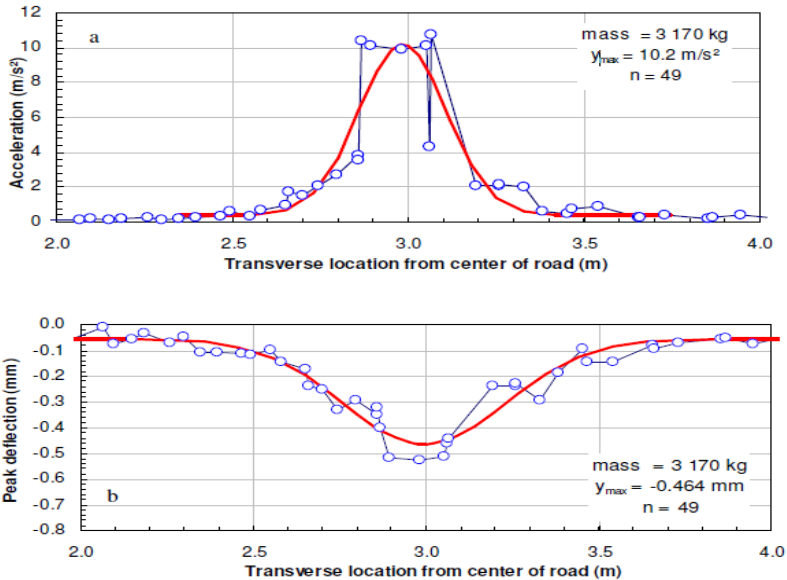


Figure 1-39. Front wheel accelerations obtained by gathering seven accelerometer measurements and comparison with calculated deflections (Ryynänen et al., 2014)

These pavement deflections are compared with the modelled pavement deflections obtained using the Kenlayer software, based on a multilayer linear elastic model. The elastic moduli of the pavement layers were estimated from the loading as a function of stress. The estimated moduli were high, compared to the typical values expected, which was attributed to the error in the displacements obtained from the accelerometer measurements. Figure 1-40 shows the comparison of the accelerometer deflections with the transverse deflection bowl calculated with the software.

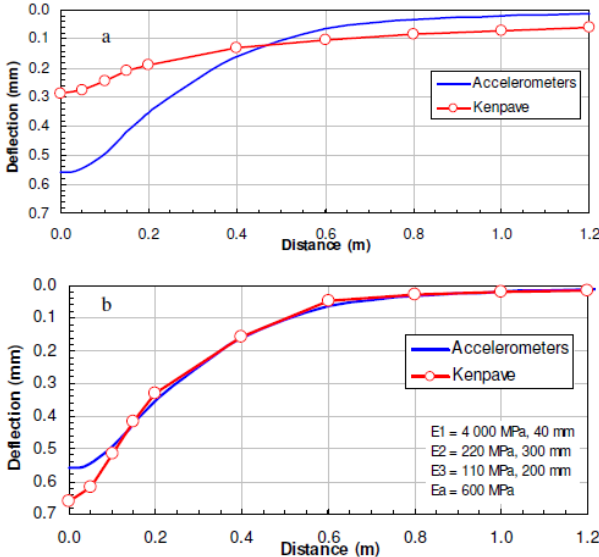


Figure 1-40. Calculated deflections a) shows the when the initial modulus values were used and b)

| Pavement layers             | Thickness (mm) | Initially modulus (A) (MPa) | Changed modulus (B) (MPa) |
|-----------------------------|----------------|-----------------------------|---------------------------|
| Asphalt concrete , AC (E1)  | 50             | 4 000                       | 4000                      |
| Crushed rock aggregate (E2) | 170            | 941                         | 220                       |
| Natural gravel (E3)         | 130            | 347                         | 110                       |
| Rock layer (E4)             | 200            | 226                         | 600                       |

shows when the modulus values are changed (Ryynänen et al., 2014)

Initially the measured deflections at the center are larger than the calculated ones, therefore the layer moduli were modified to match the deflection bowls. The modulus values of the pavement layers are given in Table 1.2.

Table 1.2 pavement structure with initial and changed modulus values to obtain a good match

This analysis led to a good match between the deflections bowls, however did not match very well with the measured stresses. Figure 1-41 shows the stresses obtained with the two different sets of elastic moduli A and B, at the depth of 0.13m. The Boussinesq elastic half space stresses for a single wheel circular loading area are also compared with the measured stresses. The figure also shows that the new values for the kenlayer B show good match to the half space analysis and also suggest that the calculated values are similar.

The authors concluded that the modelling approach is not suitable for the real pavement, because it assumes continuous material properties and infinite pavement layers whereas the real pavement has a finite transverse geometry and thin asphalt but thick unbound layer layers.

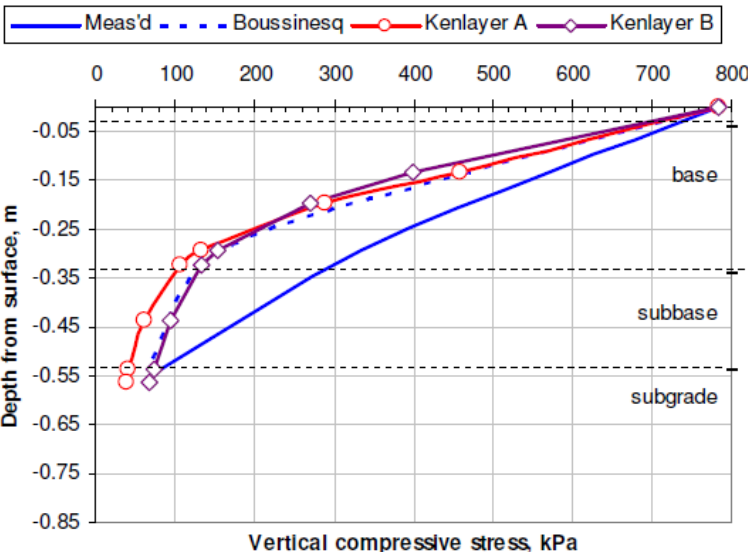


Figure 1-41. Vertical stress values calculated with the two sets of moduli of table 1, and comparison with measured values (Ryynänen et al., 2014)

**1.7.2. Long term monitoring**

Recently, advances in instrumentation technologies and data storage capacities have made possible to perform continuous monitoring of pavement performance over long periods. The studies in this section focus on long term field data collection and large-scale structural monitoring applications. These experiments are focused on developing methods to study pavement distresses, deformations and to estimate the pavement structure. They also focus on instrumentation of the pavement done during the construction phase and installation of sensors into the pavement materials, to monitor in detail the response of the different pavement layers.

*Instrumentation project: Virginia Smart Road* (Al-Qadi et al., 2004)

An experiment was conducted by the Virginia Department of Transportation to study the impact of structural and environmental parameters on pavement response. In 1999, 12 flexible pavement sections of 100 m length were built. Different sensors like strain gauges, pressure cells, thermocouples, humidity probes, resistivity probes were used for the instrumentation. These sensors were connected with two data acquisition systems with different settings; one unit was used to store the static data that doesn't require frequent recording (like temperatures, moisture contents). The other unit was used to store the dynamic data, which require high frequency measurements, like deformations and strains.

The experiment consisted in applying several passages of a heavy vehicle, with a front axle (with single wheels) loaded 25.8 kN, at four different speeds: 8 km/h, 24 km/h, 40 km/h and 72 km/h. The objective of the study was to analyze the impact of the various parameters (temperature, vehicle speed, etc.) on the structural response of the pavement. The mechanical response of the pavement, for the different experimental conditions, was also modelled, using different modelling assumptions.

The results showed that a better prediction of the pavement response was obtained with a viscoelastic model. Figure 1-42 shows transversal strains measured at the bottom of the bituminous layer, for different speeds and temperatures. A strong influence of temperature on the measured strains can be observed. Figure 1-43 presents an example of modelling of the transversal strains measured at different temperatures, with a finite element model, taking into account the viscoelastic behaviour.

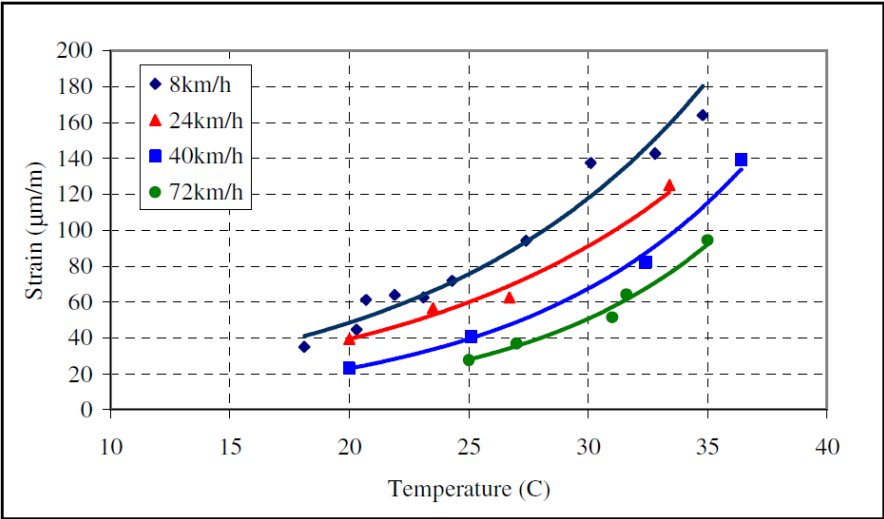


Figure 1-42. Transversal deformations measured at the bottom of the bituminous layer for different speeds and temperatures (Al-Qadi et al., 2004)

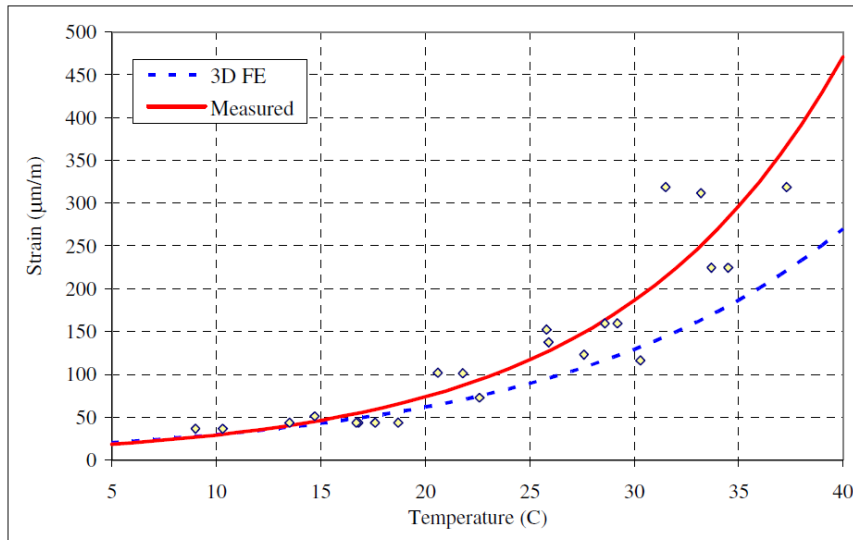


Figure 1-43. Comparison of the measured transversal deformations with values predicted using a finite element model (Al-Qadi et al., 2004)

**Section of Route 15 from Guildford, Maine, USA** (Swett et al., 2008)

A first instrumented section of flexible pavement was installed in 2005 by the Maine Department of Transportation and the data was collected over a 5 months period. Every year, the state of Maine spends 50 million dollars for the design, construction and rehabilitation of pavements, following design procedures based on the 1986 and 1993 AASHTO design guides (American Association of State Highway and Transportation Officials). In this project the instrumented site was located on Route 15 in Guilford, Maine, installed with the following sensors (Figure 1-44):

- 16 strain gauges (12 gauges in bituminous layers, 4 gauges in the subgrade)
- 30 thermocouples (6 probes at the base of the bituminous layers, 24 probes in the subgrade)
- 6 humidity probes
- 2 resistivity probes

A Data acquisition system was used to connect the sensors to the computer system. The temperature readings were recorded hourly and the strain measurements were carried out under the passage of two axle and three axle vehicles at different speeds and different temperatures.

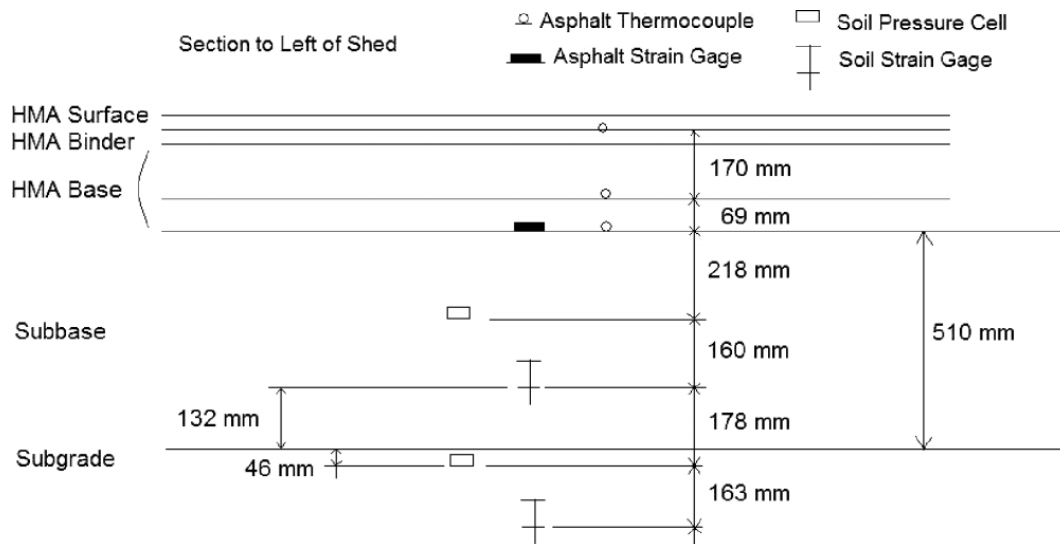


Figure 1-44. Instrumentation of the pavement on Route 15(Swett et al., 2008)

The measurements were used to evaluate the pavement response, and compare it with modelling, with the program BISAR, based on a multi-layer linear elastic model. The predicted vs measured responses showed good agreement at lower temperatures and lower loading times for the bituminous layer as shown in Figure 1-45. The strains in the bituminous layer were under-predicted at high loading times (low speeds) and this is probably due to the constant elastic moduli used with no correction with frequency. For the subbase layer, the stresses were typically underestimated and showed small increase with the loading time, as shown in Figure 1-46.

The study concluded that the effect of temperature on the measurements can be taken into account using a thermal model of the pavement. It also indicated an important effect of the loading time on the measured strains that needs to be taken into account. Finally the instrumentation could be used to monitor the effect of seasonal climatic variations on the pavement.

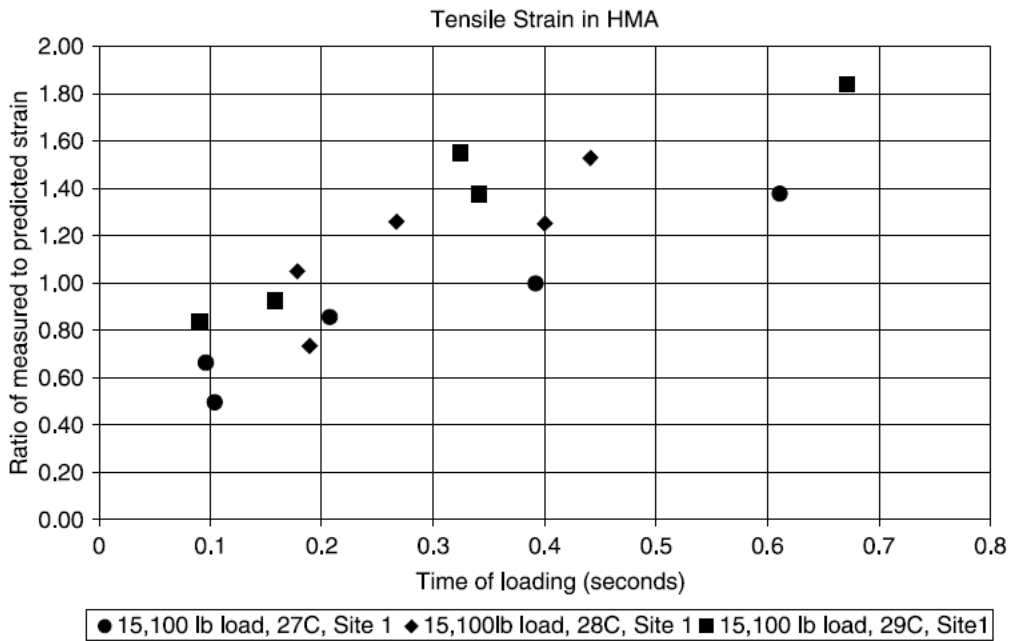


Figure 1-45. Comparison of the measured and calculated horizontal strains at the base of the bituminous layer at different loading times (Swett et al., 2008)

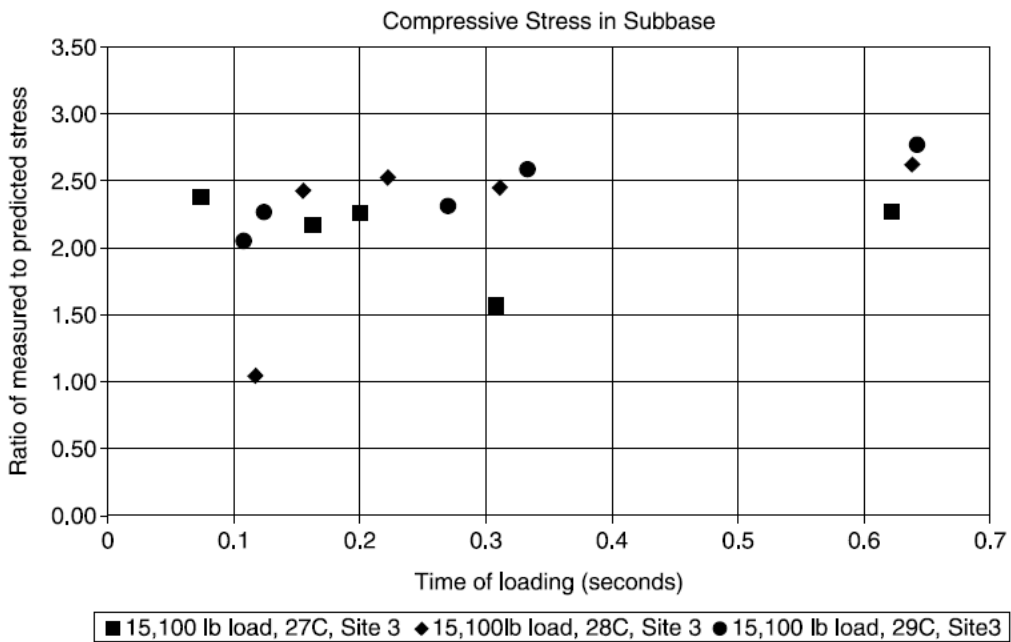


Figure 1-46. Comparison of measured and calculated vertical stresses in the subbase layer at different loading times (Swett et al., 2008)

**Virginia State Road Experimental Section** (Xue et al., 2014)

This study focused on the main goals of health monitoring, traffic analysis and back-calculations of the pavement properties with the smallest number of sensors possible. A test section on a highway in Virginia was instrumented with different types of sensors in October 2011. All the

sensors, including horizontal and vertical strain gauges, pressure sensors, thermocouple temperature sensors and moisture sensors, were placed at the bottom of the surface layer as shown in Figure 1-47. The combination of pressure cells and strain gauges (horizontal gauges in longitudinal direction, horizontal gauges in transverse direction and vertical gauges) formed a sensing group. In particular, these gauges were placed at different positions in the lateral direction, to study the effect of the wandering of vehicle passages. Vlink wireless data logger nodes were used to transfer the data from the sensors to the data base making it flexible for monitoring.

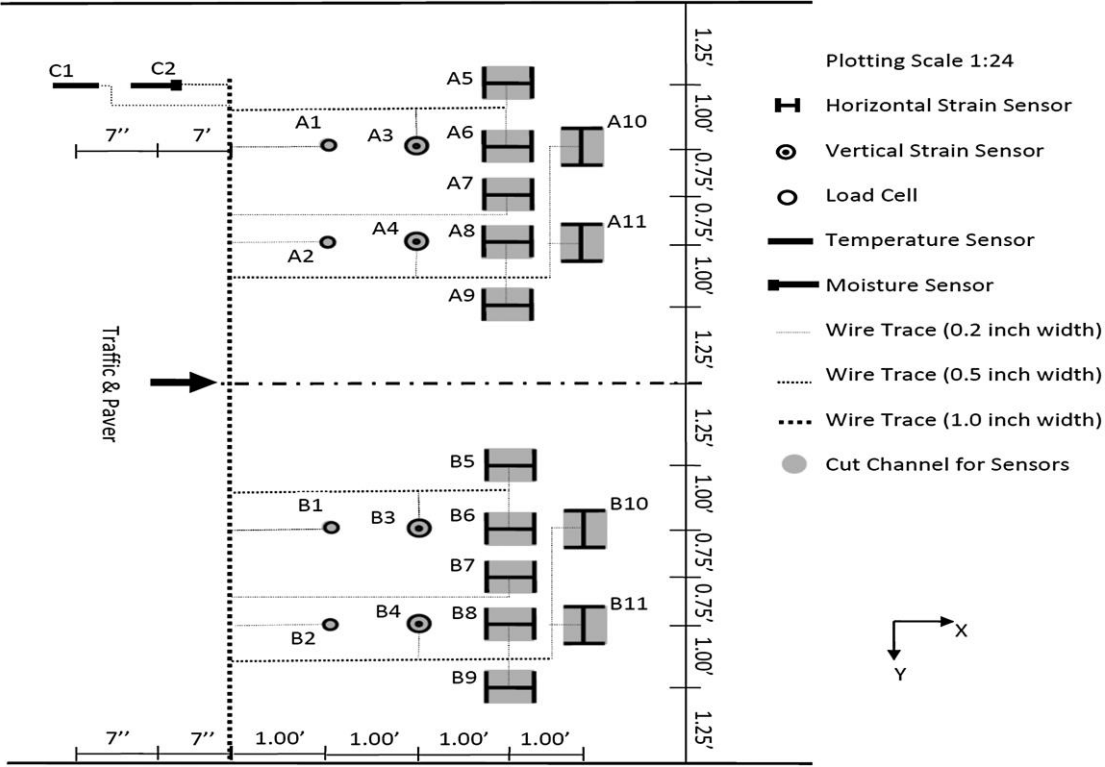


Figure 1-47. Instrumentation of the Virginia State Road Experimental Section ( Xue et al., 2014)

For the analysis of the mechanical responses of the pavement, it was important to determine the loads, speeds, vehicle configurations and temperatures. The elastic modulus was used to characterize the condition of the pavement and lifespan of the road. The data from a test vehicle was used in the back-calculation of the modulus, to assess the bearing capacity of the roadway. The initial idea was to use the measured vertical stresses and strains to determine the moduli of the pavement layers, however all the vertical gauges were damaged after 5 months, but the horizontal gauges and pressure cells were working well. The transverse strain measurements were used, together with a relationship between the vertical and longitudinal strains, to back calculate the layer moduli of the pavement. Finite element calculations made with the ABAQUS software were used to study the theoretical mechanical analysis of the pavement section.

The idea of the sensing network was to determine the vertical stresses and strains for the back-calculation, however due to the harsh environment vertical strain gauges were out of order. Hence horizontal strains were used and the parameter  $R_{ZX}$ , defined as the ratio of the vertical stress  $\sigma_z$  and the normal strain  $\epsilon_x$  in the x direction (equation (1.19)), was used to back calculate the modulus.

$$R_{ZX} = \frac{\sigma_z}{\epsilon_x} \tag{1.19}$$

The finite element calculations were used to establish a relationship between the parameter  $R_{zx}$  and the asphalt concrete modulus. Figure 1-48(a) shows this relationship, which indicates the increase of the parameter with the modulus of the asphalt concrete. For a fixed load level, Figure 1-48 (b) shows the relationship between the temperature and the parameter  $R_{zx}$  that is simulated at two speeds. Using this relationship the dynamic modulus of the asphalt concrete was back-calculated for different speeds and temperatures.

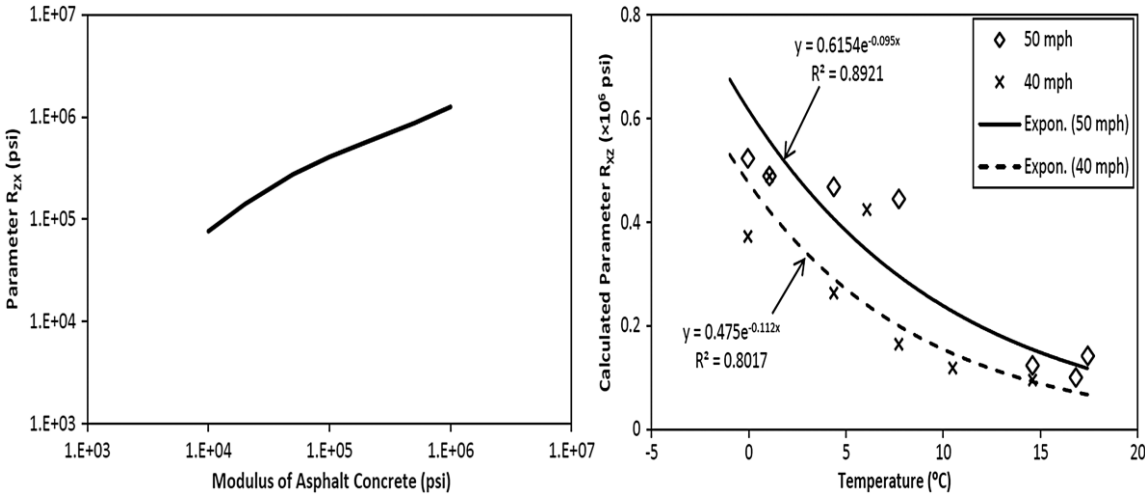


Figure 1-48. (a) Relationship between the  $R_{zx}$  and the modulus (b)  $R_{zx}$  back calculated parameter by changing temperature and speed (Xue et al., 2014)

In addition, the measurements under traffic were used to predict the damage of the roadway using fatigue and rutting criteria, based on the measured strains. The damage calculations due to each vehicle passage were made using models of the MEPDG (Mechanistic Empirical Pavement Design Guide) design method.

The monitoring of the pavement was based on the instrumented sensing network, as explained in the flow chart in Figure 1-49. The health monitoring of the pavement must comprise periodic tests with a reference load and measurements under real traffic. The periodic tests make it possible to determine the structural properties of the pavement, and the measurements under live traffic allow

to calculate the cumulative damage under the passage of vehicles. This provides criteria to determine the performance and the life span of the pavement system.

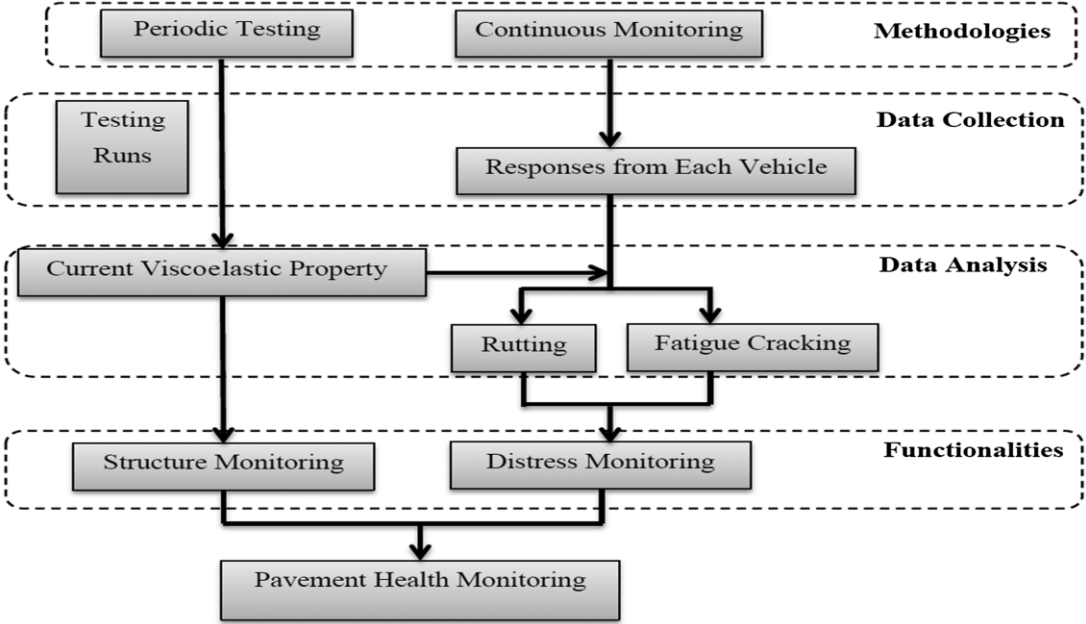


Figure 1-49. Pavement Health monitoring flowchart (Xue et al., 2014)

**Smartvia concept** (Pouteau et al., 2017)

The project was developed by the Eurovia Research Center for innovative pavement products. It implemented an automated pavement monitoring system and developed an integrated pavement system with embedded sensors, with a programmable data acquisition system. This project was implemented for a period of 5 years. It was installed in the city of Lille in 2014, with the main objective to monitor the impact of trenches on the durability of the pavement as shown in Figure 1-50. In this paper the authors only describe the instrumentation of the sensors and their installation in the pavement.

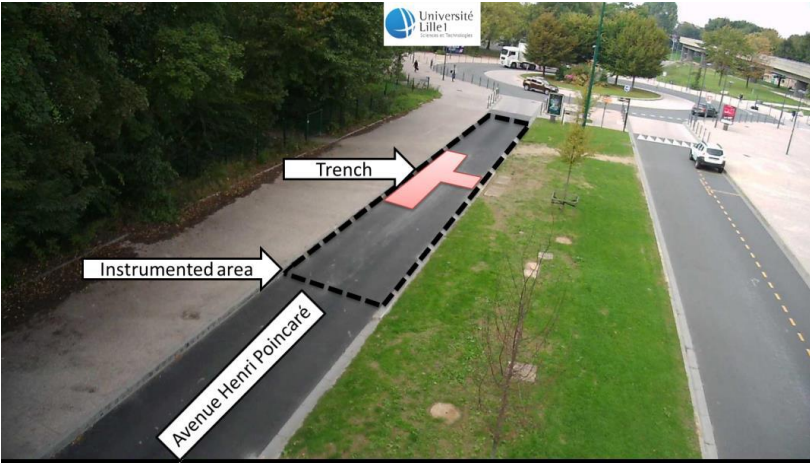


Figure 1-50. Instrumented site for the SMARTVIA project (Pouteau et al., 2017)

The test section consists of 7 instrumented sensing nodes, which include temperature sensors, strain gauges, moisture probes and Bragg grating fibre optic sensors (FBG). The data acquisition system consists of three controllers and a surveillance camera for tracking every truck passage on the sensors. 3G communication is used to transfer the data to a database. To reduce the load of the data being transferred, data is recorded only when an event (vehicle passage) is triggered.

Figure 1-51 shows examples of measurements obtained with the longitudinal strain gauges P0 (located on a reference section without trench) and P5 (located above the trench).

From this experiment, it was concluded that Smartvia was an efficient system to monitor the pavement structure under real traffic. However there was still work needed for increasing the durability of the sensors, as the gauges failed to work after 8 months.

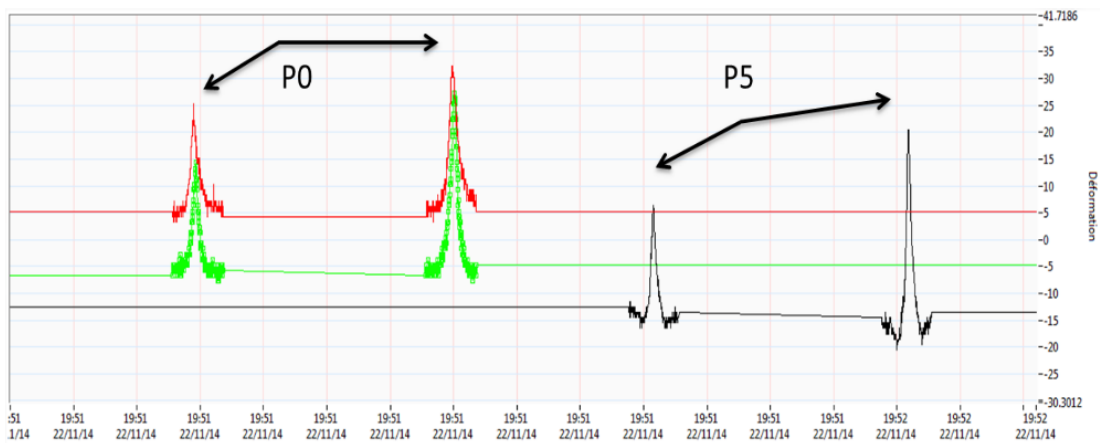


Figure 1-51. Examples of strain signals obtained with longitudinal strain gauges P0 and P5 (Xue et al., 2014)

### ***Experimental section in China*** (Ai et al., 2017)

In this project, the response of an experimental pavement under real conditions was studied, taking into account the effects of speed, configuration and loading of vehicles, and temperature of the pavement layers. Most current pavement design methods calculate the stresses and strains in the pavement under static loading conditions. The objective of the in-situ measurements was to obtain a clear picture of the structural dynamic response of the pavement.

The test road selected was a two-way road with 4 lanes, 24.5 m wide. The experimental pavement section was 900 m long, with the same subgrade, but with three different pavement structures, which included a semi-rigid pavement, an inverted asphalt pavement and a thick asphalt pavement. The sensors used were strain gauges and pressure probes, which were installed at the bottom of the base layers. Four gauges were installed in each of the three pavement sections.

To carry out the measurements, two types of heavy vehicles were used (Figure 1-52): A Heavy Duty Type 1 vehicle (with single rear axle). Three different load levels on the rear axles were used, 98 kN, 138 kN and 177 kN. The second vehicle was a Heavy Duty Type 2 vehicle with tandem rear axles. Three different load levels were used for the tandem rear axle configuration, 177 kN, 255 kN and 334 kN. The tests were made with three temperature levels: 12°C (winter), 21°C (spring) and 43°C (summer). The tests were also performed at different speeds: 20, 40, 60 and 80 km/h for vehicle T1; 20, 30, 40 and 60 km/h for vehicle T2.

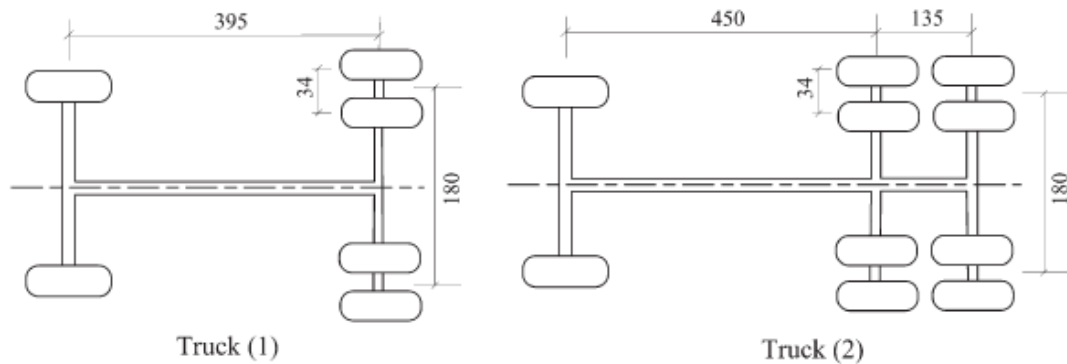


Figure 1-52. Configuration of the two types of test vehicles (Ai et al., 2017)

The results showed that, for the two types of truck loads, the temperature and the load level had the most significant effect on the deformations of the pavement. The strains increased with the increase of temperature and load, and that the combination of these two parameters (high temperature and load) leads to higher strains than predicted with a classical linear elastic model and could accelerate the fatigue damage. An exponential function was used to predict the pavement response in function of axle load, speed and temperature.

A multivariate linear regression was used to convert this relationship into 6 predictive empirical equations to model the responses depending on the influential factors like temperature, loading and the speed of the loading.

### ***Monitoring of the Motorway A10 in France*** (Blanc et al., 2019)(Duong et al., 2018)

The French motorway company Cofiroute decided to rebuild the slow lanes of the A10 and A11 motorway, near Paris, using a technique of in-place recycling with cement. To validate the mechanical performance of this innovative recycling technique, a part of the lane was selected for continuous monitoring. Four section of the motorway, located at points PR15+700, PR15+900, PR16+850, and PR17+100 were instrumented using horizontal and vertical strain gauges and temperature probes, as shown in Figure 1-53 (a). Another section (PR16+016) was instrumented with geophones and temperature probes as shown in Figure 1-53(b). These sensors were connected

with a wireless data acquisition system, based on Pegase data acquisition boards, developed by IFSTTAR. This system allows to make continuous monitoring, and transfers the sensor data to a cloud based server.

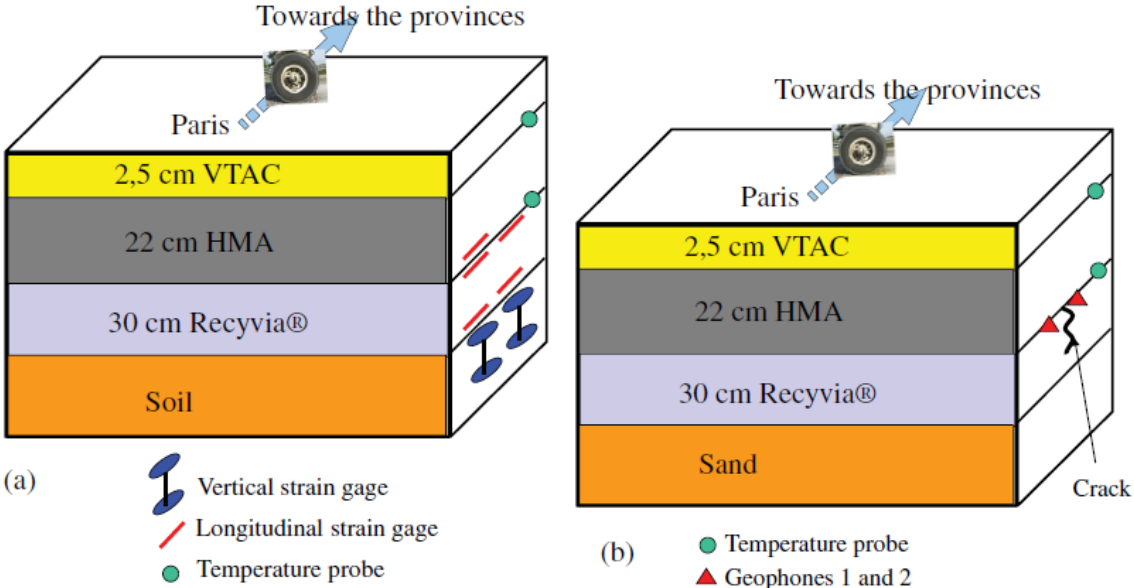


Figure 1-53. Instrumentation of the A10 motorway

- (a) sections PR15+700, PR15+900, PR16+850 and PR17+100 instrumented with gauges
- b) section PR16+016 instrumented with geophones and remote data acquisition system (Blanc et al., 2019)

Two reference trucks were used for the initial measurements: one was a two-axle truck and the second one was a 5 axles truck with loads of 17.6 and 46.5 tons respectively.

Four series of tests were conducted, at temperatures of 2°C, 12°C, 11°C and 10°C respectively. The first three series of measurements were made with the two axle truck and the last series was made with the 5 axle semi-trailer. All tests were performed at a low speed of 3km/h.

The tests were simulated using the linear elastic pavement modelling software ALIZE, and the strain gauge measurements under the passage of the reference vehicles were used to estimate the moduli of the pavement layers. A decrease of the maximum strain values with time, corresponding to an increase of the modulus of the subbase layer, due to the setting of the cement treated material, was observed, as shown in Figure 1-54.

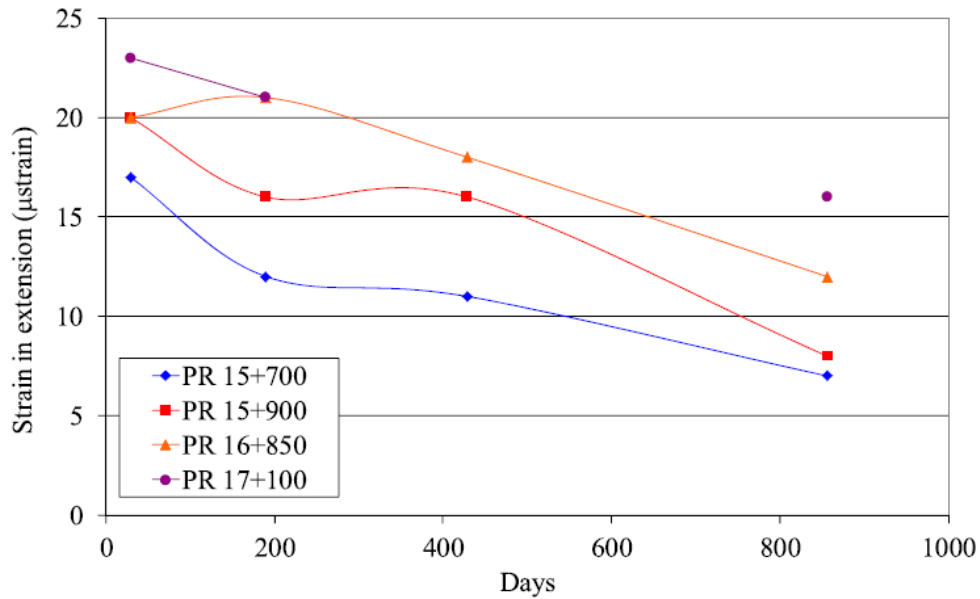


Figure 1-54. Evolution of the maximum strains at the bottom of the Recyvia layer (Blanc et al., 2019)

Comparison of the strain measurements with ALIZE allowed to back-calculate the moduli of the pavement layers. Moduli obtained for two different series of tests, at 2°C and 0.5 Hz (3km/h) and 12°C and 0.5Hz (3km/h), are given in Table 1.3. The results showed that the moduli of the cement-treated Recyvia layer increased slowly with time, and confirmed the good performance of this material, used for the pavement subbase.

Table 1.3 Pavement layer moduli of the A10 motorway obtained by fitting the sensor measurements carried out in November 2011

| Layer   | Structure (2°C, 0.5Hz)  |           |       | Structure (12°C, 0.5Hz) |           |       |
|---------|-------------------------|-----------|-------|-------------------------|-----------|-------|
|         | Layer thickness $e$ (m) | $E$ (MPa) | $\nu$ | Layer thickness $e$ (m) | $E$ (MPa) | $\nu$ |
| VTAC    | 0.025                   | 3220      | 0.35  | 0.025                   | 1886      | 0.35  |
| HMAC    | 0.11                    | 11,294    | 0.35  | 0.11                    | 7882      | 0.35  |
| HMAC    | 0.11                    | 11,294    | 0.35  | 0.11                    | 7882      | 0.35  |
| Recyvia | 0.3                     | 6500      | 0.35  | 0.3                     | 6000      | 0.35  |
| Soil    | 0.5                     | 100       | 0.35  | 1                       | 800       | 0.35  |

Another interesting aspect of this study was the analysis of the Geophone measurements, which led to various interpretations. Geophones are robust and sensitive sensors, suitable for measuring pavement response due to heavy vehicle loading, in terms of vertical velocity. The geophone signals were integrated to find the vertical displacement. The first application of the measurements was the identification of the silhouettes of the heavy vehicles. As shown in Figure 1-55, the axles of the vehicle can be easily detected through the peaks of the signals measured by the geophones.

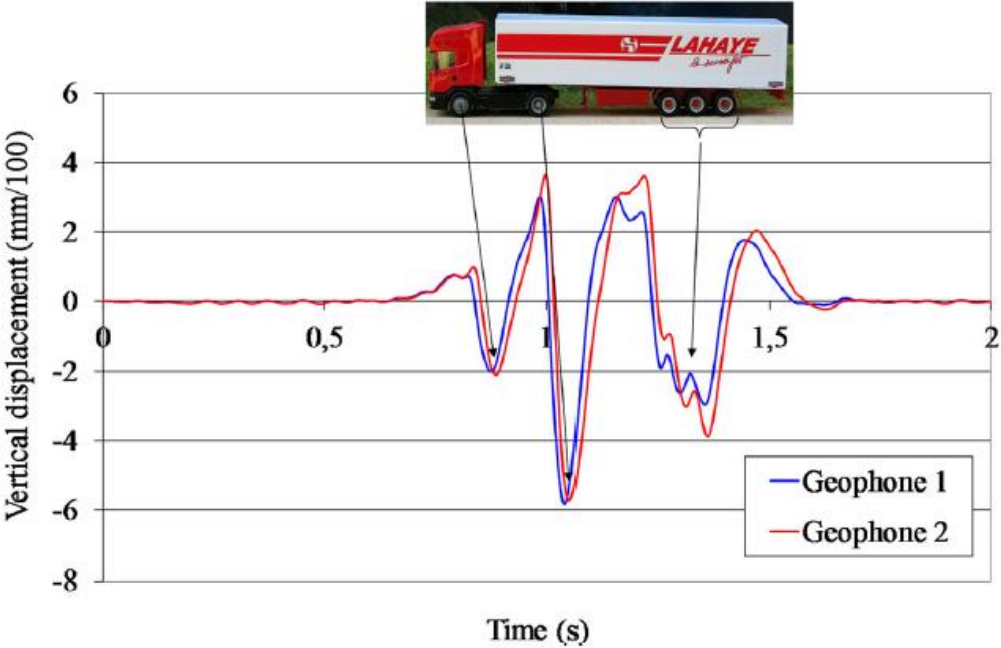


Figure 1-55. Integrated signal from the geophones under 5 axles truck (Blanc et al., 2019)

The geophone measurements were integrated directly to evaluate the pavement displacements and compared to the Alize model displacements. As shown in Figure 1-56, the displacements signals presented a positive part, indicating an upward displacement, which was not realistic, and was not predicted by the model. It was concluded that a direct integration of the vertical velocities measured by the geophones does not allow to predict accurately the displacements, and that more work was necessary to try to develop an appropriate signal treatment method, to predict pavement deflections from the geophone measurements.

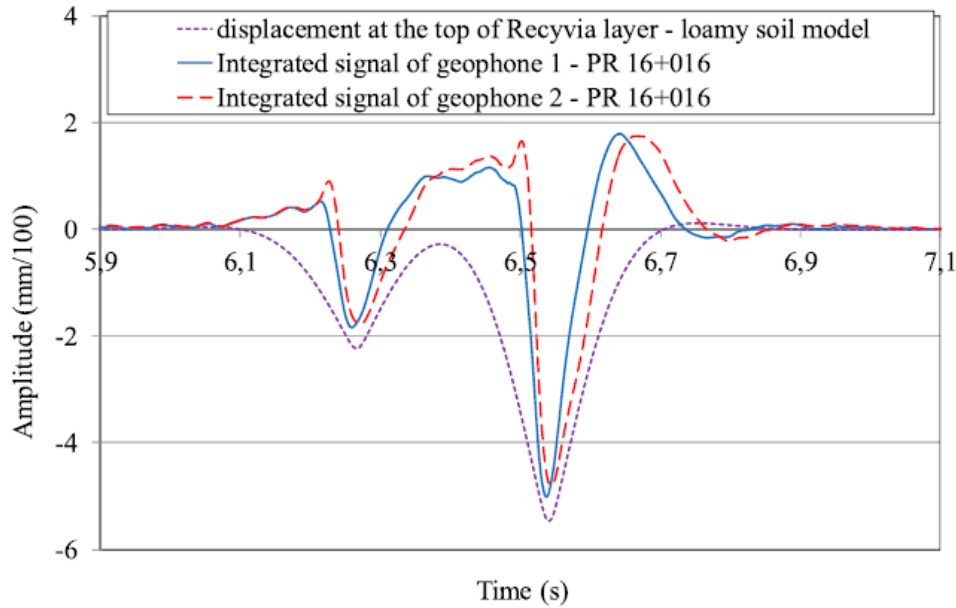


Figure 1-56. Comparison of the measured and calculated vertical displacement signals, for the measurements made on 15 November 2011 (12°C and 10 Hz).(Blanc et al., 2019)

***Monitoring of the Motorway Ax in France*** (Duong et al., 2018)

Another experimental section on a French motorway was instrumented with temperature sensors, strain gauges and geophones. Similar to the A10 motorway instrumentation, these sensors were connected with a wireless data acquisition system, in order to perform continuous monitoring under real traffic. One objective of this study was to investigate the use of geophones to measure the pavement deflections and monitor the traffic. The geophone measurements were recorded during a period of about 2 years.

The experimental pavement structure consists of five different layers, as represented in Figure 1-57. The 3 upper bituminous layers consist of a wearing course, binder course and a high modulus bituminous concrete base course. These layers were put in place in 2013, during the rehabilitation of the pavement. They rest on two layers from the old pavement structure, consisting of a cracked bituminous layer, and a cement treated subbase.

Four geophones and 8 temperature probes were installed at the base of the high modulus bituminous concrete layer as shown in Figure 1-57. The objective was to use the geophones to monitor the vertical displacements in the pavement structure. Three geophones (G1, G3 and G4) were placed 15 cm apart in the transversal direction, in order to evaluate the lateral positions of the traffic loads. Geophones G1 and G2 were placed 1 m apart in the longitudinal direction, and were used to estimate vehicle speeds.

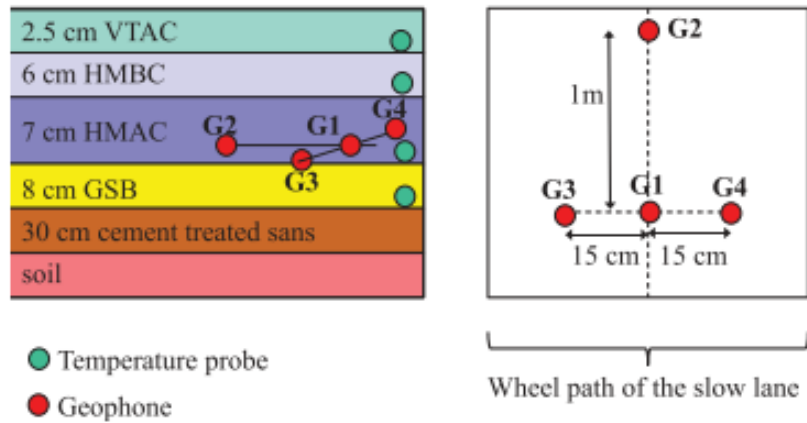


Figure 1-57. Instrumented pavement section (Duong et al., 2018)

To analyse the displacement values from the geophones, the vertical velocities were integrated. It was observed that the simple integration was not sufficient to get correct displacement signals. A signal treatment method was proposed to convert the geophone responses into vertical displacements, using in particular the Hilbert transform. The responses obtained after treatment were compared with modelling results obtained with the ALIZE software (Figure 1-58).

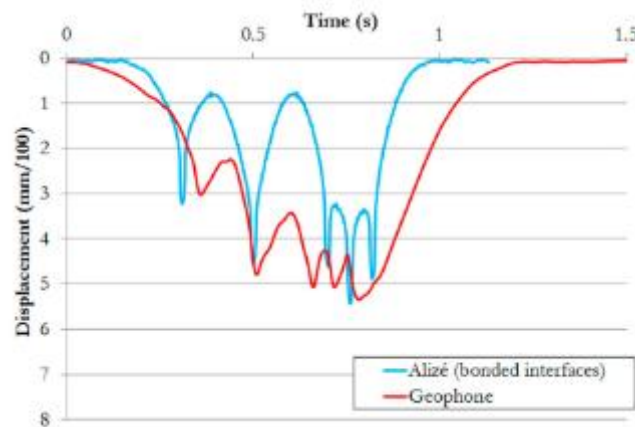


Figure 1-58. Comparison of the geophone vertical displacement response and modelled response (Duong et al., 2018)

The results from this study were not very conclusive. The shapes of the displacement signals obtained from the geophones were not very realistic, when compared with the model response, and it was decided to investigate other approaches, to exploit the full potential of the geophones for measuring vertical displacements.

The database of measurements of the Ax motorway has been reanalysed in chapter five of this thesis, using improved signal treatment methods, and several applications of the measurements have been proposed.

## 1.8 Conclusion

This project and thesis mainly focuses on pavement instrumentation, and analysis of the measured sensor data. After defining the main characteristics of pavement structures, and the factors affecting their performance, the literature review mostly focuses on instrumentation methods for pavement monitoring. The main types of sensors used for this type of instrumentation include:

- Displacement sensors
- Geophones, accelerometers
- Strain gauges
- Temperature sensors
- Pressure sensors

One of the main subjects studied in this thesis is the use of sensors for the measurement of deflections, which is one of the main parameters used to evaluate the structural characteristics of pavement structures. The literature review has shown that in addition to displacement sensors, geophones and accelerometers can be used to measure pavement deflections under moving loads.

The behaviour changes due to the environmental conditions (temperature and water content of the unbound layers) are also essential in the monitoring of pavement structures, and need to be taken into account in the interpretation of monitoring results. Knowledge (or estimation) of vehicle loads is necessary for modelling the response of the pavement, and back-calculating pavement layer properties.

Three types of modelling software have been discussed, which are used for calculating the response of pavement structures, and will be used in this work:

- ALIZE-LCPC software - French pavement design software, based on linear elastic modeling.
- Viscoroute © - analytical, multi-layer pavement modelling software which takes into account the thermo-visco-elastic behavior of bituminous materials.
- ELLEA - pavement modelling software also based on a linear elastic model.

Various case studies have been discussed in the last part of this chapter, to present in detail different instrumentation solutions used to determine pavement behaviour. These studies have been mainly categorised into:

- Short term monitoring indicating experimental setups used to measure the short term response of pavements, under a small number of vehicle passes, with known vehicle loads.
- Long term monitoring, which concerns the instrumentation of real roads, over longer periods of time, and under real traffic. With such instrumentation, it is possible to monitor the pavement structure under real traffic (with unknown loads), and to study the evolution of the pavement response under the effect of time, and of environmental variations.

However, the continuous monitoring of pavement deflections and interpretation of the vertical displacements is still a subject for research. The development of a solution for continuous monitoring of the pavement response, over a long period, under real traffic, such as the one proposed in this thesis, based on the use of geophones or accelerometers, appears to be an original approach. The proposed applications concern not only the measurement of deflections, but also the identification of vehicle types and estimation of vehicle loads, using specific signal treatment methods.

# CHAPTER 2 LABORATORY TESTING OF SENSORS (GEOPHONES & ACCELEROMETERS)

- 2.1 Introduction – Objectives of the preliminary instrumentation tests .....77
- 2.2 Selecting the sensors to measure pavement deflections .....78
- 2.3 Experimental Protocol.....79
  - 2.3.1. Objectives of the laboratory tests.....79
  - 2.3.2. Modelling of pavement deflections with the Alize software .....80
  - 2.3.3. Test Program.....81
  - 2.3.4. Determination of transfer functions.....82
- 2.4 Sensor Responses: untreated sensor signals .....83
  - 2.4.1. Results from the geophones.....84
  - 2.4.2. Results from accelerometers .....85
- 2.5 Processing and improving the geophone Signal measurements.....85
- 2.6 Method for filtering and converting the vertical velocity signals into vertical displacements .....87
  - 2.6.1. Step1: Filtering the signals .....87
  - 2.6.2. Step 2: Amplification of the signal with respect to the reference signal amplitude.....88
  - 2.6.3. Step 3: Integration and detrending to remove the continuous part of the signal .....88
  - 2.6.4. Step 4: Application of the Hilbert transform .....89
- 2.7 Method for filtering and converting the vertical acceleration signals into vertical displacements.....91
  - 2.7.1. Step1: Filtering the signals .....91
  - 2.7.2. Step 2: Amplification of the signal with respect to the reference signal amplitude.....92
  - 2.7.3. Step 3: Integration and detrending to remove the continuous part of the signal .....93
  - 2.7.4. Step 4: Application of the Hilbert transform .....94
- 2.8 Comparison of the treated geophone and accelerometer measurements with the reference laser sensor .....95
- 2.9 Results obtained with the treated sensor signals.....96
  - 2.9.1. Pulse signals.....96
  - 2.9.2. Truck signals .....101
- 2.10 Conclusion .....106



## 2.1 Introduction – Objectives of the preliminary instrumentation tests

In an actual pavement structure, moving loads induce repeated stresses and strains, which lead to fatigue and other distress mechanisms, and affect pavement layer moduli. Pavement deflection (or vertical displacement) is a parameter which is widely used to evaluate the response of pavements to traffic loads, and to assess their structural performance. Measured deflection basins can also be used to back-calculate pavement layer moduli.

Classically, in situ deflection measurements are made using anchored displacement sensors. Such sensors consist of a displacement sensor, attached to a rod, which measures the vertical displacement between the pavement surface (and a point close to the surface) and the end of the rod, which is anchored at a sufficient depth below the pavement surface (typically about 4 meters), to consider that the end of the rod is fixed. Such anchored displacement sensors give accurate results, but they are relatively expensive, and difficult to install, because it is necessary to make a borehole up to a sufficient depth. The idea in this work, is to replace the displacement sensors by accelerometers or geophones, which record respectively the vertical velocity or the vertical acceleration. By integrating once (for geophones) or twice (for accelerometers) their measurements, it is possible to calculate the pavement deflection. The advantage is that these sensors are easier to install than anchored displacement sensors, because no borehole is necessary for their installation.

This chapter focuses on the development of an appropriate methodology for measuring pavement deflections using accelerometers and geophones. For that purpose, the velocity or acceleration measured by the sensors need to be treated, to eliminate measurement noise, and then converted into vertical displacement (or deflection).

The approach for the measurement of deflections includes the following steps:

- Selection of appropriate geophones and accelerometers for the measurement of pavement deflections
- Performance of laboratory test: these tests consisted in submitting the sensors to simulated pavement deflection signals, using a vibrating table and applying different amplitudes and velocities. The responses of the sensors were then compared with displacements measured with a reference laser displacement sensor.
- Development of a signal treatment procedure, to correct the geophone and accelerometer measurements, and obtain accurate displacement measurements.

## 2.2 Selecting the sensors to measure pavement deflections

Selecting the appropriate sensors is an important step for measuring the vertical displacement. The geophones and accelerometers need to be able to resist to the environmental and loading conditions to which they will be submitted in the pavement structure. They also need to have an appropriate measurement range, to measure pavement deflections. There are several criteria to consider in order to select the appropriate geophones and accelerometers for the application of deflection measurements:

- The typical surface deflections are between 0.1 mm and 1mm hence sensors should have an appropriate range and sensitivity to measure these values.
- The resonance frequency of the sensors (for geophones) should be low when compared to the frequency of the deflection signals (typically between 2 and 20 Hz).
- Size of the sensors is also important, as the sensors should be small, in comparison with layer thickness, and easy to embed in the pavement layers.
- Durability and good mechanical properties are also other important factors that allow the sensors to measure the pavement response for sufficiently long periods (typically several years).
- Installation of these sensors is done to further increase the durability by coating them with resin.
- Relatively limited cost, to enable a widespread use of this type of instrumentation.

These criteria have led to select two types of geophones and two accelerometers described in Figure 2-1.



**Geophone  
(Geospace)**

- GS-11D
- Sensitivity : 89.2 V/m/s
- Natural frequency: 4.5Hz
- Tolerance: ±10%



**Geophone ION**

- LF-24
- Sensitivity 15.2 V/m/s
- Natural frequency: 1 Hz
- Tolerance:±10%



**Accelerometer  
silicon design**

- Model 22106-002
- Sensitivity : 2000mV/g
- Input Range ± 2 g
- Max Frequency : 300 Hz
- Non- linearity : ±0.4%



**Accelerometer-  
Memsic**

- Model (MEMSIC) CXL04GP1
- Sensitivity: 500mV/g
- Input range: ±4g
- Max Frequency: 100 Hz
- Non- linearity : ±0.2%

Figure 2-1. Sensors used for instrumentation

**2.3 Experimental Protocol**

**2.3.1.Objectives of the laboratory tests**

The sensors come out with a predefined set of characteristics given by the manufacturers. However, the actual performance of the sensors might differ from the theoretical characteristics, therefore carrying out laboratory tests before deploying them in the field pavement appeared necessary to verify the sensor performance. The tests were performed using a vibrating table. This vibrating table uses a closed-loop servo hydraulic actuator, which applies the displacement to a horizontal platform, on which the transducers were installed. The displacements applied by the vibrating table were measured with a non-contact laser displacement sensor (Keyence, model LC2100, range ± 8 mm) which was used as a reference sensor. The aim of these tests was to find and verify the properties of the sensors, mostly to control sensor response before instrumenting them on an actual test site. For the pavement instrumentation application, the sensitivity of these sensors is of utmost important, to see if this sensitivity level is sufficient to measure the response with a sufficient accuracy. In addition, the noise of these sensors and the signal to noise ratio also need to be determined.

Several types of tests were successively performed to determine different characteristics of the geophones:

- The intrinsic parameters (noise level, sensitivity) that affect the response of the sensors
- The sensitivities and frequency response of the geophones
- The responses for different amplitudes and velocities, using simulated vehicle deflection signals
- The results of the noise and the sensitivity tests are presented in the annex A.

### 2.3.2. Modelling of pavement deflections with the Alize software

In France there are number of technical standards and documents that are followed for the structural design of pavements. To define reference deflection signals for the laboratory tests, aimed at evaluating the response of the geophones, pavement calculations have been performed with the pavement design software *Alize*. This software is used to model pavement structures, and is based on a multi-layer, linear elastic, semi-infinite model. The interfaces between these layers can be bonded or un-bonded depending on the pavement materials used. It allows calculating the mechanical response of the pavement when subjected to static pressure loads in terms of strains, stresses and deflections. (see chapter 1 for the description of *Alize*). For our work, it was decided to perform calculations for a typical pavements structure, submitted to the loading of a 5 axes truck, with a total weight of 44 tons. The pavement structure considered is a classical flexible pavement for medium traffic (150 trucks /day) with a bituminous wearing course and granular base. This structure is similar to the one that was tested on the IFSTTAR accelerated pavement testing facility, as part of this work (see chapter 3). Its characteristics are defined in Table 2.1. The deflection calculated with *ALIZE* for the flexible pavement, under the loading of a T2S3 (5-axes) truck, with a total load of 40 tons as shown in Figure 2-2, and moving at a speed of 70 Km/h, is presented in Figure 2-3. Each peak of the signal represents the displacement produced by each wheel load as shown in the Figure 2-3.

Table 2.1 Pavement model used for simulation of deflections

| Materials                 | Elastic Modulus(MPa) | Thickness (cm) |
|---------------------------|----------------------|----------------|
| Bituminous mixture        | 7000                 | 11             |
| Unbound granular material | 200                  | 30             |
| Subgrade                  | 80                   | 250            |

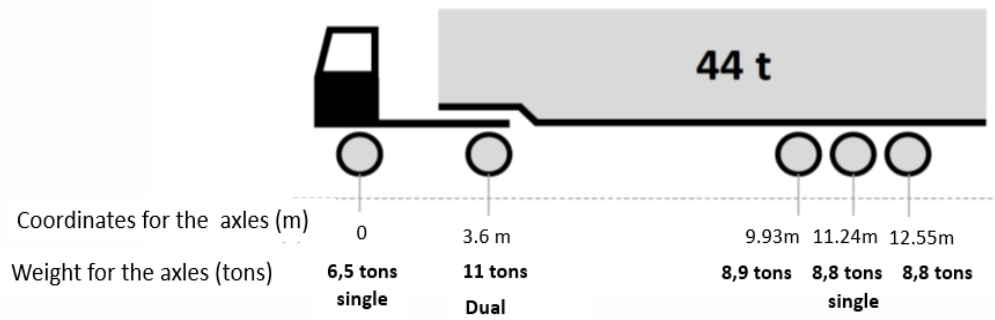


Figure 2-2. Standard 5 axle truck loading

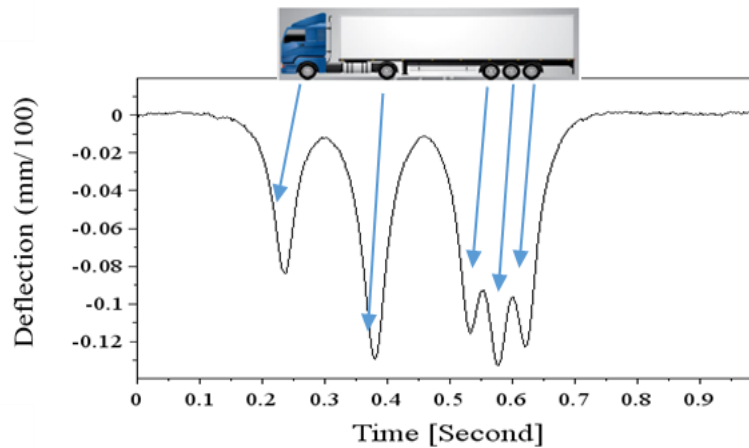


Figure 2-3. Reference deflection signal calculated with ALIZE, for a 5-axle truck

### 2.3.3. Test Program

Different tests were conducted to provide the sensor responses at different test settings. These tests were defined to evaluate the sensor performance and indicate the proficiency of the sensors to measure the vertical displacement. As indicated above, several factors are needed to define their performance. One factor is the sensitivity level that defines the resolution which can be achieved, for the measurement of the displacement. Furthermore these sensors were subjected first to a sinusoidal pulse signal simulating the vertical displacement at different amplitudes and speeds. Then, other tests were performed using a more realistic truck signal calculated with the Alize pavement design software, as input for the vibrating table, at different speeds and amplitudes. The tests carried on the vibrating table are presented in Table 2.2 below:

Table 2.2. Test settings

| S.no | Tests                    | Details  |
|------|--------------------------|--|
| 1    | Sinusoidal pulse signals | Amplitude: 0.1mm and 1mm<br>Speed: 35Km/h and 70km/h |
| 2    | Truck signals            | Amplitude: 0.1mm and 1mm<br>Speed: 35Km/h and 70km/h |

The tests carried out on the vibrating table at IFSTTAR are shown in Figure 2-4. The table reproduces the vertical displacements corresponding to the sinusoidal pulses and to the deflections calculated with the Alize software. The response of the sensors is recorded and compared with the theoretical signal. Four sensors can be tested at a time on the vibrating table, as the data acquisition system of the device has four channels. Out of four, one channel is reserved for a Keyence laser displacement sensor that is used as a reference sensor, to measure the displacements from the vibrating table; the response of the geophones and accelerometers is compared with this reference. The experimental setup is shown in Figure 2-4.



Figure 2-4. Vibrating table with various sensors attached to test

#### 2.3.4. Determination of transfer functions

In a second step, tests were performed to determine the transfer functions of the different sensors. For this purpose, the sensors were subjected to sinusoidal signals of different amplitudes (0.1 and 1mm). The coherence between the channels allows to determine the frequency range of the sensors and the geophone coherence function represent the frequency range of 1-100 Hz. The range of accelerometers is around 1-50 Hz. The transfer functions obtained for the geophones are shown in Figure 2-5. More detailed results are presented in annex A.

The results represent the ratio between the signal delivered by the geophone and the velocity applied in the tests, for different frequencies. The results show that the response of the geophones is considerably attenuated at low frequencies (below 10 Hz). The response is constant only at frequencies higher than about 10 Hz for geophone ION and 20 Hz for geophone GS11D. The flat part of the transfer function curves corresponds to the sensitivity of the sensors. For geophone Geospace GS11D, the sensitivity obtained is 89 V/m/s for the geophone with 18Kohm resistance it was found to be 83V/m/s and for geophone, ION the value is 15.25 V/m/s.

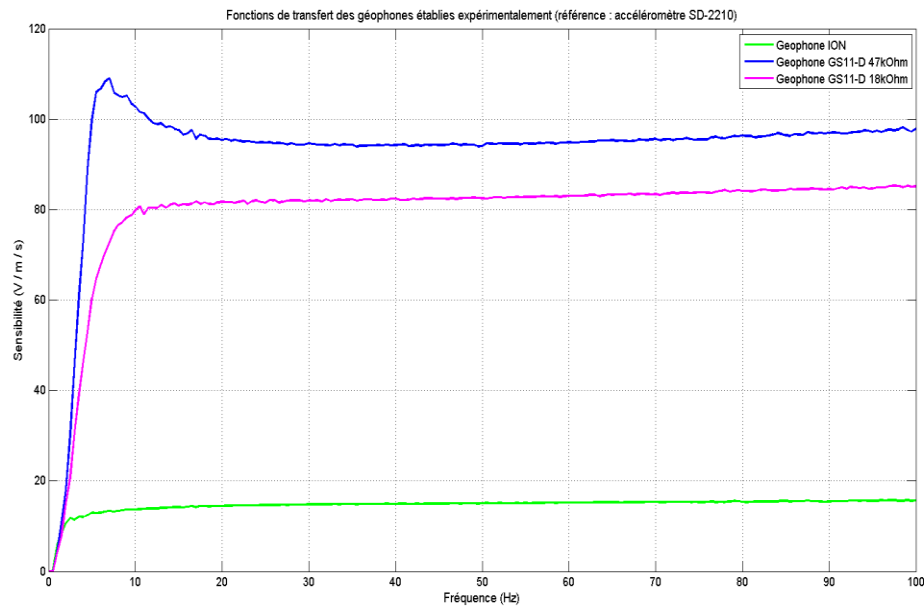


Figure 2-5. Transfer functions of the geophones

## 2.4 Sensor Responses: untreated sensor signals

This section presents the untreated sensor signals obtained in the tests simulating the deflection produced by a 5 axes truck in the pavement. In these tests, the signal applied was a deflection signal calculated with ALIZE, and reproduced by the vibrating table with a pulse amplitude of 0.1mm and a frequency corresponding to a speed of 70 Km/h. The results (presented in Figure 2-6, Figure 2-7, Figure 2-8 and Figure 2-9) show the displacements, velocities and accelerations obtained with the displacement sensor, the geophones and accelerometers respectively. These results will need to be treated and converted in order to get the vertical displacements.

### *Reference signal from the Keyence laser displacement sensor*

The deflection signal obtained from the Keyence laser sensor is considered as the reference for comparing the other sensor signals. This sensor measures directly the vertical displacements

produced by the vibrating table, and the recorded displacements reproduce closely the signal calculated with ALIZE (see Figure 2-6), with an amplitude of 0.1 mm.

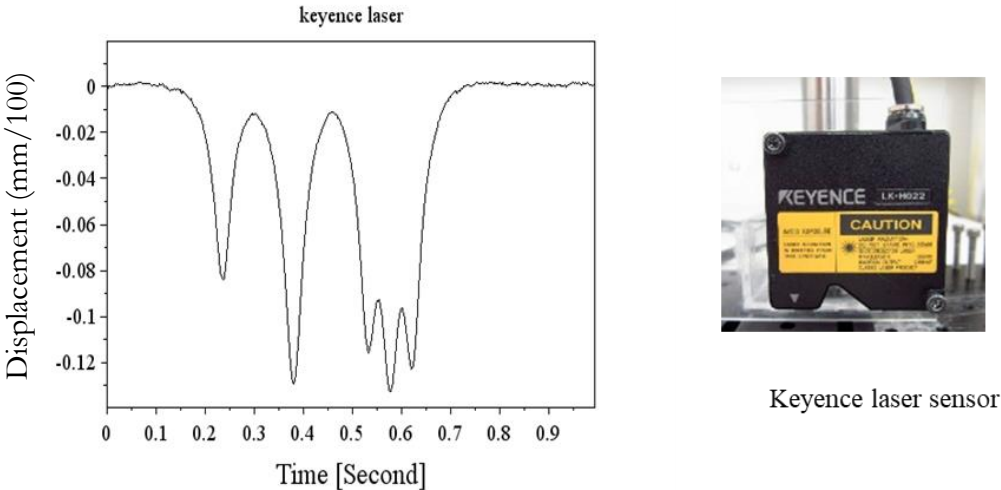


Figure 2-6. Displacements measured with the Keyence laser sensor

**2.4.1. Results from the geophones**

The geophone results correspond to the raw vertical velocity data, without any processing. Figure 2-7 shows the untreated vertical velocity signal from Geophone Ion whereas Figure 2-8 shows the results of the signals obtained with Geophone GS11D, with two different resistance values (47 kohms and 18 kohms). These results show that the velocity values need to be processed, to reduce the measurement noise, and integrated, to get the displacement values, comparing with the reference signal coming from the laser.

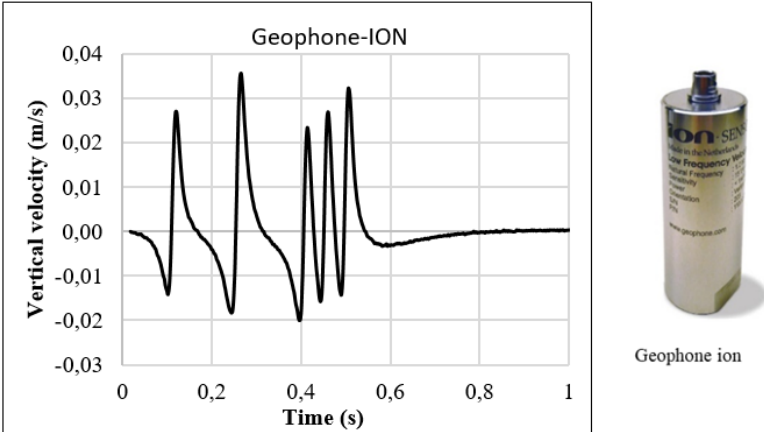


Figure 2-7. Velocity measured with geophone Ion

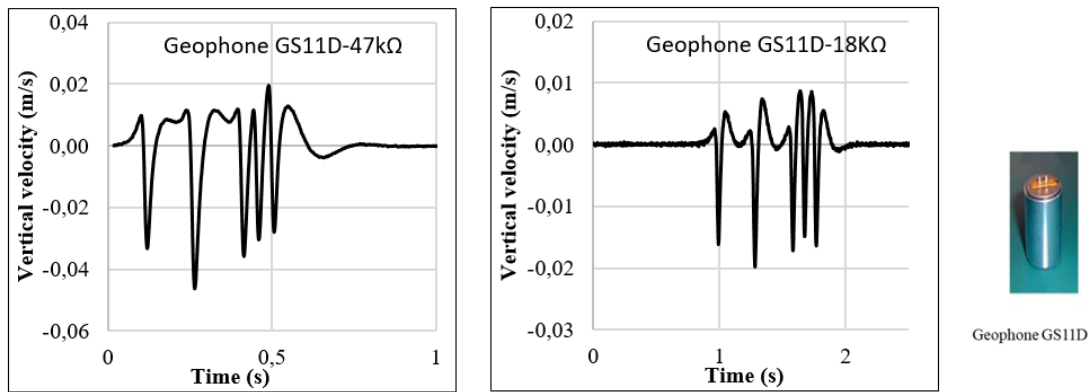


Figure 2-8. Velocities measured with geophone GS11D with different resistances

### 2.4.2. Results from accelerometers

The results in Figure 2-9 present the vertical accelerations measured by the accelerometers (Silicon design 2210 and CXL04GP1). They are obtained for the same test setting as the measurements made with the geophones and the Keyence laser sensor, but show a lot of noise, due to the small acceleration levels, hence making it extremely important to process the results to reduce the noise and obtain realistic displacement values.

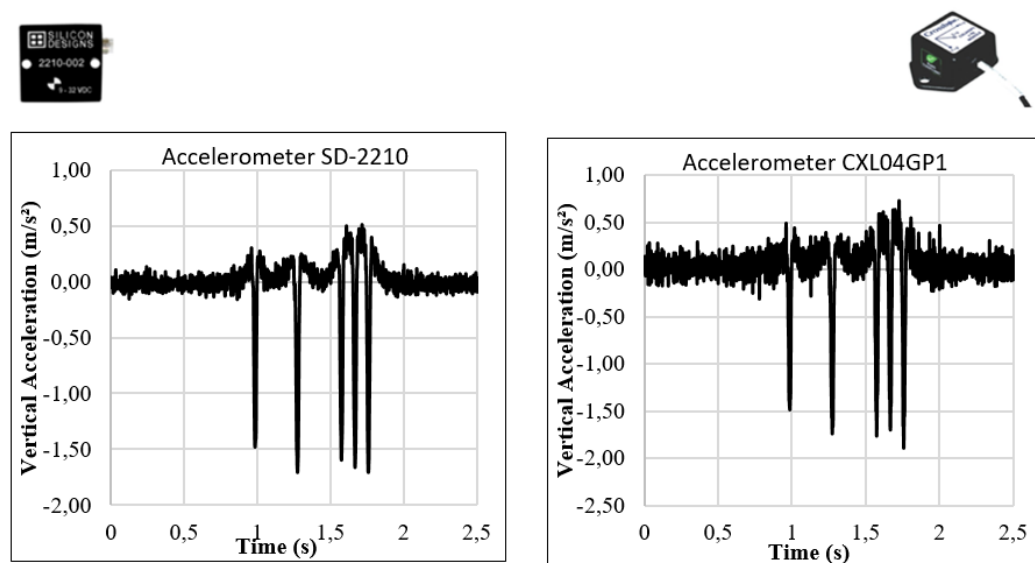


Figure 2-9. Accelerations measured by the two models of accelerometers

## 2.5 Processing and improving the geophone Signal measurements

The measurements of the geophones and accelerometers require some treatment in order to convert them into appropriate values of vertical displacements or deflections. The measurements need in particular to be integrated from velocity and accelerations into vertical displacements (deflections). For analyses purpose, Figure 2-10 represents a raw geophone signal (measured

displacement velocity), and the signal obtained after a simple integration. The same trend is observed for the values of acceleration after a double integration. It can be seen that after a simple integration process, the displacement signal obtained does not correspond exactly to the reference signal applied to the vibrating table (signal calculated with Alize). As can be seen in Figure 2-10, the amplitude of each peak of the signal is different from the reference signal. The shape is also different, with the presences of positive upward displacements in the signal. These upward lifts in the signal are not realistic as only a downward displacement is applied to the sensors. It is noted that these differences between the reference signal and sensor signals are due to two main reasons:

- The direct integration process tends to attenuate the low frequency components of the signal (Arraigada et al., 2009). The integration process also introduces a constant, and thus adds a continuous component to the signal. This may explain the unrealistic shape of the signal, with positive displacement values.
- In addition, as can be seen, the raw geophone and acceleration signals present some noise, which can also lead to inaccurate results. Each type of sensor has its advantage and its drawback: a geophone is not very sensitive to electronic measurement noise but has drift problems (inductive system); an accelerometer does not drift but is sensitive to noise (capacitive system). The electrical noise generates high frequency variations in the signals, which do not correspond to the actual vertical displacement applied in the tests. The signal comprises a wide range of frequencies, and we are only interested in a particular range of frequencies, corresponding to the vertical displacement in the pavement (N. Bahrani et al., 2019).

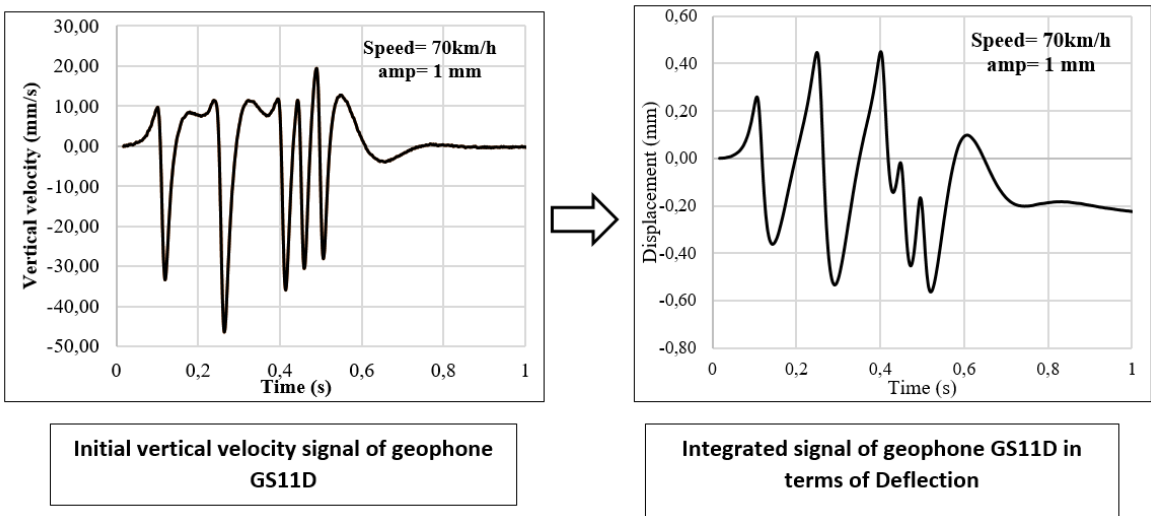


Figure 2-10. Example of raw and integrated signal of geophone GS11D, for a 5 axle truck loading.

## 2.6 Method for filtering and converting the vertical velocity signals into vertical displacements

Because the single integration of the geophone or accelerometer signals did not give sufficiently realistic deflection shape, different signal-processing methods have been tested to improve the displacement signals, and a methodology to correct the measurements has been developed. This procedure has been applied to the measurements of the two types of geophones used (Geospace GS11D and Ion LF-24). In the following figures explaining the treatment procedure, only the responses obtained with the geophone GS11D are shown for illustration. This methodology is described in the following steps.

### 2.6.1.Step1: Filtering the signals

The first step consists in suppressing the lower frequency components of the signal using a high pass filter. The advantages of using filters are that the noise suppression is very efficient and the computation is fast (Raita-aho, T, Saramaki, 1994). In this work a high pass IIR filter gave the best results, as it allows certain frequencies to pass and suppresses the lower frequencies containing noise and unwanted frequency content. It also eliminates the DC component due to the integration constant. For this purpose we have used a 4.5 Hz high pass filter. It was observed that the cut-off frequency of the filter has a huge impact on the filtering process, as this values changes the shape of the signal and needs to be adapted to the vehicle speed. For lowest speeds, a cut-off frequency of 4.5 Hz was selected, and this frequency was increased as the speed increased. For the maximum simulated speed (20m/s), a cut-off frequency of 18Hz was used. Figure 2-11 represents an example the filtered signal.

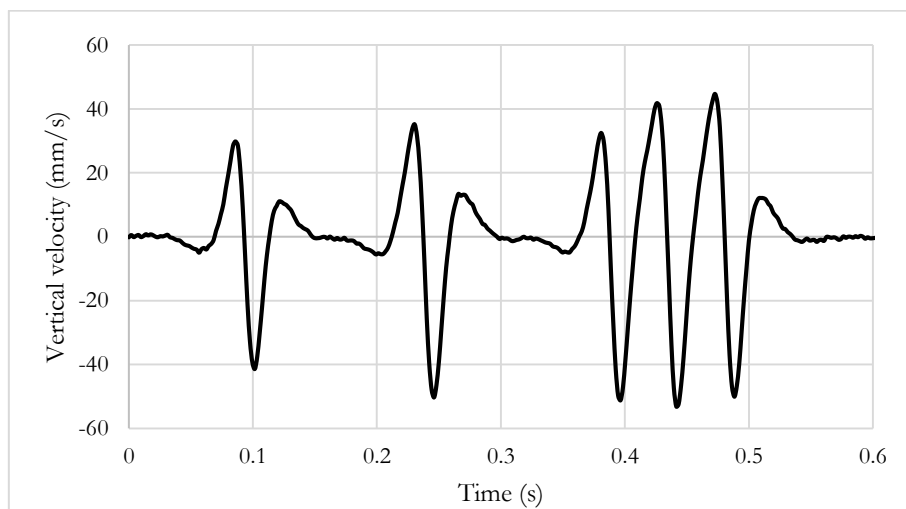


Figure 2-11. Filtering of the geophone GS11D signal, with a high pass filter at the speed of 70km/h and 1mm amplitude

### 2.6.2. Step 2: Amplification of the signal with respect to the reference signal amplitude

It was observed that when the cut off frequencies are kept lower than the values indicated above, the noise is not sufficiently reduced; hence, the shape of the signal was deteriorated. With high cut off frequencies, filtering improved the overall shape of the signal but reduced the amplitude of the signal. When the final filtered signal was compared to the reference signal, the amplitude was much lower. For this reason, after filtering, the signal had to be amplified (by a linear constant amplification factor), to keep the initial maximum amplitude as shown on Figure 2-12.

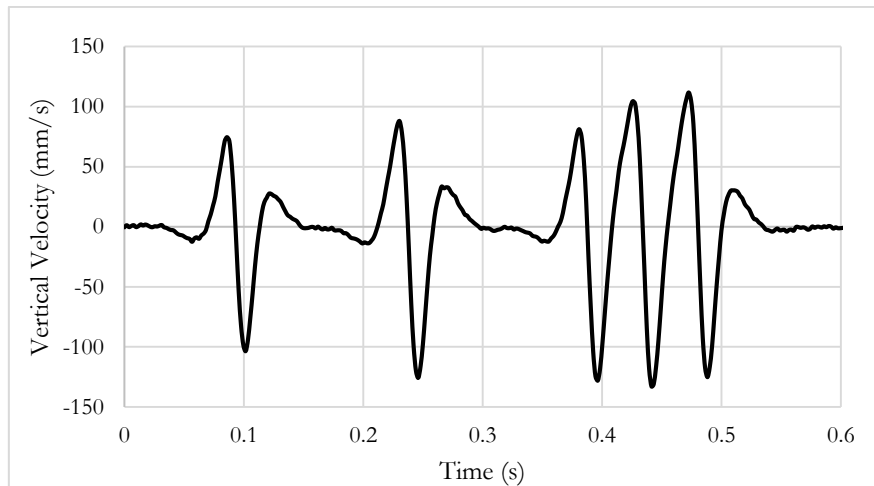


Figure 2-12. Amplification of the geophone GS11D signal after filtering at the speed of 70km/h and 1mm amplitude

### 2.6.3. Step 3: Integration and detrending to remove the continuous part of the signal

After filtering, the vertical velocity is integrated to be converted into vertical displacement. Simply integrating the velocity would increase small frequencies in the signal as well. Hence pre-processing is necessary before integration of the signals.

As mentioned above, the integration step adds a continuous component to the signal as described by equations (2.1) hence, a detrending function is applied to subtract the mean or best fit line (in the least square sense) from the data and suppress this continuous component. The signal after integration and detrending is shown on Figure 2-13.

$$D(t) = \sum_{i=1}^n V(t_i) \times \Delta t \quad (2.1)$$

Where  $V(t_i)$  is the velocity at time  $t_i$  and the  $D(t_i)$  is the displacement measured and  $\Delta t$  is the time interval between the two consecutive points of the signal.

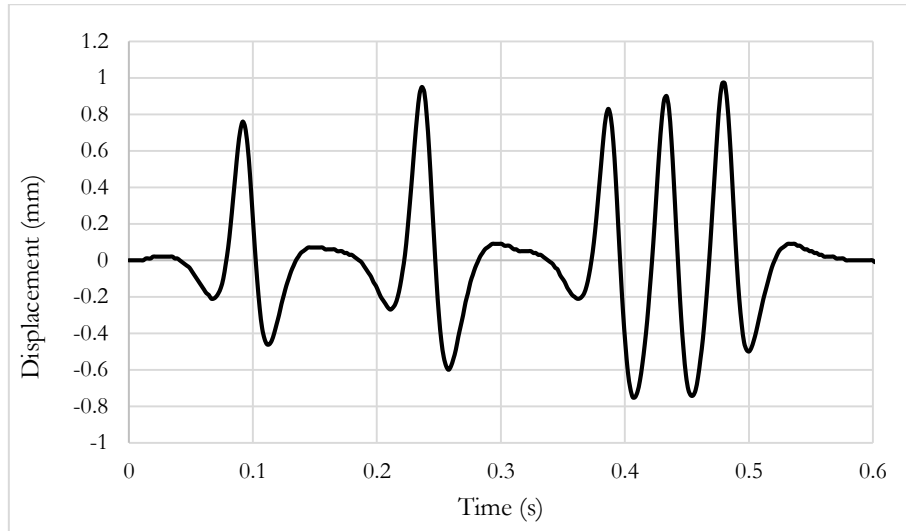


Figure 2-13. Integration of the geophone GS11D signal at the speed of 70km/h and 1mm amplitude

#### 2.6.4. Step 4: Application of the Hilbert transform

The final step consist in applying a Hilbert transform to remove the oscillations in the signal and further enhance the shape of the signal. As explained in the section 2.5 and Figure 2-10 the integration alone produce positive oscillation that have no physical meaning. Therefore, in addition to the filtering and amplification of frequencies, which should make it possible to find maximum deflection values closer to reality, we neutralize the positive oscillations of the signal by "inverting" them in the frequency domain. The Hilbert transform consists in shifting the phase of a signal by  $90^\circ$  (= its imaginary part) and thus the Hilbert transform of a sine signal would be a cosine signal with the same magnitude. By combining the initial signal with the Hilbert transform of the signal, we obtain a new signal (called the analytical signal) whose amplitude corresponds to the complex envelope of the initial signal and we obtain only variations in the same half-plane i.e. negative values.

In the time domain, the resulting signal is the convolution of the signal and the Hilbert transform of the signal, as expressed in equation (2.2), where  $\hat{x}(t)$  is the Hilbert transform  $H$  of the signal  $x(t)$

$$\begin{aligned}\hat{x}(t) = H\{x(t)\} &= \int_{-\infty}^{+\infty} \frac{1}{\pi} \times \frac{x(\tau)}{(t - \tau)} d\tau \\ &= (h * x)(t)\end{aligned}\quad (2.2)$$

Where  $h(t) = \frac{1}{\pi t}$

In the frequency domain, it is obtained with the Fourier transform and corresponds to the multiplication of the complex signal by  $-j\text{sgn}(\omega)$ , where the signum function ( $\text{sgn}$ ) is defined by equation 2.3 (Blackledge, 2006). Hence, in the frequency domain, Hilbert transform is actually a phase shift of the real signal.

$$\text{FT}\{\hat{x}(t)\} = X(\omega) [-j \times \text{sgn}(\omega)] \quad (2.3)$$

$$\text{Sgn}(\omega) = \begin{cases} -1 & \text{for } \omega < 0 \\ 0 & \text{for } \omega = 0 \\ 1 & \text{for } \omega > 0 \end{cases}$$

The principle of the Hilbert transform is to combine a signal that is the real part  $s(t)$  (analytical signal) of the signal and  $\hat{s}(t)$  an imaginary part of the signal used to extract the envelope of the signal. Hence the corrected signal is given by:

$$S_a(t) = s(t) + j\hat{s}(t) \quad (2.4)$$

The corrected signal  $a(t)$  at the end of the process corresponds to the envelope of the signal  $S_a(t)$ .

$$a(t) = \sqrt{\{\text{Real part}(S_a(t)^2)\} + \{\text{imaginary part}(S_a(t))^2\}} \quad (2.5)$$

$$= \sqrt{S^2(t) + \hat{S}^2(t)} = |S_a(t)| \quad (2.6)$$

In this case, this transform drastically improves the shape of the signal, and leads to a response close to the theoretical deflection under a five-axle vehicle, as evident in Figure 2-14.

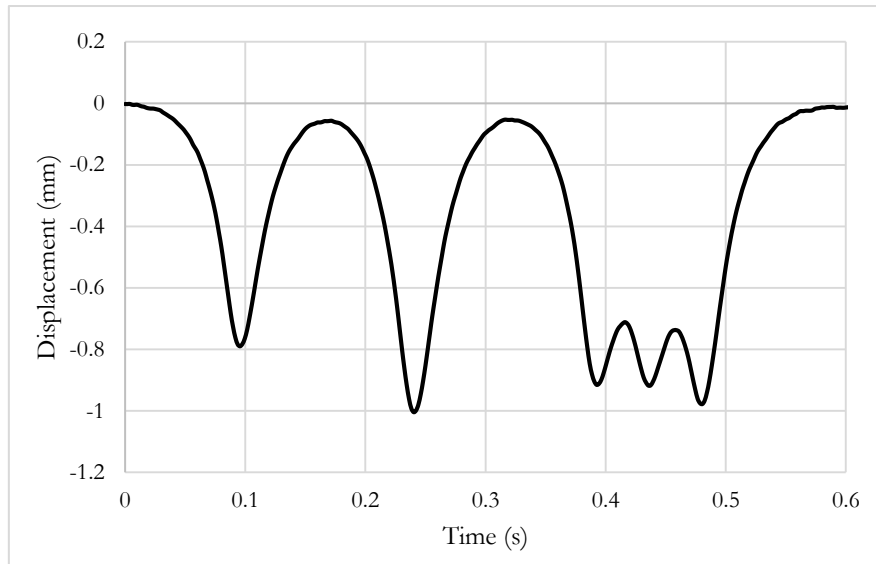


Figure 2-14. Final signal of geophone GS11D after application of the Hilbert transform at the speed of 70km/h and 1mm amplitude

## 2.7 Method for filtering and converting the vertical acceleration signals into vertical displacements

As explained in the section 2.6 simple single integration and double integration in the signal do not replicate the realistic signal hence the same methodology is used for converting the vertical acceleration effectively into vertical displacements. In this section, the same procedure applied in section 2.6 is applied to the acceleration from two types of accelerometers (MEMSIC and CXL04GP1). The difference in the procedures is that double integration is used in this process and the amplification is changed accordingly.

### 2.7.1.Step1: Filtering the signals

Similar to the section 2.6.1 first step was to suppress the lower frequency component. As the accelerometers are more sensitive to noise, it was observed that this noise suppression could be achieved using a high pass filter. The filtering also eliminate the DC component due to double integration. The suitable cut-off frequency was impacted by the speed, in the same way as for the vertical velocity. Hence for lowest speed the cut-off was set to 4.5 Hz and for higher speed the cut-off was set to 18 Hz. An example of signal after the filtering process is shown in Figure 2-15.

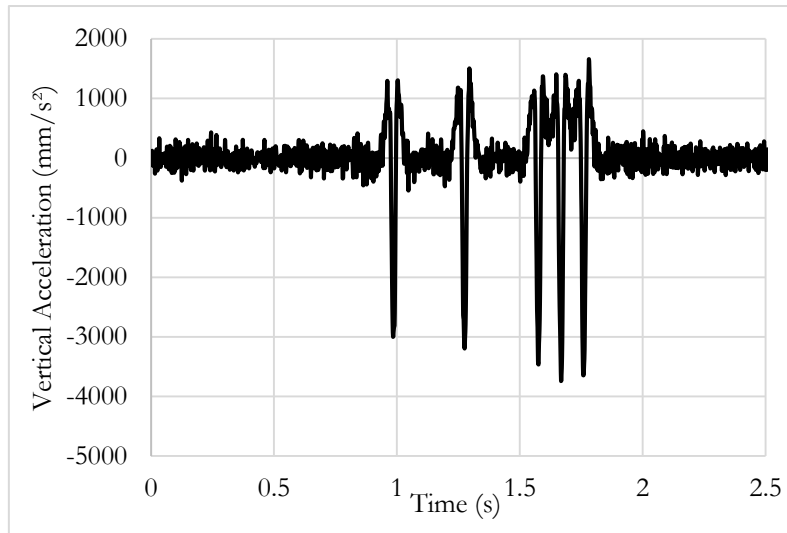


Figure 2-15. Filtering of the Accelerometer CX signal, with a high pass filter at the speed of 70km/h and amplitude of 1mm

**2.7.2.Step 2: Amplification of the signal with respect to the reference signal amplitude**

Similar to the vertical velocity signals (see section 2.6.2), after the filtering the vertical acceleration signals are amplified, by the linear constant amplification factor, to keep the initial amplitude of the signal. The amplification factor that was different for each sensor. The signal after amplification is given in Figure 2-16.

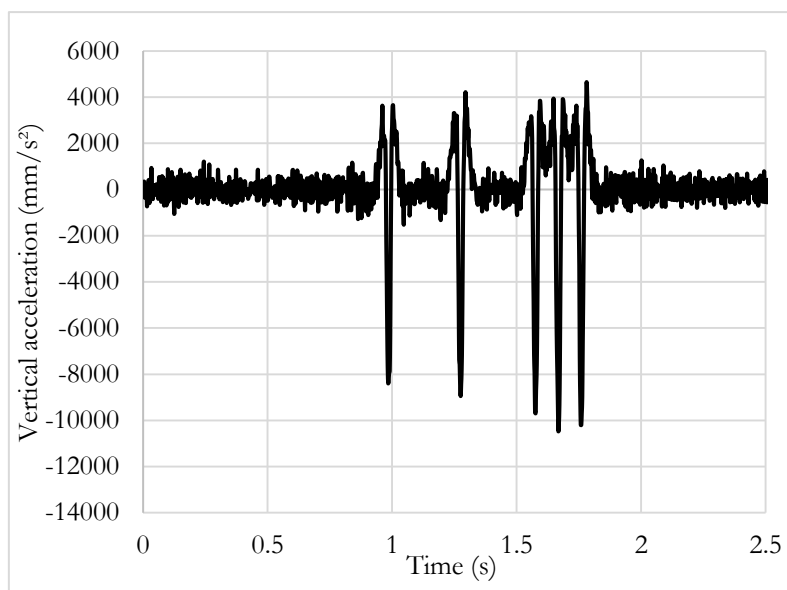


Figure 2-16. Amplification of the Accelerometer CX signal after filtering at the speed of 70km/h and amplitude of 1mm

### 2.7.3. Step 3: Integration and detrending to remove the continuous part of the signal

After the amplification the signal is integrated converting the acceleration into velocity signal using the equation (2.7). It is then integrated a second time, to convert the vertical velocity signal into the a displacement signal, using the equation 2.1. The signal after the first integration is shown in Figure 2.17. As explained in the section 2.6.3, the integration step introduces a continuous component and due to the double integration the effect is heightened. The detrending function is used after the double integration, to remove this component and the vertical displacement is represented in Figure 2-18.

$$V(t) = \sum_{i=1}^n f(A(t_i) \times \Delta t) \quad (2.7)$$

Where V is the velocity, A is the acceleration and  $\Delta t$  is the time interval between the two consecutive points of the signal

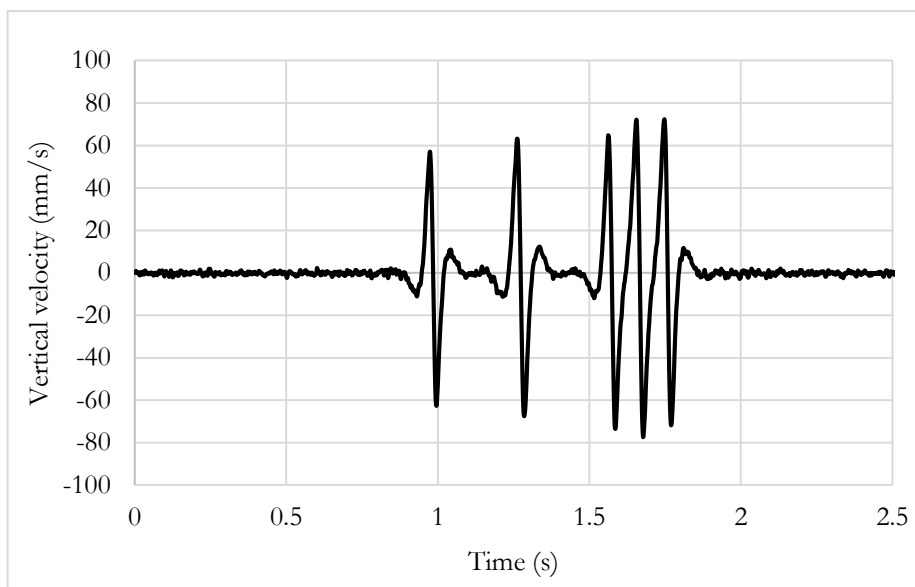


Figure 2-17. First integration of the Accelerometer CX signal at the speed of 70km/h and amplitude of 1mm

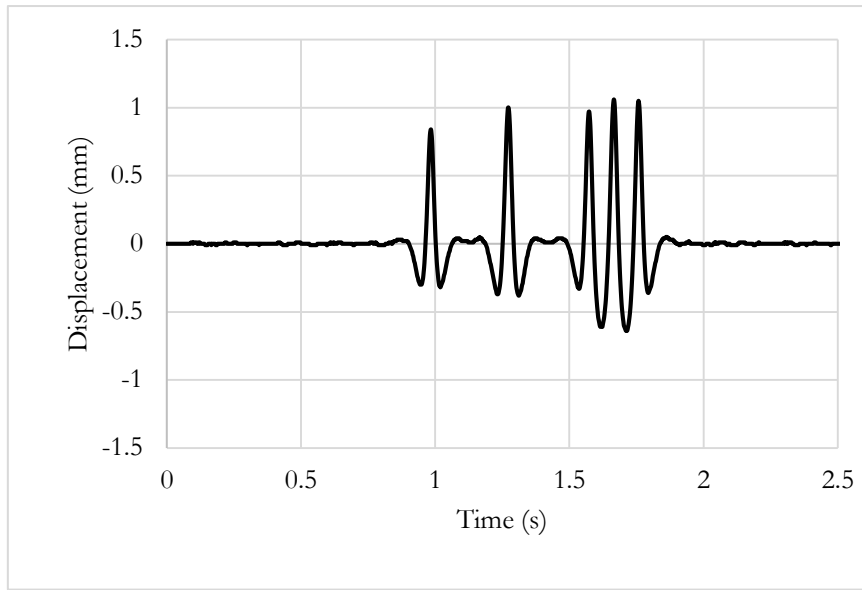


Figure 2-18. Double Integration of the Accelerometer CX signal at the speed of 70km/h and amplitude of 1mm

#### 2.7.4. Step 4: Application of the Hilbert transform

Finally the last step is the same as for the geophones and consist in applying the Hilbert transform as explained in section 2.6.4. This eliminates the positive upward lifts and corrects the signal shape, as shown in the Figure 2-19.

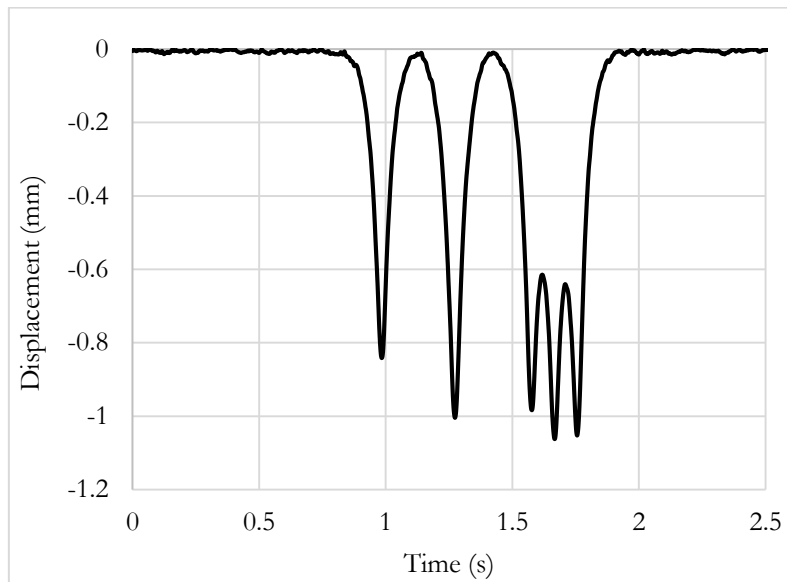


Figure 2-19. Final signal of Accelerometer CX after application of the Hilbert transform at the speed of 70km/h and amplitude of 1mm

## 2.8 Comparison of the treated geophone and accelerometer measurements with the reference laser sensor

Finally, the proposed correction procedure was applied to the geophone and accelerometer signals obtained at different speeds and amplitudes, and the results have been compared with the reference displacement values obtained with the Keyence Laser sensor. Globally, the procedure improves the geophone measurements very significantly and leads to realistic signal shapes and displacement amplitudes, for all the applied tests conditions, as shown in the example of Figure 2-20.

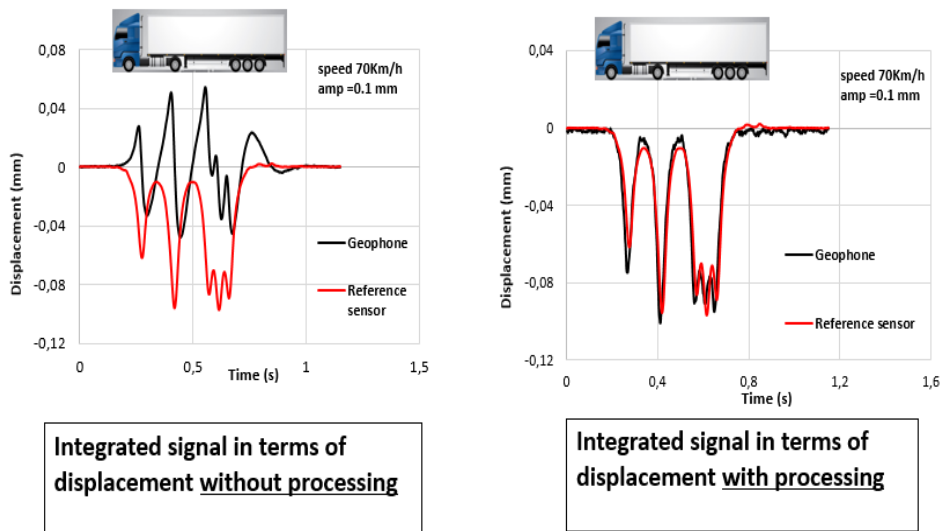


Figure 2-20. Example of comparison between the geophone signals obtained with and without the improved processing method

Figure 2-21 show the comparison of the signal of the accelerometer CX at the speed of 70km/h and the amplitude of 1mm with the processing techniques. It is very evident that the direct integration of the signal without any filtering is not comprehensible, this is due to the DC component introduced because of the double integration. After the proposed treatment, the signal is very realistic and close to signal obtained with the reference. This confirms the efficiency of the applied treatment procedure.

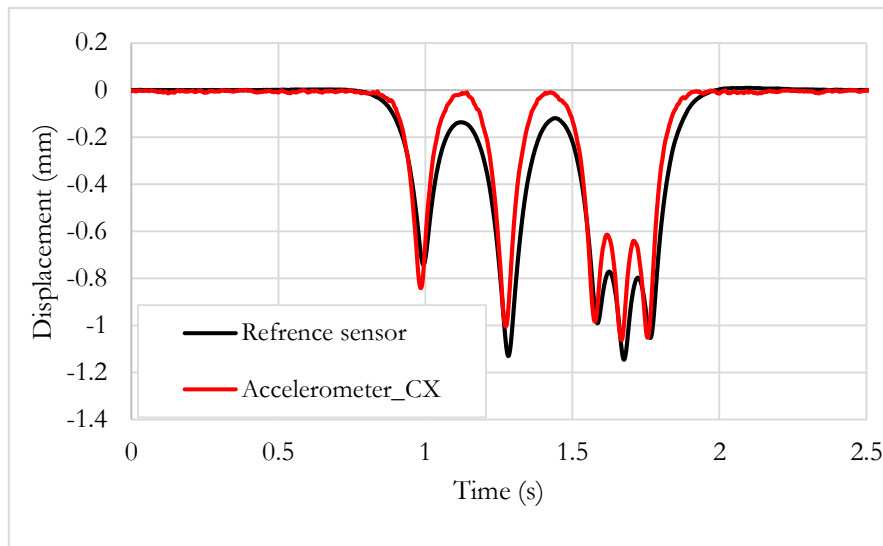


Figure 2-21. Example of comparison between the Accelerometer CX signals obtained with the improved processing method at 70 km/h

## 2.9 Results obtained with the treated sensor signals

This section presents examples of treated displacement measurements obtained with the geophones and accelerometers for different speeds and amplitudes. This processing was applied to the responses obtained from the different tests as described in Table 2.1. The treated signals are compared with the response of the Keyence laser displacement sensor. It is important to note that the treatment procedure is the same for all the amplitudes and speeds for both the geophones and accelerometers. The only parameter, which is different, is the cut-off frequency of the high pass filter. It has been noted that as the speed increases, it is necessary to increase the cut off frequency of the filter. For the speed of 35km/h, the suitable cut off frequency is 4.5 Hz, and for 70 km/h it needs to be increased to 18 Hz. With these cut off frequencies, the optimal shape of signal is achieved, which is very close to the reference signal.

### 2.9.1.Pulse signals

The following results present the processed pulse signals corresponding to a single axle load, with speeds of 35 km/h and 70 km/h and with amplitudes of the vertical displacement of 0.1 and 1 mm. After applying the improved processing procedure, realistic displacements amplitudes were obtained for all the test conditions when compared with the reference sensor signals. Figure 2-22, Figure 2-23, Figure 2-24 and Figure 2-25 represents the pulse displacement signals obtained for geophones at the speeds of 35 km/h and 70 km/h and with the two amplitudes. For the geophones, slightly better results were obtained with the geophone GS11D. Figure 2-26, Figure 2-27, Figure 2-28 and Figure 2-29 represents the pulse displacement signals obtained for accelerometers at the

same speeds and amplitudes. For the accelerometers, more noise is observed compared to geophones and the signals obtained with the accelerometer CX-Memsic present less noise and give slightly better results than the accelerometer SD, especially at the lowest amplitude of 0.1 mm. It can be noted that for all the sensors, the signals of low amplitude are more affected by noise. An error indicator, R, was calculated, for each test, to determine the overall difference between the measured signal of each sensors and the reference signal of the laser displacement sensor. The error indicator is defined by equation 2.8, where N is the total number of points of the signal Table 2.3 shows the differences in percentage. It is evident from the table that at lower speed and amplitude the overall difference is higher, with accelerometer SD having the maximum difference of 10% and geophone ion having a difference of 6%. Whereas at higher speed and higher amplitude the differences are lower.

$$R = \frac{1}{N} \sum_{i=1}^N \frac{|Reference\ value_i - Calculated\ value_i|}{Max(Reference\ value)} \times 100 \quad (2.8)$$

Where: N is the total number of points of the signal

Table 2.3. Percentage difference between the reference signal and the measured signal, for the different sensors (geophones and accelerometers)

| Sensor                  | Speed 35km/h                                    |   | Speed 70km/h                                    |   |
|-------------------------|---|---|---|---|
|                         | Percentage difference (%)<br>Amplitude<br>0.1mm | Percentage difference (%)<br>Amplitude<br>1mm | Percentage difference (%)<br>Amplitude<br>0.1mm | Percentage difference (%)<br>Amplitude<br>1mm |
| <b>Geophone GS11D</b>   | 10  | 6.8   | 5.5   | 3.5   |
| <b>Geophone Ion</b>     | 6   | 4.5   | 5.7   | 3   |
| <b>Accelerometer CX</b> | 6.8   | 5.6   | 2.8   | 1.7   |
| <b>Accelerometer SD</b> | 10.2  | 7.0   | 9.9   | 3.5   |

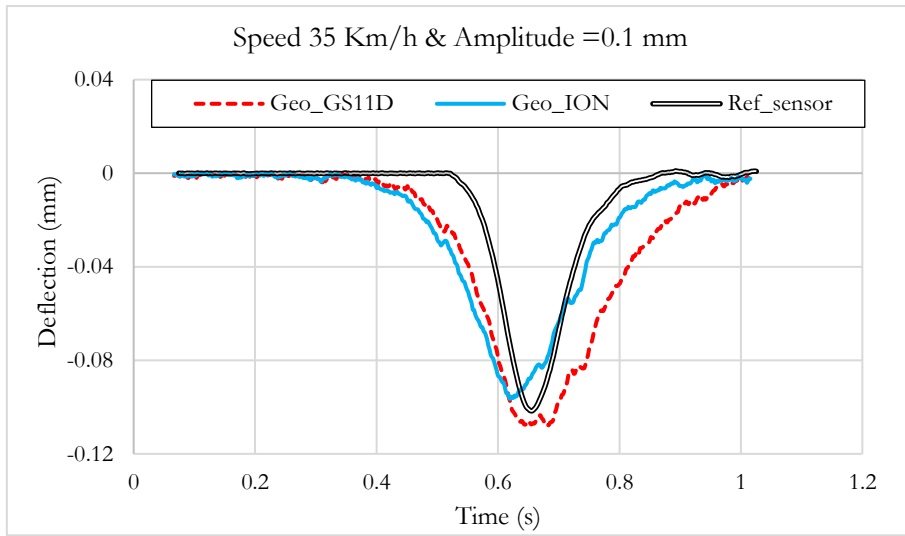


Figure 2-22. Displacement signals obtained for the geophones at the speed of 35km/h with amplitude of 0.1mm

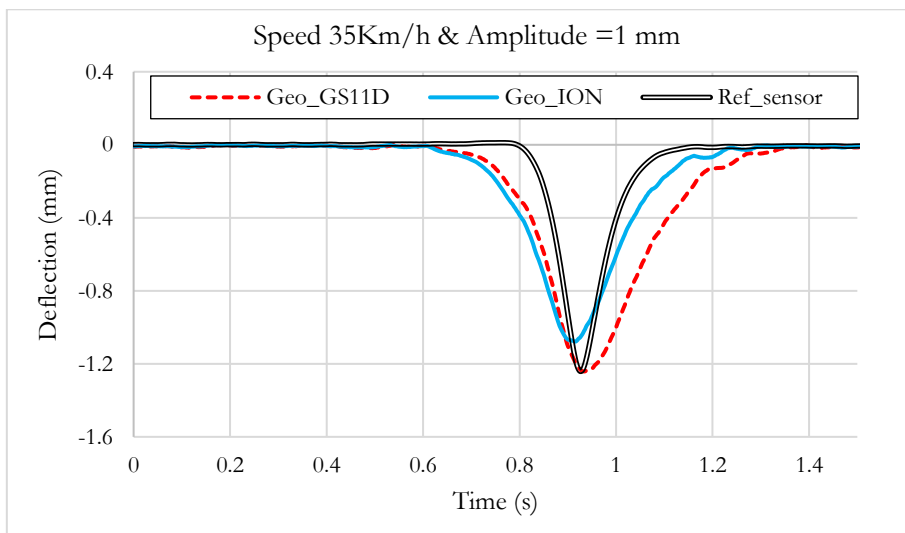


Figure 2-23. Displacement signals obtained for the geophones at the speed of 35km/h with amplitude of 1mm

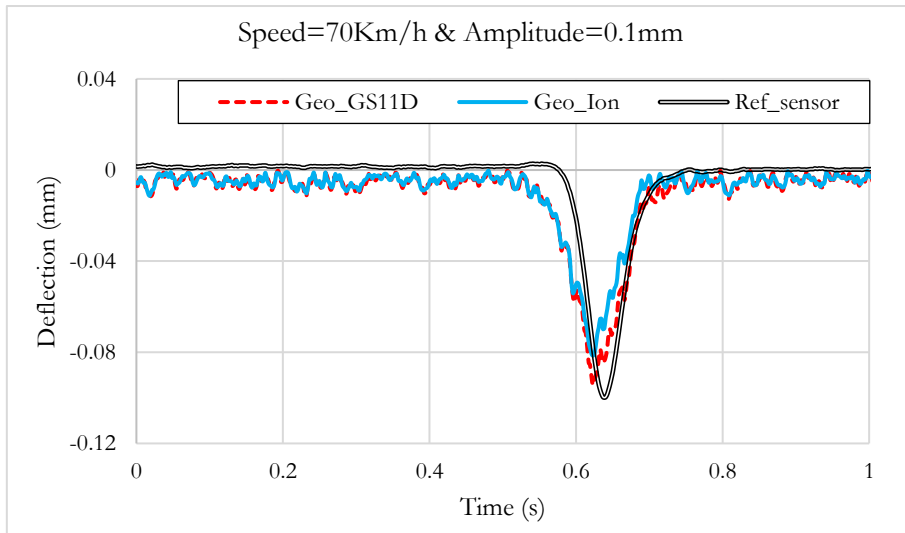


Figure 2-24. Displacement signals obtained for the geophones at the speed of 70 km/h with amplitude of 0.1mm

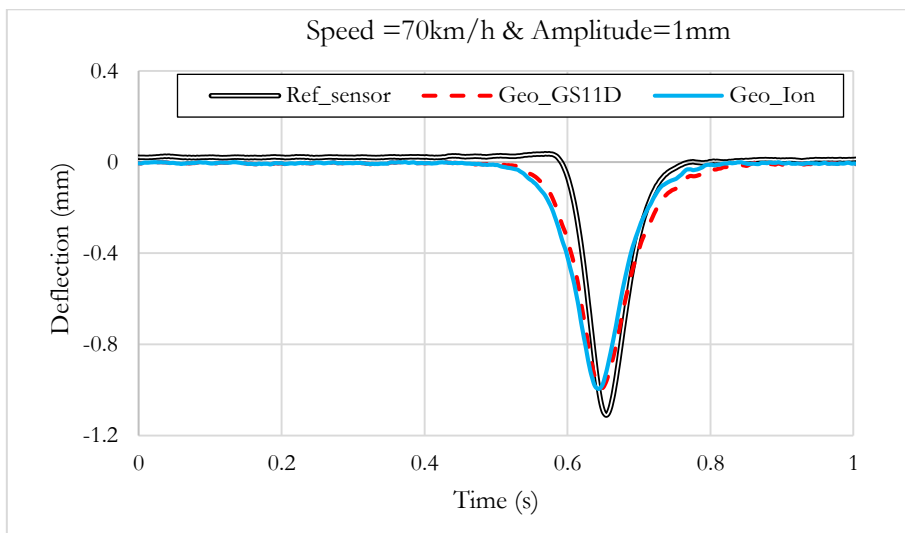


Figure 2-25. Displacement signals obtained for the geophones at the speed of 70 km/h with amplitude of 1mm

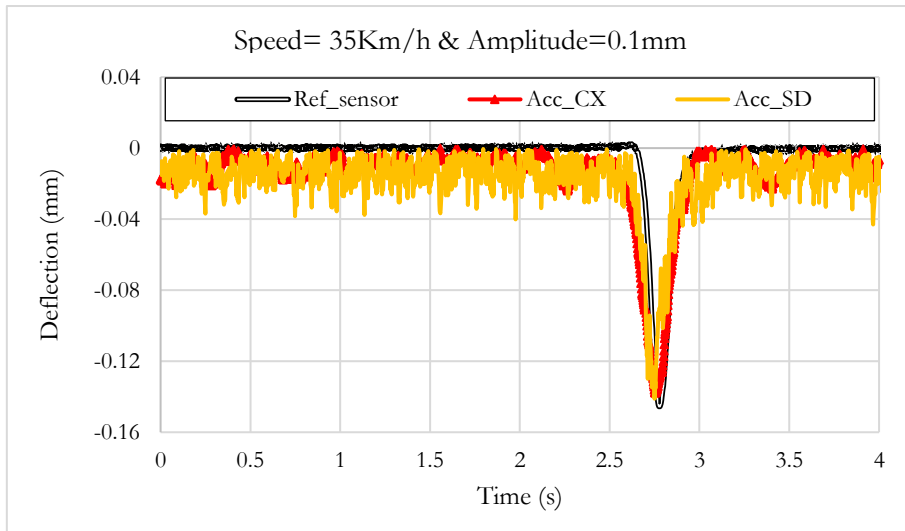


Figure 2-26. Displacement signals obtained for the accelerometers at the speed of 35 km/h with amplitude of 0.1mm

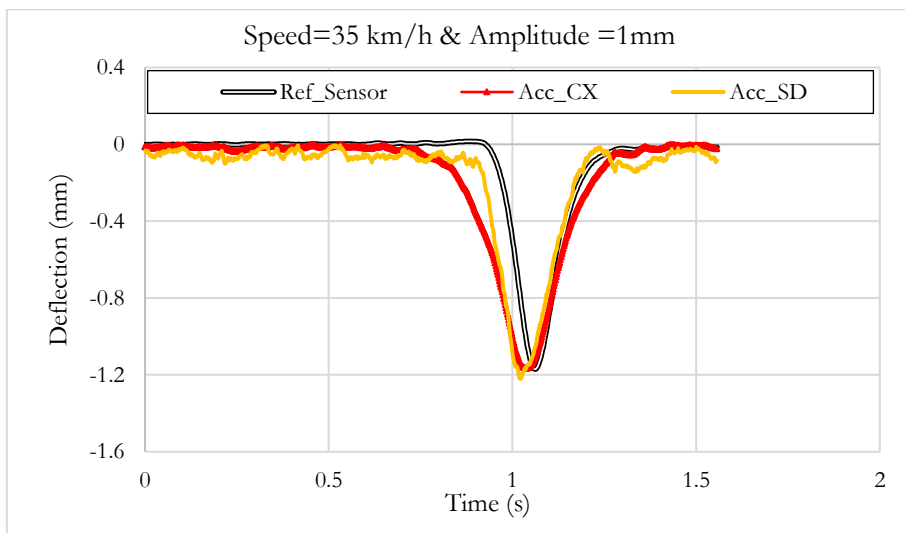


Figure 2-27. Displacement signals obtained for the accelerometers at the speed of 35 km/h with amplitude of 1mm

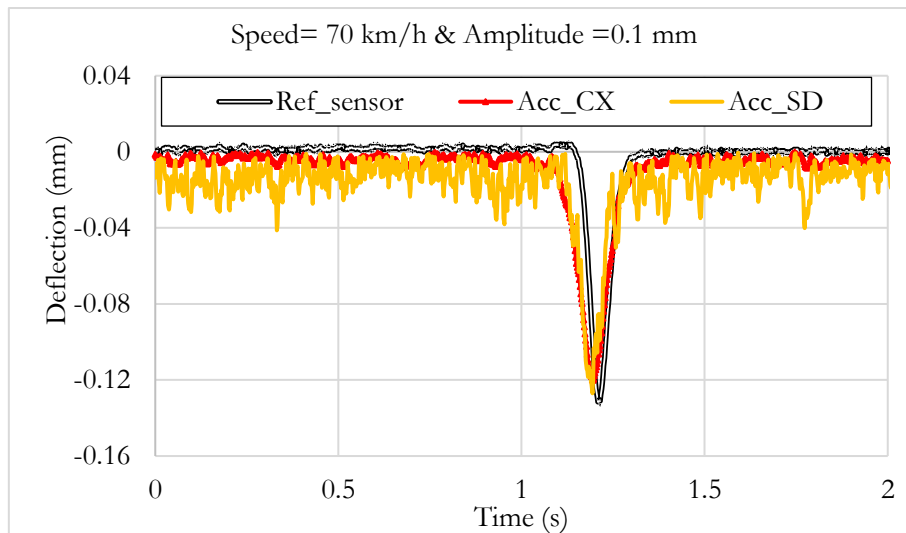


Figure 2-28. Displacement signals obtained for the accelerometers at the speed of 70 km/h with amplitude of 0.1mm

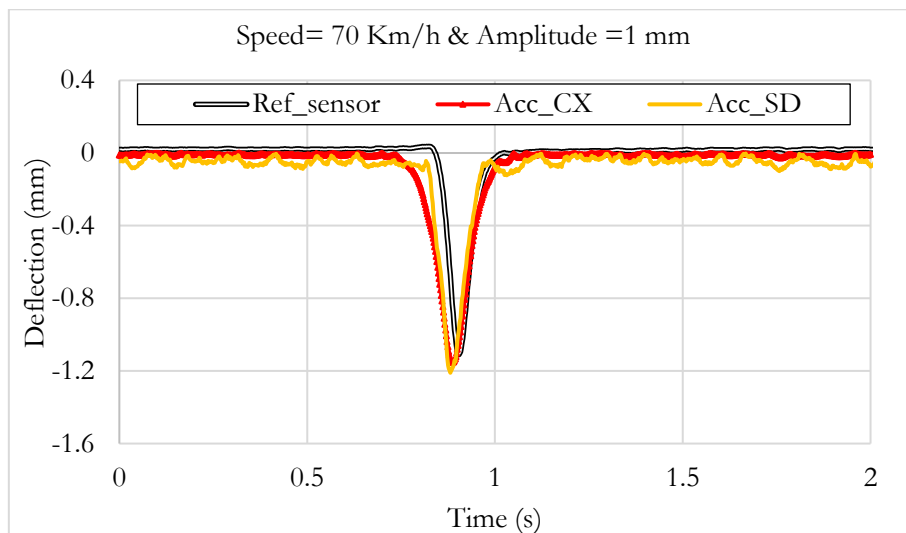


Figure 2-29. Displacement signals obtained for the accelerometers at the speed of 70 km/h with amplitude of 1mm

### 2.9.2. Truck signals

The following results present the processed truck signals, corresponding to five axle loads, with speeds of 35 km/h and 70 km/h and with vertical displacement amplitudes of 0.1, 0.3 and 1 mm. The results are similar to those obtained for the pulse signals. Figure 2-30, Figure 2-31, Figure 2-32 and Figure 2-33 represents the displacement signals for geophones at the speed of 35 km/h and 70 km/h and with the two amplitude. The processed geophone signals present amplitudes and shapes in good agreement with the reference signals and again the geophone GS11D predicts

slightly better signal amplitudes. Figure 2-34, Figure 2-35, Figure 2-36 and Figure 2-37 represents the displacement signals for accelerometers at the speed of 35 km/h and 70 km/h and with the two amplitude. For the accelerometers, the results obtained with accelerometer CX-Memsic are slightly better than Accelerometer SD. As for the pulse signals, at lower amplitudes, the signals display more noise. Table 2.4 shows the percentage differences of the truck signals calculated with the equation 2.8 for geophones and accelerometers. The results indicate the difference with the reference signal are lower than for the pulse signal with difference in percentage under 7% for all the test conditions.

Table 2.4. Percentage difference between the reference signal and the signals measured with the sensors (geophones and accelerometers)

| Sensor                  | Speed 35km/h                                    |   | Speed 70km/h                                    |   |
|-------------------------|---|---|---|---|
|                         | Percentage difference (%)<br>Amplitude<br>0.1mm | Percentage difference (%)<br>Amplitude<br>1mm | Amplitude<br>Percentage difference (%)<br>0.1mm | Percentage difference (%)<br>Amplitude<br>1mm |
| <b>Geophone GS11D</b>   | 7.2   | 3.4   | 4.1   | 5.3   |
| <b>Geophone Ion</b>     | 6.6   | 6.1   | 4.9   | 6.9   |
| <b>Accelerometer CX</b> | 6.4   | 3.5   | 5.04  | 4.47  |
| <b>Accelerometer SD</b> | 4.5   | 3.5   | 5.2   | 4.79  |

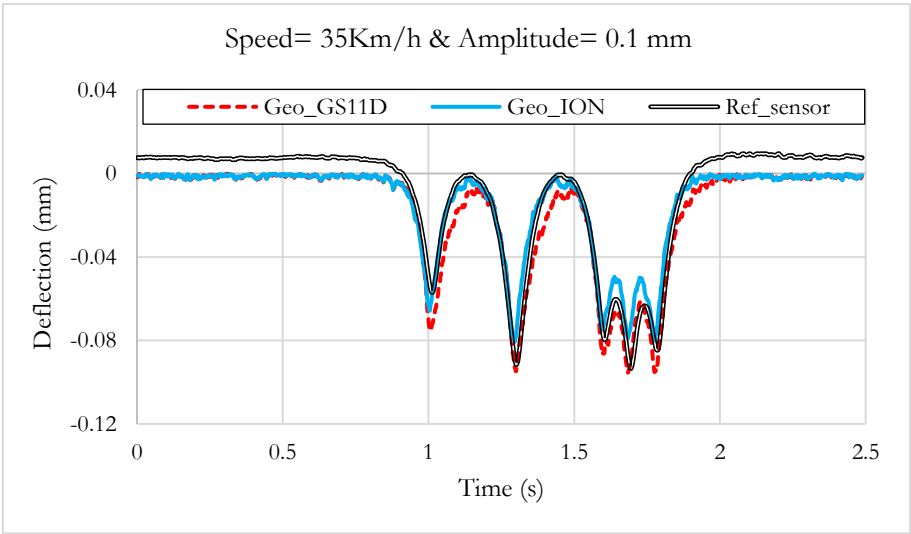


Figure 2-30. Displacement signals obtained for the geophones at 35 km/h with amplitude of 0.1mm

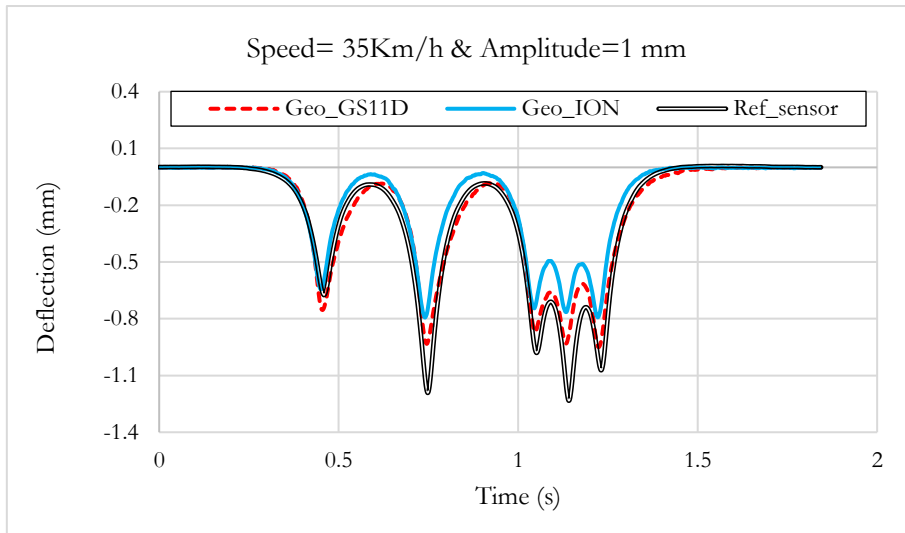


Figure 2-31. Displacement signals obtained for the geophones at 35 km/h with amplitude of 1mm

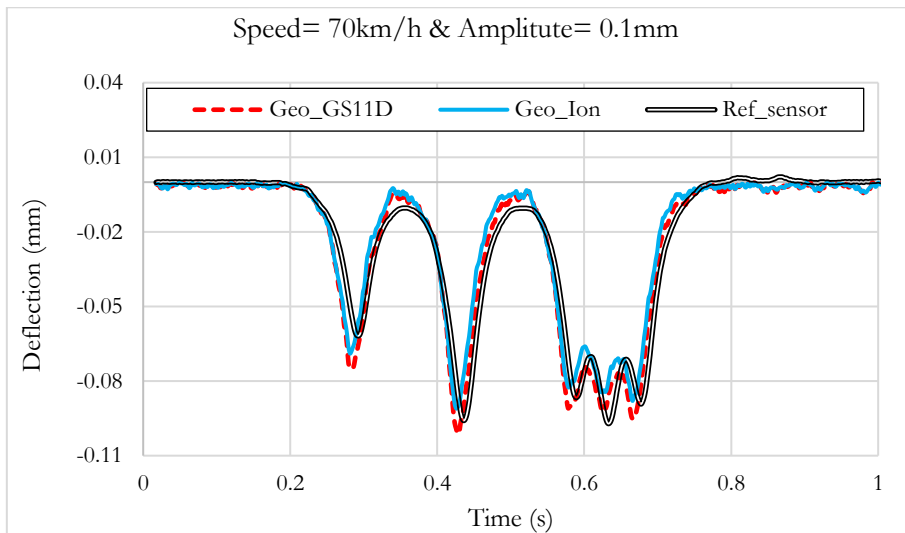


Figure 2-32. Displacement signals obtained for the geophones at 70 km/h with amplitude of 0.1mm

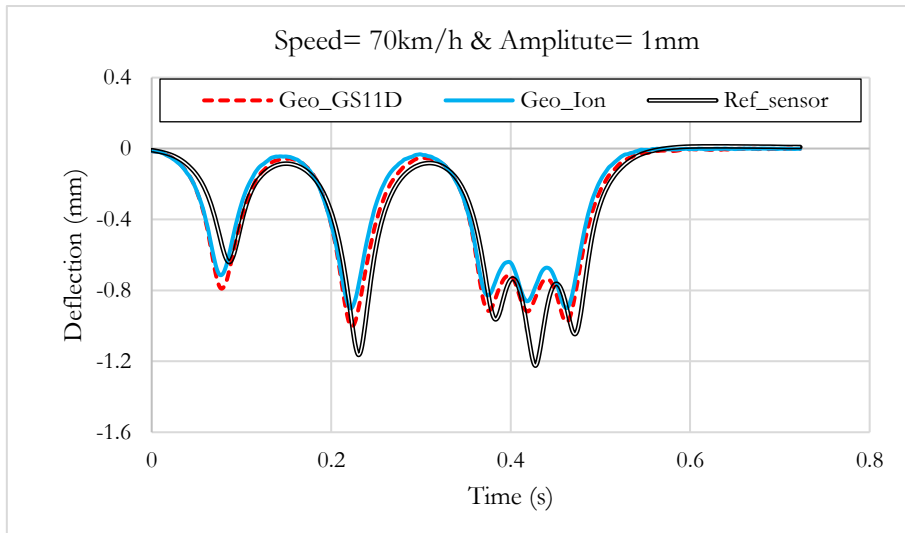


Figure 2-33. Displacement signals obtained for the geophones at 70 km/h with amplitude of 1mm

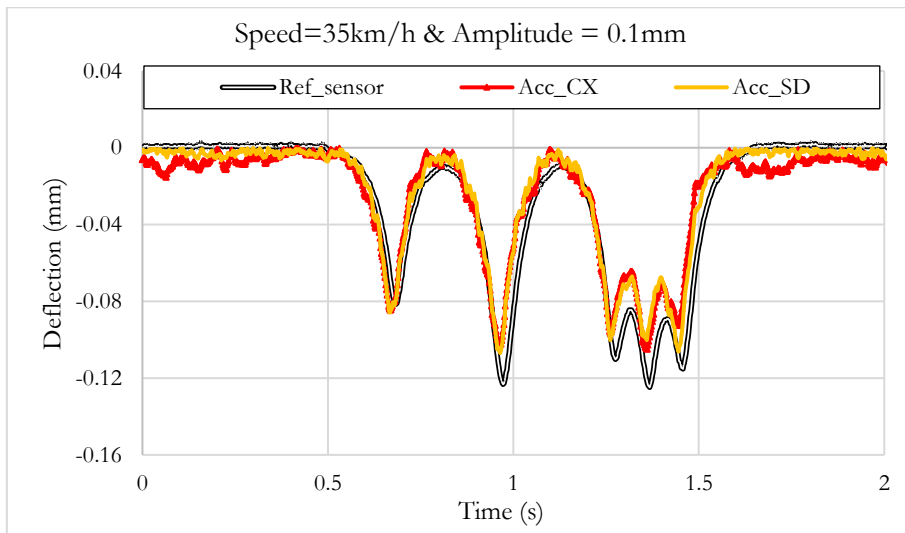


Figure 2-34. Displacement signals obtained for the accelerometers at 35km/h with amplitude of 0.1mm

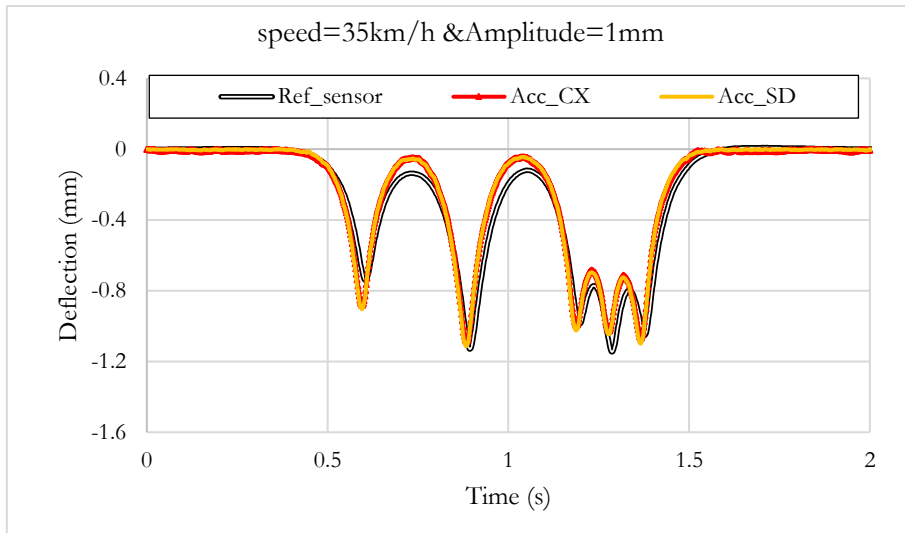


Figure 2-35. Displacement signals obtained for the accelerometers at 35km/h with amplitude of 1mm

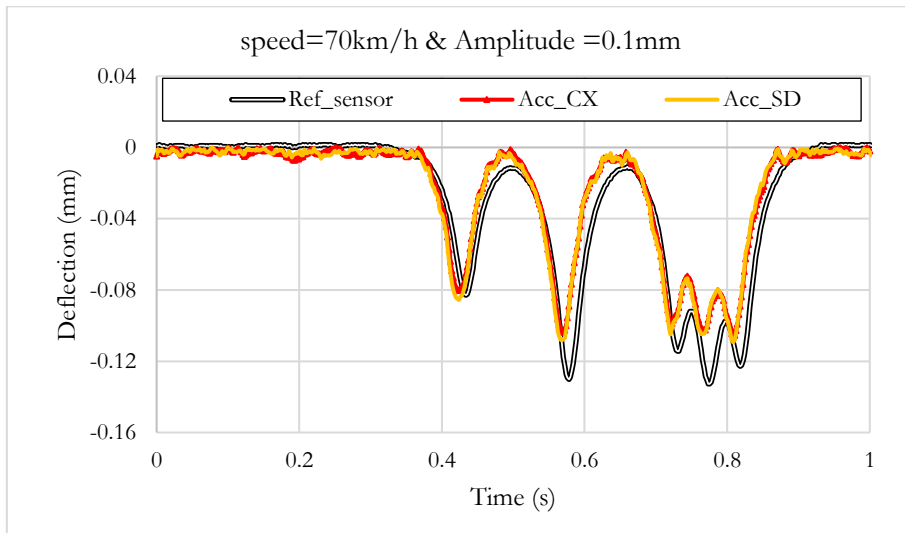


Figure 2-36. Displacement signals obtained for the accelerometers at 70 km/h with amplitude of 0.1mm

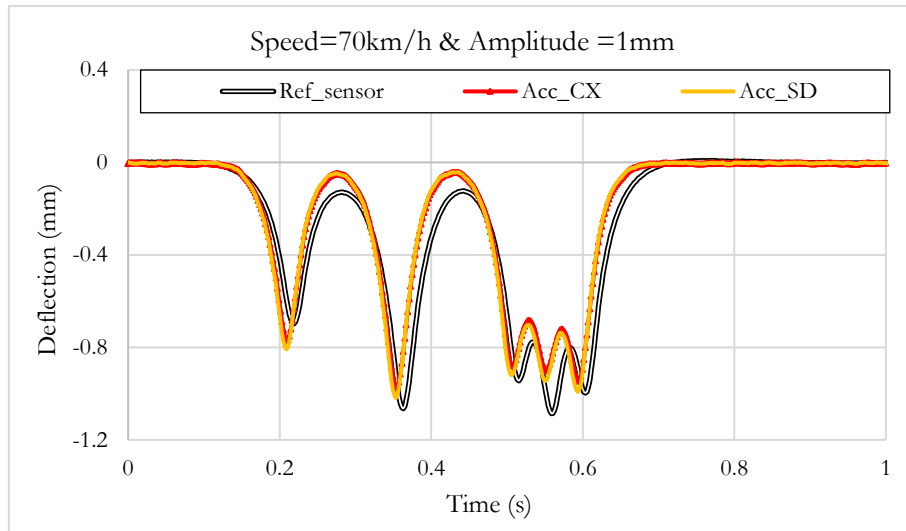


Figure 2-37. Displacement signals obtained for the accelerometers at 70 km/h with amplitude of 1mm

## 2.10 Conclusion

Geophones and accelerometers are sensors developed for the measurement of displacement velocities and accelerations respectively. They are used in various applications, such as detection of ground motions, for seismic applications. The objective of this study was to evaluate the possibility to use geophones and accelerometers for pavement instrumentation, to monitor pavement deflections under vehicle traffic. After defining the requirements for such measurements, two types of geophones and two types of accelerometers have been selected for the study: a geophone Geospace GS11D, a geophone Ion LF-24, accelerometers Silicone design and Memsic. Before testing the sensors in real conditions in a pavement, a laboratory study was performed, to evaluate their response to simulated pavement deflection signals, generated by a hydraulic vibrating table.

The sensors were submitted to sinusoidal pulse signals, and to signals reproducing the deflection under a five axle truck. These signals were applied with different amplitudes, and different frequencies, corresponding to the range of conditions encountered in real pavements.

The first results indicated that a simple integration of the signals, to convert the measured displacement velocity and accelerations into displacement is not sufficient to obtain accurate displacement values. Different treatments of the signals have been tested to improve the response, and a correction procedure has been proposed. This procedure includes five steps: noise filtering, amplification, integration of the signal, detrending, and application of a Hilbert transform. The treated signals have been compared with reference displacement measurements, carried out with a

reference laser displacement sensor, and it has been shown that after treatment, realistic deflection values can be obtained for typical pavement loading conditions.

These results confirm the possibility of using embedded geophones and accelerometers for the measurement of pavement deflections. These sensors present interesting characteristics for this type of measurements, due to their high sensitivity, good robustness, and relatively low cost. Following these results, the next step is to validate the results obtained in the laboratory by a full scale experiment, on a real pavement section.



# CHAPTER 3 ACCELERATED PAVEMENT TESTS

- Chapter 3 Accelerated pavement tests ..... 109**
- 3.1 Introduction .....110
- 3.2 Instrumentation of the pavement structure .....110
  - 3.2.1. Objectives of the Full scale testing.....110
  - 3.2.2. The Fatigue carrousel .....111
  - 3.2.3. The pavement structure .....111
  - 3.2.4. Loading configuration .....112
  - 3.2.5. Instrumented section .....113
  - 3.2.6. Sensor Arrangement .....115
- 3.3 Test program.....116
  - 3.3.1. Test scheme.....116
- 3.4 Data processing of the signals .....117
  - 3.4.1. Validation of correction method on the APT data .....117
  - 3.4.2. Methodology .....118
- 3.5 Tests Results.....118
  - 3.5.1. Deflection values at different speeds .....119
  - 3.5.2. Deflection values at different wheel positions .....126
- 3.6 Comparison between accelerometers, geophones, and deflectometer sensor .....129
- 3.7 Conclusion.....130

### **3.1 Introduction**

After the evaluation of the geophones and accelerometers in the laboratory, this chapter presents a full scale experiment performed on the IFSTTAR accelerated pavement testing (APT) facility, to evaluate the response of the sensors in a pavement, under moving wheel loads.

The four types of sensors tested previously in the laboratory were embedded in the experimental pavement section. The goal of the APT tests was to evaluate the different types of sensors in real field conditions, with a continuous data acquisition, with different loading speeds and different load positions, and to propose methods for interpreting measurements carried under controlled traffic, for monitoring the pavement. Finally, the objective was also to use the sensors to evaluate the performance of the pavement materials, and their evolution with time and loading conditions.

In this chapter, we present the main characteristics of the instrumented section and effectiveness of the sensors to measure the vertical deflections; the chapter presents successively:

- The sensor instrumentation and the methods used for their implementation
- Data processing with the same techniques developed in Chapter Two for carrying out the deflection measurements.
- The analysis of the different measurement results, with respect to different parameters.

### **3.2 Instrumentation of the pavement structure**

#### **3.2.1.Objectives of the Full scale testing**

In recent years, sensing technologies have been widely used for pavement monitoring and instrumentation, mainly to characterize the pavement mechanical properties and measuring the in situ deteriorations. The mechanical properties of the pavement can be measured with the aid of laboratory tests done on the materials. However, after pavement construction, it is difficult to test the materials in the laboratory without damaging the structure and to monitor the changes in the mechanical properties with the passage of time.

The approach of this study is to use embeddable sensors to estimate the evolution of the pavement moduli and the ultimate idea is to back-calculate the mechanical properties of the flexible pavements using the sensor response. To validate the approach, the idea is to measure the vertical velocities and accelerations using embedded geophones and accelerometers, on a pavement tested on the accelerated pavement testing facility, with respect to different conditions. These sensors were subjected to different speeds, positions and environmental conditions to detect the vertical deflections.

The responses of the sensors can be used to determine the deflection basin of the pavement, under a wheel load, and then to use classical back-calculation methods, to determine the moduli of the pavement layers. The objective is also to verify that the sensors are robust enough to resist to the installation, and to traffic loads, and that their accuracy is sufficient to measure the deflection of a real pavement, for different loading conditions (typical deflection levels range from 0.1 to 1 mm).

### **3.2.2. The Fatigue carousel**

This study was carried out on the Fatigue Carousel of IFSTTAR, a circular outdoor Accelerated Pavement Testing (APT) facility that can apply moving loads to full-scale test pavements, with speeds up to 100 km/h. A picture of the facility is shown in Figure 3-1. As can be seen the test track is split into several sectors, each accommodating a different pavement structure. There are four identical loading arms at right angles, each housing a wheel carriage at the end. These wheel carriages can accommodate different tire arrangements, different total load levels up to 13 tons multiple axles and different wander positions. The mean travel radius of the loading carriage is 19 m, i.e. a circumference of about 120 m. The width of the test pavement is generally 3m, but can go up to 6 m.

The sensors described in chapter 2 (two geophones and two accelerometers) were embedded in one pavement structure tested on the IFSTTAR accelerated pavement testing (APT) facility. A reference anchored deflectometer was also installed, to serve as reference for the measurement of the deflection response.



Figure 3-1. Carousel APT at IFSTTAR

### **3.2.3. The pavement structure**

The tests have been performed on a classic French design flexible pavement structure, consisting of 11 cm of bituminous materials (in two layers), over an unbound granular base. The

characteristics of the asphalt pavement layers were determined from laboratory complex modulus tests performed on the bituminous mix. The elastic modulus at 15 °C and 10 Hz of the mix is 9441 MPa. FWD tests and Benkelman beam deflection measurements have also been performed, giving an average elastic modulus of 110 MPa for the subgrade, and 145 MPa for the granular layer. The characteristics of the pavement structure where the sensors were installed are given in Table 3.1. The characteristics of the pavement layers were determined using the following tests:

- Thicknesses of the different layers were determined from the controls made during and after construction.
- Bituminous material complex moduli were determined from laboratory tests on the field produced mix.
- The moduli of the granular layer were determined by back calculation, from FWD measurements.
- The moduli of the subgrade were determined from Benkelman beam deflection measurements.

Table 3.1 Characteristics of the pavement structure

| Pavement Layer      | Thickness (cm) | Modulus (MPa)        |
|---------------------|----------------|----------------------|
| Bituminous material | 11             | 9441 (15°C and 10Hz) |
| Granular base       | 30             | 145                  |
| Subgrade            | 260            | 110                  |

**3.2.4.Loading configuration**

The carrousel has four loading arms. For our test, each wheel carriage was equipped with a dual wheel load (Figure 3-2).

In this experiment, dual wheels were used, with the characteristics shown on Figure 3-3 and a tire-pavement contact stress of 0.6 MPa. For the pavement calculations, the tire loads were described by circular contact surfaces, with radii of 129 mm (each) and center-to-center spacing of 352 mm.



Figure 3-2. Loading configurations used for the test: dual wheel



Figure 3-3. Dual wheel load dimensions

### 3.2.5. Instrumented section

The pavement section instrumented with the geophones and accelerometers was section S1 (see Figure 3-4), which is 22 m long, composed of (top to bottom): 11 cm of asphalt concrete in 2 lifts, 5 cm upper and 6 cm lower, consisting of 0/10 mm asphalt concrete (BBSG), 30 cm of unbound granular material (UGM 0/20), overlaying a soil subgrade extending to a depth of 2.6 meters, resting on a concrete slab. The subgrade soil, consisting of clayey sand, was processed and compacted in 2011. The granular layer was put in place in September 2017, in two separate layers. The two AC layers were also paved in September 2017.

In addition to the above, section S1 was recently (2018) instrumented with five new sensors: two different single-axis geophones (Geospace GS-11D and ION LF-24), two different single-axis accelerometers (Silicon Design 2210-002 and MEMSIC CXL04GP1), and one anchored vertical displacement sensor (Model LVDT S-series displacement sensors) as shown in Figure 3-5. The geophones and accelerometers were placed about 1 cm below the pavement surface, in the center

of the wheel path. They were glued with resin inside blind-holes drilled into the upper AC lift. They were oriented to measure vertical responses in the z direction. The effective measurement depth corresponds to the height of the sensor + 10 mm (from AC surface to bottom of sensor casing). The anchored deflectometer consists of an LVDT which is connected to a rod, anchored at a significant depth (here 3 meters), and which measures the total vertical displacement between the pavement surface and the bottom of the rod, supposed fixed.

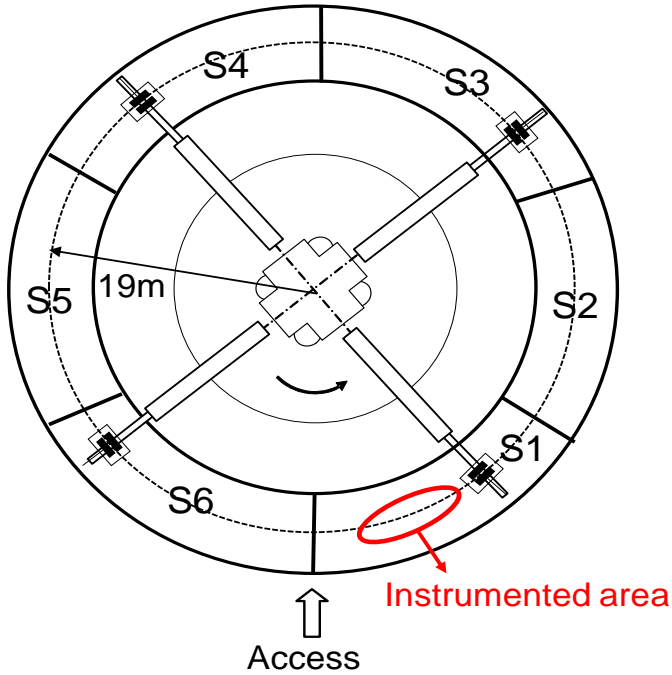


Figure 3-4. Layout of the APT sections

**Instrumentation of pavement structures**

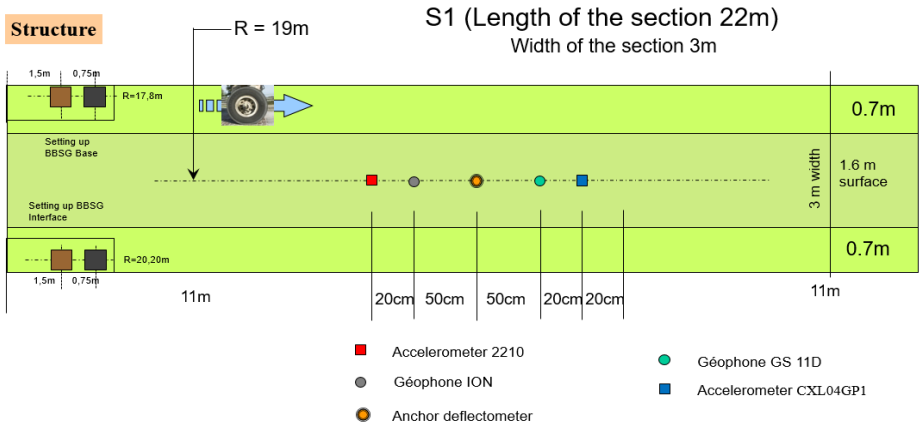


Figure 3-5. Position of the sensors on the experimental pavement section

### 3.2.6. Sensor Arrangement

The sensors, which include geophones, accelerometers and an anchored deflectometer, were installed on section 1 as shown in Figure 3-6. To measure the total pavement deflection, the sensors were installed very close to the pavement surface (1 cm below the surface). All the sensors were installed in the middle of the wheel path of the test section, close to each other (Figure 3-7).

The displacement sensor used for the deflectometer is a Model S-series LVDT, which is a linear variable differential transformer which consists of a movable core and primary and secondary coils. The coils are wound to measure the change in position of the core due to an external displacement. When the core is in central position the coupling from primary to secondary is equal and the output is 0. When the core is displaced, an output voltage proportional to the displacement is generated. The geophones used (Geospace GS-11D and ION LF-24), measure the rate of change in the displacement during the passage of the vehicle. They comprise a spring-mounted wire coil moving within the field of a permanent magnet to generate an electrical signal. The voltage is proportional to the vertical velocity, depending on the sensitivity of the sensors, which defines the minimum change that can be measured with the device.

The accelerometers (Silicon Design 22106-002 and MEMSIC CXL04GP1) are based on MEMS technology, and consist of a mass attached to a spring, which moves in one direction between two fixed outer parallel plates. During a passage of vehicle when acceleration is applied in a particular direction, the mass moves, the air gap between the mass and one plate decreases, while the other gap increases and the capacitance between the plates changes. This change in capacitance is used to determine the acceleration.

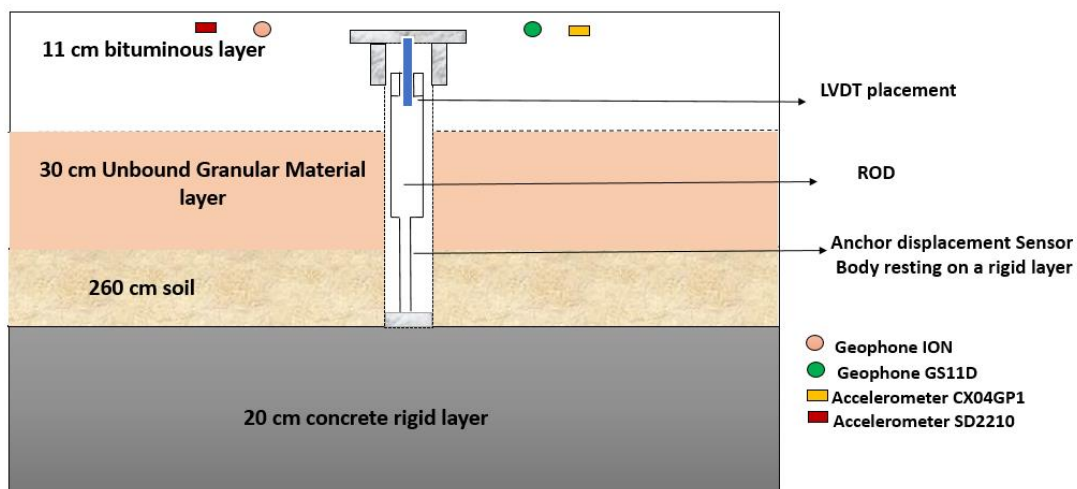


Figure 3-6. Instrumented Pavement structure



**Accelerometer-Silicon design  
2210-002 and Geophone ion**



**Accelerometer CXL04GP1 &  
Geophones GS11D**



**Anchored Deflectometer**

Figure 3-7. Sensor placement

### 3.3 Test program

#### 3.3.1. Test scheme

The tests on the fatigue carousel were carried out at different load levels, different lateral positions of the wheels and variable speed. The study has been carried out at the early stage of the test, where the structure had not experienced any damage. In total, more than 1 million loadings were applied in the experiment, with different temperatures and environmental conditions. The principal test configurations applied for the evaluation of the sensors are shown in Table 3.2.

Tests have been made for 3 different half- axles load levels (45 kN, 55kN and 65 kN), different loading speeds (from 3 to 10 rounds per minute, corresponding to approximately 21 to 70 km/h) and different lateral wheel positions, with respect to the position of the sensors, as shown in Figure 3-8. The wheels can move in the transverse direction, over 11 different positions, with a spacing of 10.5 cm. Position 6 corresponds to the central position, where the sensors are placed between the two wheels. For positions 4 and 8, the sensors are placed under the center of one wheel. The speed of the wheel loading is calculated with the number of rounds per minute, which is then converted into the equivalent speed in m/s or km/h. The equation (3.1) used to convert rounds per minute to linear velocity is:

$$V = \text{RPM} \times R \times 2 \times \pi / 60 \quad (3.1)$$

Whereas

V= velocity in m/s

RPM= rounds per minute

R= radius corresponding to the wheel position (near 19m)

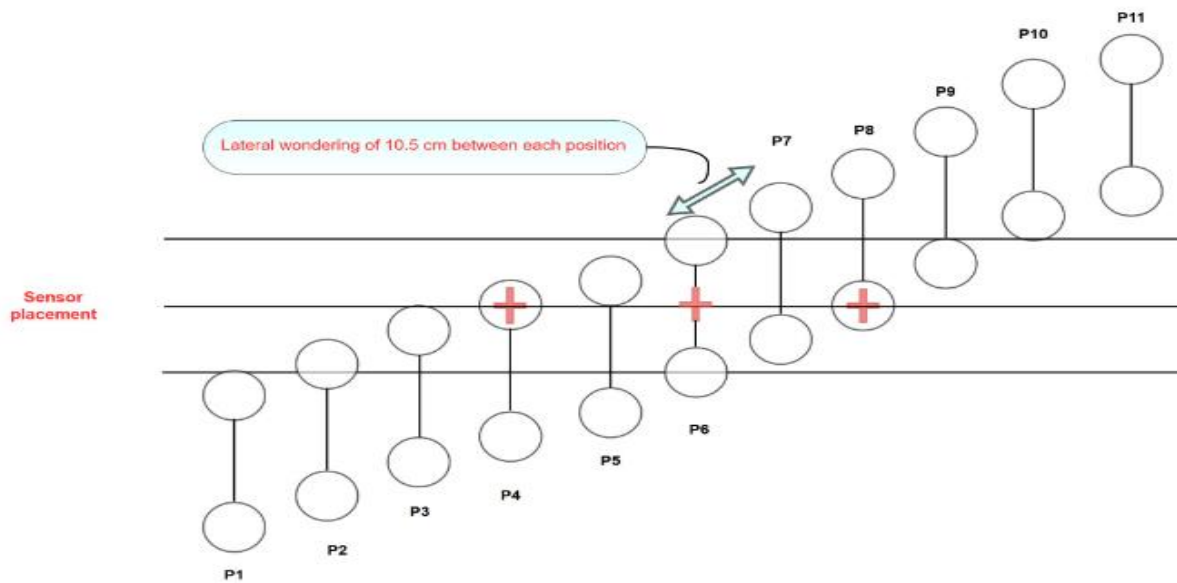


Figure 3-8. Different wheel positions with respect to the sensors

Table 3.2 test settings of the carousel

| S.no | Load     | Lateral position      | Speed                     |
|------|----------|-----------------------|---------------------------|
| 1    | 4.5 tons | From position 1 to 11 | 3 to 10 rounds per minute |
| 3    | 5.5 tons | From position 1 to 11 | 3 to 10 rounds per minute |
| 5    | 6.5 tons | From position 1 to 11 | 3 to 10 rounds per minute |

### 3.4 Data processing of the signals

#### 3.4.1. Validation of correction method on the APT data

The signal processing techniques developed in chapter two were used for the data measured on the fatigue carousel, to convert the sensor signals into vertical deflections. The procedure includes filtering, amplification, integration and application of the Hilbert transform.

The vertical deflections measured by the anchored deflectometer were used as a reference. This sensor, which measures the pavement vertical deflection with reference to a fixed point, presents range of measurement of  $\pm 5\text{mm}$ .

The measurements of the other sensors will be compared with the reference deflectometer after the treatment and the difference with the reference sensor deflection signals will be used to evaluate the accuracy of the geophones and accelerometers.

### 3.4.2. Methodology

As described in the chapter 2 section 2.6, the geophones and accelerometers measure respectively the vertical velocity and acceleration. To determine the displacements, the same treatment procedure as in chapter 2 has been applied. Figure 3-9 recalls the steps of the procedure used for the signal treatment. This procedure was applied for the geophones and accelerometers. The main difference is that for the accelerometers, a double integration is performed. And for each sensor the amplification factor was varied depending on the speed.



Figure 3-9. Signal Treatment method

### 3.5 Tests Results

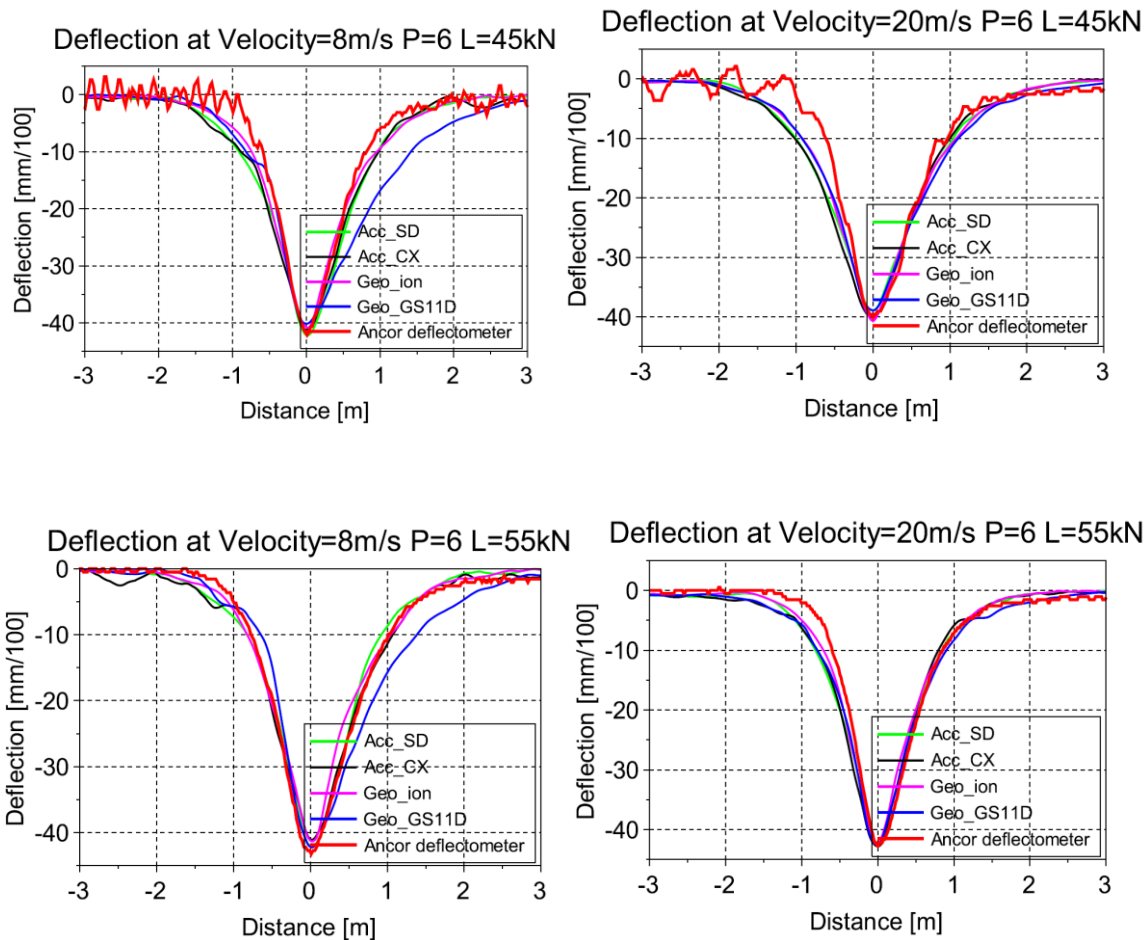
This section presents the vertical deflection measurements obtained with the accelerometers and geophones, and evaluates their accuracy. In addition, variations of these values with the magnitude of the applied load and with the loading speed are analysed. The following factors are assessed:

- The accuracy and repeatability of the deflection measurements.
- The influence of the applied load, operating speed and lateral distance between the wheel load and the sensor positions.

The tests were carried out at 3 load levels (45, 55 and 65 kN), at speeds varying from 6m/s to 20m/s and at surface temperatures of 19°C and 20°C. For each test condition, the deflections measured with the two types of geophones and two types of accelerometers were compared with the anchored deflectometer measurements. On Figure 3-10 to Figure 3-22, the acronyms used for the sensors are the following: Geophone ion designates by Geo\_ion, Geophone GS11D by Geo\_GS11D, and Accelerometer Silicon Design by Acc\_SD and accelerometer CXL04GP1 by ACC\_CX.

### 3.5.1. Deflection values at different speeds

At the fatigue carousel, the tests are conducted at controlled operating speeds which allows to study the effect of speed on the induced vertical deflections. Figure 3-10 shows the variations of the deflection signals with increasing speed, from 6 to 20 m/s at position 6 which is when each sensor is placed between the two wheels, and at 3 different load levels. The repeatability of the fatigue carousel produced by the each arm is explained in the Annex B which is considered to be negligible. In general, a slight decrease of deflections is observed when the speed increases, except for the speed of 8 m/s. We can observe that the scatter of the signals is more important for the 45kN load, especially for the deflectometer; this can be explained by the fact that it was the beginning of the tests, and that the pavement was settling down, probably because of the post compaction of the unbound granular material. The results of Figure 3-10 show that the deflections obtained with the two geophones and two accelerometers, using the proposed signal processing method, are all very close to each other, and to the reference deflections measured with the deflectometer (Bahrani et al., 2020).



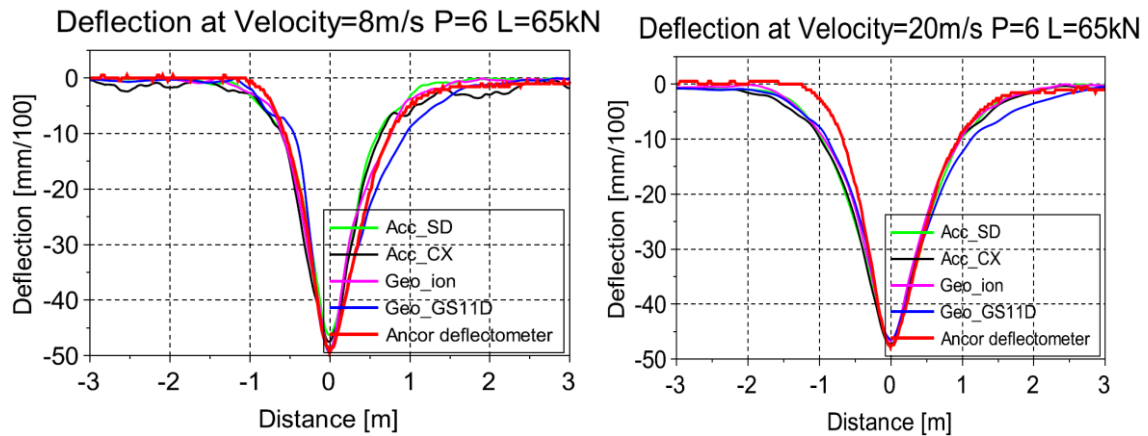


Figure 3-10. Deflection values measured for 45, 55 and 65 kN loads and speeds of 8m/s and 20m/s (wheel position 6)

In order to validate the measured deflection values, comparisons were made with modelling results. The simulations were performed for different experimental conditions, with a linear elastic model (ALIZE Software) and a viscoelastic model (ViscoRoute Software). For the multilayer elastic model, the modulus of the asphalt layer was changed according to the recorded speed and temperature (with the hypothesis that a frequency of 10 Hz corresponds to a speed of 70km/h) (Bodin et al., 2017).

Figure 3-11 shows the pavement structure model corresponding to a speed of 20m/s (10Hz) and a temperature of 19°C. As in the experiment, 3 load levels were considered for the modelling: 45, 55 and 65 kN. Figure 3-12 shows the details of the 65kN load characteristics. The maximum deflections were calculated for speeds of 20, 16, 12, 8 and 6 m/s and load levels of 45, 55 and 65kN.

- Basis structure

|        | thick. (m) | modulus (MPa) | Nu    | material type |
|--------|------------|---------------|-------|---------------|
| bonded | 0,110      | 8769,0        | 0,350 | other         |
| bonded | 0,300      | 145,0         | 0,350 | other         |
| bonded | 2,600      | 110,0         | 0,350 | other         |
|        | infinite   | 9999999       | 0,350 | other         |

Figure 3-11. Alize pavement model for 20m/s and 19°C (10Hz and 19°C)

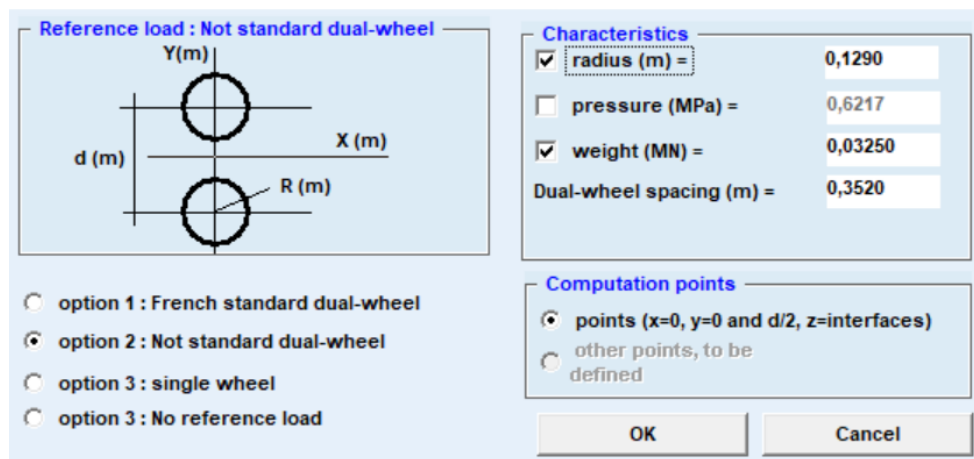


Figure 3-12. Load configuration of 65kN load in Alize

For the multilayer viscoelastic simulations (ViscoRoute software), the Huet-Sayegh model was used to describe the behaviour of the asphalt material, for the different experimental conditions. The material was characterized in the lab, using complex modulus tests (EN 12967-26). The specimens were prepared from loose material collected during the pavement construction. The material was compacted using a slab compactor with rubber-tire wheels (EN 12697-33+A1, 2007), to produce 600 mm by 400 mm and 120 mm thick slabs. After compaction, the slabs were cored to produce cylindrical specimens, which were tested in traction-compression mode, to measure their complex modulus norm ( $|E^*|$ ) and phase angle ( $\delta$ ). Temperature and frequency sweeps were carried out from  $-10^\circ\text{C}$  to  $30^\circ\text{C}$  and from 3 to 40 Hz (EN 12697-26, 2012).

Model parameters for the mixture were fitted from complex modulus tests results and the relative master curves at  $T_{ref} = 15^\circ\text{C}$ , using the software Viscoanalyse®, developed for the interpretation of complex modulus tests (Chailleux et al., 2006). Model parameters (Huet-Sayegh parameters) are presented in Table 3.3. The Figure 3-13 shows the pavement structure used for the visco-elastic calculations and Figure 3-14 shows the characteristics of the 65KN load.

Table 3.3. Huet-Sayegh viscoelastic parameters of the asphalt mix.

| $E_0$<br>(MPa) | $E$<br>(MPa) | $\delta$ | $k$     | $h$     | $\tau$ ( $\theta$ ) | $A_0$   | $A_1$  | $A_2$     |
|----------------|--------------|----------|---------|---------|---------------------|---------|--------|-----------|
| 1.9348         | 27152.7      | 1.64785  | 0.18918 | 0.57923 | 2577                | 3.82048 | -0.431 | 0.0027654 |

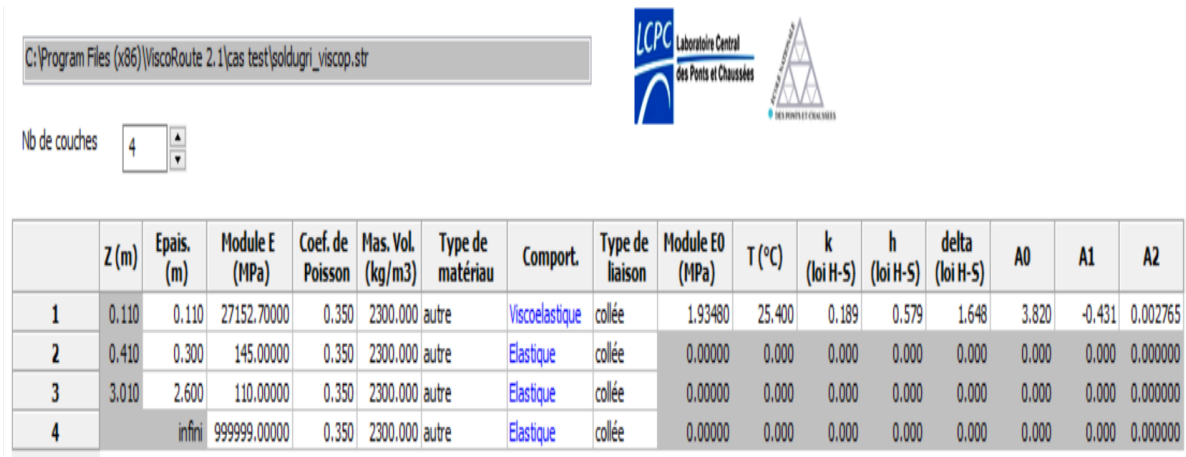


Figure 3-13. Pavement model used for the calculations with ViscoRoute

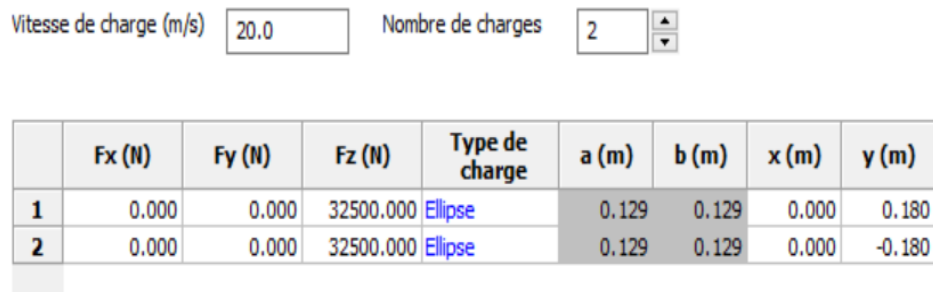


Figure 3-14. Characteristics of the 65kN load used in ViscoRoute

Figure 3-15 shows the vertical deflection calculated for the speed of 16 m/s at temperature of 18°C and the load of 65kN. In the figure it is compared to the measured response of anchor deflectometer. Similarly, the pavement deflections were calculated for speeds of 20, 16, 12, 8 and 6 m/s and loads of 45, 55 and 65KN.

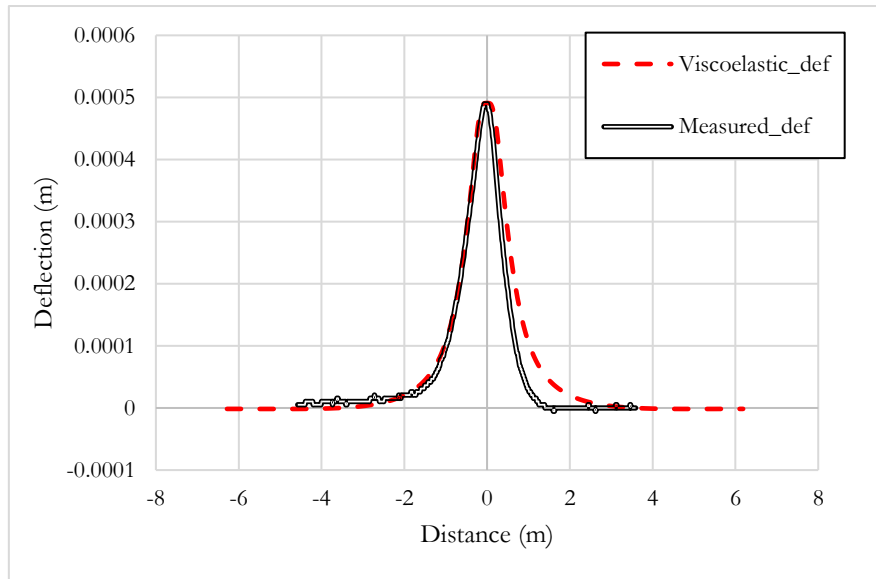


Figure 3-15. Vertical deflection calculated with ViscoRoute and the measured deflection at the speed of 16m/s, temperature 18°C and 65kN load

Figure 3-16, Figure 3-17 and Figure 3-18 present comparisons between the measured and calculated maximum deflections, for different speeds, varying from 6 to 20m/s, and for wheel position 6. To evaluate the accuracy of the simulations, the relative difference (named  $R_{max}$ ) between the maximum measured and calculated deflections was calculated, according to (equation (3.2)).

$$R_{max} = \frac{|MAX_{calculated\ signal} - MAX_{measured\ signal}|}{MAX_{calculated\ signal}} * 100 \quad (3.2)$$

For the 45kN load, the measured deflections are higher than the model predictions for the initial lower speed, and the difference percentage between the measured sensors values and calculated values with Alize is higher than for the other speeds, as described in Table 3.4. As indicated previously, this could be due to a post-compaction of the unbound granular material during the first load applications. For the other speeds the percentage is generally under 10%. Similarly, for 55kN the overall difference seems to be under 8% (see Table 3.4) and for the 65kN the percentage difference seems to be under 7% (see Table 3.4). Similarly, Table 3.5 represent the difference between the measured values and the calculated viscoelastic response. The differences between the results obtained with the elastic and viscoelastic models are also very small. Similar to the elastic responses at 45kN loads and lower speed the difference percentage seems higher however; the overall difference is under 9%. For 55kN and 65kN it is under 7%. In general, a slight decrease of deflections is observed when the speed increases, which is logical, except for the speed of 6 m/s, for which the results present more scatter. Evolution with speed is well reproduced, but the

difference with the models could be due to differences between laboratory and field properties of the materials.

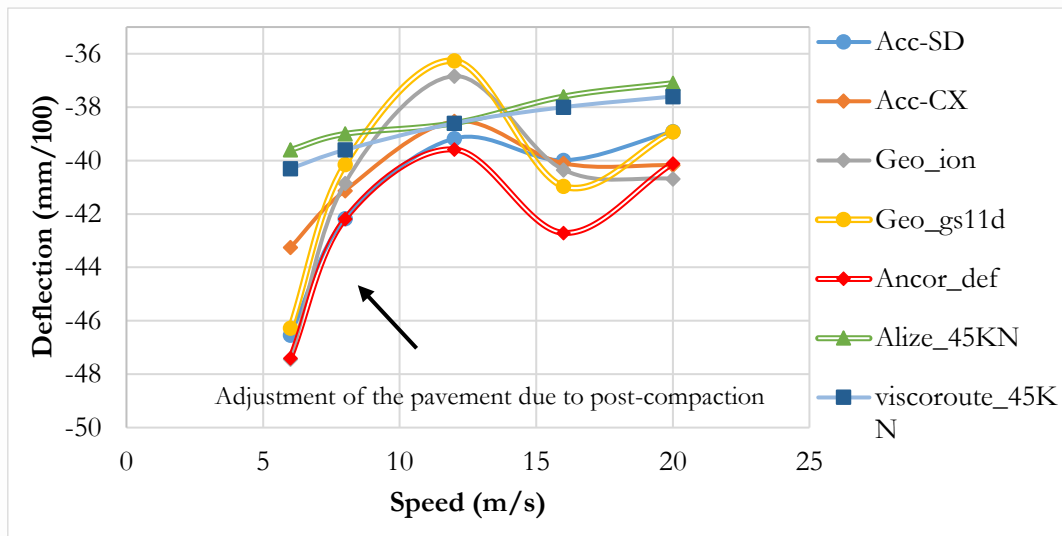


Figure 3-16. Deflection evolution of sensors for the 45 kN load at different speeds from 6 m/s to 20m/s

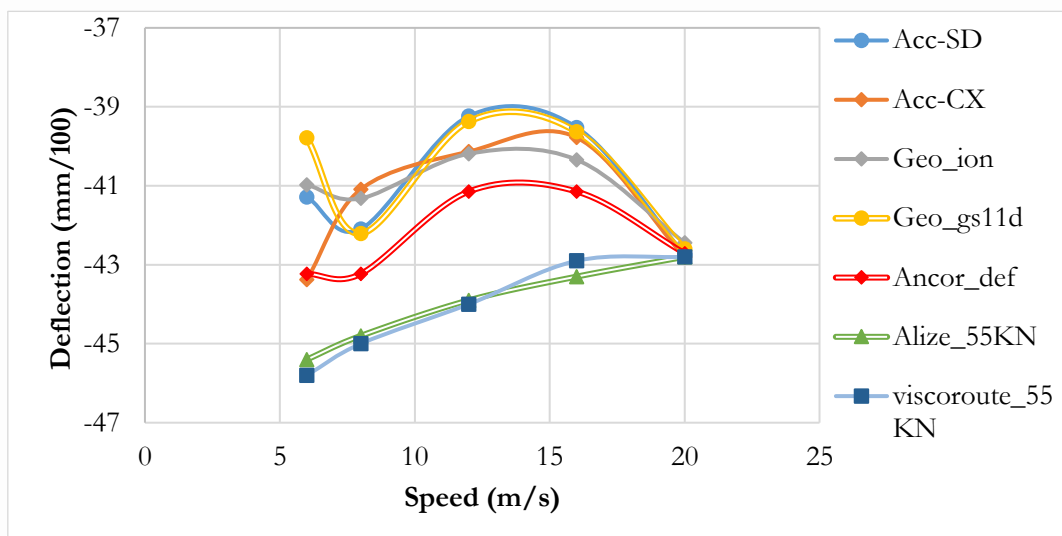


Figure 3-17. Deflection evolution of sensors for the 55 kN load at different speeds from 6 m/s to 20m/s

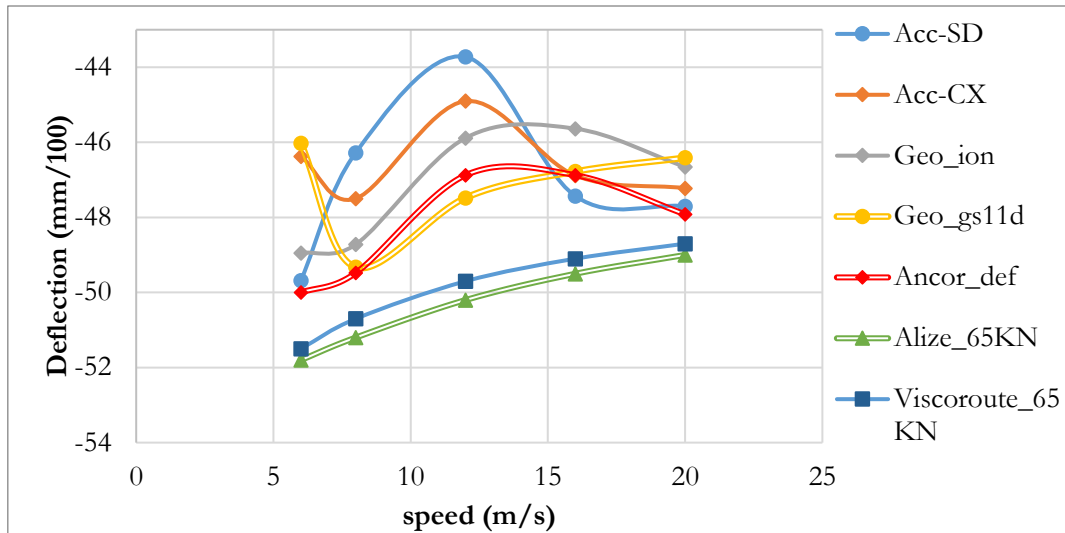


Figure 3-18. Deflection evolution of sensors for the 65 kN load at different speeds from 6 m/s to 20m/s

Table 3.4. Relative difference percentage ( $R_{max}$ ) between the maximum deflections measured with the sensor and the deflections calculated with Alize for different loads

| LOAD 45 kN & SPEED (m/s) | Anchor Deflectometer (%) | ACC-SD (%) | ACC-CX (%) | Geophone-Ion (%) | Geophone-GS11D (%) |
|--------------------------|--------------------------|------------|------------|------------------|--------------------|
| 6                        | 19.7                     | 17.5       | 9.2        | 19.8             | 16.8               |
| 8                        | 8.2                      | 8.13       | 5.4        | 4.7              | 2.9                |
| 12                       | 2.5                      | 1.48       | 0.17       | 4.5              | 6.04               |
| 16                       | 13.58                    | 6.35       | 6.65       | 7.3              | 8.94               |
| 20                       | 8.09                     | 4.88       | 8.27       | 9.6              | 4.8                |
| Mean                     | 10.414                   | 7.896      | 9.18       | 5.938            | 7.668              |
| LOAD 55 kN & SPEED(m/s)  | Anchor Deflectometer (%) | ACC-SD (%) | ACC-CX (%) | Geophone-Ion (%) | Geophone-GS11D (%) |
| 6                        | 4.78                     | 9.067      | 4.45       | 9.74             | 12.37              |
| 8                        | 3.50                     | 6.04       | 8.2        | 7.76             | 5.78               |
| 12                       | 6.27                     | 10.625     | 8.57       | 8.45             | 10.31              |
| 16                       | 4.975                    | 8.72       | 8.13       | 6.83             | 8.470              |
| 20                       | 0.21                     | 0.12       | 0.008      | 0.83             | 0.46               |
| Mean                     | 3.947                    | 7.478      | 6.722      | 5.8716           | 6.9144             |
| LOAD 65 kN & SPEED(m/s)  | Anchor Deflectometer (%) | ACC-SD (%) | ACC-CX (%) | Geophone-Ion (%) | Geophone-GS11D (%) |
| 6                        | 3.47                     | 4.09       | 10.47      | 5.507            | 11.15              |
| 8                        | 3.36                     | 9.61       | 7.23       | 4.84             | 3.65               |
| 12                       | 6.62                     | 12.90      | 10.55      | 8.59             | 5.4                |
| 16                       | 5.30                     | 4.17       | 5.28       | 7.80             | 5.49               |
| 20                       | 2.21                     | 2.65       | 3.62       | 4.78             | 5.28               |
| mean                     | 4.192                    | 6.194      | 6.3034     | 7.43             | 6.684              |

Table 3.5 Relative difference percentage ( $R_{max}$ ) between the maximum deflections measured with the sensor and the deflections calculated with ViscoRoute for different loads

| <b>LOAD 45 kN<br/>&amp; SPEED<br/>(m/s)</b> | <b>Anchor<br/>Deflectometer<br/>(%)</b> | <b>ACC-SD<br/>(%)</b> | <b>ACC-CX<br/>(%)</b> | <b>Geophone-<br/>Ion (%)</b> | <b>Geophone-<br/>GS11D<br/>(%)</b> |
|---|---|-----------------------|-----------------------|------------------------------|------------------------------------|
| 6   | 17.61                                   | 15.45                 | 7.32                  | 17.71                        | 14.81                              |
| 8   | 6.5                                     | 6.49                  | 3.85                  | 3.16                         | 1.37                               |
| 12  | 2.54                                    | 1.48                  | 0.17                  | 4.56                         | 6.04                               |
| 16  | 12.3                                    | 5.23                  | 5.52                  | 6.17                         | 7.79                               |
| 20  | 6.65                                    | 3.48                  | 6.83                  | 8.20                         | 3.50                               |
| Mean  | 9.14                                    | 6.43                  | 4.74                  | 7.96                         | 6.70                               |
| <b>LOAD 55 kN<br/>&amp; SPEED(m/s)</b>      | <b>Anchor<br/>Deflectometer<br/>(%)</b> | <b>ACC-SD<br/>(%)</b> | <b>ACC-CX<br/>(%)</b> | <b>Geophone-<br/>Ion (%)</b> | <b>Geophone-<br/>GS11D (%)</b>     |
| 6   | 5.61                                    | 9.86                  | 5.29                  | 10.53                        | 13.13                              |
| 8   | 3.93                                    | 6.46                  | 8.68                  | 8.17                         | 6.20                               |
| 12  | 6.48                                    | 10.82                 | 8.78                  | 8.66                         | 10.51                              |
| 16  | 4.08                                    | 7.87                  | 7.27                  | 5.96                         | 7.61                               |
| 20  | 0.21                                    | 0.12                  | 0.008                 | 0.83                         | 0.46                               |
| Mean  | 4.06                                    | 7.02                  | 6.01                  | 6.83                         | 7.58                               |
| <b>LOAD 65 kN<br/>&amp; SPEED(m/s)</b>      | <b>Anchor<br/>Deflectometer<br/>(%)</b> | <b>ACC-SD<br/>(%)</b> | <b>ACC-CX<br/>(%)</b> | <b>Geophone-<br/>Ion (%)</b> | <b>Geophone-<br/>GS11D (%)</b>     |
| 6   | 2.91                                    | 3.53                  | 9.95                  | 4.95                         | 10.63                              |
| 8   | 2.40                                    | 8.73                  | 6.31                  | 3.90                         | 2.70                               |
| 12  | 5.68                                    | 12.02                 | 9.65                  | 7.67                         | 4.47                               |
| 16  | 4.53                                    | 3.39                  | 4.51                  | 7.05                         | 4.72                               |
| 20  | 1.60                                    | 2.05                  | 3.03                  | 4.19                         | 4.7                                |
| mean  | 3.43                                    | 5.94                  | 6.69                  | 5.55                         | 5.44                               |

### 3.5.2. Deflection values at different wheel positions

The influence of the position of the wheels was also studied. Figure 3-19 shows the deflection responses corresponding to different lateral positions of the dual wheels with respect to the sensors. In position 6, the sensors are placed between the wheels whereas in position 4, the sensors are under the center of one wheel, as shown in Figure 3-8. The maximum deflection is obtained at positions 4 and 8. (N. Bahrani et al., 2020)

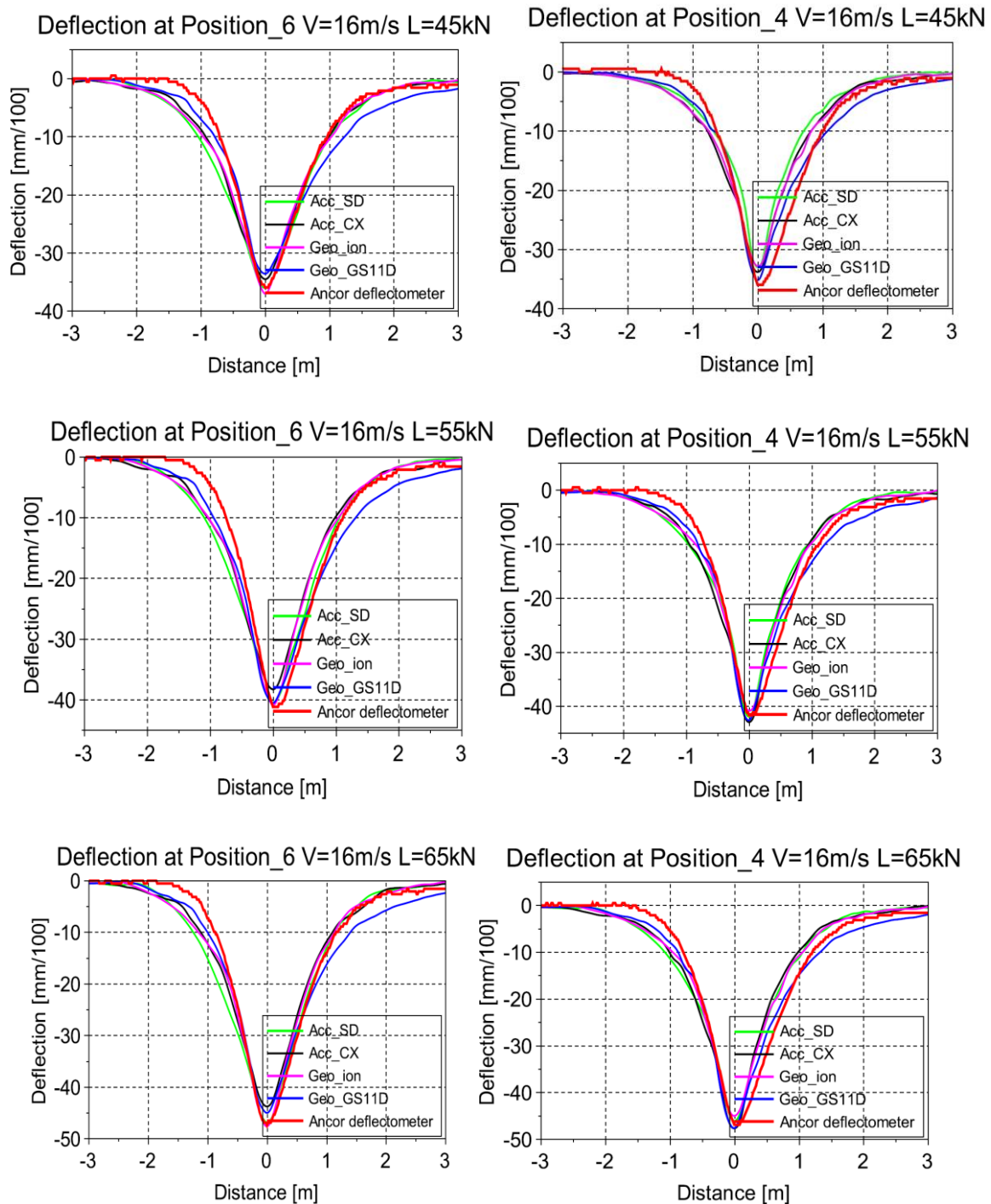


Figure 3-19. Deflection with respect to the different positions of the wheels

Figure 3-20, Figure 3-21 and Figure 3-22 shows the variation of the maximum deflections with different wheel positions and a speed of 16 m/s. For all positions, the results obtained with all the sensors are very similar. The results indicate that the maximum deflection is observed between the positions 4 and 6, which is when the wheels pass over the sensor and between the sensors, and that the deflection decreases as the wheels drive away from the sensors. There is also a slight

dissymmetry in the response, the deflection being higher at position 4 than at position 8. This indicates that the loads applied by the two wheels are not exactly the same (according to the graph the left wheel has a higher load). In addition, the deflections obtained with each sensor are very close to each other, for all positions.

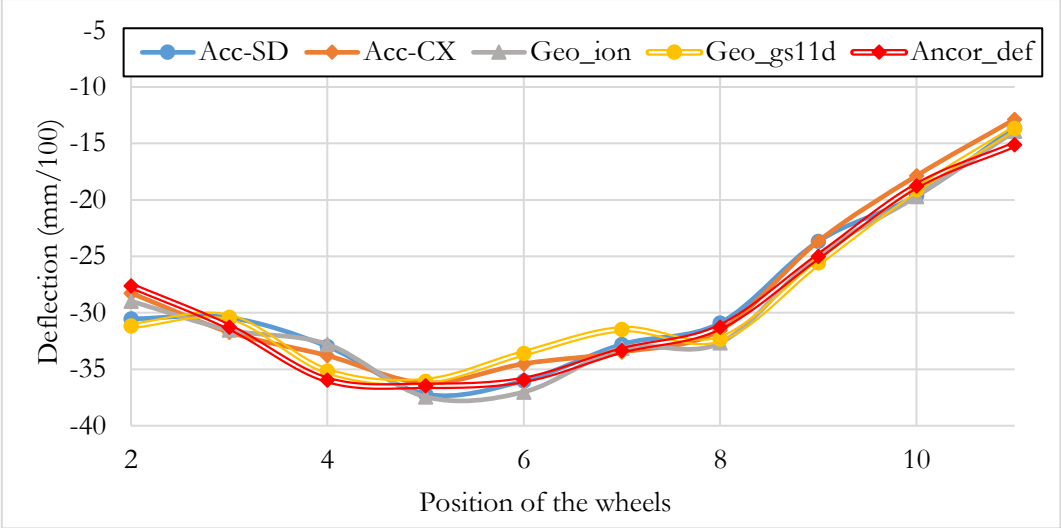


Figure 3-20. Deflection evolution with respect to 45 kN loads, at different wheel positions

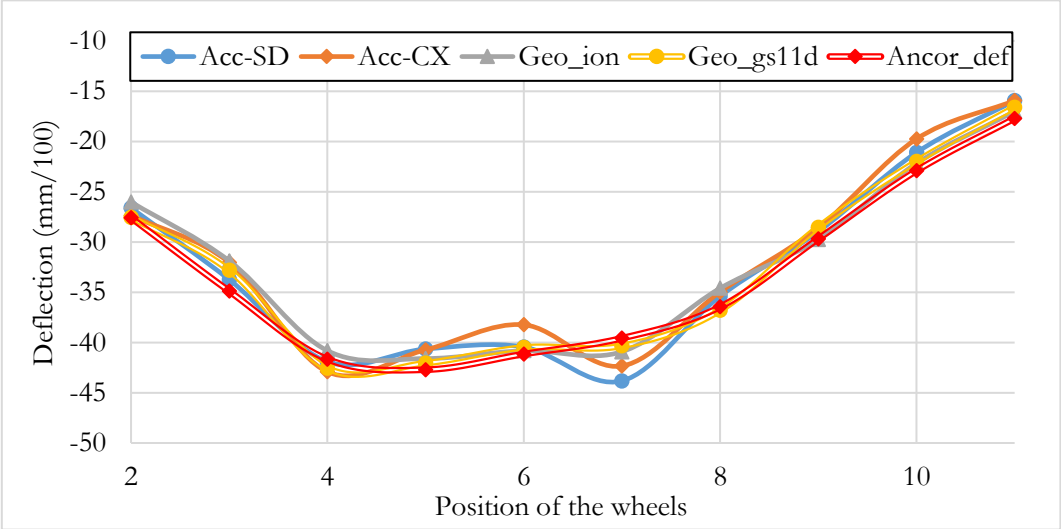


Figure 3-21. Deflection evolution with respect to 55 kN loads, at different wheel positions

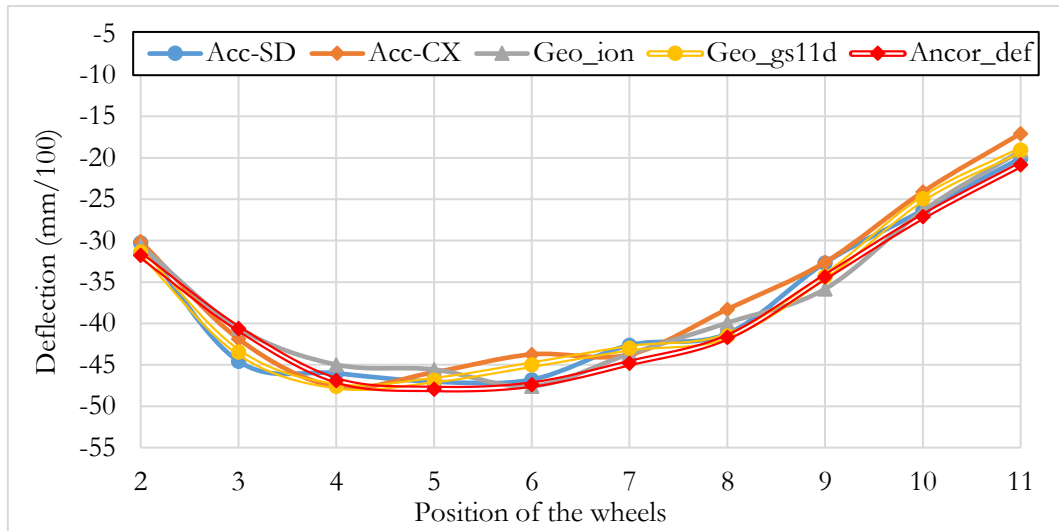


Figure 3-22. Deflection evolution with respect to 65 kN loads, at different wheel positions

### 3.6 Comparison between accelerometers, geophones, and deflectometer sensor

To evaluate more precisely the difference between the anchored deflectometer signal, and the signals of the evaluated sensors, an error indicator R was defined. This indicator considered the entire shape of the experimental signal, and not only the maximum value. The signal is considered from -3m to 3m.

This indicator is expressed by equation (3.3). It is defined as the mean relative difference, in percentage, between the values measured by each evaluated sensor (the two geophones and the two accelerometers) and the reference anchored deflectometer, at each point  $i$  of the signal, divided by the total number of measurement points  $N$  of the signal.

$$R = \frac{1}{N} \sum_{i=1}^N \frac{|Reference\ deflection(i) - sensor\ deflection(i)|}{Max(Reference\ deflection)} \times 100 \quad (3.3)$$

Table 3.6 summarizes the values of the percentages of difference (error indicator R) obtained between the signals of the geophones and accelerometers, and the signals of the reference anchored deflectometer, for the different test conditions. A mean value of error indicator R is also given for the measurements made for the same load level, and different speeds. This gives us an estimate of the accuracy of the measurements for this particular application. It is possible to conclude that:

- The error values are relatively low for all the sensors and test conditions (the highest error is 13.7%).

- The errors are slightly higher for the 45 kN load level than for the 55 kN and 65 kN load levels. A possible explanation is that the tests at 45 kN were performed right at the start of the APT test, and that some post compaction, and movement of the transducers may have occurred during these first load cycles, and affected the accuracy of the measurements.
- For the 55 kN and 65 kN load levels, mean error values for all the transducers are similar, and very satisfactory (between 3.55 and 5.03 %). This validates the original signal treatment procedure used for the calculation of deflections.

Table 3.6 relative difference in percentage for 45, 55 and 65 kN loads

| LOAD 45 kN<br>& SPEED (m/s) | ACC-SD  | ACC-CX  | Geophone-<br>ion | Geophone-<br>GS11D |
|-----------------------------|---------|---------|------------------|--------------------|
| 6                           | 7.78 %  | 12.27 % | 9.36 %           | 7.28 %             |
| 8                           | 7.95 %  | 7.70 %  | 5.44 %           | 11.54 %            |
| 12                          | 13.74 % | 9.90 %  | 6.87 %           | 11.13 %            |
| 16                          | 6.30 %  | 5.86 %  | 5.93 %           | 4.70 %             |
| 20                          | 6.07 %  | 6.21 %  | 5.50 %           | 5.52 %             |
| Mean                        | 8.37 %  | 8.39 %  | 6,62 %           | 8.03 %             |
| LOAD 55 kN<br>& SPEED(m/s)  | ACC-SD  | ACC-CX  | Geophone-<br>ion | Geophone-<br>GS11D |
| 6                           | 4.52 %  | 9.39 %  | 4.49 %           | 4.59 %             |
| 8                           | 2.76 %  | 2.51 %  | 2.89 %           | 4.71 %             |
| 12                          | 4.33 %  | 4.54 %  | 3.63 %           | 3.39 %             |
| 16                          | 4.19 %  | 4.31 %  | 3.75 %           | 4.39 %             |
| 20                          | 3.71 %  | 4.40 %  | 3.28 %           | 3.60 %             |
| Mean                        | 3.90 %  | 5.03 %  | 3.61 %           | 4.14 %             |
| LOAD 65 kN<br>& SPEED(m/s)  | ACC-SD  | ACC-CX  | Geophone-<br>ion | Geophone-<br>GS11D |
| 6                           | 2.65 %  | 6.25 %  | 2.66 %           | 3.84 %             |
| 8                           | 3.24 %  | 3.64 %  | 2.25 %           | 2.84 %             |
| 12                          | 4.86 %  | 4.27 %  | 4.69 %           | 2.70 %             |
| 16                          | 4.84 %  | 5.15 %  | 4.63 %           | 4.11 %             |
| 20                          | 4.09 %  | 4.52 %  | 3.54 %           | 4.73 %             |
| mean                        | 3.94 %  | 4.77 %  | 3.55 %           | 3.64 %             |

### 3.7 Conclusion

In a second phase of the study, the sensors have been tested under real moving wheel loading, on the IFSTTAR accelerated pavement testing facility. They have been tested under different test conditions (wheel loads, speeds and wheel positions). The same signal treatment method has been applied as in the laboratory, and the measurements have been compared with those of an anchored deflectometer, taken as reference. In all cases, a good match has been obtained between deflection values measured with the geophones and accelerometers, and the reference, with similar error levels

for all the sensors, proving that the 4 types of sensors are suitable for the measurement of deflections on real pavements.

There is also good agreement with the modelling of the pavement response both with elastic and viscoelastic models.

The next step is to use the deflection basins obtained from the accelerometer and geophone measurements to back-calculate pavement layer moduli, using the Alize pavement design software, which includes a back-calculation tool. This type of back-calculation is standard for the analysis of FWD tests, and the objective is to verify if realistic back-calculated moduli can also be obtained with the sensors, indicating that the measured deflection basins are sufficiently accurate to carry this type of analysis, and to monitor pavement layer moduli.

# CHAPTER 4 CALCULATION OF PAVEMENT LAYER MODULI

|   |            |
|---|------------|
| <b>Chapter 4 Calculation of pavement layer moduli .....</b>   | <b>132</b> |
| 4.1 Introduction .....  | 133        |
| 4.2 Pavement material and properties.....   | 134        |
| 4.3 Methodology of back-calculation of the mechanical properties of the pavement .....              | 135        |
| 4.4 Modelling and back calculation with <i>Alize</i> .....  | 135        |
| 4.4.1. Calculation scenario .....   | 135        |
| 4.4.2. Estimation of Pavement layer moduli .....  | 136        |
| 4.5 Modelling and back-calculation with <i>Ellea</i> .....  | 141        |
| 4.5.1. Calculation scenario .....   | 141        |
| 4.5.2. Optimization of layer moduli with <i>ELLEA</i> .....   | 142        |
| 4.5.3. Comparison of measurements and model prediction and estimation of pavement layer moduli .... | 142        |
| 4.6 Comparison of the two back-calculation approaches.....  | 148        |
| 4.7 Conclusion.....   | 150        |

## 4.1 Introduction

This chapter focuses on the development of a method for identifying asphalt pavement layer properties based on the deflection measurements obtained from accelerometers and geophones, using the signal treatment procedures developed in chapter 2. The measurements that will be used in this chapter are those of the sensors embedded near the ride surface, in the accelerated pavement fatigue carousel experiment described in chapter 3.

These sensors are relatively small in size and easily embeddable, making them an ideal choice for wide-area applications in the live transportation network. As described in chapter 3, a section within the IFSTTAR accelerated pavement testing (APT) facility was instrumented with accelerometers and geophones; an anchored displacement sensor was also installed to serve as a reference/validation device. The APT facility offers the ability to control the loading configuration and intensity, travel speed, and wander (i.e., lateral offset) position relative to the sensor locations. Thus, it becomes possible to isolate the task of layer property identification through inverse analysis from other real-world complications.

After the description of the experimental setup and the signal processing of the data from APT tests in chapter 3, the next step is to investigate the application of near-surface single-axis geophones and accelerometers to determine pavement layer properties. The considered geophones and accelerometers measure, respectively, the vertical velocity and vertical acceleration of the pavement ride surface resulting from a passing vehicle.

Assuming a layered-elastic model, two methods are proposed and demonstrated in this chapter for estimating the pavement moduli. These methods are based on best-matching of measured deflections, velocities and accelerations for the deflectometer, geophones and accelerometers (respectively) with the calculated responses.

A classical approach for determining pavement layer moduli consists in using a back-calculation method based on the analysis of deflection basins. This method is frequently used to analyse FWD measurements, and is implemented in the ALIZE pavement design software. Here, this method was applied to the geophone and accelerometer measurements. The sensor signals were first integrated with respect to time (once for the geophones and twice for the accelerometers), in order to arrive at deflections. Then, the deflection basins were used to back-calculate pavement layer properties, using Alize. Then, a second method was used to best match the measured sensor responses with the model predictions, without integrating the signals to convert them into deflections. This method consists in using the elastic model to calculate the vertical velocities and accelerations at the pavement surface, and then directly matching these calculated values with the

sensor measurements. The advantage of this approach is that it completely avoids the need for integration, and is therefore well suited for noisy signals. An iterative optimization procedure can be used to adjust the model parameters and determine the sought layer properties. In this chapter both methods are applied to analyse the geophone and accelerometer measurements made on the IFSTTAR accelerated pavement testing (APT) facility as a means of back-calculating the elastic moduli of the pavement layers. The quality of the results is checked against measurements made with an anchored displacement sensor, and also with layer moduli back-calculated from FWD measurements.

## 4.2 Pavement material and properties

The modelling is carried out with experiment data of the Accelerated pavement test at different test settings as explained in chapter 3. The pavement structure consisted of two asphalt concrete (AC) layers, with a total thickness of 11 cm and a 30 cm thick 0/20 mm granular subbase, overlaying a clayey-sandy soil subgrade extending to a depth of 3 m and resting on a 20 cm concrete slab which is supposedly fixed. Laboratory complex modulus tests have been performed on the AC, characterizing the material across different temperatures and frequencies. FWD tests and Benkelman beam measurements have also been performed, giving an average elastic modulus of 110 MPa for the subgrade, and 145 MPa for the granular layer.

Measurements made on the 22 m long instrumented section, at different speeds and position are used to model the mechanical properties of the pavement. The back-calculation could be used to follow the evolution of the modulus with temperature.

Table 4.1. Characteristics of the pavement structure

| <b>Pavement Layer</b>           | <b>Thickness (cm)</b> | <b>Modulus (MPa)</b>                      |
|---------------------------------|-----------------------|---|
| Bituminous material<br>concrete | 11                    | 9441(15°C and 10Hz)<br>9038(15°C and 8Hz) |
| Granular base                   | 30                    | 145                                       |
| Subgrade                        | 260                   | 110                                       |

### **4.3 Methodology of back-calculation of the mechanical properties of the pavement**

The objective is to propose a non-destructive approach, based on the sensor measurements, to determine the elastic stiffness of each layer using the technique of back-calculation. The approach consist in using the measured responses (deflection basins, vertical velocity and vertical accelerations) and proposing an iterative approach for matching the measurements with the calculated response of the pavement generated by a pavement design software or tool. By continuously monitoring the pavement, it will thus be possible to follow the evolution of the layer properties under the effect of traffic and climatic conditions.

In the back-calculation approach, modeling of the pavement response is performed using a linear elastic model, with bonded interfaces. Two different software will be used, Alize and then ELLEA, which offers the possibility to calculate directly the displacements, and also the velocities and accelerations. Both softwares are described in chapter 1 of the thesis, devoted to the bibliography. For each software, different modeling cases are successively considered, corresponding to different loading conditions (load levels, loading speeds, and wheel positions).

### **4.4 Modelling and back calculation with Alize**

#### **4.4.1. Calculation scenario**

The first procedure used for the back-calculation of pavement layer moduli is based on the linear elastic pavement design software ALIZE. This software is used to calculate the response of the experimental pavement (Table 4.1) under the APT dual wheel loading, and the corresponding deflection basin. This theoretical deflection basin is then compared with the measured basin, obtained by processing and integrating the accelerometer or geophone signals. An iterative method is used to adjust the layer moduli, until the best match between the calculated and measured response is obtained.

The methodology used for the optimization of the layer moduli is the following:

- The initial characteristics of the pavement (layer thicknesses, initial layer moduli) are entered in Alize.
- The characteristics of the wheel load are entered in Alize.
- The measured deflection basin is discretized into a certain number of points (17 points) to be inputted in the software.

- Lower and upper limits are defined for the moduli of each layer, for the optimization process, (the values used are given in Table 4.2).
- Successive pavement response calculations are carried out, adjusting successively the layer moduli, until the best match between the calculated and measured deflections, and thus the best estimate of the pavement layer moduli is obtained.

#### 4.4.2. Estimation of Pavement layer moduli

To evaluate the back-calculation method, measurements made during the APT test at speeds of 16m/s and 20m/s, a temperature of 19°C and for position 6 (sensor placement between the wheels) were used. The initial moduli and thicknesses of the pavement layers used for the calculations are defined in Table 4.1.

The loading considered was the 65 kN dual wheel load of the APT tests. The deflection signals are those presented in Figure 3-11 (chapter 3). For the back-calculations with Alize, only half of the deflection basins are considered, and the deflection basin of each sensor has been described by a series of points, represented by the red dots on Figure 4-1. Points located at the same distance are considered for the geophones and accelerometers, and for the deflectometer. In the calculations, the maximum and minimum attainable modulus values have been limited for each layer, as shown in Table 4.2. These limits are needed to facilitate the convergence, and avoid getting unrealistic solutions. The final back calculated moduli are defined in Table 4.4 and Table 4.5, they are obtained using the measurements of all the different sensors at two speed limits of 16m/s and 20m/s.

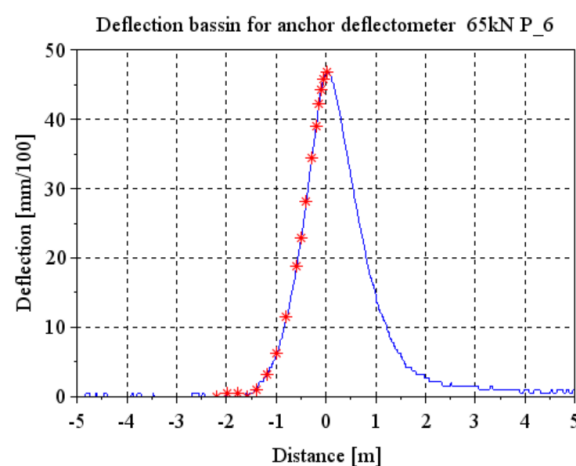


Figure 4-1. Deflection points selected on the deflection basin for the back calculation with Alize

Table 4.2. Limit values of layer moduli defined for the back calculation

| <b>Pavement layer</b> | <b>Lower modulus limit (MPa)</b> | <b>Upper modulus limit (MPa)</b> |
|-----------------------|----------------------------------|----------------------------------|
| E1                    | 8000                             | 12000                            |
| E2                    | 100                              | 200                              |
| E3                    | 50                               | 150                              |

Figure 4-2, Figure 4-3, Figure 4-4, Figure 4-5 and Figure 4-6 represent the fitted deflection basins obtained with Alize, and compare them with the measured deflections. On each figure, the blue lines represent the measured values, and the orange lines are the adjusted calculated deflection curves. A global error indicator is defined, R, characterizing the relative difference (in percent) between the model response and the reference values (measured sensor response). This indicator calculates the pointwise difference between the two signals, divided by the absolute maximum value of the measured response as defined in Equation 4.1, where N is the total number of reference points.

$$R = \frac{1}{N} \sum_{i=1}^N \frac{|Reference\ value\ (i) - Calculated\ value(i)|}{Max(Reference\ deflection)} \times 100 \quad (4.1)$$

The R indicator is calculated to quantify the difference between the measured and calculated responses. Table 4.3 shows the differences in percentage for all the sensor at speeds of 16m/s and 20m/s. For the two geophones and accelerometers, a very good fit is obtained between the measured and calculated deflections. For the anchored deflectometer, however, comparatively larger differences between the measured and calculated basins are obtained after the optimization. The difference is 2.4 % for 16m/s and 6.6 % for the speed of 20m/s, as presented in Table 4.3. For the speed of 16m/s, the minimum difference is observed with the geophone Ion, and for the 20m/s speed Geophone GS11D shows better results. Overall, the geophones give slightly better fitting of the curves, with minimum error values R (N. Bahrani et al., 2020).

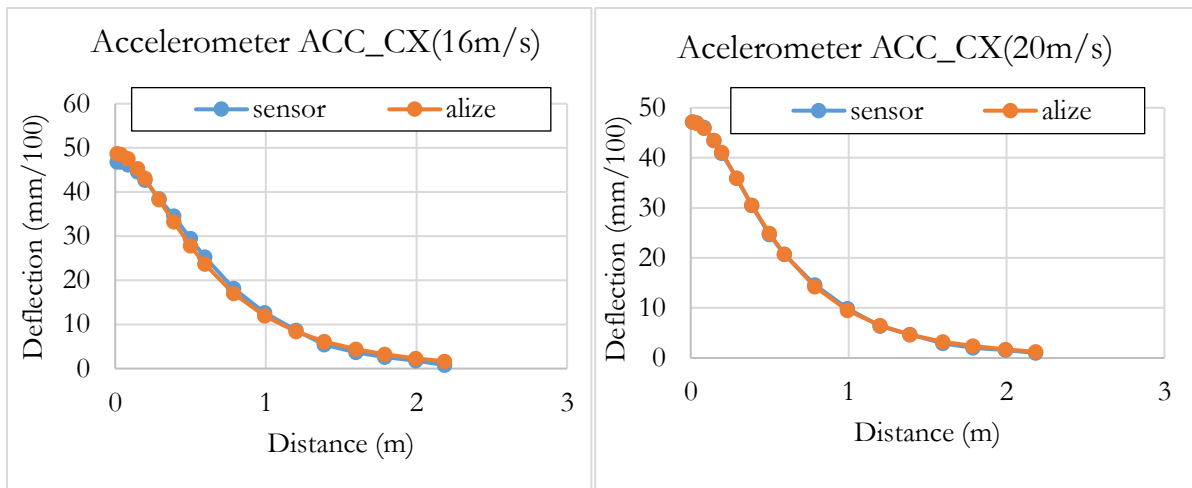


Figure 4-2. Deflection fitting for Accelerometer CX for 65kN dual wheel load (a) Speed:16m/s  
(b) Speed:20m/s

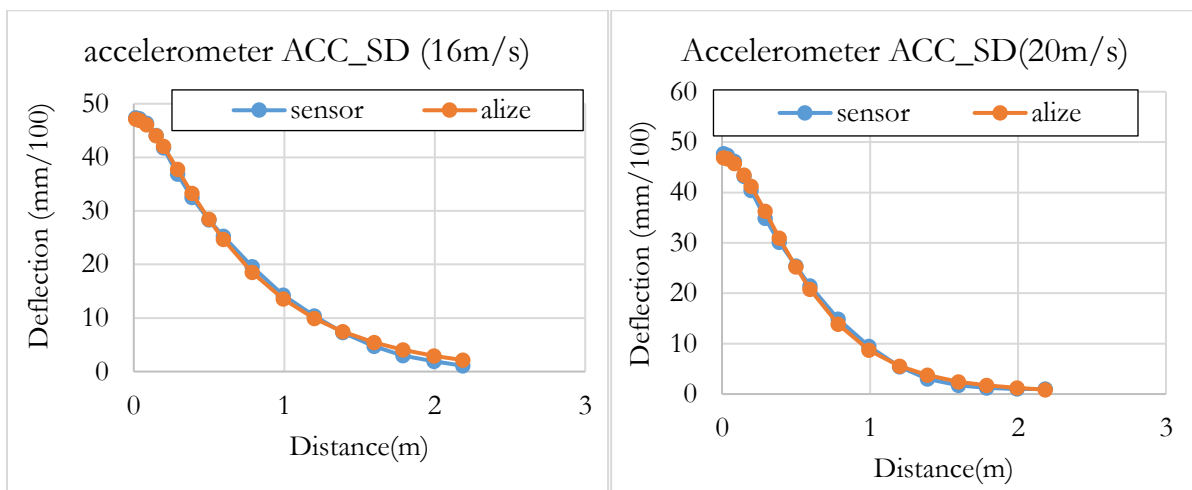


Figure 4-3. Deflection fitting for Accelerometer SD for 65kN dual wheel load (a) Speed:16m/s  
(b) Speed:20m/s

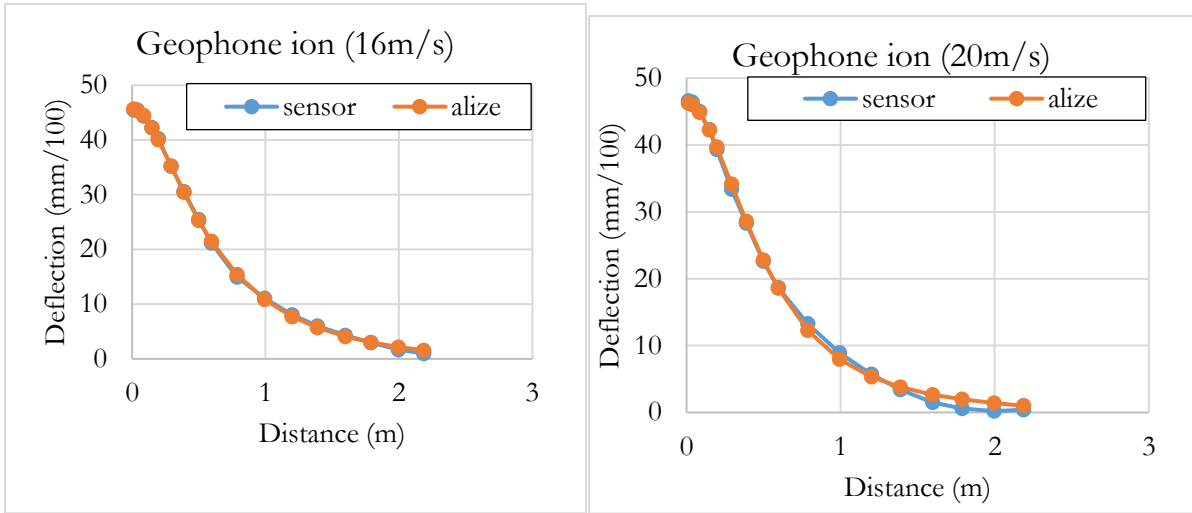


Figure 4-4. Deflection fitting for Geophones ION for 65kN dual wheel load (a) Speed:16m/s (b) Speed:20m/s

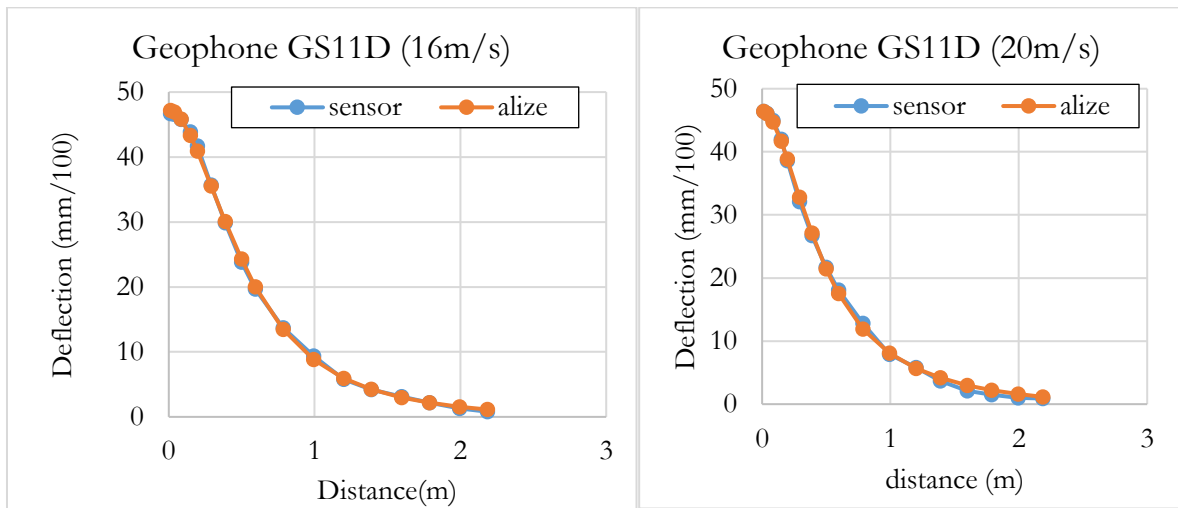


Figure 4-5. Deflection fitting for Geophones GS11D for 65kN dual wheel load (a) Speed:16m/s (b) Speed:20m/s

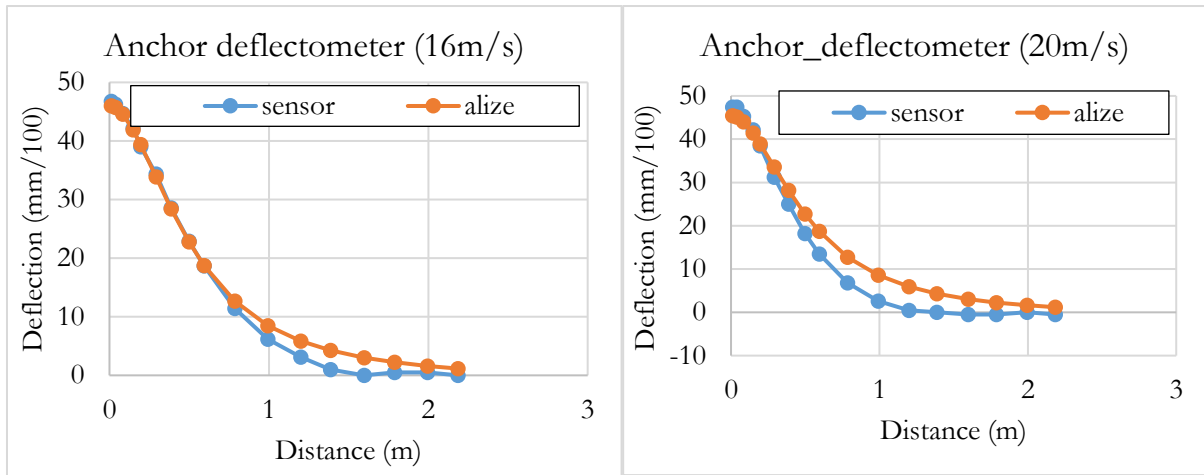


Figure 4-6. Deflection fitting for Anchored deflectometer for 65kN dual wheel load (a) Speed:16m/s (b) Speed:20m/s

Table 4.3. Relative Differences between the measured and calculated responses

|                     | Anchor Deflectometer | Accelerometer SD | Accelerometer CX | Geophone Ion | Geophone GS11D |
|---------------------|----------------------|------------------|------------------|--------------|----------------|
| Difference at 16m/s | 2.4%                 | 1.24%            | 2.0%             | 0.5%         | 0.64%          |
| Difference at 20m/s | 6.6%                 | 1.3 %            | 0.35 %           | 1.2%         | 0.88%          |

The pavement layer moduli back-calculated for each transducer, at two speeds, are given in Table 4.4 and Table 4.5. These are compared with the reference modulus values obtained previously, from laboratory tests and FWD measurements (Table 4.1). In this first example, all the sensors give realistic modulus values, which are close to the reference moduli. For the asphalt layer modulus, the maximum difference with the reference is about 2500 MPa. For the granular layer and soil, the maximum difference with the reference is 40 MPa. These first results are encouraging, and show that, with the developed signal treatment method, realistic deflection values, and realistic back-calculated moduli can be obtained using the geophones and accelerometers.

Table 4.4. Back calculated pavement layer moduli obtained with ALIZE for the different sensors, and comparison with reference values 16m/s.

| Pavement layer | Reference Moduli (MPa) | Anchored deflectometer (MPa) | ACC-SD(MPa) | ACC-CX(MPa) | Geophone-ion(MPa) | Geophone-GS11D(MPa) |
|----------------|------------------------|------------------------------|-------------|-------------|-------------------|---------------------|
| Asphalt layer  | 9038                   | 8285                         | 11549       | 11556       | 10133             | 10001               |
| UBG            | 145                    | 139                          | 151         | 143         | 182               | 108                 |
| Soil           | 110                    | 127                          | 97          | 95          | 101               | 126                 |

Table 4.5. Back calculated pavement layer moduli obtained with ALIZE for the different sensors and comparison with reference values 20m/s.

| Pavement layer | Reference Moduli (MPa) | Anchored deflectometer (MPa) | ACC-SD(MPa) | ACC-CX(MPa) | Geophone-ion(MPa) | Geophone-GS11D(MPa) |
|----------------|------------------------|------------------------------|-------------|-------------|-------------------|---------------------|
| Asphalt layer  | 9441                   | 8520                         | 10681       | 10357       | 9115              | 8007                |
| UBG            | 145                    | 144                          | 102         | 118         | 110               | 123                 |
| Soil           | 110                    | 126                          | 123         | 117         | 138               | 139                 |

## 4.5 Modelling and back-calculation with Ellea

### 4.5.1. Calculation scenario

In this second approach, the analysis of the deflection sensor, geophone and accelerometer measurements is based on the use of the multilayer linear elastic pavement calculation software ELLEA1(ver0.96), developed by Levenberg (2009). The approach consists in using the software to calculate the vertical displacement, vertical velocity and vertical acceleration at the position of each sensor, and matching the model predictions with the sensor measurements. For that purpose, an iterative procedure is used to adjust the model parameters (the pavement layer moduli), until the best match between the modelling results and the measurements is obtained. The final set of moduli corresponds to the estimated moduli of the pavement layers. This modelling methodology is successively applied to the deflection sensor, the geophones and the two accelerometers, and the pavement layer moduli obtained with each sensor will be compared.

#### **4.5.2. Optimization of layer moduli with ELLEA**

For the pavement modelling, the initial characteristics considered for the pavement layers (elastic modulus and thickness of each layer) are those given in Table 4.1. Characteristics of the pavement structure except for the AC modulus which was adjusted according to the real test temperature and frequency. The wheel loading is 65 kN and the dual wheel load distribution described in chapter 3 was considered for the simulation, assuming circular contact areas. The Poisson ratio for all layers was set to 0.35, and the tire-pavement contact stress to 0.6 MPa. The vertical displacements are calculated over a horizontal distance of approximately 5m from the center of the load.

The optimization method, to determine the pavement layer moduli, is similar for all the sensors, and is based on the following steps:

- Computing the pavement response (vertical displacement) with the modelling software for a passing wheel.
- Calculating vertical velocities and accelerations by numerical derivation (finite difference formulas).
- Comparing the computed response traces to the measured traces.
- Finding the best match between the two responses by adjusting iteratively the modulus parameters of the pavement.
- The procedure allows obtaining a “best estimate” of the pavement layer moduli. Only the modulus values of the pavement model are adjusted in the optimization process, the other parameters are fixed.

#### **4.5.3. Comparison of measurements and model prediction and estimation of pavement layer moduli**

The optimization procedure described above was applied to the measurements made in the APT experiment using the different sensors, for different loading conditions (different load levels, loading speeds and load positions). The data presented in this chapter correspond to measurements made at an average temperature of 18°C in the AC layers, and speeds of 16 m/s and 20 m/s (corresponding to AC layer moduli of 9038 MPa at 16m/s and 9441 MPa at 20 m/s). The sensors were placed in the center of the wheel path, between the dual wheels represented in Figure 3-3 of chapter 3. For each load condition, measurements were made during several successive load applications, but for the modelling, dual wheel load signal was considered. The duration of the signal was about 1 s to 1.5 s, corresponding to about 500 to 600 recorded measurement points.

A global error, calculating the difference between the measured response and the responses calculated by the Ellea tool are indicated.

This difference is then minimized by optimizing the modulus values of the model to obtain the best match of the calculated and measured values. The minimization is carried out using the Solver which is the gradient optimizer in Excel (Fylstra, 1998). In the solver, maximum and minimum attainable modulus values are fixed for each layer, as represented in Table 4.6 to avoid getting unrealistic solutions. The choice for these bounds can be considered inconsequential, as long as they surround the optimal solution.

Table 4.6. Limits of layer moduli for the optimization of the back calculation

| <b>Pavement Layer</b> | <b>Min Modulus<br/>(MPa)</b> | <b>Max Modulus<br/>(MPa)</b> |
|-----------------------|------------------------------|------------------------------|
| Bituminous layer      | 8000                         | 12000                        |
| Granular base         | 100                          | 200                          |
| Subgrade              | 50                           | 150                          |

The different signals selected for the comparison with the ELLEA model predictions are presented in Figure 4-7, Figure 4-8, Figure 4-9, Figure 4-10 and Figure 4-11. Each graph represents the response measured by one sensor (displacement sensor, geophone or accelerometer), under the passage of the moving dual wheels at 16 m/s or 20 m/s, and the corresponding predicted values, before and after optimization. Positive values represent downwards displacements, velocities and accelerations.

The displacement signals (Figure 4-7) indicate a positive deflection when the wheel is approaching, and then a return to zero when the wheel drives away. The measured displacement signal is not completely symmetrical, most probably due to the viscoelastic behaviour of the AC layers (the return to zero is slower). The vertical velocity signals (Figure 4-8) are positive when the wheel approaches, and then negative. The signals obtained with geophone Ion are close to the calculated Ellea signals, indicating a good fit after the optimization.

In these comparisons, it can be noted that the velocity signals of geophone GS11D are not predicted correctly with Ellea (Figure 4-9), and present a significantly different shape from the model results. The signals present two significant positive peaks and one negative peak, which is

different from the calculated velocity signals. This type of behaviour was observed for all GS11D signals at different loadings and speeds. However, after filtering and conversion of the signals into displacements (in section 4.4), the comparisons with the ALIZE calculations were satisfactory. Therefore, the Geophone GS11D signals were omitted from the back-calculation using the Ellea method.

The vertical acceleration signals (Figure 4-10 and Figure 4-11) are first positive, when the wheel is approaching, then negative under the wheel, and then positive again when the wheel drives away. The acceleration signals are also slightly asymmetrical, and present more noise than the other signals, due to the low acceleration levels.

As can be seen in Figure 4-7, Figure 4-8, Figure 4-10 and Figure 4-11, for all sensors (excluding geophone GS11D), the modelling results are in good agreement with the measurements, except that the calculated signals are symmetrical, due to the elastic model used for the back-calculation. After optimization, the match with the measurement is only slightly improved (Bahrani, et al., 2020)

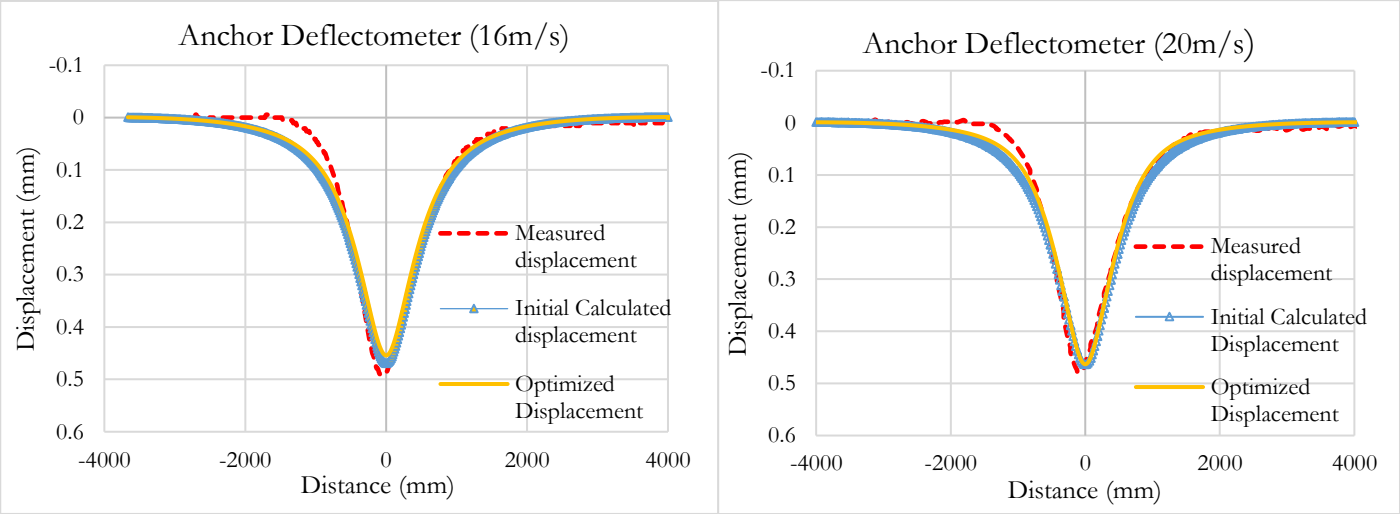


Figure 4-7. Deflection fitting for anchor deflectometer and Ellea model for the speeds of 16m/s and 20m/s

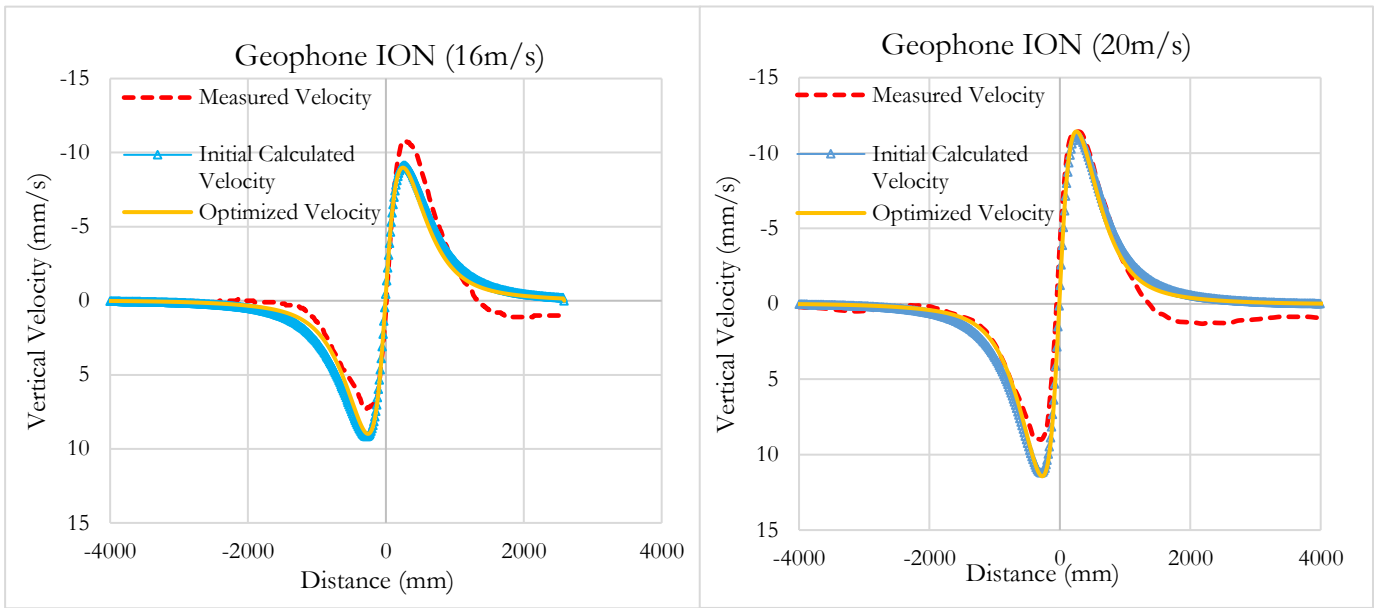


Figure 4-8. Vertical velocity fitting for Geophone ION and Ellea model for the speed of 16m/s and 20m/s

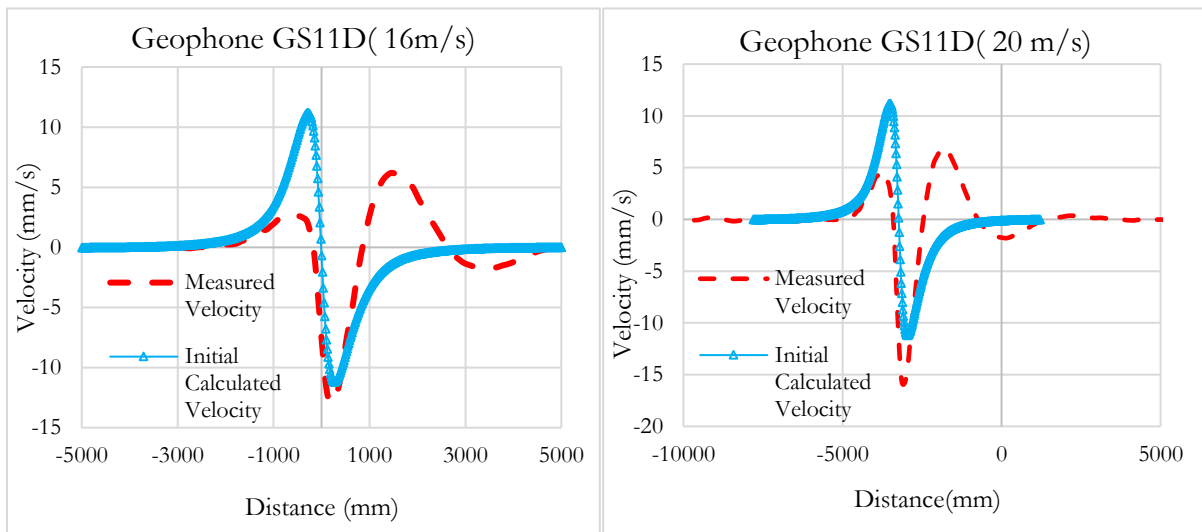


Figure 4-9. Vertical velocity fitting for Geophone GS11D and Ellea model for the speed of 16m/s and 20m/s

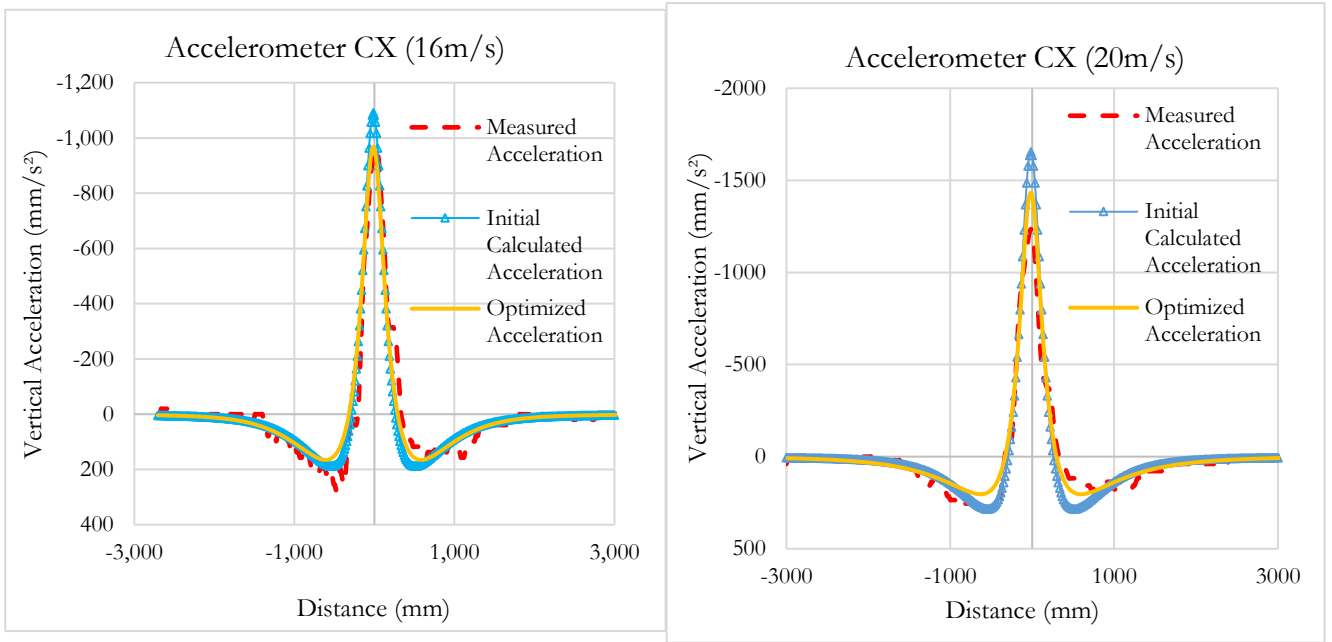


Figure 4-10. Vertical acceleration fitting for accelerometer CX and Ellea model for the speed of 16m/s

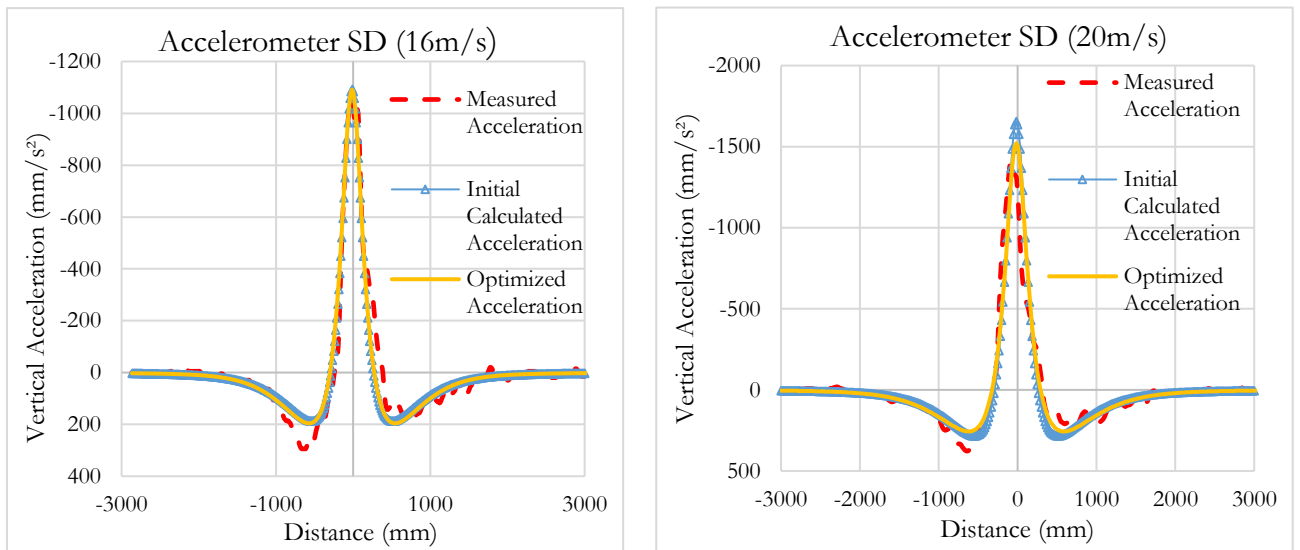


Figure 4-11. Vertical acceleration fitting for accelerometer SD and Ellea model for the speed of 16m/s

The calculated final differences between the optimized modelling results and the measurements (error indicator R equation (4.1)) are summarized in Table 4.7. The lowest differences are obtained with the anchor deflectometer. Compared to the other sensors, geophone ION gives larger differences, of up to 9.5%.

Table 4.7. Relative Differences between the measured and calculated responses

|                        | <b>Anchor<br/>Deflectometer</b> | <b>Accelerometer<br/>SD</b> | <b>Accelerometer<br/>CX</b> | <b>Geophone<br/>Ion</b> |
|------------------------|---------------------------------|-----------------------------|-----------------------------|-------------------------|
| Difference<br>at 16m/s | 2.7%                            | 2.78%                       | 3.1%                        | 9.5%                    |
| Difference<br>at 20m/s | 1.9%                            | 2.36%                       | 2.6%                        | 8.4%                    |

The average modulus values obtained after the optimization are given in Table 4.8 and Table 4.9. The back-calculated moduli of the pavement layers are generally close to the reference values obtained from laboratory tests and FWD measurements. However, in some cases, the calculated modulus is equal to the limit defined in the optimization procedure, which indicates some difficulties to converge. This occurs in particular for the asphalt layer modulus, for accelerometer CX (for the two speeds), and also for the geophone and deflectometer, for the speed of 16 m/s. This seems to indicate that the asphalt layer modulus has a relatively low influence on the calculated solution, for this pavement structure.

Table 4.8 . Modulus values obtained after the optimization compared to the reference, at the speed of 16m/s

| <b>Pavement<br/>Layer</b> | <b>Reference<br/>(MPa)</b> | <b>Deflectometer<br/>(MPa)</b> | <b>Accelerometer<br/>SD (MPa)</b> | <b>Accelerometer<br/>CX (MPa)</b> | <b>Geophone<br/>Ion (MPa)</b> |
|---------------------------|----------------------------|--------------------------------|-----------------------------------|-----------------------------------|-------------------------------|
| Bituminous<br>layer       | 9038                       | 8000                           | 9967                              | 12000                             | 8000                          |
| Granular base             | 145                        | 155                            | 100                               | 100                               | 154                           |
| Subgrade                  | 110                        | 120                            | 122                               | 107                               | 150                           |

Table 4.9. Modulus values obtained after the optimization compared to the reference, at the speed of 20m/s

| Pavement Layer   | Reference (MPa) | Deflectometer (MPa) | Acceleromete<br>r<br>SD (MPa) | Acceleromete<br>r<br>CX (MPa) | Geophone<br>Ion (MPa) |
|------------------|-----------------|---------------------|-------------------------------|-------------------------------|-----------------------|
| Bituminous layer | 9441            | 9500                | 9998                          | 12000                         | 8569                  |
| Granular base    | 145             | 100                 | 100                           | 175                           | 132                   |
| Subgrade         | 110             | 137                 | 101                           | 67                            | 150                   |

#### 4.6 Comparison of the two back-calculation approaches

Two different back-calculation procedures have been used for the calculation of the mechanical properties of the pavement layers, using the studied sensors. The results have shown that both the intrinsic responses of the sensors and the responses after signal processing could be used to calculate the pavement layer moduli. Both modelling tools used for the back-calculation (Alize and ELLEA) are based on multi-layer linear elastic pavement models. With both models, iterative methods were also used to determine the moduli leading to the best fit of the measured response. The main difference is that the Alize method uses deflection basins, whereas with Ellea, the back-calculation procedure is more direct, as it can be applied to deflection basins, vertical velocities and vertical accelerations. This avoids the need to apply a procedure to filter and integrate the sensor signals.

A comparison between the results obtained with the two back-calculation methods, for the two speeds of 16m/s and 20m/s, for the same sensor signals, is presented in Table 4.10 and Table 4.11. This comparison shows that the modulus values obtained with the two methods are in the same range. However, The values obtained with ALIZE seem to be slightly closer to the reference moduli of the different layers, than those obtained with ELLEA, which sometimes reach the limits defined for the back-calculation procedure.

In the previous comparisons, the differences in percentage observed with Alize are in terms of displacement hence it is easier to compare the fitting of all the sensors. The overall percentage difference is found to be under 7% and with geophones and accelerometers it is under 3%. For Ellea the percentage difference among the calculated and measured signals is based on the raw

signal (vertical velocity or acceleration) instead of displacement, and it was indicated to be under 10%. Here the geophones displayed more difference, with a maximum difference of about 9.5%. As the variables are different it is not possible to compare the accuracy with the Alize results. Hence, the comparison is done through the back-calculated moduli only.

Finally, these results confirm that there is great potential in building a pavement condition monitoring system with near-surface accelerometers and geophones. The deflections predicted using these sensors are very realistic, and the sensor measurements can also be used for the back-calculation of layer moduli, as in the case of FWD tests, for instance. The main advantage of the embedded sensors is that they can be used to monitor continuously the evolution of layer properties with time, and thus to detect in real time changes in the pavement response, and pavement damage. By comparison, FWD measurements are only performed at relatively long intervals (ever one or two years).

Table 4.10. Comparison between the modulus obtained with alize and Ellea for all the sensors at 16m/s

|                               | <b>Asphalt layer</b> |       | <b>UGM</b> |       | <b>Soil</b> |       |
|-------------------------------|----------------------|-------|------------|-------|-------------|-------|
|                               | Alize                | Ellea | Alize      | Ellea | Alize       | Ellea |
| <b>Reference (MPa)</b>        | 9038                 | 9038  | 145        | 145   | 110         | 110   |
| <b>Anchored deflectometer</b> | 8285                 | 8000  | 139        | 155   | 127         | 120   |
| <b>ACC-SD(MPa)</b>            | 11549                | 9967  | 151        | 100   | 97          | 122   |
| <b>ACC-CX(MPa)</b>            | 11556                | 12000 | 143        | 100   | 95          | 107   |
| <b>Geophone- Ion</b>          | 10133                | 8000  | 182        | 154   | 101         | 150   |
| <b>Geophone-GS11D(MPa)</b>    | 10001                | N/A   | 108        | N/A   | 126         | N/A   |

Table 4.11. Comparison between the modulus obtained with Alize and Ellea for all the sensors at the speed 20m/s

|                               | Asphalt layer |       | UGM   |       | Soil  |       |
|-------------------------------|---------------|-------|-------|-------|-------|-------|
|                               | Alize         | Ellea | Alize | Ellea | Alize | Ellea |
| <b>Reference (MPa)</b>        | 9441          | 9441  | 145   | 145   | 110   | 110   |
| <b>Anchored deflectometer</b> | 8520          | 9500  | 144   | 100   | 126   | 137   |
| <b>ACC-SD(MPa)</b>            | 10681         | 9998  | 102   | 100   | 123   | 101   |
| <b>ACC-CX(MPa)</b>            | 10357         | 12000 | 118   | 175   | 117   | 67    |
| <b>Geophone- Ion</b>          | 9115          | 8569  | 110   | 132   | 138   | 150   |
| <b>Geophone-GS11D(MPa)</b>    | 8007          | N/A   | 123   | N/A   | 139   | N/A   |

#### 4.7 Conclusion

After conducting several tests with the sensors, under real moving wheel loading, on the IFSTTAR accelerated pavement testing facility, under different test conditions (wheel loads, speeds and wheel positions), the same treatment procedures as in the laboratory tests (chapter 2) have been used for determining pavement deflections. In all cases, a good match has been obtained between deflection values measured with the geophones and accelerometers, and the reference, proving that the four types of sensors are suitable for the measurement of deflections on real pavements. Two methods of back-calculation have been proposed for finding the mechanical properties of the pavement layers.

The deflection basins obtained from the accelerometer and geophone measurements have been used to back-calculate pavement layer moduli, using the Alize pavement design software, which includes a back-calculation tool. Realistic back-calculated moduli have been obtained for all the sensors, indicating that the measured deflection basins are sufficiently accurate to carry this type of analysis, and to monitor pavement layer moduli.

The second back-calculation method was based on the Ellea pavement modelling tool, and on the use of vertical velocity and acceleration signals, instead of deflection signals, to model the pavement response. The measured responses have been compared with calculations performed with the multi-layer elastic model, and a procedure for back-calculation of pavement layer moduli has been

proposed. An error indicator  $R$  has been used to estimate the relative difference between the responses. Slightly better results have been obtained with the deflectometer, however this type of sensor is not very suitable for real road monitoring, due to its high cost and difficulty of installation.

It is planned to perform other tests, on different pavement structures, to further evaluate and improve this back-calculation procedure. However, these first results are very encouraging, and indicate that instrumentation with accelerometers and geophones can be used to determine pavement layer properties.

## CHAPTER 5 TEST SITE EXPERIMENT AND RESULTS

|  |     |
|--|-----|
| 5.1 Introduction .....   | 153 |
| 5.2 Presentation of the instrumented site of motorway Ax .....               | 153 |
| 5.2.1. Test site experimentation .....                                       | 153 |
| 5.2.2. Pavement structure .....  | 154 |
| 5.2.3. Instrumentation .....   | 154 |
| 5.2.4. Presentation of the data acquisition system.....                      | 155 |
| 5.2.5. Application to the instrumented site.....                             | 156 |
| 5.3 Geophone Measurements .....  | 157 |
| 5.3.1. Geophones data recording .....  | 157 |
| 5.3.2. Calculation of Deflections .....                                      | 159 |
| 5.3.3. Examples of integrated signals.....                                   | 160 |
| 5.3.4. Characterisation of heavy vehicle silhouettes.....                    | 161 |
| 5.3.5. Examples of truck signal with different load values .....             | 166 |
| 5.3.6. Calculation of vehicle speeds .....                                   | 167 |
| 5.3.7. Selection of T2S3 truck signals .....                                 | 169 |
| 5.3.8. Effect of geophone position on measured vertical displacements .....  | 170 |
| 5.4 Analysis of the influence of temperature on deflections .....            | 174 |
| 5.4.1. Temperature variations in the experimental section .....              | 174 |
| 5.4.2. Temperature correction.....   | 176 |
| 5.5 Comparison of measured deflections with pavement modelling.....          | 179 |
| 5.5.1. Objectives of the comparisons .....                                   | 179 |
| 5.5.2. Initial back-calculation of pavement layer moduli.....                | 179 |
| 5.5.3. Determination of mean deflection basins.....                          | 180 |
| 5.5.4. Modelling of the deflection basins with ALIZE .....                   | 181 |
| 5.5.5. Evaluation of heavy vehicle loads using deflection measurements ..... | 187 |
| 5.6 Conclusion.....  | 194 |

## **5.1 Introduction**

This chapter presents an application of the instrumentation using geophones to a real road test site. The site was built on motorway Ax, in collaboration with the Colas Company. The purpose of this instrumentation was to study measurements made with different types of sensors, with a continuous data acquisitions system, under real road traffic. The test section was instrumented prior to the start of this thesis, and a large database of measurements was collected, under real traffic. The work presented in this chapter consisted in re-analysing the geophone measurements and temperature measurements, using the signal treatment procedures developed in this thesis.

This chapter thus presents different possible uses of geophones for continuous monitoring of roads and highways. It presents successively:

- The characteristics of the test section and the instrumentation
- The traffic and different traffic statistics obtained using the geophone measurements
- The treatment of the geophones and temperature measurements
- Different applications of the vertical deflection measurements

## **5.2 Presentation of the instrumented site of motorway Ax**

### **5.2.1. Test site experimentation**

In 2013, Colas carried out rehabilitation works on the Ax motorway, and on this occasion, a section of this motorway was instrumented, for monitoring the pavement with geophones, strain gauges and temperature probes. A total of 24 transducers were installed, and a data acquisition system and transmission system was setup, to enable continuous monitoring of the behaviour of the pavement. The system started working in 2014 and after some preliminary tests in March, continuous measurements were carried out from October 2014 to December 2016. However, the data acquisition was interrupted from January to February 2015 and from January to March 2016 due to failure of some data acquisition boards.

In this thesis, a new exploitation of the geophone measurements (and associated temperature measurement) has been performed, with several objectives:

- To determine the silhouettes and speeds of the heavy vehicles
- To calculate vertical displacements (deflections) at the positions of the different geophones
- To analyze the evolution of deflections with temperature and time
- To evaluate pavement layer moduli, and their evolution with time

### 5.2.2. Pavement structure

The instrumented section on the Ax motorway is located at PK 12 (the position of the section is defined by the "kilometre point, PK") in the direction Bayonne-Bordeaux. The rehabilitated pavement structure consists of 3 new layers, built in September 2013 on the existing, 20 years old, road base (see Figure 5-1). The characteristics of the different pavement layers are as follows:

- 2.5 cm thick very thin asphalt concrete, (VTAC)
- 6 cm thick binder course, high modulus bituminous concrete, (HMBC)
- 7 cm thick base course, high modulus Asphalt concrete (HMAC) (EME, or “enrobé à module élevé”).
- 8 cm thick cracked layer of Gravel stabilized with bitumen (GB)
- About 30 cm thick sand-cement treated layer
- Natural sandy subgrade

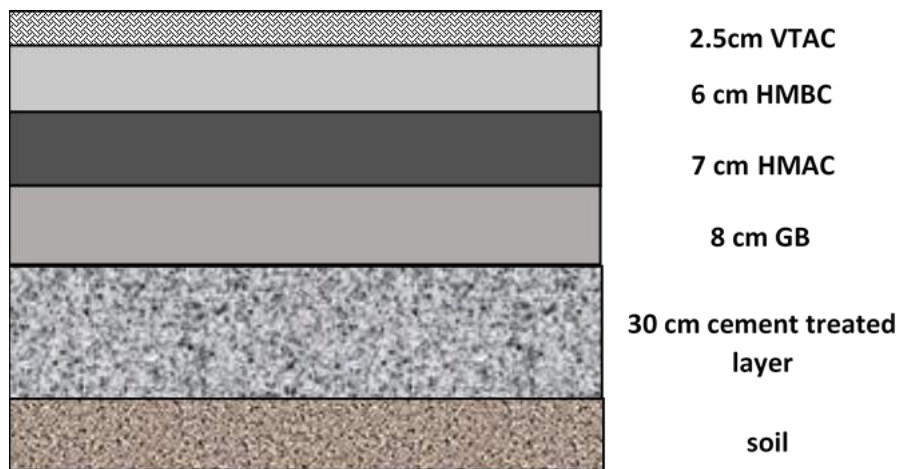


Figure 5-1. Pavement structure of the Ax motorway (Duong et al., 2018)

### 5.2.3. Instrumentation

The experimental section was instrumented with strain gauges, geophones and temperature probes. However, in this work, only geophone and temperature probe measurements are considered. The temperature sensors are of PT100 type and the geophones are of type GS11D 4000, with a closing resistance of 47 k $\Omega$ . These geophones are of the same type as those used in the laboratory tests and accelerated pavement tests presented in chapters 2 and 3. The geophones were installed in the slow lane, in the wheel path close to the emergency lane. The temperature sensors were positioned at the edge of the lane.



100% wireless was not needed as a 220V power supply was available on site. Pegase has DSP (digital signal processing) and input output ports, a 32-bit low power processor optimized to route to RAM and FLASH memories; it also has a WIFI PCMCIA module for wireless communication. The PEGASE mother board is integrated with the Blackfin 537 processor, wireless communication module and a GPS module. For a given application, the mother board is completed by specific daughter boards implementing conditioners selected according to the sensors used, like geophones, accelerometers, strain gauges, temperature Probes. The PEGASE card is Linux kernel based and configured with communication protocols, specified IP (internet protocol) and the global protocol; this allows the Wi-Fi network or 3G/4G connection to have remote sessions. The main advantage of this system is that the developer is able to retrieve the data and modify the acquisition procedures remotely from the platform, without having the need to dismantle or reprogram it physically.



Figure 5-3. PEGASE board (Cam et al., 2008)

### **5.2.5. Application to the instrumented site**

On the instrumented site, the sensors (geophones and temperature probes) are connected by wires to a road side box containing the acquisition system (Figure 5-4 (a)). This box contains the sensor conditioners, the PEGASE boards and a remote transmitter. To allow long term operation regardless of weather conditions, the cabinet is waterproof and has a heating system as shown in Figure 5-4 (b).

The geophones used have a natural frequency of 4.5 Hz and the sampling frequency of the acquisition was fixed at 2000 Hz. For every vehicle passage, a trigger with an adjustable acquisition duration, is used to record the signal. The duration is set by a pre-trigger and post-trigger, and in our application the signals of all the sensors were recorded in total for 10 seconds.

In our application, a threshold was also set for recording the geophone data. The value of this threshold was selected to record only signals corresponding to a minimum deflection of 5mm/100. This makes it possible to limit the number of recordings, by recording only deflections under heavy vehicles with a sufficiently high load, and not under passenger cars. The threshold of 5mm/100 led to record approximately 100 to 160 heavy vehicle passages per day. On the other hand, the

temperature measurements were recorded continuously (without any trigger), at a rate of one measurement every 15 minutes. All the measurements are temporarily stored in the board and transferred automatically every 4 hours to a data server using the 3G/4G network as represented in Figure 5-5.



Figure 5-4 (a): Instrumented site (Duong et al., 2020) (b): Road side box with the peagse boards and transmitters

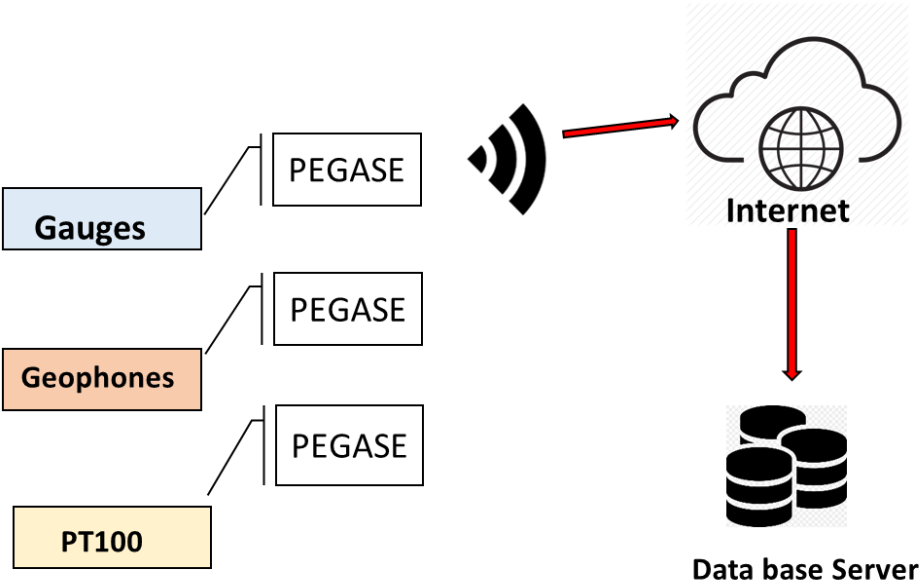


Figure 5-5. Principle of the data acquisition system

### 5.3 Geophone Measurements

#### 5.3.1. Geophones data recording

Geophones measure the vertical velocity at their location in the pavement, due the vehicle passage, as explained in the literature review. In this section, we assess the possibility of using geophones to

measure the vertical displacement or deflection in a real traffic scenario. On the instrumented site, the four geophones were placed at different lateral positions and depths in the pavement, as shown in Figure 5-2. Geophones G1 and G2 were placed 1m apart, at the same depth and lateral position, in order to double the measurements, and also determine vehicle speeds.

The first measurements were made in March 2014, however, the actual data monitoring started later that year. The data collection under real traffic was carried out from October 2014 to December 2016. During this period, on two occasions, data acquisition was interrupted due to malfunctions of the data acquisition system.

As explained in section 5.2.5, a threshold was set to record heavy vehicle signals only, hence the data analysis in this work concerns only heavy vehicles. The total number of files recorded per day is indicated in Figure 5-6. During the first months, the variation of the number of trucks is not only due to traffic variations but also due to change in the threshold setting in data acquisition.

It can also be noted that the average number of files recorded is higher on working days than on weekends, indicating that heavy vehicle traffic is more important on working days, as shown in Figure 5-7.

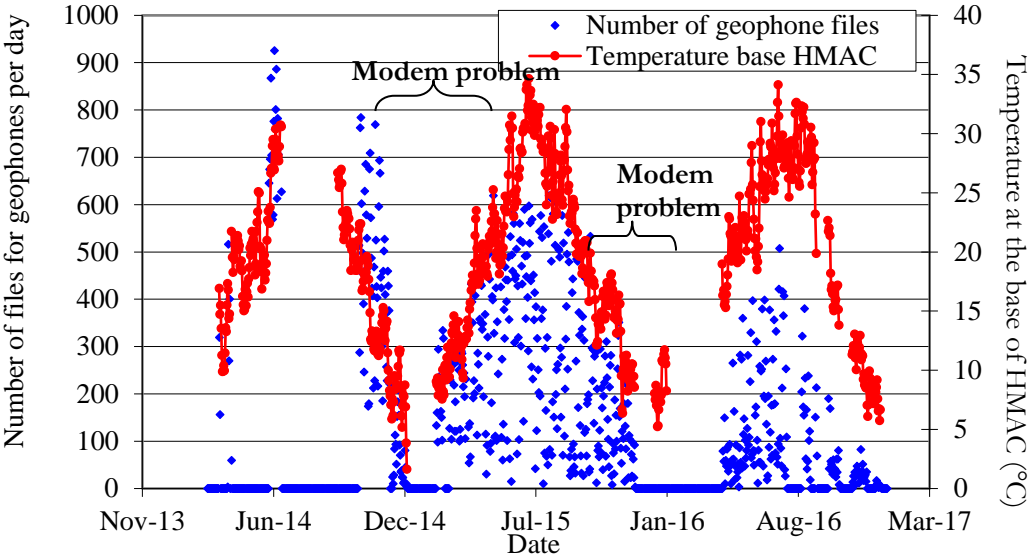


Figure 5-6. Total number of files recorded and average temperature values from 2014 to December 2016.

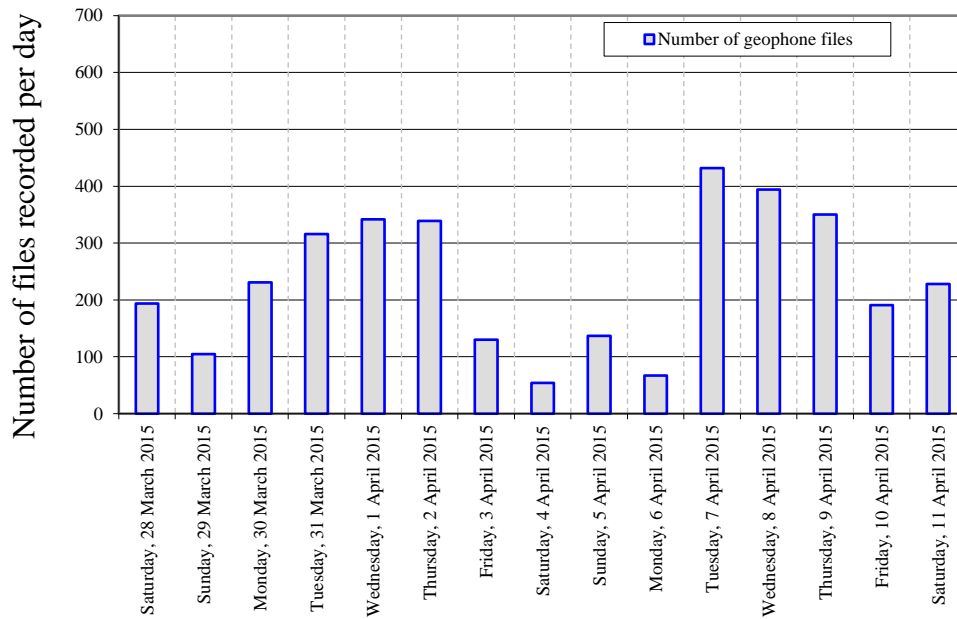


Figure 5-7. Weekly variation of number of recorded vehicle passes

### 5.3.2. Calculation of Deflections

In order to analyse the pavement displacements, the signals of the geophones were treated using the same methodology as developed in chapter 2. The same treatment steps were used: filtering, amplification, integration, and application of the Hilbert transform. To adapt to the frequency and conditions of the road traffic, the cut-off frequency of the high pass filter was set to 8.5 Hz, and an amplification factor of 3 was applied. Figure 5-8 shows the different treatment steps that were taken to convert the signal into a deflection signal. The example in Figure 5-8 corresponds to geophone 1. In this figure (and in all this chapter) negative values correspond to downward displacements.

This signal treatment approach has been implemented to correct all the geophone measurements, and convert their signals into displacements. We have also considered that the vertical displacement measured by the sensors can be considered equal to the surface deflection because the difference between the displacement at the surface and in the HMAC layer is negligible. The deflection basin of the pavement during the passage of the vehicle, depends on the silhouette of the vehicle (number of axles), the axle loads and the speed of the vehicle. For example, the 5 downwards peaks in Figure 5-8 correspond to the passage of a 5-axle semi-trailer vehicle. According to the previous observations, it is possible to propose a first application of the geophone measurements, which consists in detecting and counting the different heavy vehicle silhouettes, and calculating vehicle speeds. However as there is no reference sensor (anchored deflectometer) like in chapter 2 and 3,

it is not possible to compare the signal with a known reference, to estimate the accuracy of the measured displacements.

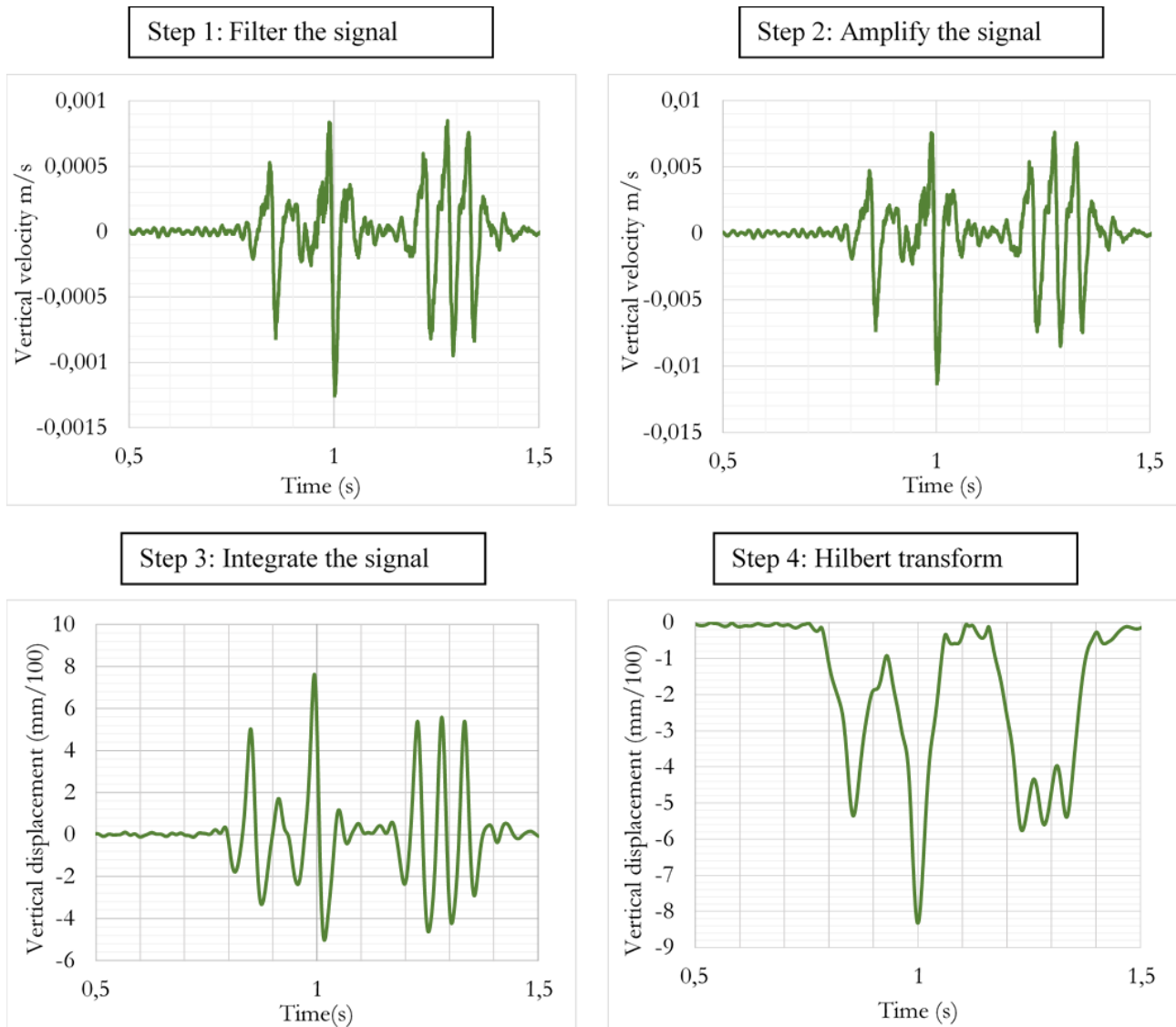
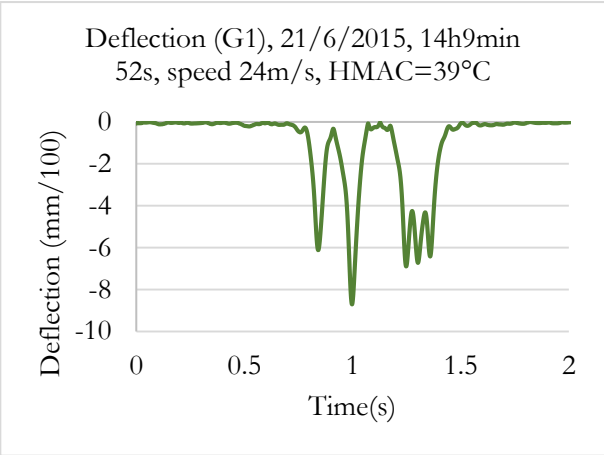


Figure 5-8. Signal treatment procedure, applied to a signal of geophone G1

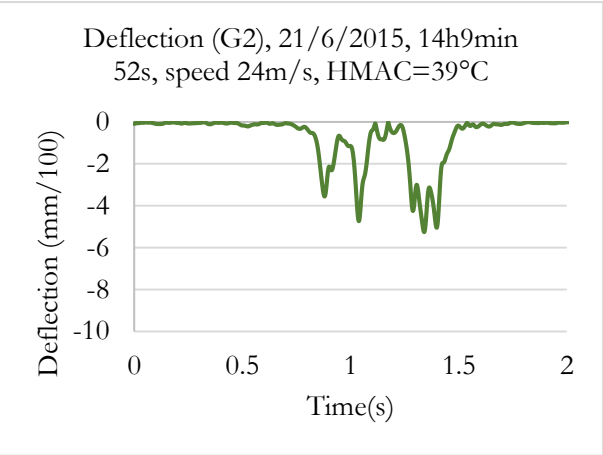
### 5.3.3.Examples of integrated signals

Figure 5-9 shows examples of treated integrated signals of geophones G1, G2, G3 and G4, obtained in June 2015, under the same truck passage. All the geophones give well-defined signals, which correspond to a five axle semi-trailer truck (defined here as T2S3 truck). The maximum amplitude of the displacement is about 8 mm/100. The differences in the deflection signals can be explained by the different positions of the geophones in the pavement. For example, when comparing signals of geophones G1, G3 and G4, which are located at the same depth, but at different lateral positions, it can be seen that the signal of geophone G1 (the central geophone) has

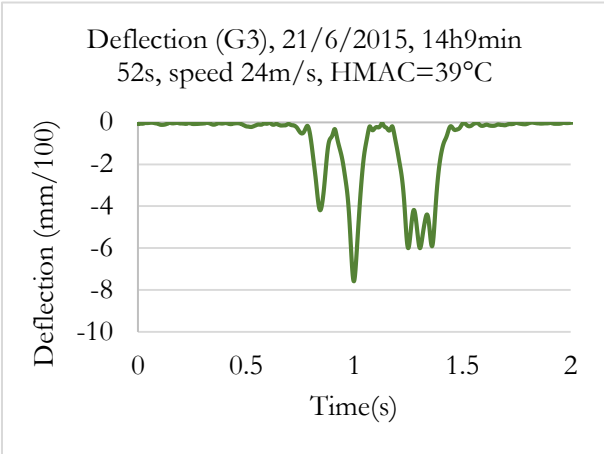
the highest amplitude, which indicates that the wheels of the vehicle are positioned over sensor G1.



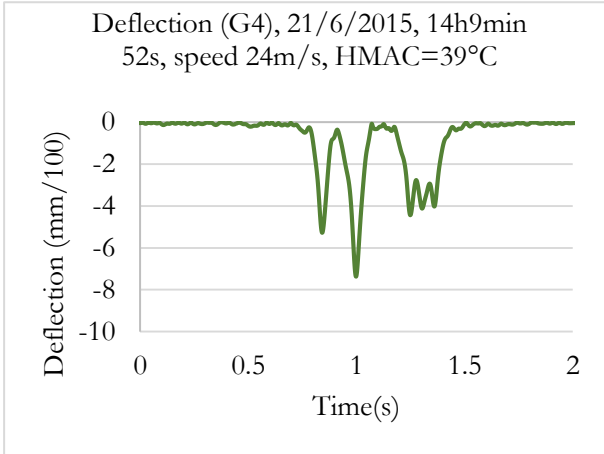
(a) Deflection – geophone G1



(b): Deflection – geophone G2



(c): Deflection – geophone G3



(d): Deflection - geophone G4

Figure 5-9. Deflection signals measured by the four geophones under the passage of the same T2S3 truck – 21 June 2015

**5.3.4.Characterisation of heavy vehicle silhouettes**

As already mentioned, the integrated geophones signals can easily be used to identify heavy vehicle silhouettes, by the number of displacement peaks of the signal, each downward peak corresponding to one axles of the vehicle.

To automate the detection of the peaks, a procedure based on the calculation of the derivative of the displacement has been proposed. The peaks of the signal are detected by the changes of sign

of the derivative. The derivative of the signal is calculated by successive intervals of 20 data acquisition points ( $A_i, \dots, A_{i+20}$ ), in order to eliminate the noise.

$$f'(A_i) = \frac{f(t_{i+20}) - f(t_i)}{t_{i+20} - t_i} \tag{5.1}$$

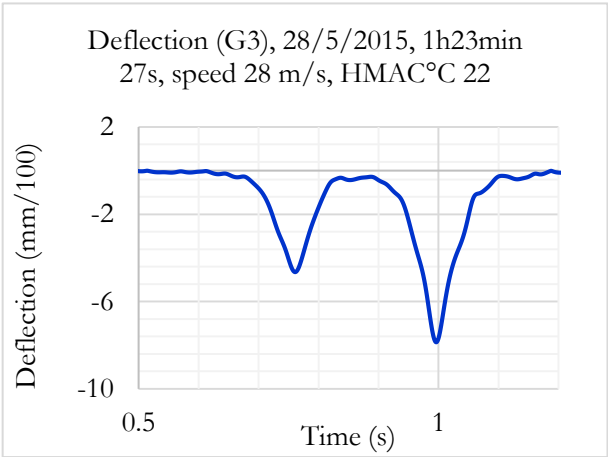
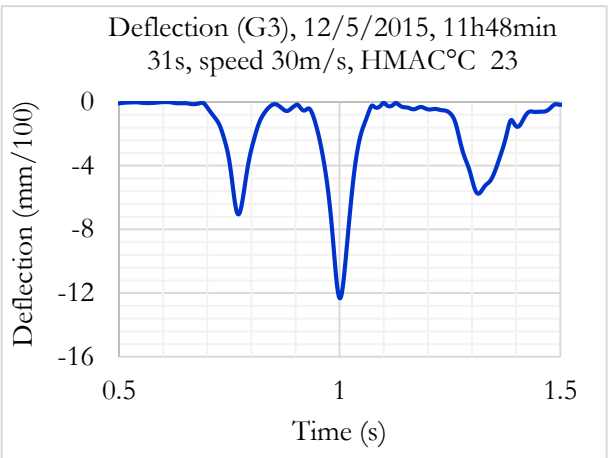
Peak detection is based on the fact that the sign of the derivative of the signal changes when a peak has passed. When the derivative changes from negative to positive, a downward peak, which is assumed to correspond to the passage of a wheel, is detected. A procedure based on this principle was programmed using the Scilab software, to identify 2-axles, 3-axles, 4-axles, 5-axles and 5-axles T2S3 type trucks. The criterion used to identify each type of vehicle is defined in Table 5.1.

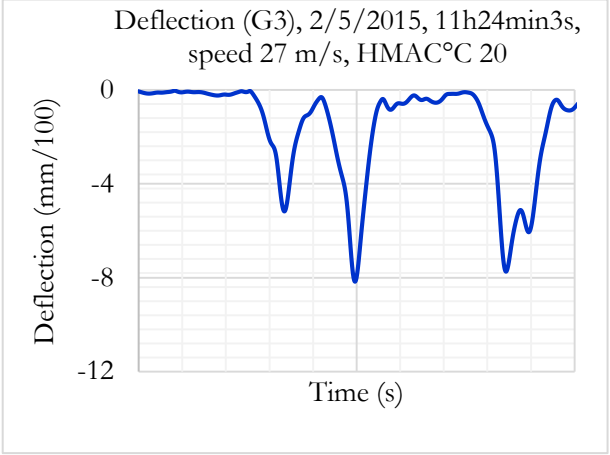
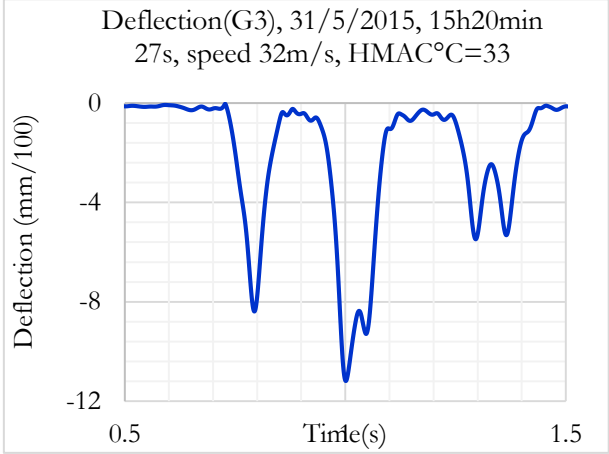
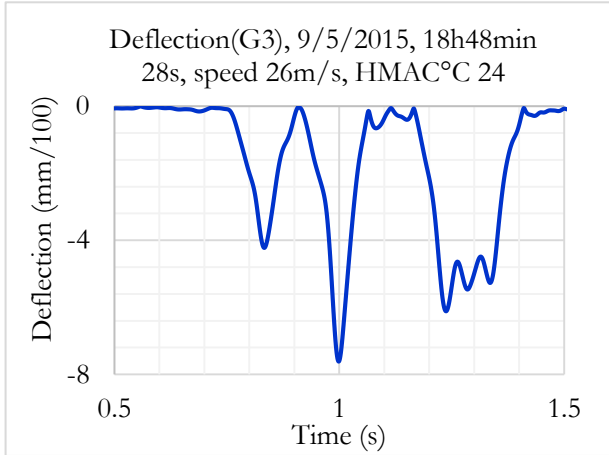
Table 5.1. Identification criteria for different types of trucks

| <b>Heavy vehicle type</b> | <b>Number of downward peaks</b>  |
|---------------------------|--|
| <b>2- axles truck</b>     | 2  |
| <b>3-axles truck</b>      | 3  |
| <b>4-axles truck</b>      | 4  |
| <b>5-axles truck</b>      | 5 peaks, time btw the 3nd and 4th peak > (time btw 4th and 5th peak)*1.2 |
| <b>5-axles T2S3 truck</b> | 5 peaks, time btw the 3nd and 4th peak < (time btw 4th and 5th peak)*1.2 |

Table 5.2 presents examples of signals corresponding to the different types of vehicles. In all the cases, the truck silhouette can be easily identified by the number of downward peaks and their distance.

Table 5.2. Examples of determination of different truck silhouettes using the deflection signals

| S.no | Silhouette of the truck  | Type of load  |
|------|--|---|
| 1    | <p>Deflection (G3), 28/5/2015, 1h23min<br/>27s, speed 28 m/s, HMA°C 22</p>    | <p><b>2-AXLES TRUCK</b></p>    |
| 2    | <p>Deflection (G3), 12/5/2015, 11h48min<br/>31s, speed 30m/s, HMA°C 23</p>  | <p><b>3-AXLES TRUCK</b></p>  |

|   |  |  |
|---|--|--|
| 3 | <p style="text-align: center;">Deflection (G3), 2/5/2015, 11h24min3s,<br/>speed 27 m/s, HMA°C 20</p>    | <p style="text-align: center;"><b>4-AXLES TRUCK</b></p>   |
| 4 | <p style="text-align: center;">Deflection(G3), 31/5/2015, 15h20min<br/>27s, speed 32m/s, HMA°C=33</p>  | <p style="text-align: center;"><b>5-AXLES TRUCK</b></p>  |
| 5 | <p style="text-align: center;">Deflection(G3), 9/5/2015, 18h48min<br/>28s, speed 26m/s, HMA°C 24</p>  | <p style="text-align: center;"><b>T2S3 5-AXLES</b></p>  |

By applying this automated truck-type detection procedure to all the recorded signals, it is possible to determine the composition of the truck traffic, and establish various statistics. Figure 5-10

presents, as an example, the average monthly traffic composition (in terms of different truck silhouettes) observed on the Ax motorway between October 2014 and December 2016. This graph shows that, on this motorway, T2S3 trucks are predominant, and represent around 80 % of the heavy vehicle traffic.

It must be mentioned that as the acquisition system was setup with a threshold, to record only vehicles creating a maximum deflection exceeding 5 mm/100, only the most heavily loaded vehicles were recorded (the exact corresponding load level is not known). This threshold was set to limit the number of signals recorded with the average of 150+ number of good files recorded every day and was thought sufficient to characterize the mechanical response of the pavement. However, by reducing this threshold, it would be possible to detect and count the total truck traffic passing on the motorway.

The accuracy of the identification procedure was verified by inspecting one hundred data files for one month and for that only one file was wrongly identified, indicating an error percentage, corresponding to a wrong detection of the truck silhouettes, of the order of 1 percent. Because the T2S3 semi-trailer trucks represent a large part of the heavy traffic on the motorway, it was decided, for this study, to focus the analysis on the deflection signals of the T2S3 trucks.

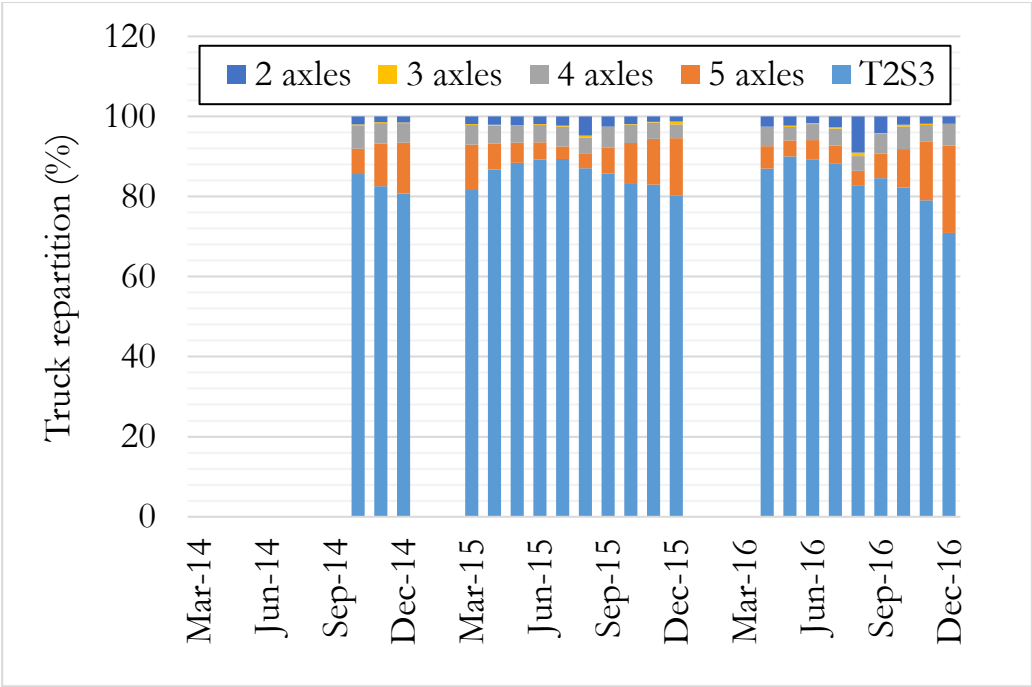


Figure 5-10. Average percentages of different types of heavy vehicles travelling on the Ax motorway, between October 2014 and December 2016

### 5.3.5. Examples of truck signal with different load values

Figure 5-11 represents examples of deflection signals of T2S3 trucks, with different deflection amplitudes, corresponding to different levels of load of the vehicles (low, medium, heavy load), for similar measurement conditions. The values are obtained with geophone G1 on 1/06/2015 and for the maximum and medium loaded vehicles, the speed is 27m/s and the temperature of the HMAC layer is 21.4 °C, for the lower load, the speed is 29m/s and the temperature of the HMAC is 23°C

It can be seen that the first two axles of the truck, which carry the weight of the front body, present similar deflection levels, because they are not much influenced by the weight of the cargo transported by the truck; the deflections under the last three axles, on the contrary, are much more influenced by the transported load, and could help determine the total weight of the truck.

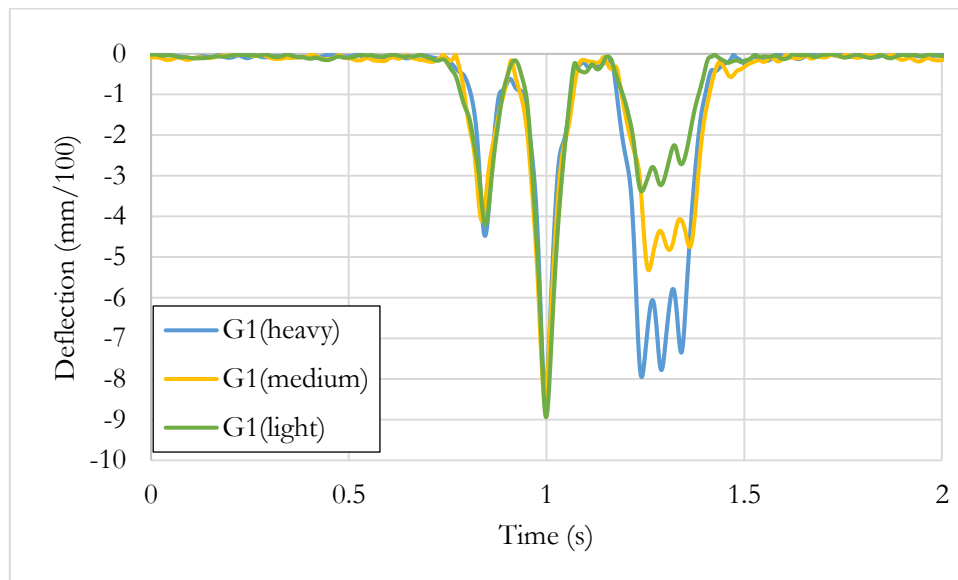


Figure 5-11. G1 deflection signals on 1/6/2015 for 3 vehicles with different loads, for similar speeds and temperatures

Figure 5-12 represent the average values of deflection peaks for each month for T2S3 trucks, recorded with geophone G1. The standard deviation of the deflection values is higher for the last three axles (see the table in annex C). The maximum amplitude is always obtained with the second peak. The evolution of the average deflections also presents important seasonal variations (the deflections are higher in the summer), due to the influence of temperature.

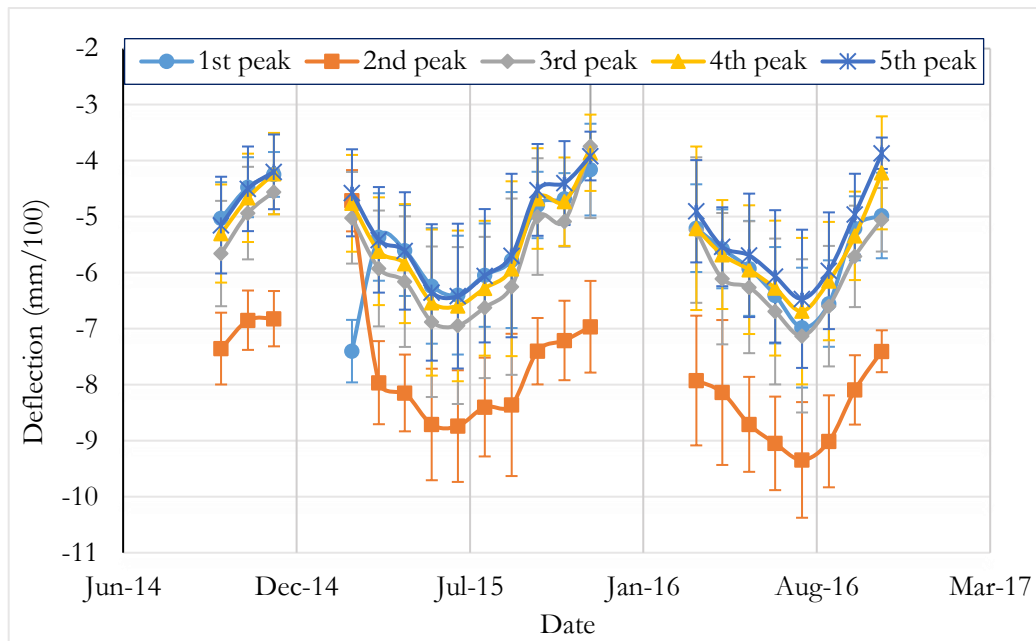


Figure 5-12. Monthly average deflections for each peak (each vehicle axle), obtained with geophone G1 for T2S3 trucks

### 5.3.6. Calculation of vehicle speeds

On the instrumented Ax section, two geophones (G1 and G2) were placed at a longitudinal distance  $D = 1$  meter from each other in the same lateral position, in order to be able to calculate vehicle speeds. Knowing the distance  $D$  between the two sensors, the time difference  $\Delta T$  between the two sensor signals, when a vehicle passes, can be used to calculate the vehicle speed. The interval  $\Delta T$  is determined by the time difference between the minimum values corresponding to the second peak of each sensor signal, as shown in Figure 5-13. This figure shows the signals obtained with the two geophones G1 and G2, placed at a distance of 1 m, and the points used to calculate  $\Delta T$ . knowing the distance  $D$  between the sensors and the time difference, the speed  $v$  of the vehicle is calculated by:

$$v = \frac{D}{\Delta T} \quad (5.2)$$

With:

D: Distance between the two geophones (here 1 m)

$\Delta T$ : Time interval between the responses of the two integrated signals (in seconds)

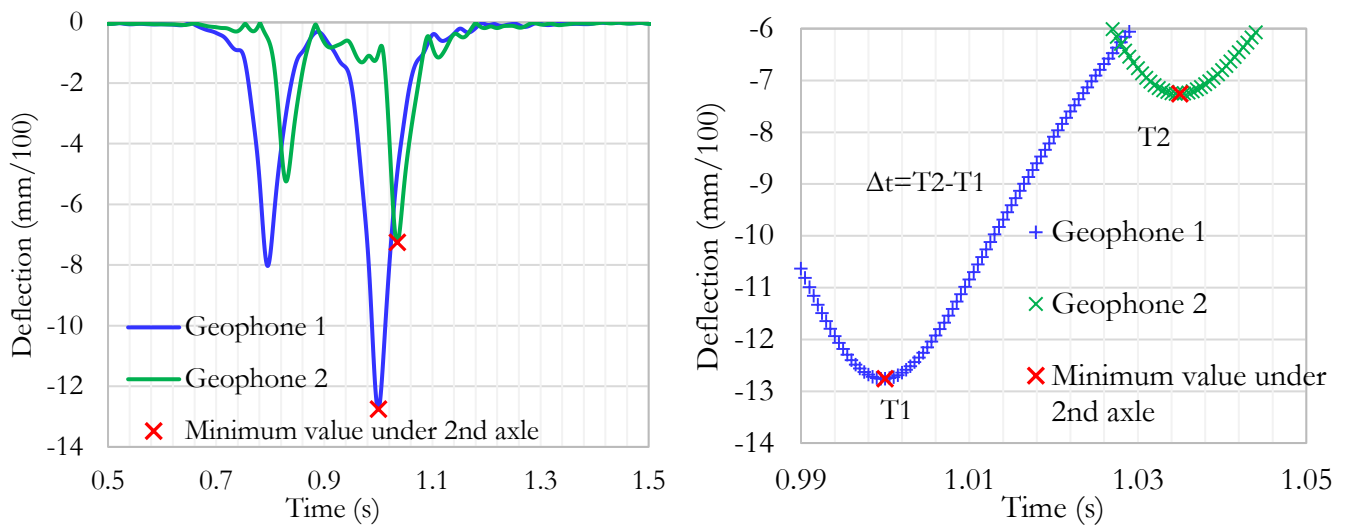


Figure 5-13. Determination of vehicle speed with the peaks of geophones G1 and G2

This procedure was implemented in a Scilab program, and used to calculate the vehicle speed corresponding to each recorded signal. From these values, the average speed of the heavy vehicle traffic, and its standard deviation, was calculated for each month, during the two years of monitoring. The calculated vehicle speeds and their standard deviations are shown on Figure 5-14. The average speed of the heavy vehicles on the Ax motorway, during the whole measurement period, is 96km/h with an average standard deviation of 8 km/h. Knowing the vehicle speeds is also important for comparisons with modelling.

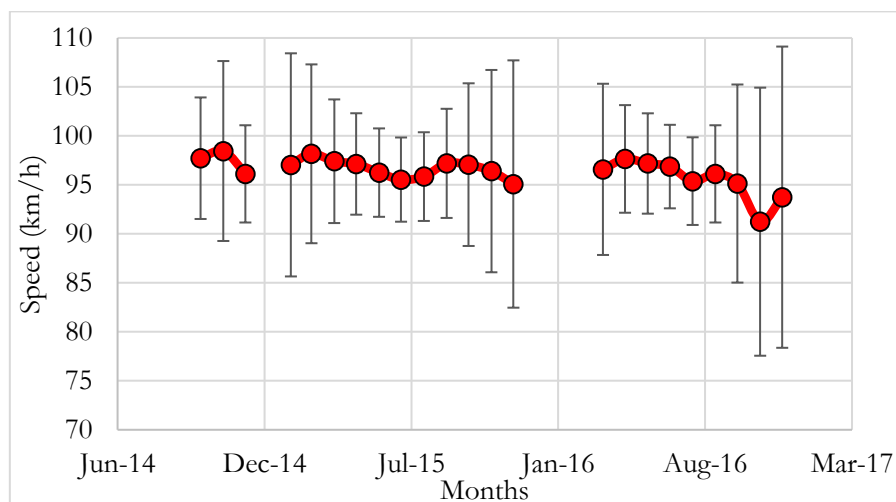


Figure 5-14. Monthly average heavy vehicle speeds on the Ax motorway

### 5.3.7. Selection of T2S3 truck signals

For further analysis of the deflection signals recorded on the Ax motorway, such as determination of mean monthly deflection values, it was decided to use only signals of T2S3 trucks, which represent about 80 % of the heavy vehicle traffic. The total number of recorded geophone signals (per geophone), and the number of signals corresponding to T2S3 vehicles retained for analysis each month are represented in Figure 5-15. The number of selected T2S3 signals varies approximately between 3200 and 10100 per month (during the months without interruption of the acquisition). The highest number of vehicles (highest traffic) is recorded during the summer months.

On the instrumented section, geophones G1, G3 and G4 were placed at the same depth in the HMAC layer, and approximately 15 cm apart in the transversal direction (Figure 5-2). Geophone G1 was assumed to be located in the middle of the wheel path. This arrangement was chosen in order to detect the lateral position of the vehicles, which has a strong influence on the sensor measurements. The position is detected by assuming that the wheels of the vehicle pass close to the sensor giving the maximum deflection amplitude.

Figure 5-16 represents the number of files where the maximum deflection value is recorded with geophones G1, G3 and G4 respectively, for each month. It can be concluded that in most cases, the highest deflection is obtained with geophone G3, which means that most vehicle drive with their wheels close to geophone G3, which is the geophone located on the right of the wheel path, closest to the emergency lane. Less than 20 % of the vehicles drive with their wheels aligned with the central geophone (G1), and only few with their wheels close to geophone G4.

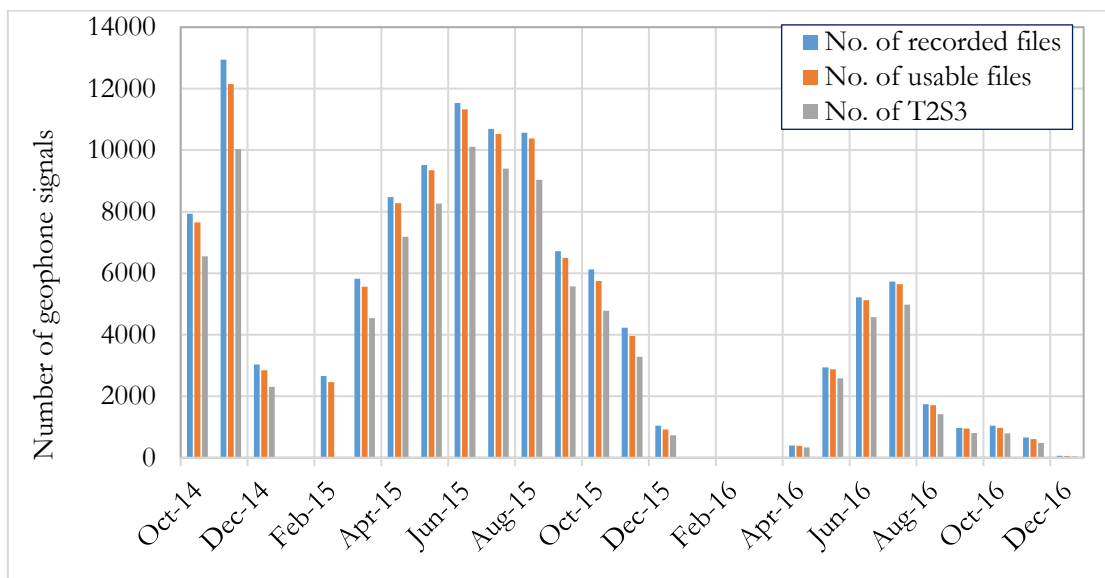


Figure 5-15. Total number of geophone signals recorded on the Ax motorway per month

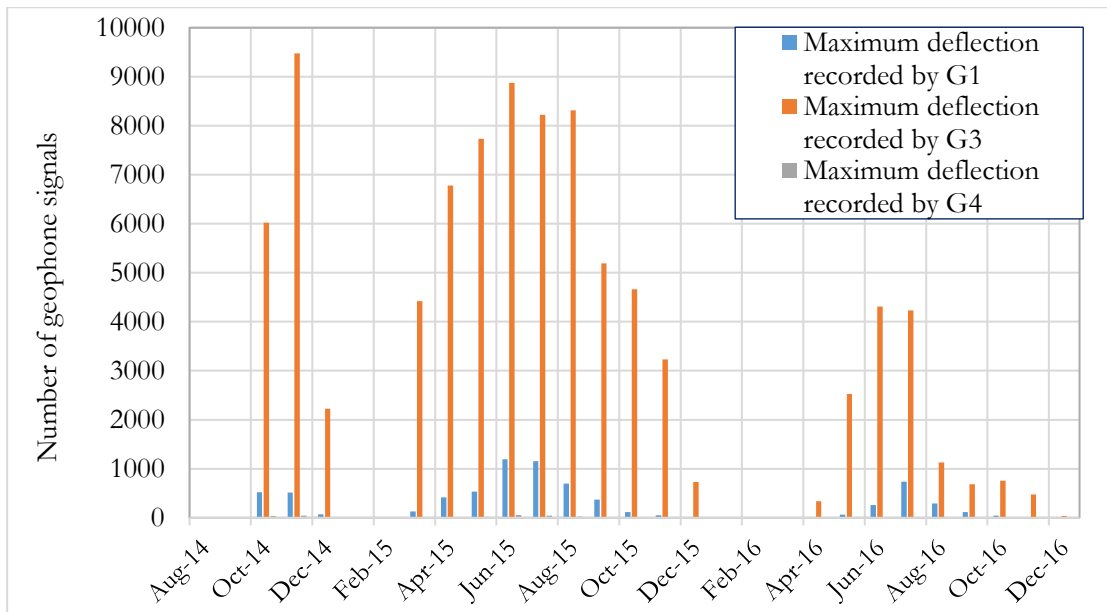


Figure 5-16. Number of files with a maximum deflection recorded by geophones G1, G3 and G4 respectively

### 5.3.8. Effect of geophone position on measured vertical displacements

On the Ax motorway section, geophones were installed at different lateral positions (see Figure 5-2). In particular, 3 geophones (G1, G3 and G4) were placed in the transverse direction, in order to be able to study the lateral wandering of heavy vehicles, as shown in Figure 5-17.

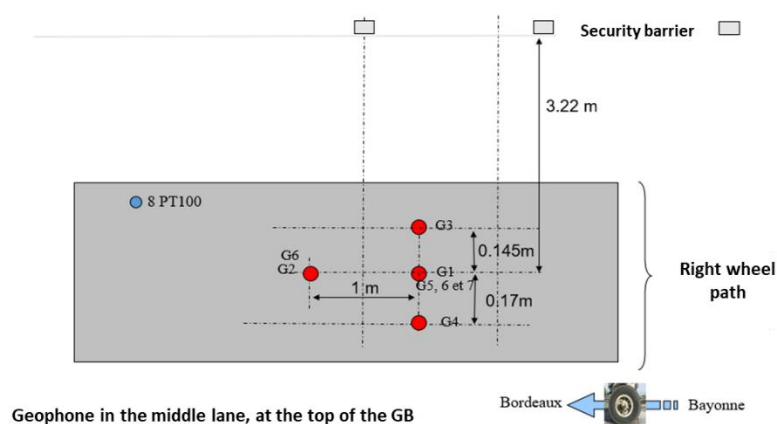


Figure 5-17. Lateral position of the geophones in the wheel path.

Measurements made with these 3 geophones clearly show that the amplitude of the deflections is affected by the lateral position of the geophone, relatively to the vehicle wheels. As also shown in

chapter 3 section 3.5.2 (Figure 3-19), the maximum amplitude of the deflection is obtained when the wheel is positioned directly over the sensors. Hence it is convenient, for the analysis of deflection basins, to consider the geophone giving the maximum deflection amplitude.

To illustrate the influence of the lateral position of the wheels, Figure 5-18, Figure 5-19 and Figure 5-20 present cases where the wheels are located above geophones G3, G1 and G4 respectively. The results of the analysis of all the data indicate that maximum amplitudes of deflection are obtained most frequently for geophone G3 (for about 80 % of vehicles), less frequently for geophone G1, and rarely for geophone G4 (as already shown on Figure 5-15). This indicates that most heavy vehicles drive with their right wheels close to the emergency lane, where geophone G3 is located.

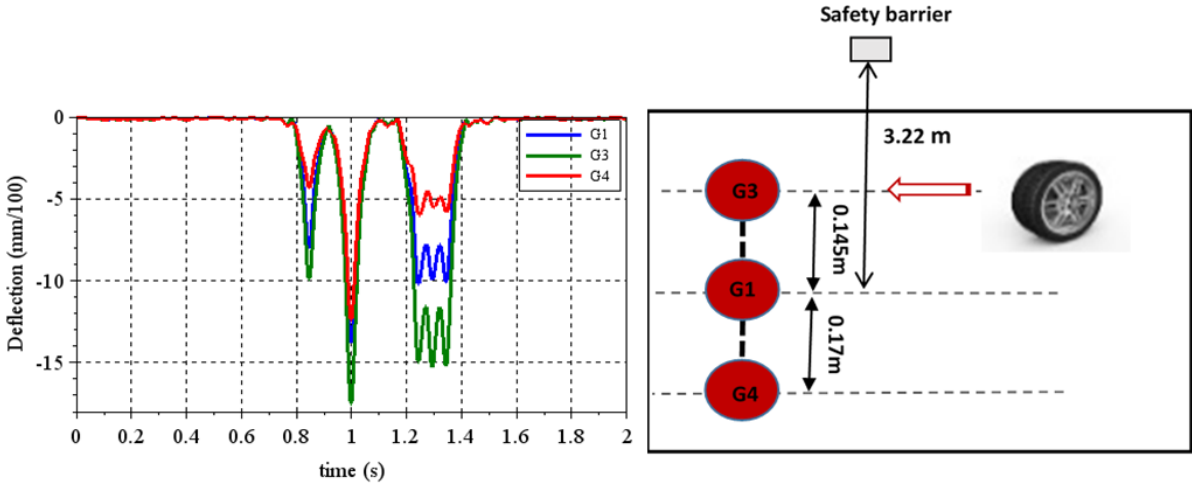


Figure 5-18. Example of deflection signals when the wheels are passing close to geophone G3

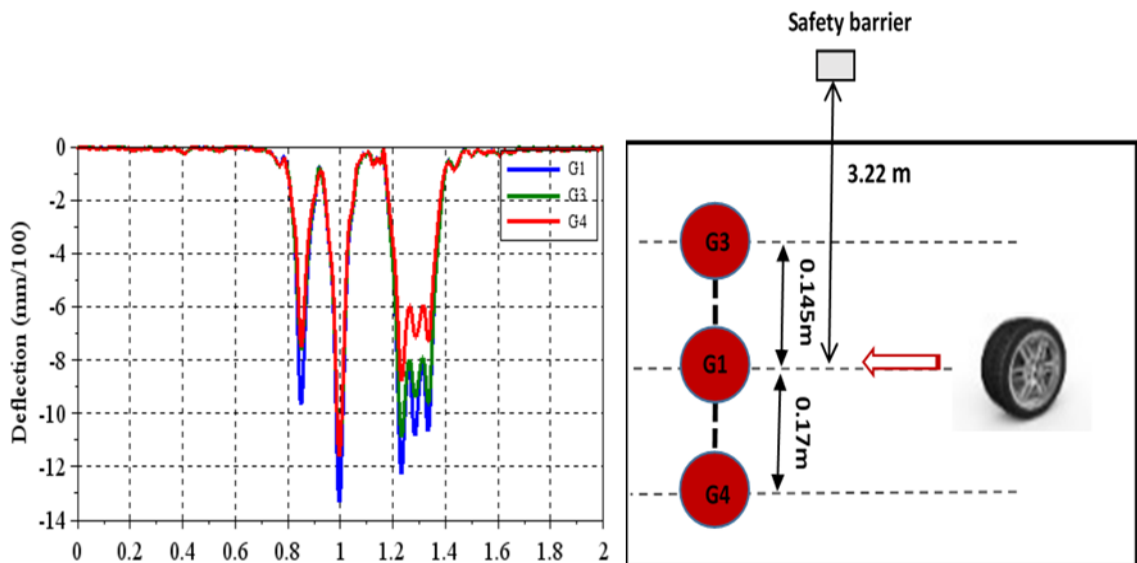


Figure 5-19. Example of deflection signals when the wheels are passing close to geophone G1

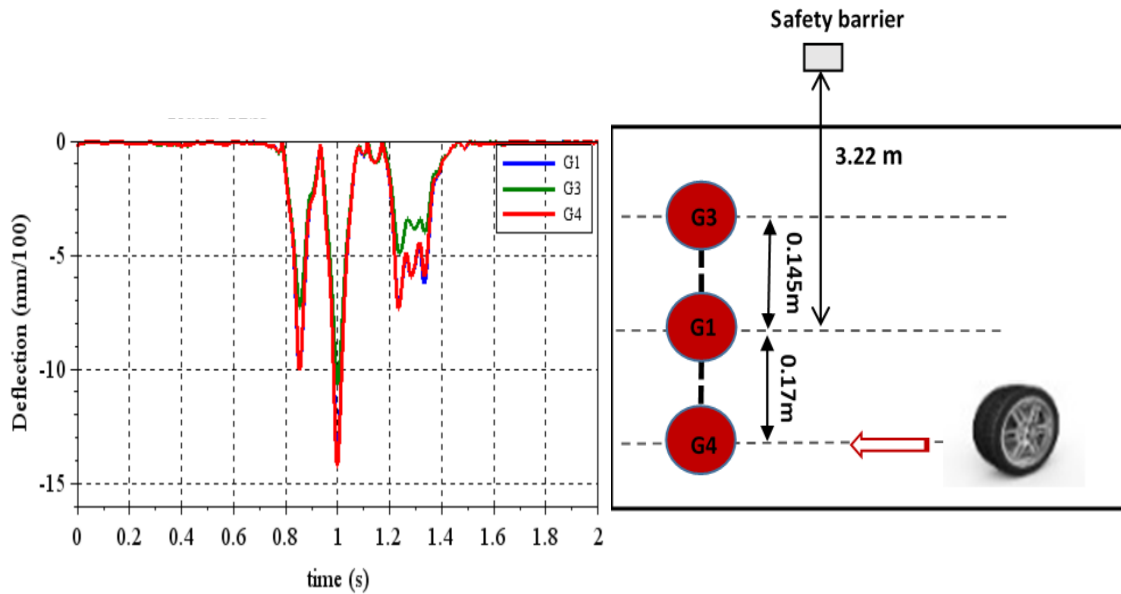


Figure 5-20. Example of deflection signals when the wheels are passing close to geophone G4

To study the evolution of deflections with time on the Ax motorway, a first simple approach was used, which consisted in calculating monthly average values of deflection, for the three geophones G1, G3, and G4, using all the T2S3 heavy vehicle signals. These monthly average values of deflection are shown on Figure 5-21 and Figure 5-22, which present respectively the deflection amplitudes obtained for the 1<sup>st</sup> peak of the signals (corresponding to the first axle of the vehicles) and for the 2<sup>nd</sup> peak (corresponding to the second axle). These figures indicate the following trends:

- The highest average deflection values are obtained for geophone G3; those of geophone G1 come second, and those of geophone G4 are the smallest. As already discussed, these differences can be explained by the lateral positions of the vehicles, which drive mostly with their wheels close to G3.
- For all geophones, the deflections under the second axle (Figure 5-22) are higher than those under the first axle; this is logical, since on T2S3 trucks, the second axle generally carries the highest load.
- For all geophones, the monthly average deflection values present important seasonal variations, due to temperature variations. The deflections increase significantly in the summer, when the pavement temperatures increase, and decrease in the winter, when the pavement temperatures decrease. These variations are due to the high sensitivity to temperature of bituminous materials. Due to these effects of temperature, it is difficult to determine if there is any long-term variation of deflections, due for instance to pavement

damage. For this reason a procedure for temperature correction of deflection measurements is proposed in the next section.

- Geophone G4 seems to be damaged at the end of the experiment, as the data obtained from it after the month of July 2016 doesn't seem to be correct and cannot be used.

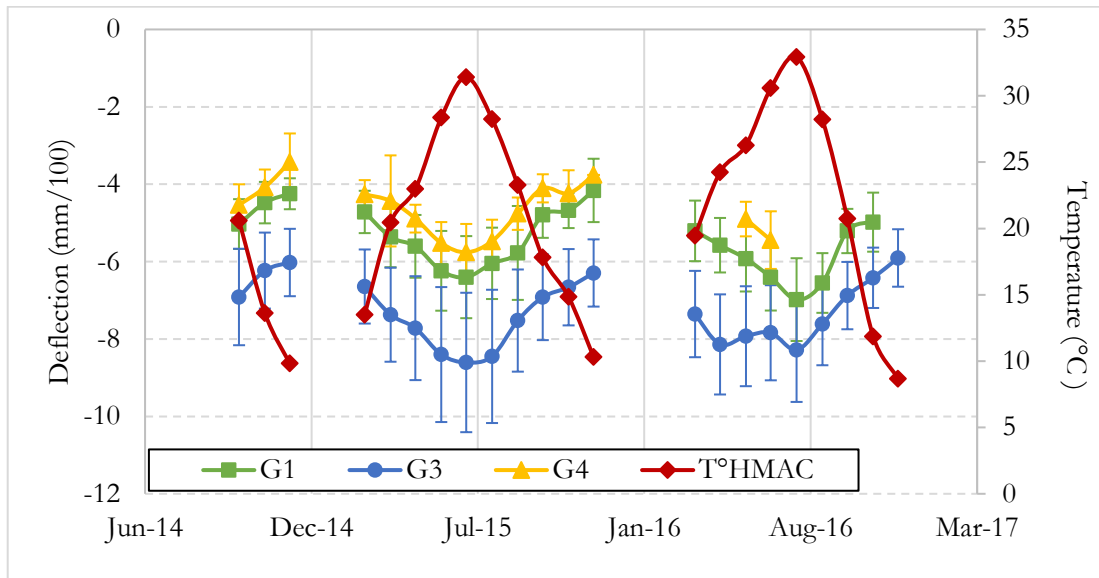


Figure 5-21. Monthly average deflections measured by geophones G1, G3 and G4 (under first axle of T2S3 trucks)

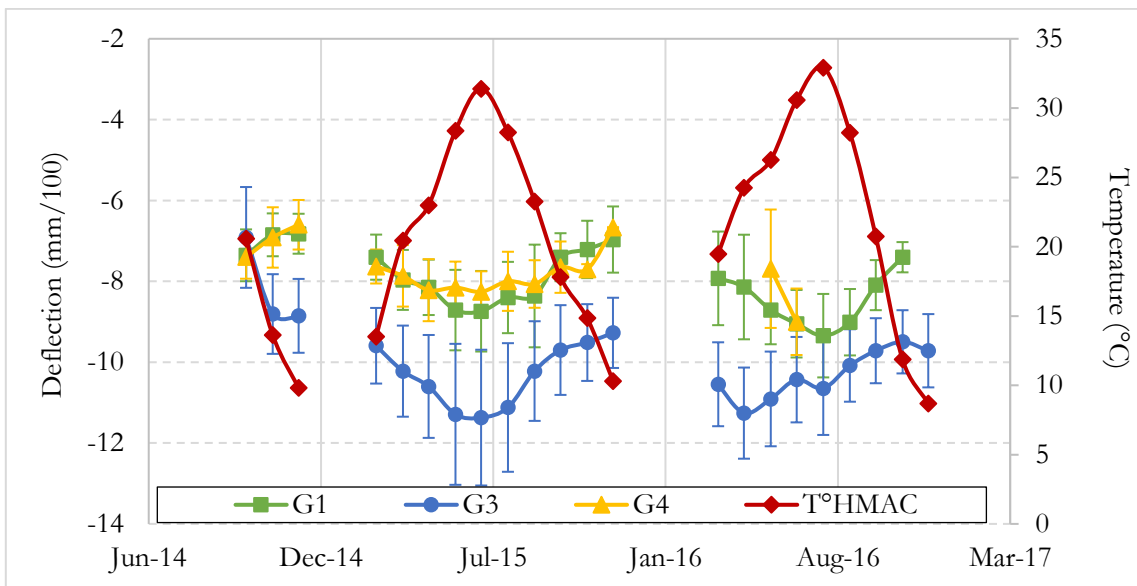


Figure 5-22. Monthly average deflections measured by geophones G1, G3 and G4 (under second axle of T2S3 trucks)

## 5.4 Analysis of the influence of temperature on deflections

### 5.4.1. Temperature variations in the experimental section

To take into account the effects of temperature on the performance of the experimental pavement, the Ax motorway section was instrumented with temperature probes, placed at the bottom of each layer of the pavement (VTAC, HMBC, HMAC, GB). The temperatures were recorded every 15 minutes during the two years of monitoring. Figure 5-23 represents the average temperatures measured each day from March 2015 to December 2015 in each pavement layer. The highest average temperatures are close to 50°C during the summer months, and the lowest average temperatures are close to 1°C during the winter months. Figure 5-24 shows the daily variation in the pavement layers within 10 days. Logically the VTAC surface layer presents somewhat larger temperature variations than the other layers.

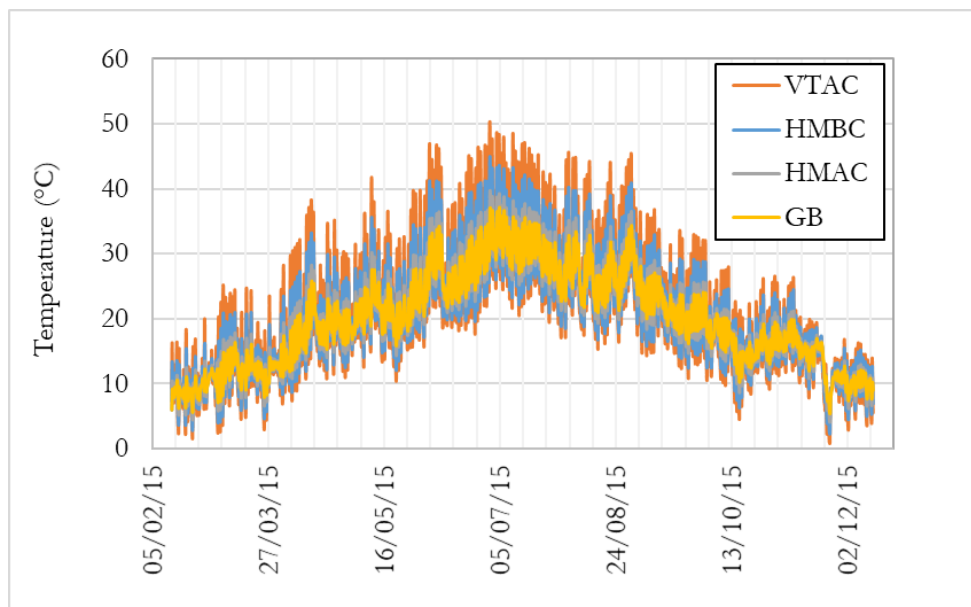


Figure 5-23. Daily temperature variations at the base of each pavement layer from February 13<sup>th</sup> 2015 to December 12<sup>th</sup> 2015

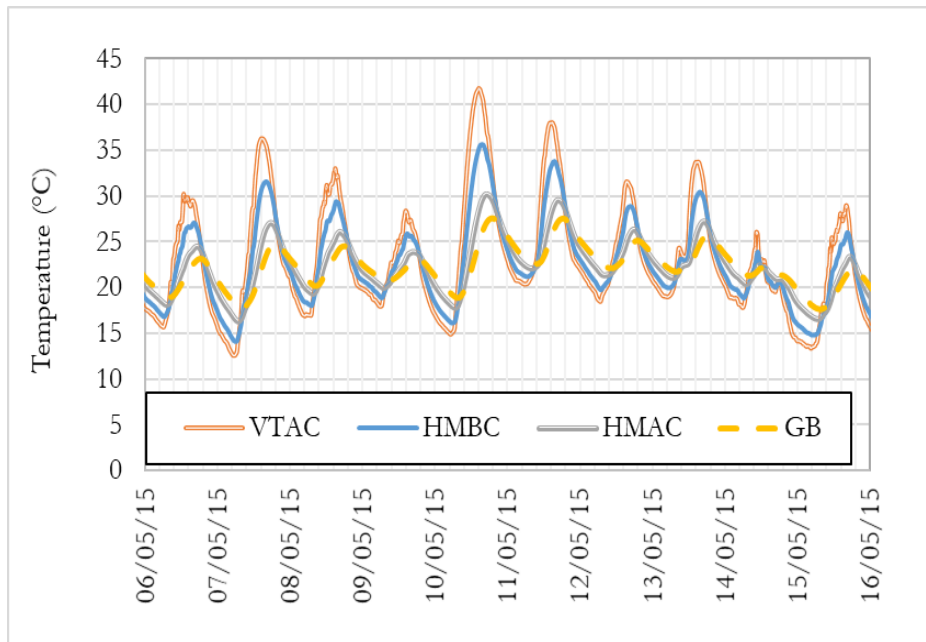


Figure 5-24. Temperature variation for 10 days, from May 6<sup>th</sup> 2015 to May 16<sup>th</sup> 2015

Figure 5-25 shows the evolution of the average values of the maximum deflection (without any temperature correction) of each month for the entire period from 2014 to 2016, calculated for geophone 1, 3 and 4 and the monthly average temperatures of the HMAc layer. This figure shows that:

- Despite the variability of traffic loads, the monthly average amplitudes of vertical deflections present a coherent evolution.
- The average deflection amplitudes vary between about 8 mm/100 and 12 mm/100, and deflections increase with the increase of temperature.

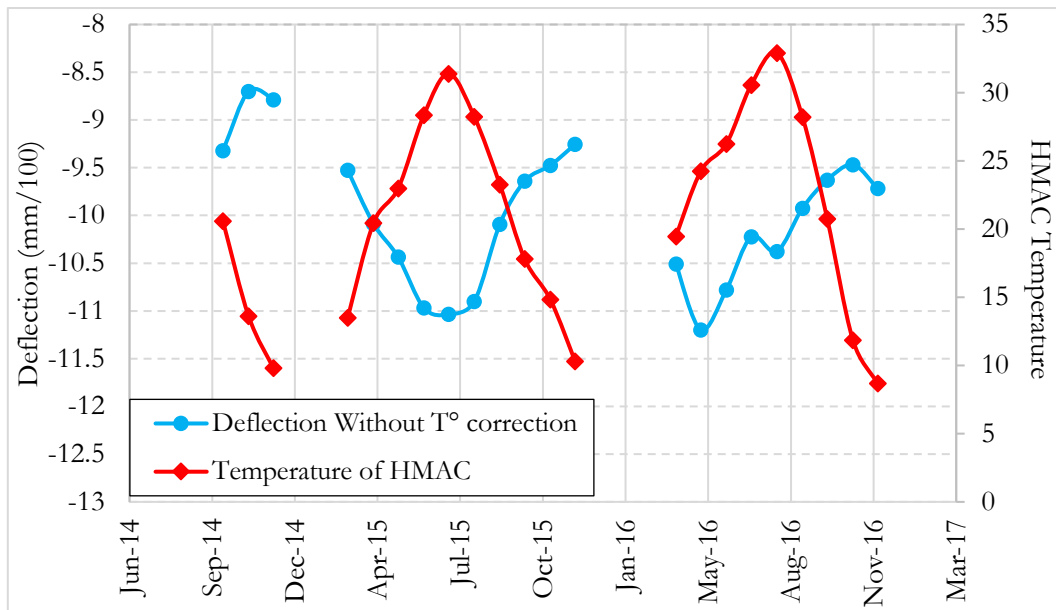


Figure 5-25. Evolution of average monthly deflections of the three geophones with temperature

#### 5.4.2. Temperature correction

To eliminate the influence of temperatures on the measured deflection, two temperature correction methods were tested. The temperature corrections were applied to geophones G1 and G3, located in the HMAC base layer, and at lateral positions where most of the vehicle wheels pass. For this reason, the temperature at the base of the HMAC layer was selected for the correction.

The first temperature correction method used consisted in trying to establish a relationship between the average temperature values, and the average deflections. This approach was applied to geophones G1 and G3 separately, and only the measurements made during the first six months of 2015 (beginning of the continuous monitoring period) were used, to avoid, as much as possible, any influence of evolution or damage of the pavement on the measured deflections.

The resulting deflection versus temperature relationships are shown in Figure 5-26. For both geophones, a practically linear variation of deflections with temperature was observed, and therefore, a linear correction function was proposed. This correction was then applied to the remaining years, and very consistent deflection values were obtained. Figure 5-27 and Figure 5-28 show the variations of the average deflections obtained with and without correction, for geophones G1 and G3 respectively.

The temperature corrections could be explained with the following equations, which were calculated on the recordings of the months from March 2015 to July 2015 at the average temperature of 13°C, 20°C, 23°C, 28°C and 31°C respectively.

For geophone 1

$$D(15^{\circ}\text{C}) = D(\text{measured}) + 0.1058(T_{\text{Measured}} - 15) \quad (5.3)$$

For geophone 3

$$D(15^{\circ}\text{C}) = D(\text{measured}) + 0.0792(T_{\text{Measured}} - 15) \quad (5.4)$$

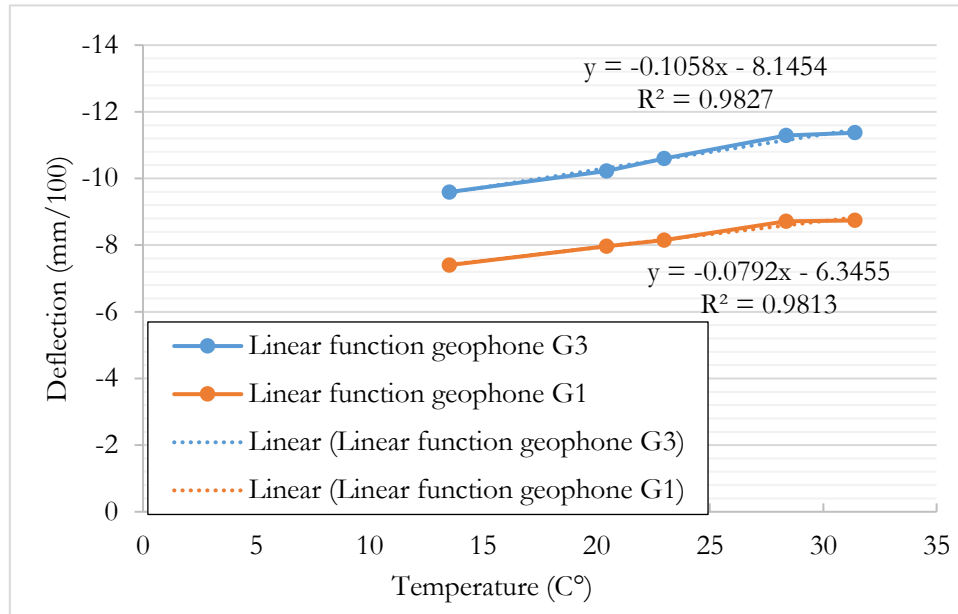


Figure 5-26. Temperature correction equation corresponding to the months of March 2015 to July 2015

The second approach, for correcting the effect of temperature, consisted in using the method proposed in the French Technical Guide on Pavement Reinforcement (CEREMA-IDRRIM, 2016). This guide provides the following equation (5.5), for the temperature correction of deflection measurements:

$$d_{15^{\circ}\text{C}} = \frac{d_{\theta_{mes}}}{1 + K * (\theta_{mes} - 15)/15} \quad (5.5)$$

Where:

$d_{15}$  is the deflection observed at 15°C

$d_{\theta_{mes}}$  is the measured deflection at the temperature  $\theta_{mes}$

K is a constant function of pavement type, which value is equal to  $k=0.2$  for the Ax section (thick bituminous pavement)

Figure 5-27 and Figure 5-28 show the evolution of deflections with and without temperature correction, for geophones G1 and G3 respectively. Both temperature correction methods are compared and it can be seen that the two correction methods give very similar results, maximum difference percentage between the two corrections is about 2% for geophone G1 and for G3 it is 1 %. This confirms the validity of the formula proposed in the Pavement Reinforcement Guide (CEREMA-IDRRIM, 2016).

The following observations can be made concerning the temperature correction methods:

- Both correction methods are efficient, and eliminate the seasonal variations of deflections with temperature. It may be noted, however, that for this pavement structure, the variations of deflections with temperature are relatively limited, probably due to the cement-treated subbase.
- For geophone G1, a slight difference is observed between the two corrections. For geophone G3, there is practically no difference.
- After correction, both geophones indicate relatively stable deflection values during the whole monitoring period; there are no seasonal variations of deflection (once the temperature effect is corrected), and no continuous evolution, which could be due to pavement deterioration.

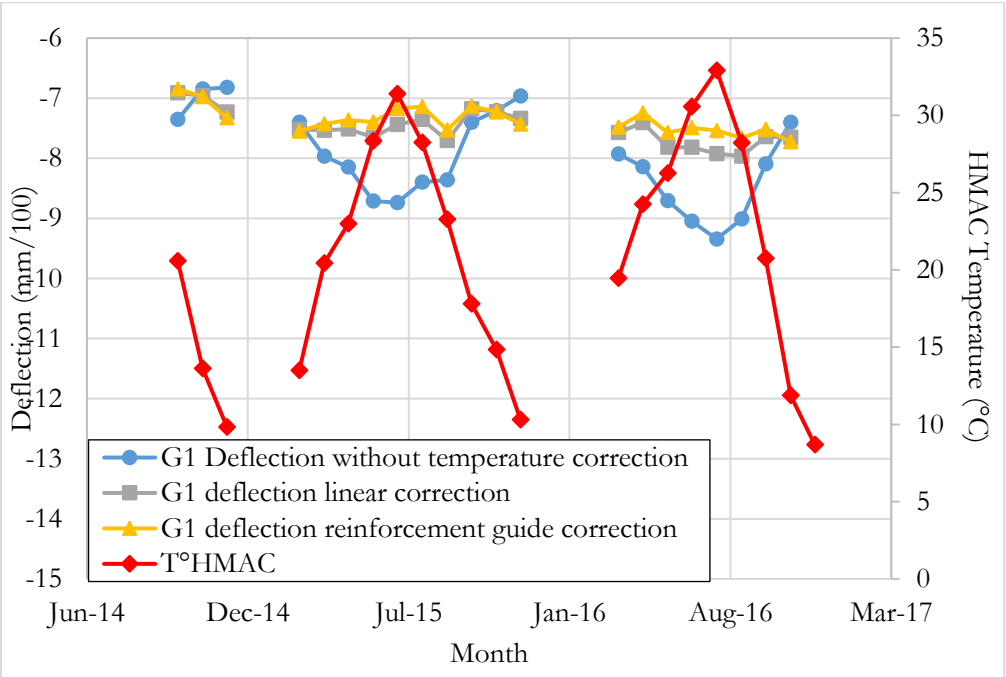


Figure 5-27. Evolution of deflections of Geophone G1 with and without temperature correction

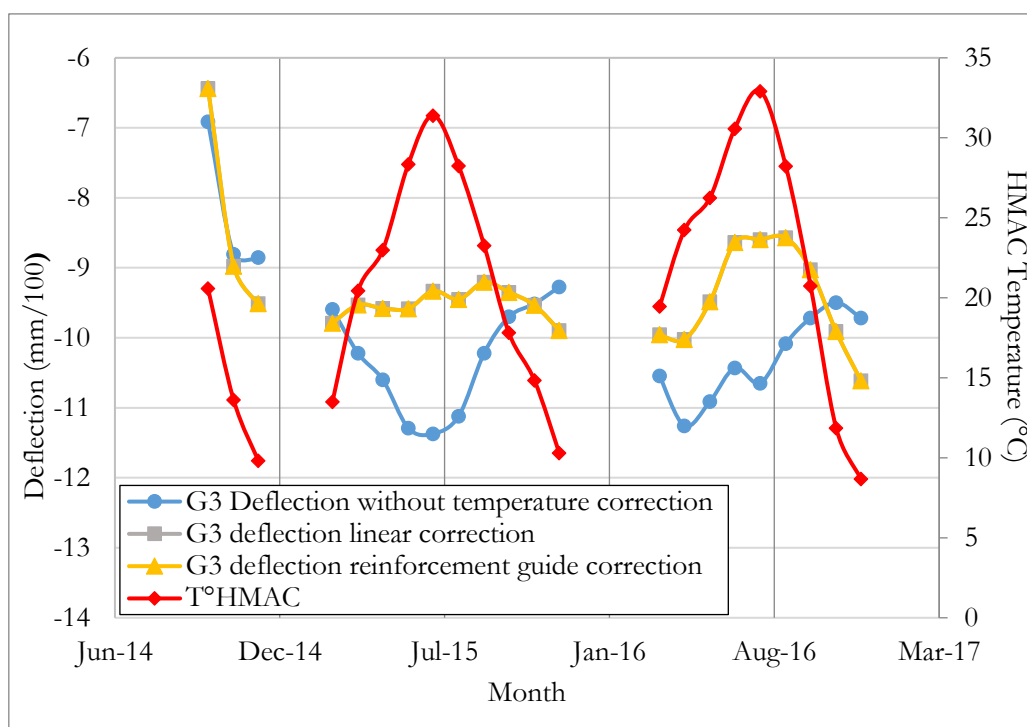


Figure 5-28. Evolution of deflections of Geophone 3 with and without temperature correction

## 5.5 Comparison of measured deflections with pavement modelling

### 5.5.1. Objectives of the comparisons

As on the Ax motorway section, there is no reference sensor to compare the geophone measurements with, as it was in the laboratory tests and the APT tests in chapters 2 and 3, it was found important to make a comparison with calculated theoretical signals. This was done by comparing the measurements with deflections calculated with the linear elastic pavement modelling software Alize, after identification of the initial pavement layer moduli.

### 5.5.2. Initial back-calculation of pavement layer moduli

Before comparing the geophone signals with calculated signals, it was necessary to define the initial pavement model. To determine the initial moduli of the pavement layers, Falling Weight Deflectometer (FWD) tests performed on the experimental section in October 2013 were used. FWD test were performed on three measurement points. These measurements were used to back-calculate the moduli of the cement treated layer and of the soil, using the back-calculation tool of the ALIZE software. The calculations were made with the following assumptions:

- The pavement structure considered is defined on Figure 5-29 (a). In the absence of precise information, the thickness of the subgrade was assumed equal to 1m. The thickness of the cement treated layer is 0.30m.
- A loading frequency of 30 Hz was considered.
- The moduli of the bituminous layers (VTAC, HMBC, HMAC) were defined using the materials library available in ALIZE (depending on the type of mix), and adjusted according to the temperature of each layer, and loading frequency. Only the moduli of the subgrade and of the cement-treated layer were back-calculated.
- The Poisson ratios of all the materials were set to 0.35, and all layers were assumed perfectly bonded.
- The results of the back-calculation are illustrated on Figure 5-29(b), which compares the measured deflection basin with the calculation results. A modulus of 3969 MPa was obtained for the cement-treated layer, and a value of 50 MPa for the subgrade.

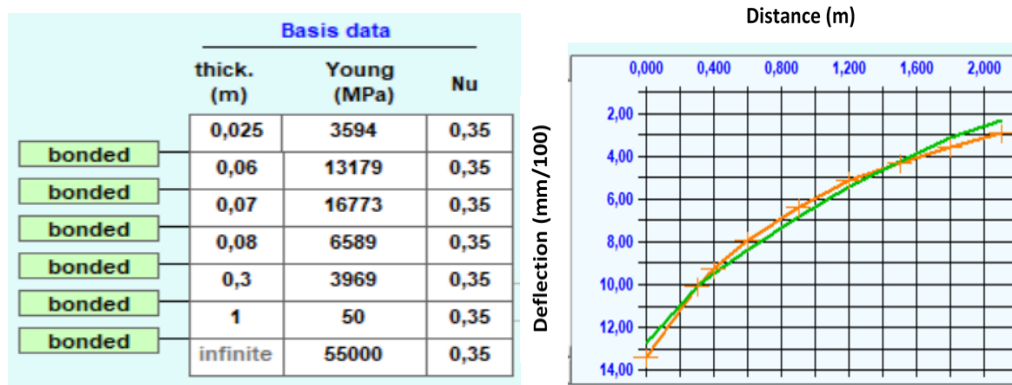


Figure 5-29(a). Pavement structure at temperature 15°C and frequency 30Hz (b). Comparison of measured and calculated deflection basin

### 5.5.3.Determination of mean deflection basins

For the comparisons with ALIZE, it was decided to use only one experimental signal per month. Firstly, the deflection basins measured with geophone G1 was used. The reason is that when the maximum deflection value is measured with geophone G1, which has a central position in the wheel path (in comparison with G3 and G4) it is certain that the vehicle wheels pass above G1. When the maximum deflection is obtained with G3 or G4, the position of the wheels is less accurate, because the wheels may not be located above the sensors, but may pass on the left of G4 or on the right of G3.

As the data acquisition system records a large number of deflection signals each month, it was necessary to choose a limited number of representative signals for the comparisons with the modelling. For that purpose, it was decided to select a “representative” geophone signal for each month, defined as the recorded signal whose maximum deflection is closest to the monthly average deflection value, calculated previously (see section 5.3.8 and Figure 5-21 and Figure 5-22). This “representative” signal can also be determined as the signal for which the error  $e$  (defined by equation 5.6) is minimal. Whereas  $e$  represents the difference between the measured peak deflection values, and the monthly average values (adapted from BROUTIN, 2014)

$$e_i = \frac{\sqrt{(d_{max,1st\ peak} - d_{mean,1st\ peak})^2 + (d_{max,2nd\ peak} - d_{mean,2nd\ peak})^2 + \dots + (d_{max,5th\ peak} - d_{mean,5th\ peak})^2}}{5} \quad (5.6)$$

Where  $d_{max,i^{th}peak}$  is the measured deflection corresponding to the  $i^{th}$  peak of the signal

$D_{mean,i^{th} peak}$  is the monthly average deflection, for the  $i^{th}$  peak of the signal.

$n$  is the number of peaks of the deflection signal ( $n=5$  for T2S3 trucks).

#### 5.5.4. Modelling of the deflection basins with ALIZE

To compare the “representative” deflection basins with the ALIZE modelling, the following approach was used:

- The ALIZE model, defined from the FWD measurements (section 5.5.2) was used as initial model.
- The moduli of the bituminous layers (VTAC, HMBC and HMA layer, GB layer) were adjusted to the measured temperature and frequency of each “representative” deflection signal.
- For the cement treated layer, the modulus back-calculated using the FWD tests was used in the pavement model.
- For the soil, it was necessary to take into account the variations of its bearing capacity with time, and in particular with changes of water content (Ksaibati et al., 2000). Therefore, the modulus of the soil was adjusted, in order to fit the selected deflection basins
- The Poisson’s ratio was set to 0.35 for all the materials, and all interfaces were assumed to be bonded.

Figure 5-30 shows an example of pavement model obtained for the month of March 2015, for a temperature of  $HMAC = 20^{\circ}C$  and a frequency of 14 Hz which corresponds to 28m/s, the speed of the vehicle (chupin et al., 2010).

**Basis structure**

|        | thick. (m) | modulus (MPa) | Nu    | material type |
|--------|------------|---------------|-------|---------------|
| bonded | 0,025      | 2436,0        | 0,350 | bbtm          |
| bonded | 0,060      | 9426,0        | 0,350 | eb-bbme3      |
| bonded | 0,070      | 13653,0       | 0,350 | eb-eme2       |
| bonded | 0,080      | 5449,0        | 0,350 | bbm           |
| bonded | 0,300      | 3964,0        | 0,350 | other         |
| bonded | 1,000      | 150,0         | 0,350 | other         |
| bonded | infinite   | 10000,0       | 0,350 | other         |

Figure 5-30. Pavement structure defined for the simulation of the deflection basins (month: March 2015, temperature:  $20^{\circ}C$ , frequency 14 Hz)

The truck load used for the ALIZE calculation was that corresponding to a reference T2S3 semi-trailer truck, loaded at 44 tons. Deflections were calculated under the load passage at different temperatures and frequencies corresponding to mean signals of each month. The geometry and axle loads of the considered T2S3 truck are given in Figure 5-31.

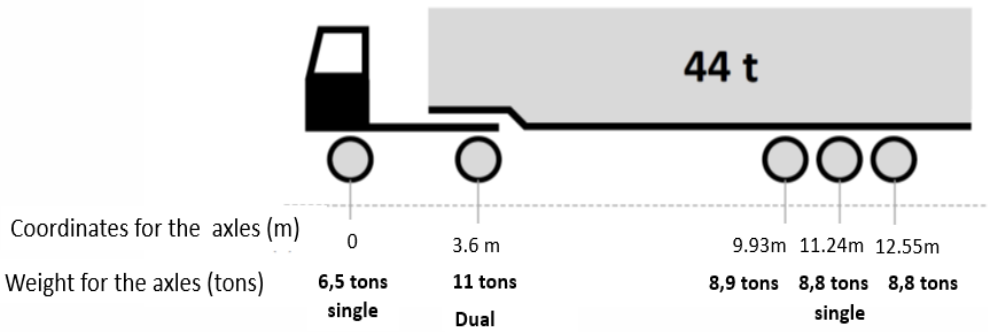


Figure 5-31. Reference T2S3 Truck dimensions and weights

It is also known, from previous studies (Blanc et al., 2019) that for a T2S3 truck, the load of the front axle is very little influenced by the weight of the transported cargo, and is, in average, equal to 6.5 tons (Schmidt et al., 2016). For this reason, it was decided, in the calculations, to keep the load of the first axle constant, and equal to 6.5 tons, and to adjust the loads of the other axles, to fit the experimental values. In order to do that first it is necessary to adjust the values of the soil modulus to fit the measured sensor values. As described in the paper (Saevarsdottir et Erlingsson,

2013), the pavement response is highly susceptible to moisture content. The cement treated layer being more resilient to the moisture content (Y. Liu et al., 2019), only the modulus values of the subgrade were adjusted.

For adjusting the values of the soil modulus, the following approach was used:

- First, a calculation was performed with the initial pavement layer moduli, and with the reference 44 tons vehicle load, and compared with the geophone measurements.
- Then, assuming that the load of the first axle is known and equal to 6.5 tons, the modulus of the soil was adjusted, until the best fit with the measured deflection was found for the first axle.

Figure 5-32, Figure 5-33, Figure 5-34 and Figure 5-35 present some examples of the initial comparison of the deflections measured with geophone G1 and calculated with ALIZE for the different months of 2015. These figures show that, as expected, the measured and calculated deflections are very similar in amplitude for the first axle, (and also relatively close for the second axle) but that the measured deflections are lower for the 3 rear axles. This was explained by the fact that the real weight of the vehicle (which is unknown) is lower than the standard value of 44 tons, assumed in the modelling, which the maximum weight allowed in France.

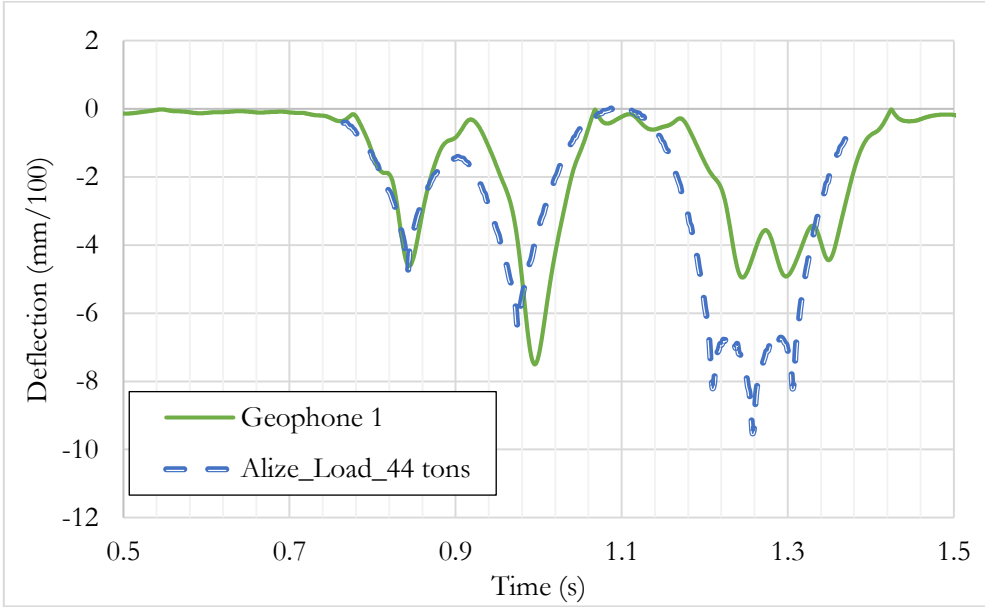


Figure 5-32. Comparison of the deflection obtained with representative signal of March 2015 (13/3/2015, 10h 59 min 39s, 28m/s and temp= 20°C) and simulation with Alize with a truck loaded at 44 tons

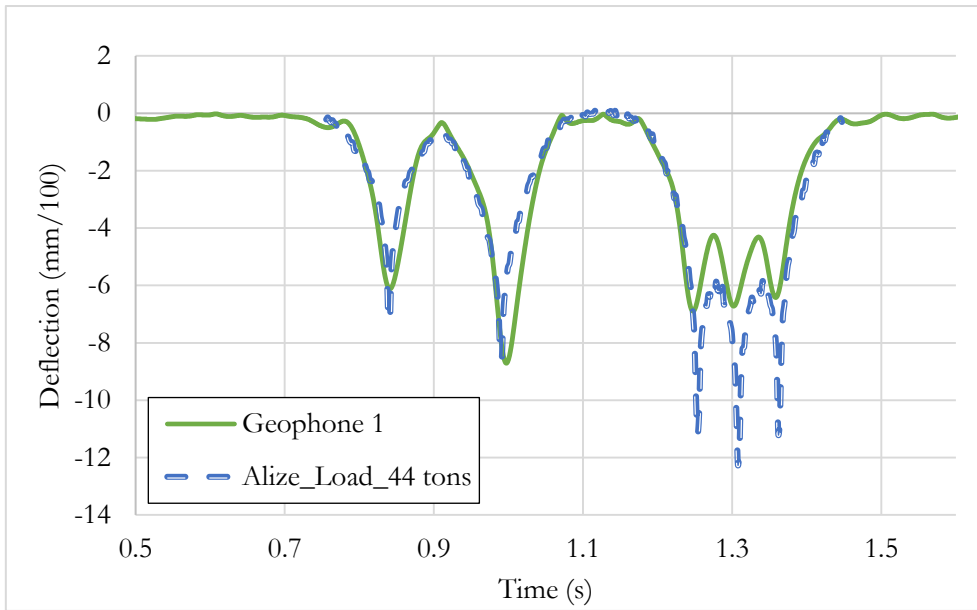


Figure 5-33 Comparison of the deflection obtained with the representative signal of June 2015 (21/06/2015, 14h 9 min 52s, 24m/s and HMAc= 39°C and the simulation with Alize with a truck loaded at 44 tons

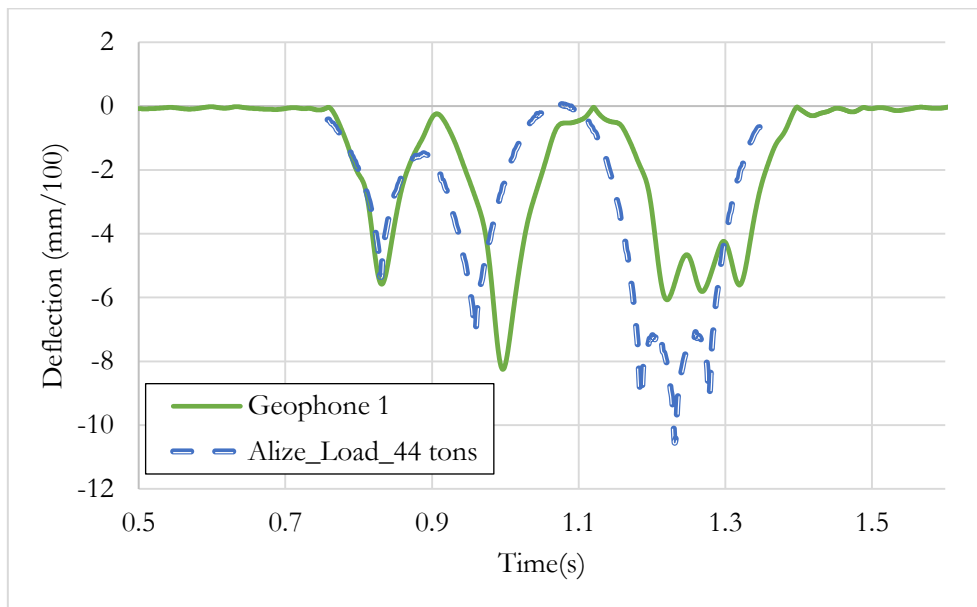


Figure 5-34. Comparison of the deflection obtained with the representative signal of September 2015 (07/09/2015, 23h 11 min 30s, 28m/s and temp= 21°C) and the simulation with Alize with a truck loaded at 44 tons

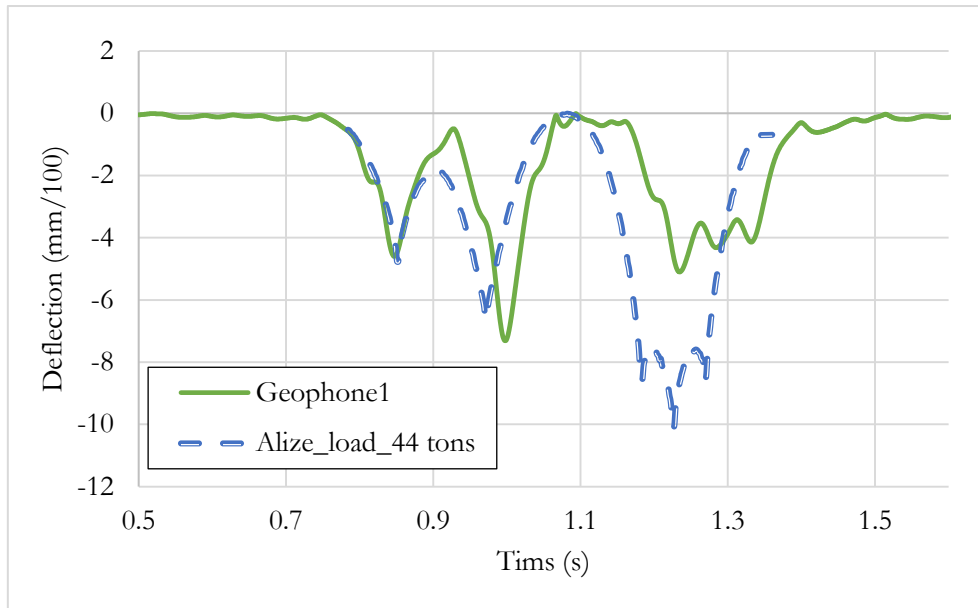


Figure 5-35. Comparison of the deflection obtained with the representative signal of November 2015 (14/11/2015, 12h 24 min 31s, 30m/s and HMAC= 16°C) and the simulation with Alize with truck loaded at 44 tons

The subgrade moduli have been adjusted using such calculations, for each month during the monitoring period and the corresponding values are given in Table 5.3. Figure 5-36 shows the seasonal variations of the average monthly subgrade moduli, during the two years period. Following the trend, it is evident that during the summer dry months, the modulus is higher whereas during the winter months the modulus decreases. In the summer, the soil modulus varies between 180 and 200 MPa, and in the winter, the values vary between 90 and 140 MPa. The same trend is observed during the two years (2015 and 2016). These variations of modulus are probably due seasonal water content variations of the subgrade, with lower water contents (corresponding to higher moduli) in the summer, and higher water contents in the winter. From these first calculations, it was concluded that the ALIZE modelling could be used as a simplified and approximate method to estimate the modulus of the soil.

Table 5.3. Estimated modulus of the soil for each month of the monitoring period

| Date<br>Year & Month | Temperature of the<br>reference signal<br>(°C) | Speed of the<br>reference signal<br>(m/s) | Soil modulus<br>(MPa) |
|----------------------|--|---|-----------------------|
| March 2015           | 15   | 28  | 150                   |
| April 2015           | 16   | 24  | 150                   |
| May 2015             | 23   | 26  | 160                   |
| June 2015            | 32   | 24  | 200                   |
| July 2015            | 23   | 27  | 200                   |
| Aug 2015             | 32   | 25  | 200                   |
| Sept 2015            | 23   | 28  | 140                   |
| Oct 2015             | 15   | 29  | 110                   |
| Nov 2015             | 14   | 30  | 120                   |
| Dec 2015             | 10   | 29  | 140                   |
| April 2016           | 20   | 27  | 150                   |
| May 2016             | 29   | 26  | 160                   |
| June 2016            | 25   | 27  | 180                   |
| July 2016            | 30   | 26  | 180                   |
| Aug 2016             | 33   | 26  | 190                   |
| Sept 2016            | 30   | 27  | 170                   |
| Oct.2016             | 18   | 27  | 90                    |
| Nov 2016             | 13   | 28  | 140                   |
| Dec 2016             | N/A  | N/A                                       | N/A                   |

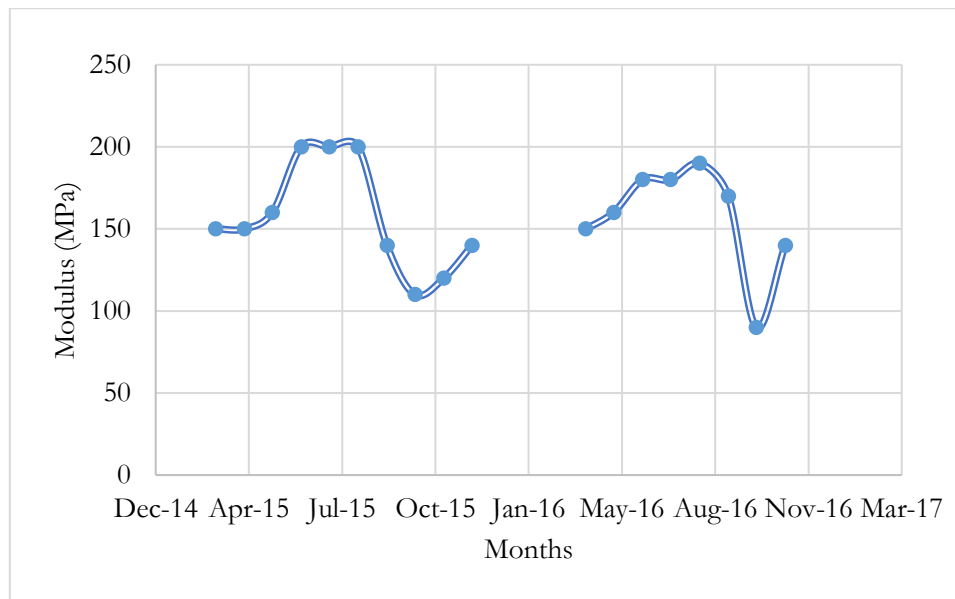


Figure 5-36. Monthly variations of the subgrade modulus during the years 2015 and 2016

### 5.5.5. Evaluation of heavy vehicle loads using deflection measurements

After having defined the soil moduli, for each month, a similar method of adjustment with ALIZE was also proposed, for trying to estimate the heavy vehicle loads. For that, the following approach was used:

- After fixing the soil modulus, a comparison was made between the calculated and measured geophone responses. It was found that when making the calculations with the standard 44 ton reference vehicle loads (see Figure 5-31), the first two peaks of the deflection signal were relatively well predicted, but significant differences between the measurements and calculations were still observed for the last three peaks, corresponding to the rear tridem axles.
- Then, the loads of the 3 last axles of the truck were adjusted in ALIZE (assuming the loads of the 3 axles equal), and the model response was compared with the geophone measurements, and the load was adjusted again until the best match was found.

Figure 5-37, Figure 5-38, Figure 5-39 and Figure 5-40 represent several examples of modelling of geophone deflection signals, for the months of March, June, September and November 2015. The deflection signal obtained after adjusting the axle loads is shown on the given figures. The figures show that, with the corrected loads, the deflections under the first two axles are not significantly modified, but the deflections under the last three axles are much better predicted. The total truck weight found after the adjustment is indicated on each figure.

The Figure 5-37, Figure 5-39 and Figure 5-40 also indicate, in some cases, a difference between the calculated and measured positions of the deflection peaks, due to the change between the real and theoretical truck dimensions (and axle spacing). To eliminate these differences, the distances between the axles were adjusted in ALIZE, in order to improve the modelling, as represented in these figures. The predictions are improved with the corrected axle positions.

The comparison of the other representative signals for the remaining months are given in the figures in annex D.

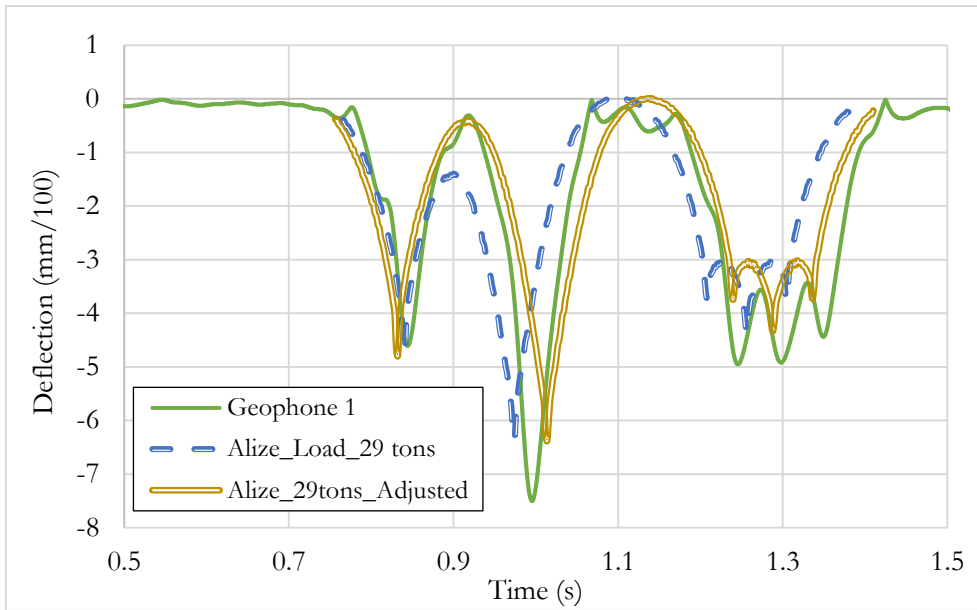


Figure 5-37. Comparison of the deflection obtained with the representative signal of March 2015 (13/3/2015, 10h 59 min 39s, 28m/s and 20°C) and the simulation with Alize with a truck loaded at 29 tons and with the adjusted axles spacing

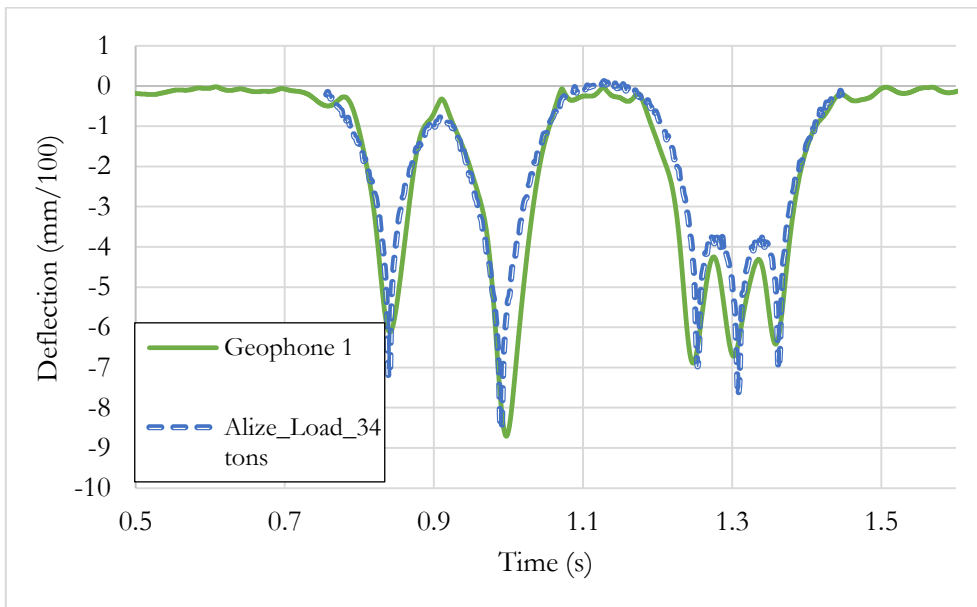


Figure 5-38. Comparison of the deflection obtained with the representative signal of June 2015 (21/06/2015, 14h 9 min 52s, 24m/s and 39°C) and the simulation with Alize with a truck loaded at 34 tons

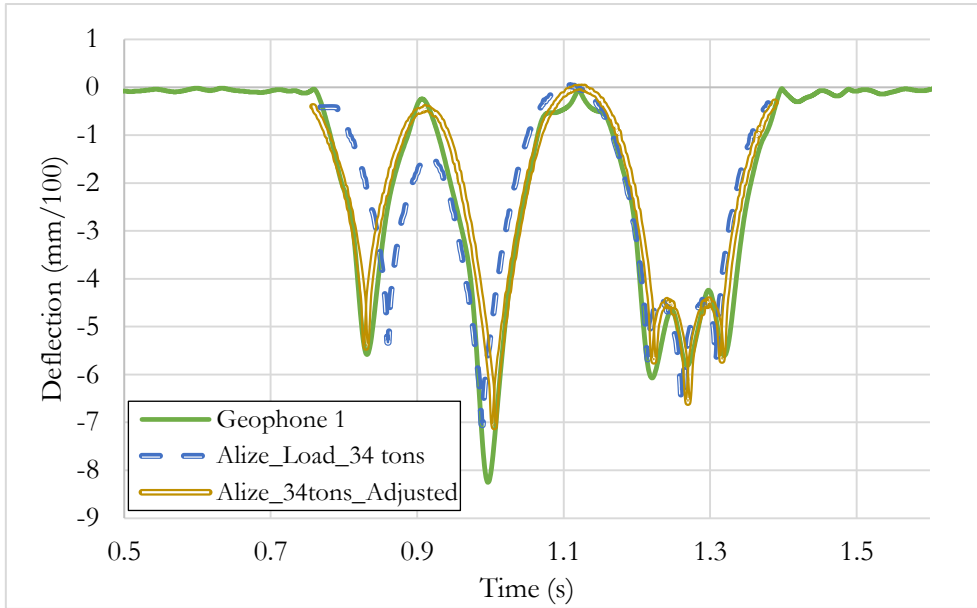


Figure 5-39. Comparison of the deflection obtained with the representative signal of September 2015 (07/09/2015, 23h 11 min 30s, 28m/s and 21°C) and the simulation with Alize with a truck loaded at 34 tons and with the adjusted axle spacing

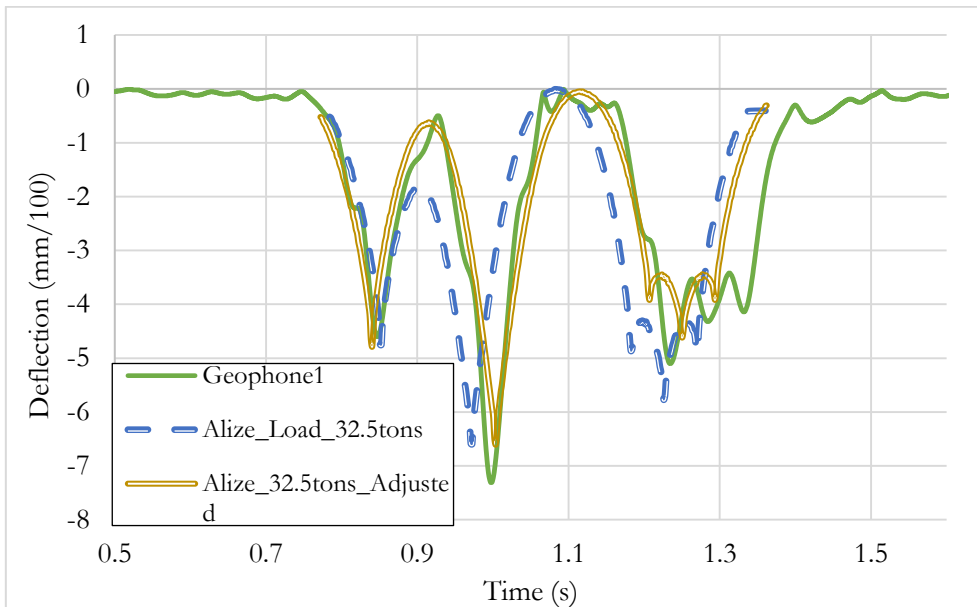


Figure 5-40. Comparison of the deflection obtained with the representative signal of November 2015 (14/11/2015, 12h 24 min 31s, 30m/s and 16°C) and the simulation with Alize with a truck loaded at 32.5 tons and with the adjusted axles spacing

The variations of the “average” monthly vehicle loads, obtained with the selected representative deflection signals, during the two years of monitoring are presented in Figure 5-41. This figure shows that the “average” loads remain relatively stable during the two years, with values varying approximately between 30 and 34 tons except in the month of December when less traffic was recorded and no recording was observed with geophone G1. The estimated mean loads corresponding to these “representative” load signals are presented in Table 5.4.

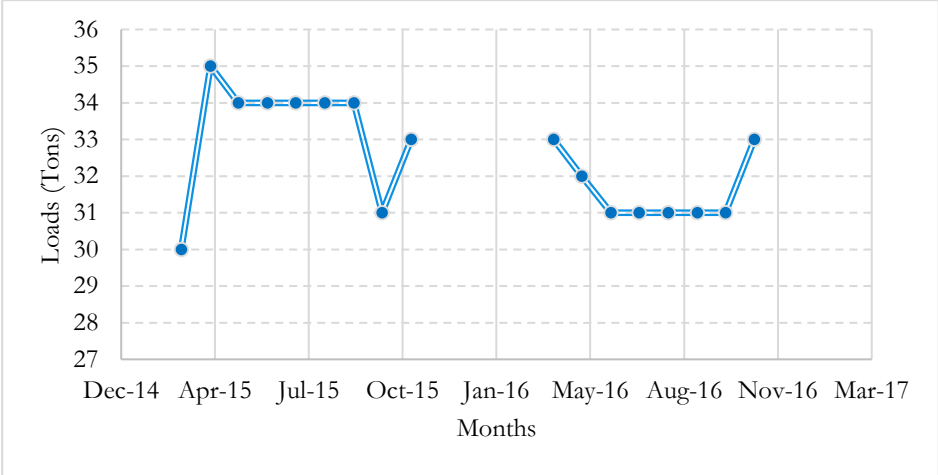


Figure 5-41. Monthly variations of the average vehicle loads, during the years 2015 and 2016

Table 5.4. Load values obtained with the “representative” deflection signals for each month of the years 2015 and 2016

| Date Year & Month | Temperature (°C) | speed of the representative signal (m/s) | load of three last axles per wheel (tons) | Total load (tons) |
|-------------------|------------------|--|---|-------------------|
| March 2015        | 15               | 28                                       | 2   | 30                |
| April 2015        | 16               | 24                                       | 2.9                                       | 35                |
| May 2015          | 23               | 26                                       | 2.75                                      | 34                |
| June 2015         | 32               | 24                                       | 2.75                                      | 34                |
| July 2015         | 23               | 27                                       | 2.75                                      | 34                |
| Aug 2015          | 32               | 25                                       | 2.75                                      | 34                |
| Sept 2015         | 23               | 28                                       | 2.75                                      | 34                |
| Oct 2015          | 15               | 29                                       | 2.2                                       | 31                |
| Nov 2015          | 14               | 30                                       | 2.5                                       | 33                |
| April 2016        | 20               | 27                                       | 2.5                                       | 33                |
| May 2016          | 29               | 26                                       | 2.4                                       | 32                |
| June 2016         | 25               | 27                                       | 2.2                                       | 31                |
| July 2016         | 30               | 26                                       | 2.2                                       | 31                |
| Aug 2016          | 33               | 26                                       | 2.2                                       | 31                |
| Sept 2016         | 30               | 27                                       | 2.2                                       | 31                |
| Oct.2016          | 18               | 27                                       | 2.2                                       | 31                |
| Nov 2016          | 13               | 28                                       | 2.5                                       | 33                |

Similarly to what was done in previous chapter, an error indicator has been calculated, to evaluate the differences between the calculated and measured deflections, after adjustment of the vehicle loads in ALIZE. For that, the five peaks of the measured and calculated signals have been determined for each monthly “representative” signal, and the relative difference, in percentage, between the calculated and measured points was calculated (see Figure 5-42). The relative difference (R) of these five peak points has been calculated using the equation 5.7.

$$R = \frac{1}{N} \left( \sum_{i=1}^N \frac{|Calculated\ deflexion\ of\ peak\ i - Measured\ deflexion\ of\ peak\ i|}{Calculated\ deflexion\ of\ peak\ i} \right) * 100 \tag{5.7}$$

Where N is the number of axles of the truck (here, N=5).

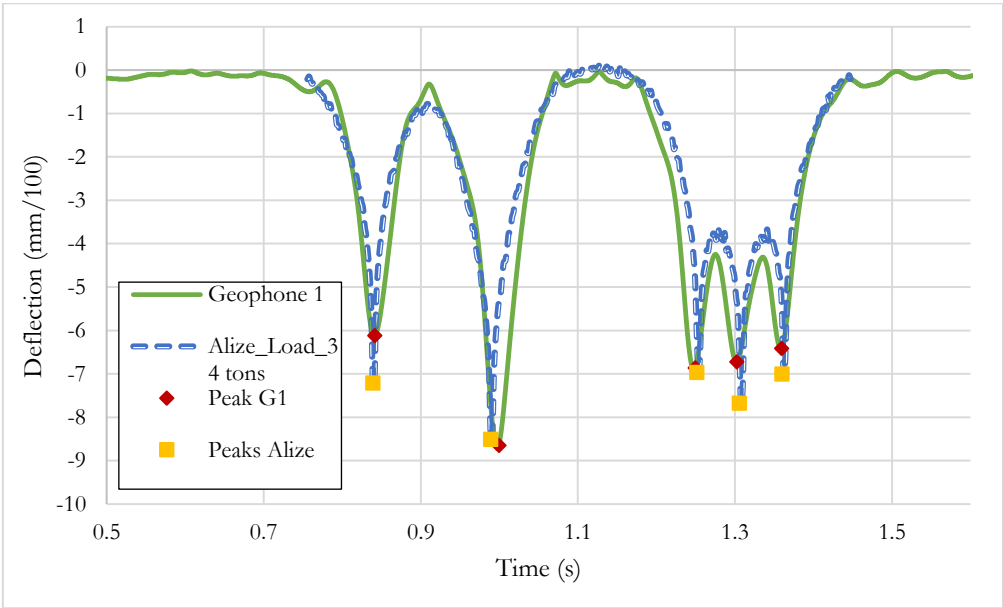


Figure 5-42. Mean signal of June 2015 and the Alize signal with indicated peaks of each signal. For each month, the relative differences between the measured “representative” signal and the calculated signal are given in Table 5.5.

Table 5.5. Percentage difference of the maximum peak measured and calculated deflection values

| <b>Time</b> | <b>Difference (%)</b> |
|-------------|-----------------------|
| March- 2015 | 17                    |
| April- 2015 | 14                    |
| May-2015    | 9                     |
| June-2015   | 8                     |
| July-2015   | 12                    |
| Aug-2015    | 8                     |
| Sept-2015   | 8                     |
| Oct-2015    | 13                    |
| Nov-2015    | 11                    |
| Dec-2015    | 15                    |
| April-2016  | 7                     |
| May-2016    | 10                    |
| June-2016   | 8                     |
| July-2016   | 9                     |
| August-2016 | 9                     |
| Sept-2016   | 7                     |
| Oct.-2016   | 22                    |
| Nov-2016    | 12                    |

The maximum allowable weight for T2S3 trucks in France is 44 tons, whereas for the whole of Europe, the maximum load for T2S3 trucks is 40 tons. On the motorway Ax, there is mostly international traffic between France and Spain, so it is expected that the maximum load will be 40 tons rather than 44 tons. As the “representative” deflection signals over the two-year period do not correspond to the maximum allowable loads, it was decided to select two signals (for the months of May and June 2015) where the rear axle deflections were maximum. To verify the levels of load corresponding to these two selected signals, they were compared with simulations made with Alizé. For these calculations:

- The bituminous mix moduli were adjusted in function of the speed and temperature.
- The soil modulus used was the one determined in previous calculations, for the same months (Table 5.3)
- The load of the truck was set to 40 tons in the calculations

Figure 5-43 and Figure 5-44 present the comparisons between the selected “maximum” signals and the simulation, with the 40 tons total load. The results indicate a good agreement between the

model and the measurements, confirming that the loads of the heaviest vehicles are close to 40 tons.

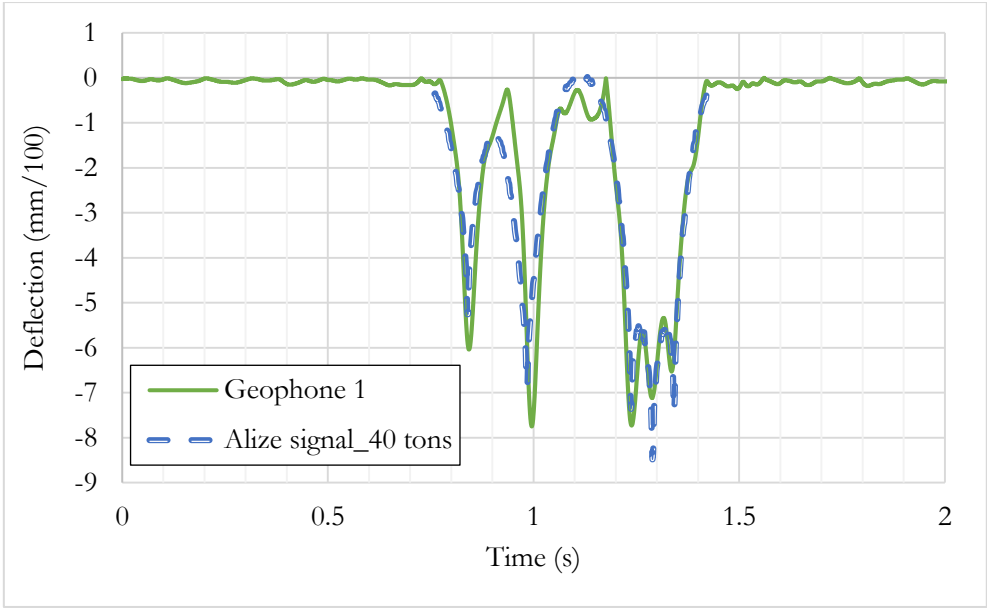


Figure 5-43. Comparison of the deflection obtained with the maximum signal of May 2015 (03/05/2015, 16h 54 min 10s, 26.8 m/s and HMAC= 27°C) and the simulation with Alize with a truck loaded at 40 tons

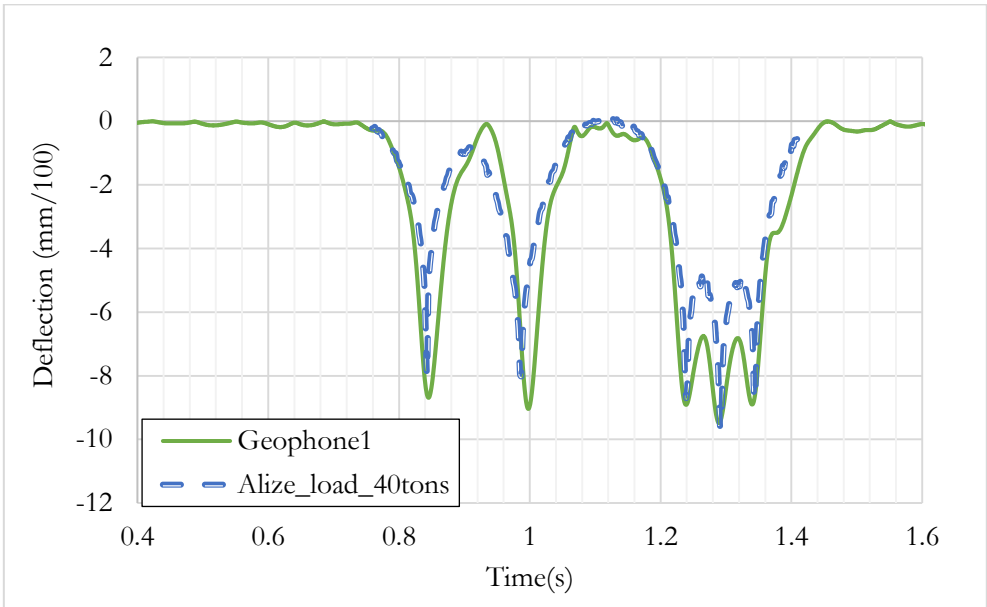


Figure 5-44. Comparison of the deflection obtained with the maximum signal of June 2015 (08/06/2015, 19h 9 min 56s, 28 m/s and HMAC= 36°C) and the simulation with Alize with a truck loaded at 40 tons

In conclusion, it has been shown that by adjusting the pavement model on the measured deflections, it is possible to estimate vehicle loads. This approach has been applied to the “representative” deflection signals, obtained with geophone G1 for each month, during all the monitoring period (from March 2015 to November 2016).

## **5.6 Conclusion**

In this chapter, we have presented an application of geophones for the monitoring of deflections on a test section of the Ax motorway, under real traffic. The motorway section was instrumented with 4 geophones and 8 temperature probes, located at the base of each pavement layer. These sensors were connected to a data acquisition system based on the PEGASE data acquisition boards, associated with a wireless transmitter, which sends the data via 3G/4G wireless technology. The data received from the geophones is treated with the same processing techniques used in the chapter 2 and 3. Deflection and temperature data recorded from October 2014 to December 2016 was used to analyse the pavement performance.

The geophones installed at different lateral position were used to determine the deflections. These signals were used to determine vehicle speeds, estimate vehicle lateral positions, and to identify types of heavy vehicles. This information was used to get statistics about the types of trucks passing on the Ax motorway.

Temperature data was used to evaluate the influence of temperature on pavement deflections values. From these results, two different temperature correction formulas were proposed and compared, and it was shown that they give very similar results. After correcting the effects of temperature, it was concluded that the pavement deflections present no significant evolution during the two years of monitoring, and no significant seasonal variations.

Finally, to compare the measured deflections with modelling, the geophone signals were sorted, and only signals corresponding to T2S3 trucks, and passing in the center of the wheel path (with their wheels centered on geophone G1) were selected. From these signals, a “representative” signal, was selected, for each month. These “representative” signals were compared with calculations with the linear elastic software ALIZE.

The modelling with ALIZE was carried out, at first, with the loading of a standard T2S3 vehicle, loaded at 44 tons (maximum legal weight in France). These comparisons indicated that for the front axle of the vehicle, (loaded at 6.5 tons), the calculated deflections were very close to the measurements, whereas for the other axles, there were more important differences. This was explained by the fact that for T2S3 trucks, the load of the front axle is not influenced by the weight

transported by the truck, and is close to 6.5 tons. For the other axles, the load depends much more on the weight of the cargo transported by the truck. This result was used to estimate truck weights, by adjusting the axle loads (except for the front axle), to match the measured deflections. This result shows that, if the pavement properties are known, the geophone measurements can be used to estimate the loads of passing vehicles.

The objective of this approach is not to measure the weight accurately, but to get a reasonable approximation, with a low cost sensor, which could be very interesting, for example, for estimating effective pavement damage due to traffic, and thus the remaining life of the pavement.

Finally, the comparisons with the modeling also allowed to estimate the variations of the subgrade modulus during the 2 years of monitoring. The results have shown seasonal variations of the subgrade modulus, certainly related with moisture variations.

The next steps would be to compare the loads estimated with the geophones with more accurate measurements made with a weight in motion system, to evaluate the accuracy of the approach based on the geophones.



## GENERAL CONCLUSION

This thesis presents an extensive study about the use of geophones and accelerometers for instrumentation and monitoring of pavements. The objectives were to assess the efficiency of the sensors for measuring pavement deflections, and then to test them in real conditions, for the instrumentation of a heavy traffic pavement, under continuous traffic. The objective was also to develop methods of analysis of the sensor measurements, suitable for long-term pavement monitoring, under real traffic.

Geophones and accelerometers present several interesting characteristics for pavement instrumentation. They present the advantage of being relatively small and robust sensors, which makes them suitable for embedment in the pavement. For deflection measurements, they can be placed close to the surface, and can thus easily be installed in the pavement even after the construction. Finally, due to their measurement principle (measurement of velocity or acceleration), they do not require a fixed reference point to measure the displacement.

The first objective of this work was to verify the possibility of using the sensors for monitoring of pavement deflections. For that purpose, a laboratory test program was set up, to evaluate the characteristics of the sensors, and their response to displacement signals simulating real pavement deflections, with different amplitudes and frequencies. The results of these tests were presented in chapter 2. When processing these signals, it was found that a simple integration of the velocity (or double integration of the acceleration) leads to a signal of incorrect shape, which presents positive and negative oscillations. To eliminate these oscillations, the idea was to apply the Hilbert transform, which is used in particular in signal modulation methods to distinguish the signal envelope from its carrier. Finally, an original signal processing method was defined for the calculation of deflections. The processing includes five steps: noise filtering, amplification, integration of the signal (or double integration for the accelerometers), detrending, and application of the Hilbert transform. The results obtained with this procedure were compared with reference measurements, made with a laser displacement sensor, and it was shown that realistic values are obtained for all the tested sensors, for a range of frequencies and amplitudes corresponding to real pavement deflections.

The second objective, in chapter three, was to evaluate the response of the sensors embedded in a pavement, under moving wheel loading. For this purpose, a test section built on the IFSTTAR accelerated pavement testing facility was instrumented with geophones, accelerometers and temperature probes. This study was a necessary step to validate the response of the sensors, and

the signal processing method, in realistic conditions. In these tests, different controlled loading conditions (wheel loads, speeds, and wheel positions) were applied. The results were compared with measurements of a reference anchored deflectometer, which is difficult to install on in-service pavements, but gives accurate deflection measurements. The results indicated a good agreement between the measurements of the accelerometers and geophones, and of the reference deflectometer, for different loading speeds. It was also shown that the position of the wheels with respect to the sensors has a large influence on the measurements. The maximum deflection is obtained when one of the wheels is centered on the sensors.

The results obtained with the sensors were compared with predictions obtained with a linear elastic model (Alize software) and with a visco-elastic model (Visco-route software). The calculations were performed with bituminous mix parameters determined from laboratory complex modulus tests, and taking into account the experimental conditions (loading speed and temperature). The results indicated a good agreement between the measured and calculated responses with maximum differences of 10% for the elastic model and 7% for the viscoelastic model.

The objective of Chapter 4 was to develop two back-calculation procedures, for the determination of pavement layer moduli, based on the deflection basins measured by the geophones and accelerometers. Two different procedures were tested for the calculation of the pavement layer moduli. The first, classical approach, consisted in using the back-calculation tool of the ALIZE Software. This approach consists in comparing the measured and calculated deflection basins, and adjusting, iteratively, the layer moduli, until the best fit with the measured deflection basin is obtained. A second approach, initially proposed by Levenberg (2012), was also tested. This approach consists in performing the optimization using directly the acceleration or velocity signals delivered by the sensors. This second approach was implemented in the linear elastic calculation tool ELLEA. After calculating the pavement deflections using the elastic model, they were converted to velocity and acceleration, by numerical derivation. The calculated velocity (respectively acceleration) signals were then compared with the sensor measurements. An optimization procedure was used to adjust iteratively the pavement layer moduli, until a good match with the measurements was obtained. The advantage of the second method is that it uses directly the sensor signals, without the need for any processing or integration, which could reduce their accuracy. The moduli back-calculated by the two methods were compared with reference values, obtained from FWD tests and laboratory modulus tests. The results indicated that the two methods lead to realistic moduli, with a slight advantage for the ALIZE-based approach.

The objective of the last chapter was to apply the different instrumentation and treatment methods developed in the thesis to data from a real instrumented site, located on motorway Ax. The

experimental section was instrumented with geophones and temperature probes placed at different depths in the pavement, and connected with a PEGASE data acquisition system, with remote data transfer capabilities.

A large amount of data was recorded during a period of 22 months, and several procedures were developed to follow the evolution of the performance of the pavement, and also characterize the passing traffic. The same signal processing methods developed and tested in the previous chapters were applied to the geophones measurements on the Ax motorway. In a first step, a procedure was developed to identify the silhouettes of heavy vehicles passing on the road. This process is based on the detection of negative peaks (number of peaks, the position of peaks) of geophone signals after integration. The results have shown that about 80 % of heavy vehicles traveling on the motorway are T2S3 (5 axle) semi-trailers. The speeds of heavy vehicles were also estimated, using the measurements of two geophones placed in the direction of circulation (longitudinal direction) and separated by one meter. The average speed of heavy goods vehicles was around 96 km/h.

In a second step, for the analysis of deflections, a sorting procedure was defined, to reduce the amount of data to analyze. First, only 5 axle T2S3 trucks were selected; then using the measurements of 3 geophones placed at different lateral positions, only vehicles with their wheels centered on the central geophone, G1, were selected, in order to eliminate the effect of variable lateral positions on the measurements. This sorting process allowed to reduce significantly the variability of the deflection signals, by selecting only vehicles of the same type, and passing at the same lateral position. After this sorting, variations of the maximum deflections were analysed, and a strong influence of temperature on deflections was observed. Two different temperature correction procedures, giving very similar results, were proposed, to eliminate temperature effects, and correct the deflections to a constant temperature of 15 °C. After applying this correction, the evolution of deflections with time, during the 22 month monitoring period, was studied. The results indicated no significant evolution of the corrected deflections, which led to conclude that no significant deterioration occurred during this period; this seems logical, as the pavement had been recently reinforced (In 2013).

Finally, the measured deflections were compared with pavement calculations, performed with the ALIZE software. The pavement model used in ALIZE, and in particular the layer moduli, were determined from FWD measurements, combined with the use of standard modulus values for some layers. The ALIZE results were compared, for each month, with a “representative” signal. This “representative” signal was defined as the real recorded signal giving peak deflection values, for each axle, which were closest to the monthly average values.

From these results, an original method for estimating the vehicle loads was proposed. Initially, the real loads of the T2S3 vehicles passing on the motorway being unknown, the ALIZE calculations were performed with loads corresponding to a “reference” T2S3 truck, loaded at 44 tons, with standard axle loads. The initial comparisons between the calculations and the measured signals showed that for the first axle, the measured and calculated deflections were similar, whereas for the other axles, and in particular the 3 rear axles the measured deflections were lower than those calculated with the reference 44 tons truck. This result could be explained by the fact that the load of the front axle of T2S3 trucks is very little influenced by the weight of the cargo, and is, in average, equal to 6.5 tons. Then, new calculations were performed with ALIZE, by adjusting the load values of the last 3 axles, until a good fit was obtained with the measured signals, and these loads were used to estimate the total weight of the T2S3 vehicles. This approach was applied to the “representative” deflection signals of each month, and the weights of the vehicles were estimated. Truck weights generally varying between 30 and 35 tons were obtained. This approach provides a relatively simple means of estimating vehicle weights, which could be interesting for estimating effective pavement damage due to traffic. In this project, it was not possible to validate the estimated weights, by comparison with reference measurements, made with a weight in motion system; but such comparisons will be performed in the next months, to determine the accuracy of this approach.

In conclusion, in the last chapter, different applications of the geophone measurements to the monitoring of a real road, under continuous traffic, over a significant period of time, were proposed. With the different calculation procedures developed, it was shown that a relatively limited instrumentation with geophones and temperature probes (or possibly also with accelerometers) can provide very useful data for road managers, including:

- Counting of heavy vehicles, identification of their silhouettes, and estimation of their speeds.
- Monitoring of variations of pavement temperatures and pavement deflections with time; by applying a temperature correction to the deflections, it is possible to follow pavement deterioration (inferred from the evolution of deflections).
- After calibrating a pavement model (by carrying for example deflection measurements under a test vehicle of known load), it is also possible to use the measured deflections to estimate vehicle weights.

The different information obtained (deflections, temperatures, vehicle loads) could also be used to calculate, by an incremental procedure, effective pavement damage due to the real traffic loads, and real pavement temperatures, and thus also the remaining pavement service life.

## CONCLUSION GENERALE (FRANÇAISE)

Dans cette thèse, nous présentons une étude approfondie sur l'utilisation de géophones et d'accéléromètres pour l'instrumentation et la surveillance des chaussées. Les objectifs étaient d'évaluer l'efficacité des capteurs pour mesurer la déflexion des chaussées, puis de les tester en conditions réelles, pour l'instrumentation d'une chaussée à fort trafic, sous trafic continu. L'objectif était également de développer des méthodes d'analyse des mesures des capteurs, adaptées à une surveillance à long terme de la chaussée, sous trafic réel.

Les géophones et accéléromètres présentent plusieurs caractéristiques intéressantes pour l'instrumentation des chaussées. Ces capteurs présentent l'avantage d'être relativement petits et robustes, ce qui permet de les installer dans les couches de chaussées. La déflexion étant mesurée près de la surface de la chaussée, ils peuvent facilement être installés dans la chaussée, même après la construction. Enfin, de par leur principe de mesure (mesure de vitesse ou d'accélération), ils ne nécessitent pas de point de référence fixe pour mesurer le déplacement.

Le premier objectif de ce travail était de vérifier la possibilité d'utiliser ces capteurs pour la mesure des déflexions des chaussées. Pour cela, un programme d'essais en laboratoire a été défini, pour évaluer les caractéristiques des capteurs, et leur réponse à des signaux de déplacement réalistes, avec différentes amplitudes et fréquences. Les résultats de ces tests ont été présentés dans le chapitre 2. Lors du traitement de ces signaux, on a montré qu'une simple intégration de la vitesse (ou double intégration de l'accélération) conduit à un signal de forme incorrecte, qui présente des oscillations positives et négatives. Pour éliminer ces oscillations, on a choisi d'utiliser la transformée de Hilbert, qui est notamment utilisée dans les méthodes de modulation du signal pour séparer l'enveloppe d'un signal de sa porteuse. Une méthode originale de traitement des signaux a ainsi été proposée, pour la mesure de la déflexion. Le traitement comprend cinq étapes: le filtrage du bruit, l'amplification, l'intégration du signal (ou double intégration pour les accéléromètres), la suppression de la composante continue et l'application de la transformée de Hilbert. Les résultats obtenus avec cette procédure ont été comparés à des mesure de référence, réalisées avec un capteur de déplacement laser, et on a montré que des valeurs réalistes peuvent être obtenues pour tous les capteurs testés, pour une plage de fréquences et d'amplitudes correspondant aux déformations réelles de la chaussée.

Le deuxième objectif, dans le chapitre trois, était d'évaluer la réponse des capteurs installés dans la chaussée, sous charge roulante. À cet effet, une section de chaussée testée sur le manège de fatigue de l'IFSTTAR a été instrumentée avec des géophones, des accéléromètres et des sondes de température. Cette étude représentait une étape nécessaire pour valider la réponse des capteurs, et

la méthode de traitement du signal, en conditions réelles. Au cours de ces essais, différentes conditions de chargement contrôlées (charges, vitesses et positions des roues) ont été appliquées. Les résultats ont été comparés à des mesures réalisées avec un déflectomètre ancré, choisi comme référence. Ce type de capteur est peu utilisé sur des chaussées en service, mais permet de réaliser des mesures de déflexion précises. Les résultats ont montré une bonne concordance entre les mesures des accéléromètres et géophones, et du déflectomètre de référence, pour différentes vitesses. On a également montré que la position des roues par rapport aux capteurs a une grande influence sur les mesures. La déformation maximale est obtenue lorsque l'une des roues est centrée sur les capteurs.

Les résultats des mesures ont ensuite été comparés à des prédictions obtenues avec un modèle élastique linéaire (logiciel Alize) et avec un modèle visco-élastique (logiciel Visco-route). Les calculs ont été effectués avec des paramètres d'enrobés bitumineux déterminés à partir d'essais de module complexe en laboratoire et en prenant en compte les conditions expérimentales (vitesse de chargement et température). Les résultats ont indiqué une bonne concordance entre les réponses mesurées et calculées avec des différences maximales de 10% pour le modèle élastique et de 7% pour le modèle viscoélastique.

L'objectif du chapitre 4 était de développer des procédures de calcul inverse, pour la détermination des modules des couches de chaussées, à partir des bassins de déflexion mesurés par les géophones et les accéléromètres. Deux procédures différentes ont été testées pour le calcul des modules. La première approche, classique, a consisté à utiliser l'outil de calcul inverse du logiciel ALIZE. Cette approche consiste à comparer les bassins de déflexion mesurés et calculés, et à ajuster, par itération, les modules des couches, jusqu'à obtenir le meilleur ajustement du bassin de déflexion mesuré. Une deuxième approche, initialement proposée par Levenberg (2012), a également été testée. Cette approche consiste à effectuer l'optimisation en utilisant directement les signaux d'accélération ou de vitesse délivrés par les capteurs. Cette seconde approche a été implémentée dans l'outil de calcul élastique linéaire ELLEA. Après avoir calculé les déflexions de la chaussée à l'aide du modèle élastique, celles-ci ont été converties en valeurs de vitesse et d'accélération, par dérivation numérique. Les signaux de vitesse (respectivement d'accélération) calculés ont ensuite été comparés aux mesures des capteurs. Une procédure d'optimisation a été utilisée pour ajuster de manière itérative les modules des couches de chaussée, jusqu'à obtenir un bon calage des mesures. L'avantage de cette deuxième méthode est qu'elle permet d'utiliser directement les signaux des capteurs, sans effectuer de traitement ou d'intégration, qui pourrait réduire leur précision. Les modules rétro-calculés par les deux méthodes ont été comparés à des valeurs de référence, obtenues à partir d'essais FWD et d'essais de module en laboratoire. Les résultats ont indiqué que les deux

méthodes conduisaient à des modules réalistes, avec un léger avantage pour l'approche basée sur ALIZE.

L'objectif du dernier chapitre était d'appliquer des différentes méthodes d'instrumentation et de traitement développées dans la thèse aux données provenant d'un site réel instrumenté, situé sur l'autoroute Ax. La section expérimentale a été instrumentée avec des géophones et des sondes de température placées à différentes profondeurs dans la chaussée, et connectées à un système d'acquisition de données PEGASE, permettant de transférer les données à distance.

Un grand nombre de données a été enregistré sur une période de 22 mois, et plusieurs procédures ont été développées pour suivre l'évolution des performances de la chaussée, et également pour caractériser le trafic. Les mêmes méthodes de traitement du signal développées et testées dans les chapitres précédents ont été appliquées aux mesures des géophones sur l'autoroute Ax. Dans un premier temps, une procédure a été développée pour identifier les silhouettes des poids lourds passant sur la chaussée. Cette procédure est basée sur la détection de pics négatifs (nombre de pics, position des pics) des signaux du géophone après intégration. Les résultats ont montré qu'environ 80% des poids lourds circulant sur l'autoroute sont des semi-remorques T2S3 (à 5 essieux). Les vitesses des poids lourds ont également été estimées à partir des mesures de deux géophones placés dans le sens de la circulation (direction longitudinale) et séparés d'un mètre. La vitesse moyenne des poids lourds était d'environ 96 km / h.

Dans un deuxième temps, on s'est intéressé à l'analyse des déflexions, et une procédure de tri des signaux a été mise au point, afin de réduire la quantité de données à analyser. Cette procédure a consisté à sélectionner uniquement les signaux des camions T2S3 à 5 essieux. Ensuite, en utilisant les mesures de 3 géophones placés à différentes positions latérales, seuls les véhicules dont les roues étaient alignées sur le géophone central, G1, ont été retenus, afin d'éliminer l'effet de la position latérale des véhicules sur les mesures. Cette procédure de tri a permis de réduire significativement la variabilité des signaux de déflexion, en ne sélectionnant que des véhicules de même type, et passant à la même position latérale. A la suite de ce tri, les variations des déflexions maximales ont été analysées, et une forte influence de la température sur les déflexions a été observée. Deux procédures de correction de température différentes, donnant des résultats très similaires, ont été proposées pour éliminer les effets de température et ramener les déflexions à une température constante de 15 ° C. Après cette correction, on a pu étudier l'évolution des déflexions dans le temps, au cours de la période de mesure (22 mois). Les résultats n'ont pas montré d'évolution significative des déflexions corrigées, ce qui a conduit à conclure qu'aucune détérioration significative ne s'est produite pendant cette période; cela semble logique, car la chaussée avait été récemment renforcée (en 2013).

Enfin, les déflexions mesurées ont été comparées à des calculs de chaussées, réalisés avec le logiciel ALIZE. Le modèle de chaussée utilisé dans ALIZE, et en particulier les modules des couches, ont été déterminés à partir de mesures FWD, complétées par l'utilisation de valeurs de module standard pour certaines couches. Les résultats obtenus avec ALIZE ont été comparés, pour chaque mois, à un signal « représentatif ». Ce signal « représentatif » a été défini comme le signal réel enregistré donnant des valeurs de déflexion maximales les plus proches des valeurs moyennes mensuelles, pour chaque essieu.

À partir de ces résultats, une méthode originale d'estimation des charges des véhicules a été proposée. Dans un premier temps, les charges réelles des véhicules T2S3 passant sur l'autoroute étant inconnues, les calculs ALIZE ont été réalisés avec des charges correspondant à un camion T2S3 « de référence », chargé à 44 tonnes, avec des charges à l'essieu standard. Les premières comparaisons entre les calculs et les signaux mesurés ont montré que pour le premier essieu, les déflexions mesurées et calculées étaient similaires, alors que pour les autres essieux, et notamment pour les 3 essieux arrière, les déflexions mesurées étaient inférieures à celles calculées avec le camion de référence de 44 tonnes. Ce résultat s'explique par le fait que la charge de l'essieu avant des camions T2S3 est très peu influencée par le poids de la cargaison transportée, et vaut, en moyenne, 6,5 tonnes. Ensuite, de nouveaux calculs ont été effectués avec ALIZE, en ajustant les valeurs de charge des 3 derniers essieux, jusqu'à obtenir un bon ajustement des signaux mesurés, et ainsi une estimation du poids total des véhicules T2S3. Cette approche a été appliquée aux signaux de déflexion «représentatifs» de chaque mois et les poids des véhicules correspondants ont été estimés. Des poids de camions variant généralement entre 30 et 35 tonnes ont été obtenus. Cette approche fournit un moyen relativement simple d'estimer les poids des véhicules, et pourrait être utilisée pour calculer l'endommagement réel de la chaussée causé par le trafic. Dans ce projet, il n'a pas été possible de valider les poids obtenus, par comparaison avec des mesures de référence, réalisées par exemple avec un système de pesage en marche ; mais de telles comparaisons seront réalisées prochainement, pour vérifier la précision de cette approche.

En conclusion, dans le dernier chapitre, différentes applications des mesures des géophones au suivi d'une chaussée, sous trafic continu, sur une durée significative, ont été proposées. Avec les différentes procédures de calcul développées, on a montré qu'une instrumentation relativement réduite, comprenant des géophones et des sondes de température (ou éventuellement avec des accéléromètres) peut fournir des données très utiles pour les gestionnaires de réseaux routiers, incluant :

- Le comptage des véhicules lourds, l'identification de leurs silhouettes et l'estimation de leurs vitesses.

- Le suivi des variations de température et des déflexions de la chaussée dans le temps; En corrigeant les variations de la déflexion avec la température, il est également possible de suivre l'endommagement de la chaussée (déduite de l'évolution des déflexions).
- Après avoir calé un modèle de la chaussée (en réalisant par exemple des mesures de déflexion à l'aide d'un véhicule d'essai de charge connue), il est également possible d'utiliser les déflexions mesurées pour estimer les poids des véhicules.

Les différentes informations obtenues (déformations, températures, charges des véhicules) pourraient également être utilisées pour calculer, de manière incrémentale, l'endommagement de la chaussée dû aux charges réelles des véhicules, et aux températures réelles, et donc également la durée de vie résiduelle de la chaussée.

## PERSPECTIVES

This work focuses on using the geophones and accelerometer to measure the deflection. This study propose different interpretation of these measurements, and opens up several perspectives for the continuation of this research.

Firstly, the experiments showed that the sensors like geophones and accelerometers are appropriate for measuring the deflections. Also the proper functioning of the remote acquisition systems, which have collected large amounts of data to study the pavement mechanics and structures and the daily traffic variations. They also showed the potential of geophones, relatively inexpensive sensors, and very sensitive to low movements recorded on thick motorway pavements, for the assessment of the traffic composition, and the estimate of deflections.

An interesting development could be the implementation of certain treatment procedures (like directly measuring the deflections, identification and counting of silhouettes, determination of speeds, sorting of signals according to certain criteria), directly on the cards data acquisition systems, designed for this type of application. This would allow treatment in real time, avoiding storing of the complete acquisition signals.

Despite interesting results, the deployment of these sensors on a larger scale instrumented roads could be costly as the sensors are expensive, 100 € for the geophones, around 300 € for the accelerometers. Another difficulty is of implementation of these sensors, because the sensors used are currently wired sensors, which require the passage of wires between the sensor and the acquisition system. More research on development of wireless sensors and low cost sensor should be done to facilitate the applicability of the system on a large scale.

One of the prominent results that has been highlighted concerns the characteristics of the pavement that shows the behavior seems to be sensitive to temperature and that of an elastic or viscoelastic layer properties. These results deserve to be continued by studies in laboratory, on the behavior of interfaces, at different temperatures in order to confirm the observed behaviors.

Finally, the perspective concerns the exploitation of geophone signals to estimate the weights of the moving vehicle on a real road. The weight in motion device could be used to validate the accuracy of the estimation of the vehicle loads using the deflection signals of the sensors. Using of these low cost sensors to estimate the load will be a promising application to further investigate.

## REFERENCES

- AASHTO. (1986). *AASHTO Guide for Design of Pavement Structures*.
- AASHTO. (2000). Standard Specifications for Transportation Materials and Methods of Sampling and Testing and AASHTO Provisional Standards.
- AASHTO. (2008). *Mechanistic-Empirical Pavement Design Guide A Manual of Practice*.
- Ai, C., Rahman, A., Xiao, C., Yang, E. et Qiu, Y. (2017). Analysis of measured strain response of asphalt pavements and relevant prediction models. *International Journal of Pavement Engineering*, 18(12), 1089-1097. 10.1080/10298436.2016.1149836
- Al-Qadi, I., Loulizi, A., Elseifi, M. et Lahouar, S. (2004). *The Virginia Smart Road: The Impact of Pavement Instrumentation on Understanding Pavement Performance*. Baton Rouge, LA, USA (p. 427-465).
- Arattano, M. et Marchi, L. (2008). Systems and sensors for Debris-flow monitoring and warning. *Sensors*, 8(4), 2436-2452. 10.3390/s8042436
- Arraigada, M., Partl, M. N., Angelone, S. M. et Martinez, F. (2009). Evaluation of accelerometers to determine pavement deflections under traffic loads. *Materials and Structures/Materiaux et Constructions*, 42(6), 779-790. 10.1617/s11527-008-9423-5
- Aszkler, C. (2005). Acceleration, Shock and Vibration Sensor. Dans J. S. Wilson (dir.), *Sensor Technology Handbook*. 10.1016/B978-0-7506-7729-5.50045-8
- Bahrani, N., Blanc, J., Hornyh, P. et Menant, F. (2019). Pavement Instrumentation for Condition Assessment Using Efficient Sensing Solutions, 471-480. 10.1680/icsic.64669.471
- Bahrani, N., Blanc, J., Hornyh, P. et Menant, F. (2020). Alternate method of pavement assessment using geophones and accelerometers for measuring the pavement response. *Infrastructures*, 5(3). 10.3390/infrastructures5030025
- Bahrani, Natasha., Blanc, J., Hornyh, P. et Menant, F. (2020). Evaluation of the Use of Geophones and Accelerometers for Monitoring Pavement Deflections, Using Accelerated Pavement Tests. Dans *Accelerated Pavement Testing to Transport Infrastructure Innovation 2020*. Springer.
- Bahrani, Natasha., Levenberg, E., Blanc, J. et Hornyh, P. (2020). Inverse Analysis of Pavement Layer Moduli Based on Data Collected by Buried Accelerometers and Geophones. Dans *Accelerated Pavement Testing to Transport Infrastructure Innovation 2020*. Springer.
- Barriera, M., Pouget, S., Lebental, B. et Van Rompu, J. (2020). In situ pavement monitoring: A

- review. *Infrastructures*, 5(2). 10.3390/infrastructures5020018
- Blackledge, J. M. ed. W. P. (2006). *Digital Signal Processing: Mathematical and Computational Methods, Software development and applications* (2nd éd.). Woodhead Publishing.
- Blanc, J., Horny, P., Duong, N. S., Blanchard, J. Y. et Nicollet, P. (2019). Monitoring of an experimental motorway section. *Road Materials and Pavement Design*, 20(1), 74-89. 10.1080/14680629.2017.1374997
- Bodin, D., Chupin, O. et Denneman, E. (2017). Viscoelastic asphalt pavement simulations and simplified elastic pavement models based on an “equivalent asphalt modulus” concept. *Journal of Testing and Evaluation*, 45(2), 1887-1895.
- Burmister, D. (1943). (1943). The theory of stress and displacements in layered systems and applications of the design of airport runways. *The Highway Research Board*, 23.
- Cam, V. Le. (2011). Journées techniques Ouvrages d'Art Utilisation de la carte d'instrumentation PEGASE de d'IFSTTAR dans plusieurs applications Sommaire.
- Cam, V. Le et Bourquin, F. (2008). Design of a generic smart and wireless sensors network – Benefits of emerging technologies.
- CEREMA-IDRRIM. (2016). Diagnostic et conception des renforcements de chaussées.
- Chabot, A., Tamagny, P., Poché, D. et Duhamel, D. (2006). Visco-elastic modelling for asphalt pavements -- software {ViscoRoute}. *International Conference on Asphalt Pavements, \ntb{10}, 2006, Québec City, Canada, (1943), 10.*
- Chabot, Armelle, Chupin, O., Deloffre, L. et Duhamel, D. (2010). ViscoRoute 2.0 A: Tool for the Simulation of Moving Load Effects on Asphalt Pavement. *Road Materials and Pavement Design*, 11(2), 227-250. 10.1080/14680629.2010.9690274
- Chailleux, E., Such, C., Ramond, G. et de La Roche, C. (2006). A mathematical-based master-curve construction method applied to complex modulus of bituminous materials. *International Journal Road Materials and Pavement Design, Vol 7(Special Issue EATA), 75-92.*
- Chang, T. Y. et Cui, H. L. (2013). Determination of Direction of Arrival of Seismic Wave by a Single Tri-axial Fiber Optic Geophone. *Defence Technology*, 9(1), 1-9. 10.1016/j.dt.2013.02.001
- Chupin, O., Chabot, A., Piau, J. M. et Duhamel, D. (2010). Influence of sliding interfaces on the response of a layered viscoelastic medium under a moving load. *International Journal of Solids and Structures*, 47(25-26), 3435-3446. 10.1016/j.ijsolstr.2010.08.020

- D'Alessandro, A., Scudero, S. et Vitale, G. (2019). A review of the capacitive MEMS for seismology. *Sensors (Switzerland)*, 19(14), 1-22. 10.3390/s19143093
- Dessouky, S. H., Al-Qadi, I. L. et Yoo, P. J. (2014). Full-depth flexible pavement responses to different truck tyre geometry configurations. *International Journal of Pavement Engineering*, 15(6), 512-520. 10.1080/10298436.2013.775443
- Duong, N. S., Blanc, J., Horny, P., Menant, F., Lefeuvre, Y. et Bouveret, B. (2018). Monitoring of pavement deflections using geophones. *International Journal of Pavement Engineering*, 21(9), 1103-1113. 10.1080/10298436.2018.1520994
- Duong, N. S., Blanc, J., Horny, P., Menant, F., Lefeuvre, Y. et Bouveret, B. (2020). Monitoring of pavement deflections using geophones. *International Journal of Pavement Engineering*, 21(9), 1103-1113. 10.1080/10298436.2018.1520994
- Elseifi, M. A. (2009). *Analysis of Seasonal Strain Measurements in Asphalt Materials under Accelerated Pavement Testing and Comparing Field Performance and Laboratory Measured Binder Tension Properties*. 5. Report Date 13. Type of Report and Period Covered Final Report 2008 14. S.
- Goacolou, H. e. (2003). La méthode française de dimensionnement. In *Revue Générale des Routes et de l'Aménagement*, (Issue 823).
- Huet, C. (1965). *Etude par une méthode d'impédance du comportement viscoélastiques des matériaux hydrocarbonnés*. In *Thèse à l'Université de Paris*.
- Ksaibati, K., Armaghani, J. et Fisher, J. (2000). Effect of moisture on modulus values of base and subgrade materials. *Transportation Research Record*, (1716), 20-29. 10.3141/1716-03
- Lajnef, N., Rhimi, M., Chatti, K., Mhamdi, L. et Faridazar, F. (2011). Toward an integrated smart sensing system and data interpretation techniques for pavement fatigue monitoring. *Computer-Aided Civil and Infrastructure Engineering*, 26(7), 513-523. 10.1111/j.1467-8667.2010.00712.x
- Leiva-Villacorta, F. &. (2012). Simulating the effects of instrumentation on measured pavement response. In D. Jones, J. Harvey, & A. M. Al-Qadi. (Eds.), *Advances in Pavement Design through Full-scale Accelerated Pavement Testing*.
- Levenberg, E. (2009). Validation of NCAT structural test track experiment using INDOT APT facility. *Bearing Capacity of Roads, Railways and Airfields - Proceedings of the 8th International Conference on the Bearing Capacity of Roads, Railways and Airfields*, 2, 1361-1371. 10.1201/9780203865286.ch142
- Levenberg, Eyal. (2012). Inferring Pavement Properties using an Embedded Accelerometer.

- International Journal of Transportation Science and Technology*, 1(3), 229-246. 10.1260/2046-0430.1.3.229
- Liu, P., Otto, F., Wang, D., Oeser, M. et Balck, H. (2017). Measurement and evaluation on deterioration of asphalt pavements by geophones. *Measurement: Journal of the International Measurement Confederation*, 109, 223-232. 10.1016/j.measurement.2017.05.066
- Liu, Y., He, L. Q., Jiang, Y. J., Sun, M. M., Chen, E. J. et Lee, F. H. (2019). Effect of in situ water content variation on the spatial variation of strength of deep cement-mixed clay. *Geotechnique*, 69(5), 391-405. 10.1680/jgeot.17.P.149
- Michael BROUTIN. (2014). *Auscultation des chaussées souples aéronautiques au HWD- Guide technique*.
- Montalv, D. (2015). Sensors & Signal Processing Diogo Montalvão Senior Lecturer in Mechanical Systems, (November). 10.1201/b19009
- Mougenot, D. et Thorburn, N. (2004). MEMS-based 3C accelerometers for land seismic acquisition: Is it time? *Leading Edge (Tulsa, OK)*, 23(3), 246-250. 10.1190/1.1690897
- Olivier, C., Armelle, C., Didier, B. et Jean-Michel, P. (2014). Determination of an equivalent elastic system to a multilayer viscoelastic structure: Application to the case of thick flexible pavement. *Asphalt Pavements - Proceedings of the International Conference on Asphalt Pavements, ISAP 2014*, 1, 797-804. 10.1201/b17219-99
- Oome, A. J. J. A., Janssen, J. L. G., Encica, L., Lomonova, E. et Dams, J. A. A. T. (2009). Modeling of an electromagnetic geophone with passive magnetic spring. *Sensors and Actuators, A: Physical*, 153(2), 142-154. 10.1016/j.sna.2009.04.019
- Pouteau, B., Berrada, K. et Drouadaine, I. (2017). Smartvia concept : a 5 years feedback on standalone pavement structure monitoring, (June). 10.14311/ee.2016.202
- Raita-aho, T , Saramaki, T. (1994). A digital filter for ECG signal processing. *IEEE Transactions on Instrumentation and Measurement, Volume 43*, 644-649.
- Ryynänen, T., Pellinen, T. et Belt, J. (2014). The use of accelerometers in the pavement performance monitoring and analysis. *IOP Conference Series: Materials Science and Engineering*, 10(1). 10.1088/1757-899X/10/1/012110
- Saevarsdottir, T. et Erlingsson, S. (2013). Water impact on the behaviour of flexible pavement structures in an accelerated test. *Road Materials and Pavement Design*, 14(2), 256-277. 10.1080/14680629.2013.779308

- Saevarsdottir, T., Erlingsson, S. et Carlsson, H. (2016). Instrumentation and performance modelling of heavy vehicle simulator tests. *International Journal of Pavement Engineering*, 17(2), 148-165. 10.1080/10298436.2014.972957
- Sangiorgi, C., Settimi, C., Tataranni, P., Lantieri, C. et Adomako, S. (2018). Thermal Analysis of Asphalt Concrete Pavements Heated with Amorphous Metal Technology. *Advances in Materials Science and Engineering*, 2018. 10.1155/2018/6382874
- Sayegh, G. (1966). *Contribution à l'étude des propriétés viscoélastiques des bitumes purs et des bétons bitumineux. Thèse à l'Université de Paris.* Université de Paris.
- Schmidt, F. J., Jacob, B. et Domprobst, F. (2016). Investigation of truck weights and dimensions using WIM data. *Transportation Research Procedia*, 14, 811-819.
- SETRA et Lcpc. (1998). Catalogue des structures types de chaussées neuves.
- SETRA et LCPC. (1994). Conception et dimensionnement des structures de chaussée — guide technique. *Guide technique, Dec.*  
<http://scholar.google.com/scholar?hl=en&btnG=Search&q=intitle:Conception+et+dimensionnement+des+structures+de+chaussées#1>
- Sohm, J., Hornych, P., Kerzreho, J. P., Cottineau, L. M., Le Cam, V., Hautiere, N., De La Roche, C. et Van Damme, H. (2012). Remote monitoring of an experimental motorway section - an enabling technology of the 5th generation road. *International Journal of Pavement Research and Technology*, 5(5), 289-294. 10.6135/ijprt.org.tw/2012.5(5).289
- Swett, L., Mallick, R. B. et Humphrey, D. N. (2008). A study of temperature and traffic load related response in different layers in an instrumented flexible pavement. *International Journal of Pavement Engineering*, 9(5), 303-316. 10.1080/10298430701576117
- Tabatabaee, N. et Sebaaly, P. (1990). State-of-the-Art Pavement Instrumentation. *Transportation Research Record*, 246-256. <http://onlinepubs.trb.org/Onlinepubs/trr/1990/1260/1260-022.pdf>
- Tao, M., Zhang, Z. et Wu, Z. (2008). Simple Procedure to Assess Performance and Cost Benefits of Using Recycled Materials in Pavement Construction. *Journal of Materials in Civil Engineering*, 20(11), 718-725. 10.1061/(asce)0899-1561(2008)20:11(718)
- Technique, G. et Regionaux, D. E. S. M. (2003). Guide Technique Pour L ' Utilisation Des Matériaux Régionaux D ' Ile-De-France Catalogue Des Structures. [http://www.ile-de-france.cerema.fr/IMG/pdf/cat\\_str\\_ch\\_cle77b4d6.pdf](http://www.ile-de-france.cerema.fr/IMG/pdf/cat_str_ch_cle77b4d6.pdf)

- Tran, D. (2012). Sensors & Transducers A Piezoresistive Acceleration Sensor : from System to Physical Levels. *Sensors & transducers journal*, 145(10), 86-95.
- Van Cauwelaert, F. (1995). Stresses and displacements in multi-layered orthotropic systems. *Theoretical background to the stress/strain calculation program used within the NOAH software*.
- Voldman, J., Sds, T. et Adi, T. D. (2007). Joel Voldman Massachusetts Institute of Technology Outline > Accelerometer fundamentals > Analog Devices accelerometer. *Spring*.
- Xue, W., Wang, L., Wang, D. et Druta, C. (2014). Pavement health monitoring system based on an embedded sensing network. *Journal of Materials in Civil Engineering*, 26(10), 1-8. 10.1061/(ASCE)MT.1943-5533.0000976
- Zan, L., Latini, G., Piscina, E., Polloni, G. et Baldelli, P. (2002). Landslides early warning monitoring system. *International Geoscience and Remote Sensing Symposium (IGARSS)*, 1(C), 188-190. 10.1109/igarss.2002.1024983

# ANNEX

## Annex A: Results of Sensors laboratory tests

### Transfer function of Geophone Geo-space

Below are the transfer functions measured for the Geophone GeoSpace. We notice 2 peaks respectively at 100 Hz and 175 Hz. They are not to be taken into account, the peak at 100 Hz comes from the electrical network while the one at 175 Hz comes from the hydraulic group. The points around these frequencies have been removed for sensitivity calculations.

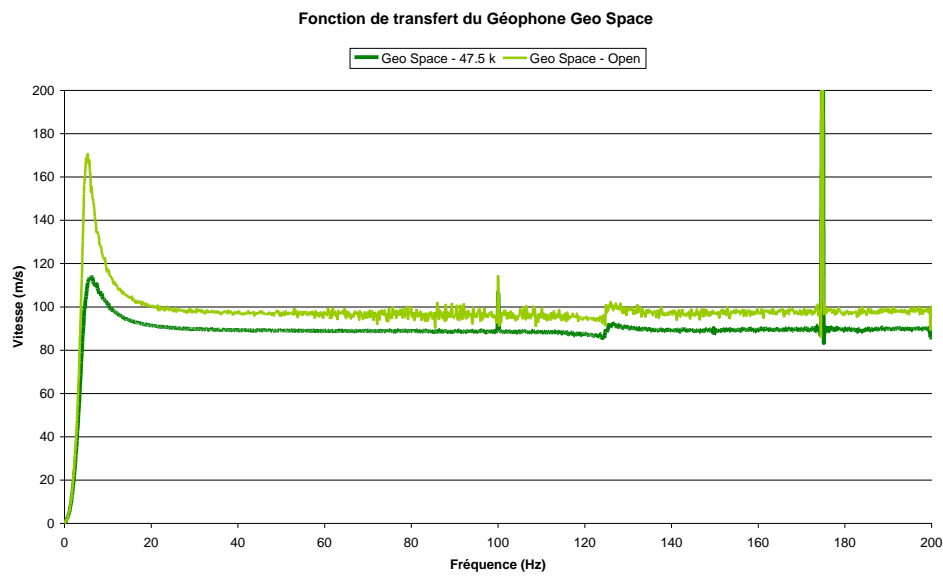


Figure A-1. (Graph n°1 : FRF GeoSpace – Open & 47k)

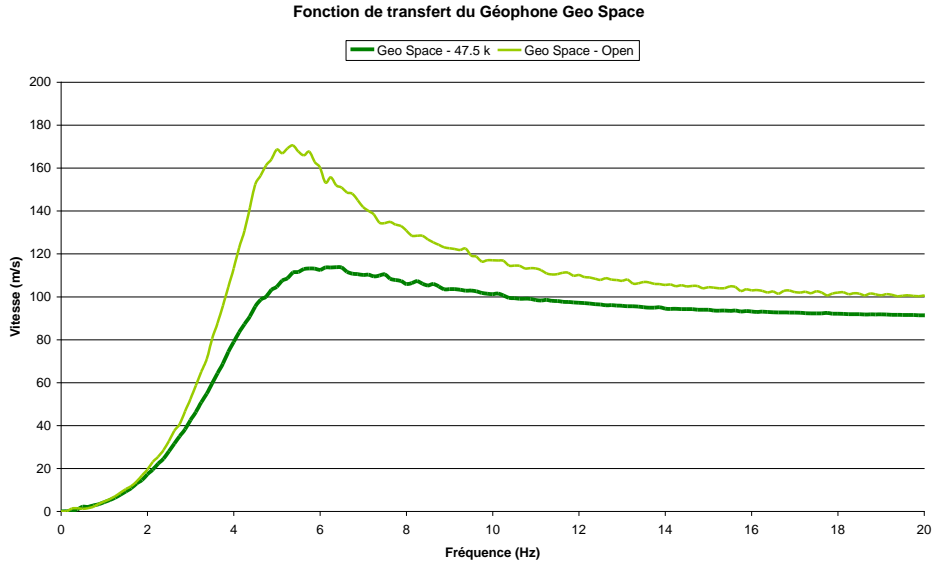


Figure A-2. (Graph n°2 : FRF GeoSpace – Open & 47k

Table A-1: summary table of measured sensitivities and results of equivalent filter modeling

| Frequency Band | Sensitivity GeoSpace « open » |                    | Sensitivity GeoSpace « 47k » |                    |
|----------------|-------------------------------|--------------------|------------------------------|--------------------|
|                | Average                       | Standard deviation | Average                      | Standard deviation |
| 30-60          | <b>97.18</b>                  | 0.71               | <b>89.19</b>                 | 0.25               |
| 30-100         | 96.80                         | 1.37               | 88.94                        | 0.32               |
| 30-200         | 96.98                         | 1.55               | 89.08                        | 0.79               |

### Transfer function of Geophone ION

Below are the transfer functions measured for the Geophone GeoSpace. Same remark as before concerning the 2 peaks at 100 Hz and 175 Hz. The two measurements were made with different levels of excitation to check the influence of the sensitivity as a function of the input level. According to the measurements, the sensitivity of the sensors varies little according to this parameter.

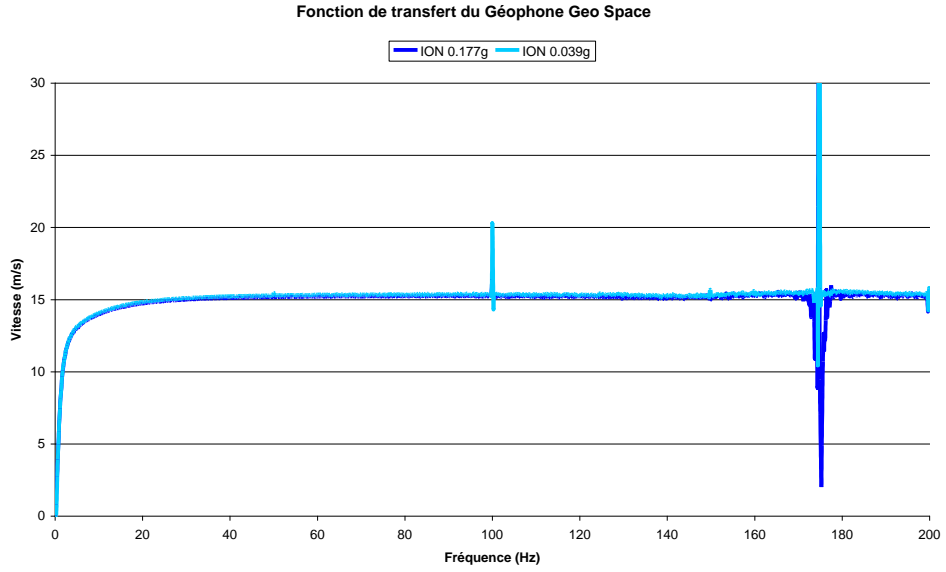


Figure A-3: (Graph n°1 : FRF ION)

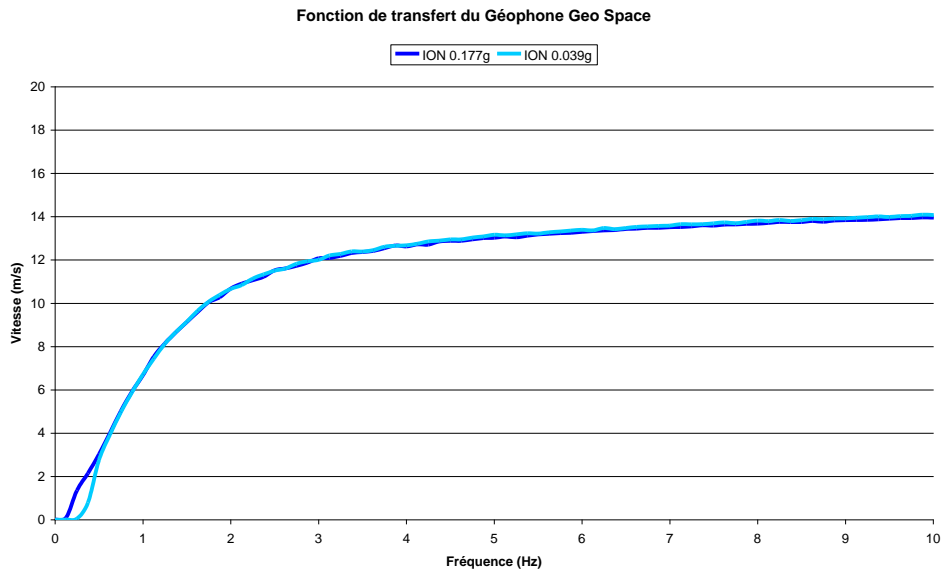


Figure A-1: (Graph n°1 : FRF ION)

Figure A-2: summary table of measured sensitivities and results of equivalent filter modeling

| Frequency Band | Sensitivity ION – 0.04 g (rms) |                    | Sensitivity ION 0.18 g (rms) |                    |
|----------------|--------------------------------|--------------------|------------------------------|--------------------|
|                | Average                        | Standard deviation | Average                      | Standard deviation |
| 30-60          | <b>15.25</b>                   | 0.07               | <b>15.13</b>                 | 0.06               |

|        |       |      |       |      |
|--------|-------|------|-------|------|
| 30-100 | 15.31 | 0.07 | 15.19 | 0.06 |
| 30-200 | 15.34 | 0.09 | 15.21 | 0.09 |

### Measurement of sensor noise

The purpose of these tests carried out with the sensors was to measure the noise level. This type of test could be helpful to indicate the amount of noise present in the signal and to select an appropriate filter to reduce this noise. Two types of geophones and two types of accelerometers, along with the reference laser sensor, were tested. The noise was measured in two different conditions :

when the hydraulic loading system was off (see the results in A-3)

when the hydraulic loading system was on (see the results in A-4)

The measurements with the loading system on were made to see if any vibrations induced by the loading system of the vibrating table affect the response of the transducers. It was found that for these two settings, the noise levels were different.

Table A-3. Noise ratio when the hydraulic system is off

| Sensors                                     | Noise( mean) | Noise (stdev) |
|---|--------------|---------------|
| Laser (m)                                   | -1.5612e-004 | 9.2372e-007   |
| Geophone GS11D-47k (m/s)                    | -5.6708e-005 | 5.1949e-005   |
| Geophone ion(m/s)                           | 3.9125e-004  | 3.1681e-005   |
| Geophone GS11D-18k (m/s)                    | -3.4436e-005 | 9.2211e-005   |
| Accelerometer SD (m/s <sup>2</sup> )        | -9.7214      | 0.0801        |
| Accelerometer MEMSIC<br>(m/s <sup>2</sup> ) | -9.7272      | 0.0386        |

Table A-4. Noise ratio when the hydraulic system is on

## Annex B

### Repeatability of the deflection measurements

The fatigue carousel has four arms hence it is possible to analyse the repeatability of the vertical signals produced by the loading of each arm during one passage. It is important to note that the repeatability of the signals was analysed before any processing was applied to the sensor data. shows the vertical displacements, velocities and accelerations generated by the loading of the 4 successive arms. A mean signal of all four arms is also calculated and represented.

To evaluate more precisely the difference between the signal under each arm, and the mean signal of the evaluated sensor, an error indicator R was defined. This indicator considered the entire shape of the experimental signal. The signal is considered from -2m to 2m.

This indicator is expressed by equation 1. It is defined as the mean relative difference, in percentage, between the values measured under each arm, by each evaluated sensor (the two geophones, the two accelerometers and the anchored deflectometer) and the mean signal, at each point i of the signal, divided by the total number of measurement points N of the signal.

$$R = \frac{1}{N} \sum_{i=1}^N \frac{|Mean\ signal(i) - raw\ signal(i)|}{Mean\ signal(i)} \times 100 \quad (1)$$

| Sensors                                  | Noise( mean) | Noise (stdev) |
|--|--------------|---------------|
| Laser (mm)                               | 1.5072831    | 0.            |
| Geophone GS11D-47k (m/s)                 | 5.4550e-005  | 1.7743e-007   |
| Geophone ion (m/s)                       | 3.6943e-004  | 2.1472e-006   |
| Geophone GS11D-18k (m/s)                 | -3.4518e-005 | 5.6026e-005   |
| Accelerometer SD (m/s <sup>2</sup> )     | -9.7209      | 0.0077        |
| Accelerometer MEMSIC (m/s <sup>2</sup> ) | -9.7240      | 0.0133        |

The relative mean difference between the signal of each arm and the mean signal is calculated for each arm. The obtained values are all very small, as shown in . These tests show that the signals produced by all the arms are very similar, and that all the sensors have a good repeatability.

Table B.1. Relative difference (in percentage) between the signal obtained under each arm of the fatigue carousel and the mean signal of each sensors.

| Sensors                 | Relative<br>Difference-<br>Arm 1(%) | Relative<br>Difference-<br>Arm 2(%) | Relative<br>Difference-<br>Arm 3(%) | Relative<br>Difference-<br>Arm 4(%) |
|-------------------------|-------------------------------------|-------------------------------------|-------------------------------------|-------------------------------------|
| Anchor<br>deflectometer | <b>0.00021</b>                      | <b>0.00033</b>                      | <b>0.00025</b>                      | <b>0.00025</b>                      |
| Geophone<br>GS11D       | <b>0.00000</b>                      | <b>0.00001</b>                      | <b>0.00001</b>                      | <b>0.00000</b>                      |
| Geophone Ion            | <b>0.00001</b>                      | <b>0.00001</b>                      | <b>0.00001</b>                      | <b>0.00000</b>                      |
| Accelerometer<br>ACC_CX | <b>0.00096</b>                      | <b>0.00090</b>                      | <b>0.00098</b>                      | <b>0.00078</b>                      |
| Accelerometer<br>ACC_SD | <b>0.00066</b>                      | <b>0.00053</b>                      | <b>0.00074</b>                      | <b>0.00052</b>                      |

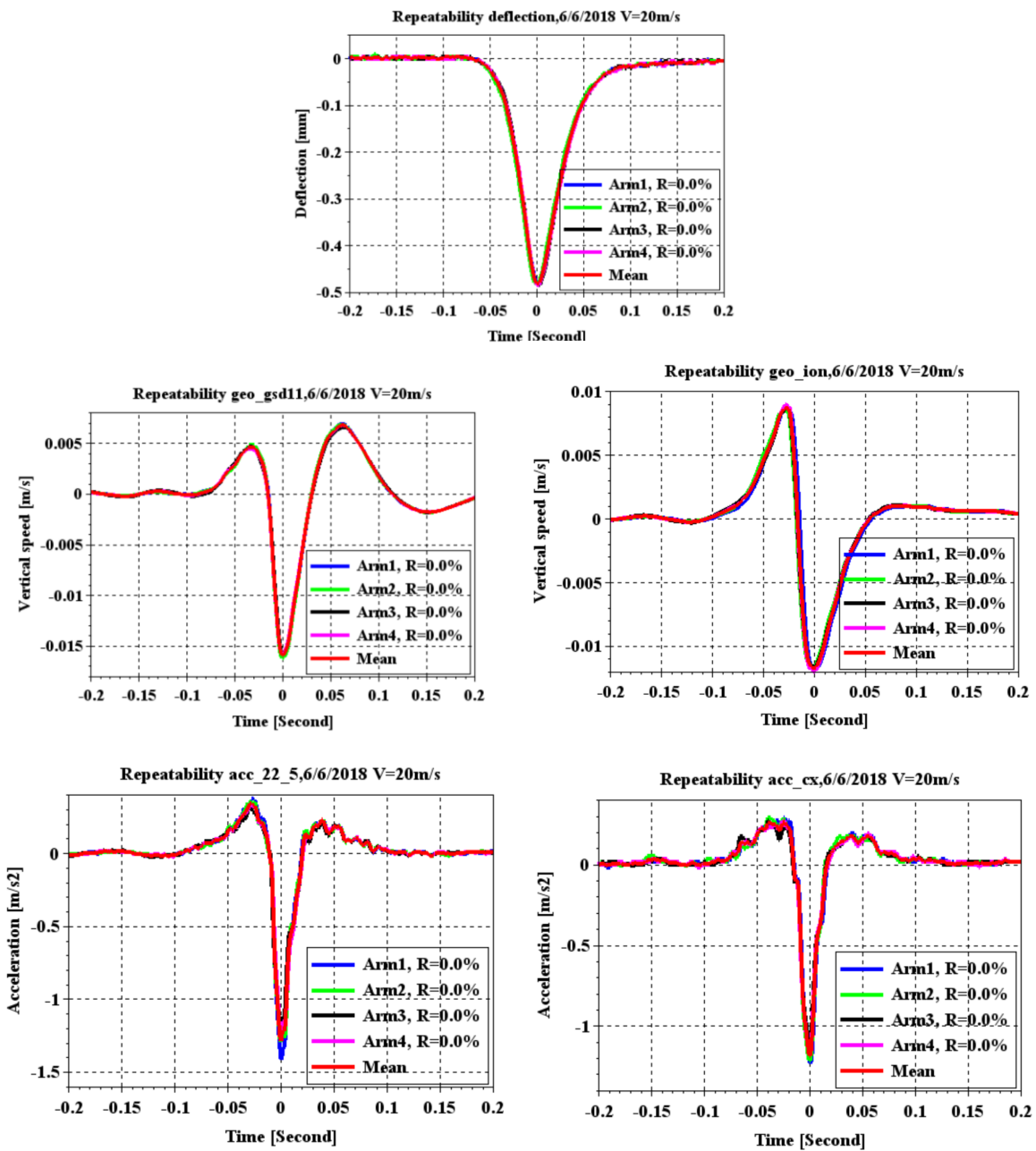


Figure B-1: Repeatability of the signals measured under the passage of each arm

## Annex C

### AX motorway experiments

#### Standard deviation of deflections

Table C.1. Standard deviation of monthly average deflection peaks measured during two years period

| <b>Date</b>   | <b>1st peak</b> | <b>2nd peak</b> | <b>3rd peak</b> | <b>4th peak</b> | <b>5th peak</b> |
|---------------|-----------------|-----------------|-----------------|-----------------|-----------------|
| <b>Oct-14</b> | 0.643457        | 0.641042        | 0.940544        | 0.875519        | 0.86358         |
| <b>Nov-14</b> | 0.535597        | 0.530061        | 0.826323        | 0.7888          | 0.75541         |
| <b>Dec-14</b> | 0.399957        | 0.493983        | 0.399957        | 0.726957        | 0.666946        |
| <hr/>         |                 |                 |                 |                 |                 |
| <b>Mar-15</b> | 0.55786         | 0.547063        | 0.817874        | 0.863878        | 0.777168        |
| <b>Apr-15</b> | 0.781059        | 0.741752        | 1.034323        | 0.961798        | 0.942248        |
| <b>May-15</b> | 0.810975        | 0.685326        | 1.165552        | 1.062178        | 1.047945        |
| <b>Jun-15</b> | 1.030707        | 0.995507        | 1.343586        | 1.304057        | 1.217744        |
| <b>Jul-15</b> | 1.060723        | 0.996596        | 1.400378        | 1.345045        | 1.292816        |
| <b>Aug-15</b> | 0.922423        | 0.881876        | 1.26083         | 1.203473        | 1.190229        |
| <b>Sep-15</b> | 1.213471        | 1.269891        | 1.573994        | 1.560648        | 1.459428        |
| <b>Oct-15</b> | 0.592952        | 0.592952        | 1.040787        | 0.897969        | 0.819536        |
| <b>Nov-15</b> | 0.454795        | 0.70937         | 0.454795        | 0.78934         | 0.749114        |
| <b>Dec-15</b> | 0.818627        | 0.818627        | 1.281671        | 0.681212        | 0.435224        |
| <hr/>         |                 |                 |                 |                 |                 |
| <b>Apr-16</b> | 0.782867        | 1.157877        | 1.298672        | 1.459853        | 0.912896        |
| <b>May-16</b> | 0.704435        | 1.293601        | 1.172351        | 0.972676        | 0.704435        |
| <b>Jun-16</b> | 0.847787        | 0.847787        | 1.177562        | 1.148973        | 1.101921        |
| <b>Jul-16</b> | 0.860431        | 0.834945        | 1.301791        | 1.204246        | 1.18181         |
| <b>Aug-16</b> | 1.069789        | 1.032226        | 1.367425        | 1.307552        | 1.233786        |
| <b>Sep-16</b> | 0.771405        | 0.821202        | 1.075454        | 1.056425        | 1.041981        |
| <b>Oct-16</b> | 0.571957        | 0.619296        | 0.905636        | 0.7897          | 0.72205         |
| <b>Nov-16</b> | 0.763178        | 0.374148        | 0.56698         | 1.008512        | 0.280601        |
| <b>Dec-16</b> |                 |                 |                 |                 |                 |

## Annex D

### AX motorway experiments

**Comparison of the representative signals of each month 2015 and 2016 with the Alize modelling for motorway Ax**

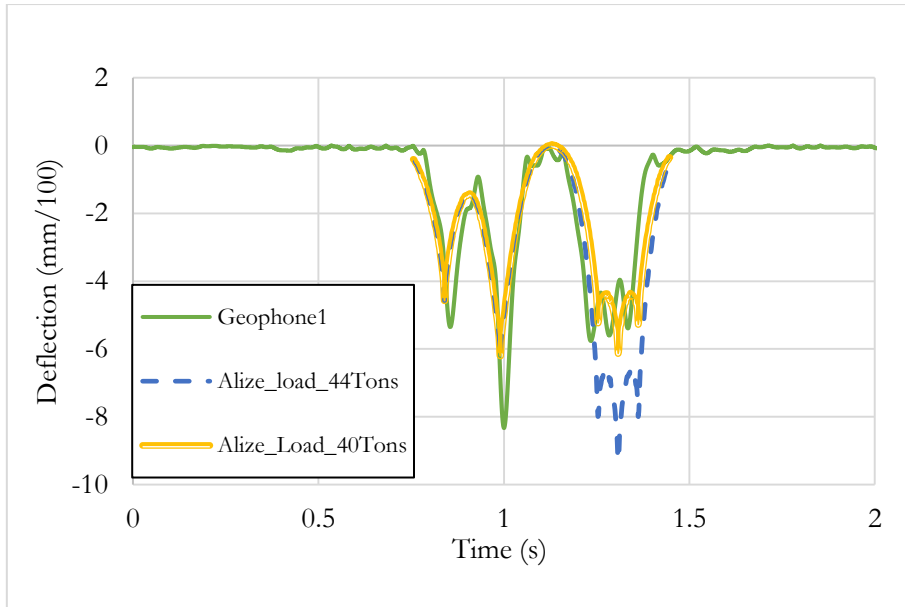


Figure D-1: Comparison of the deflection obtained with the representative signal of April 2015 (1/4/2015, 18h39min8s, 24m/s and 16°C) and the simulation with Alize with truck loaded at 32.5 tons and with the adjusted axles spacing

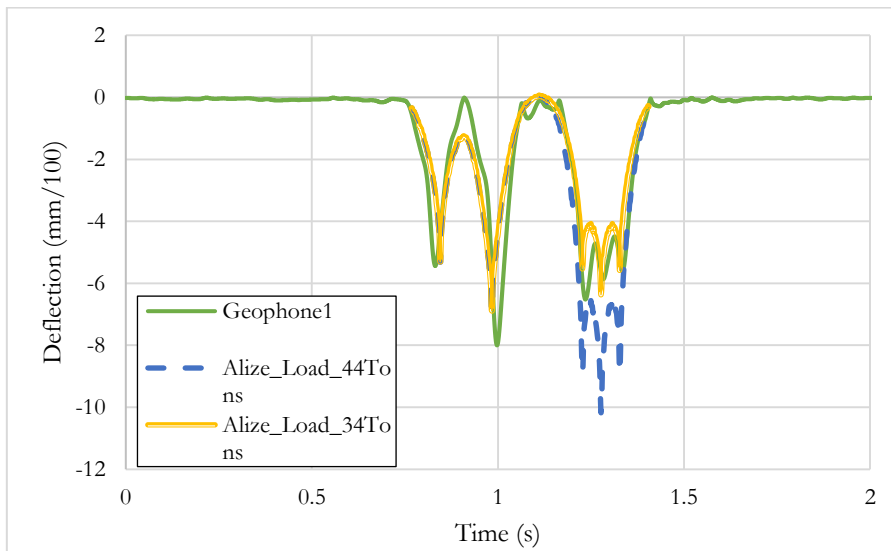


Figure D-2. Comparison of the deflection obtained with the representative signal of May 2015 (9/5/2015, 18h48min28s, 26m/s and 23°C) and the simulation with Alize with truck loaded at 32.5 tons and with the adjusted axles spacing

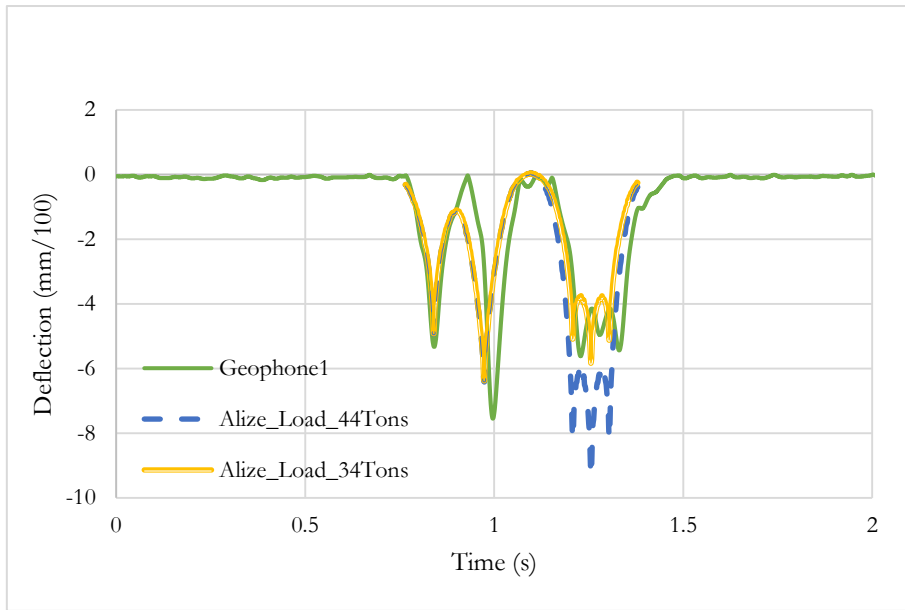


Figure D-3. Comparison of the deflection obtained with the representative signal of July 2015 (31/07/2015, 5h4mins22s,27m/s and 22°C) and the simulation with Alize with truck loaded at 32.5 tons and with the adjusted axles spacing

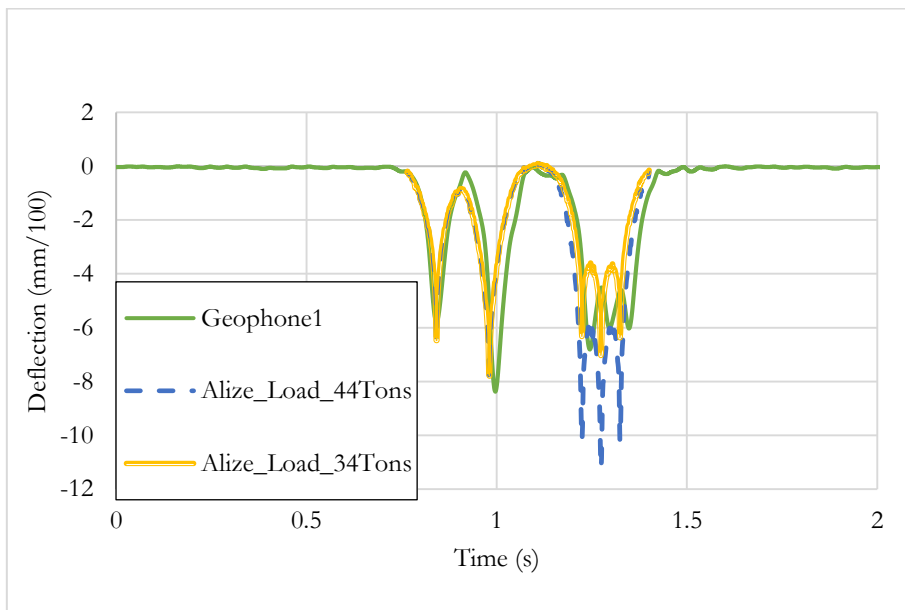


Figure D-4. Comparison of the deflection obtained with the representative signal of August 2015 (7/08/2015, 18h51min30s, 27m/s and 32°C) and the simulation with Alize with truck loaded at 32.5 tons and with the adjusted axles spacing

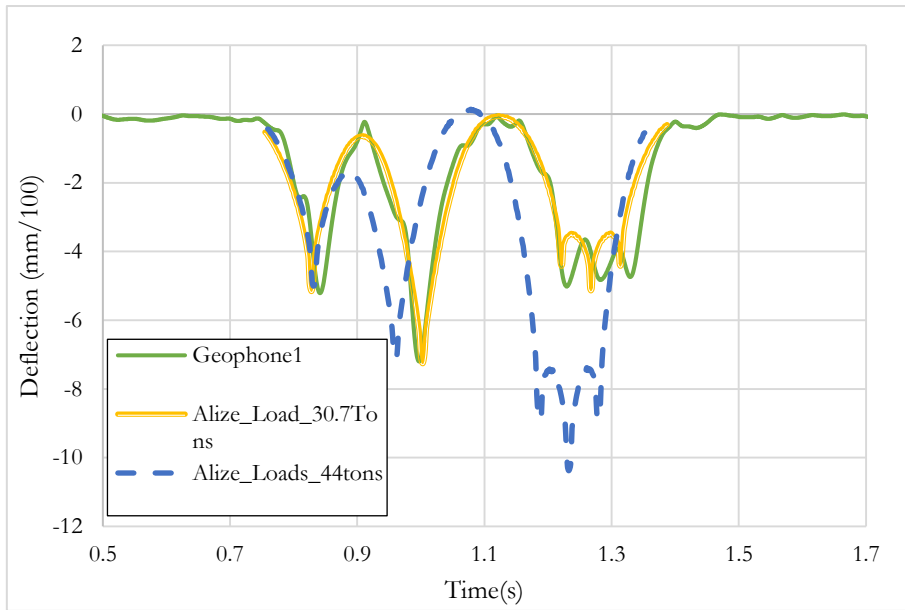


Figure D-5. Comparison of the deflection obtained with the representative signal of October 2015 (16/10/2015,17h10min27s, 29m/s and 15°C) and the simulation with Alize with truck loaded at 32.5 tons and with the adjusted axles spacing

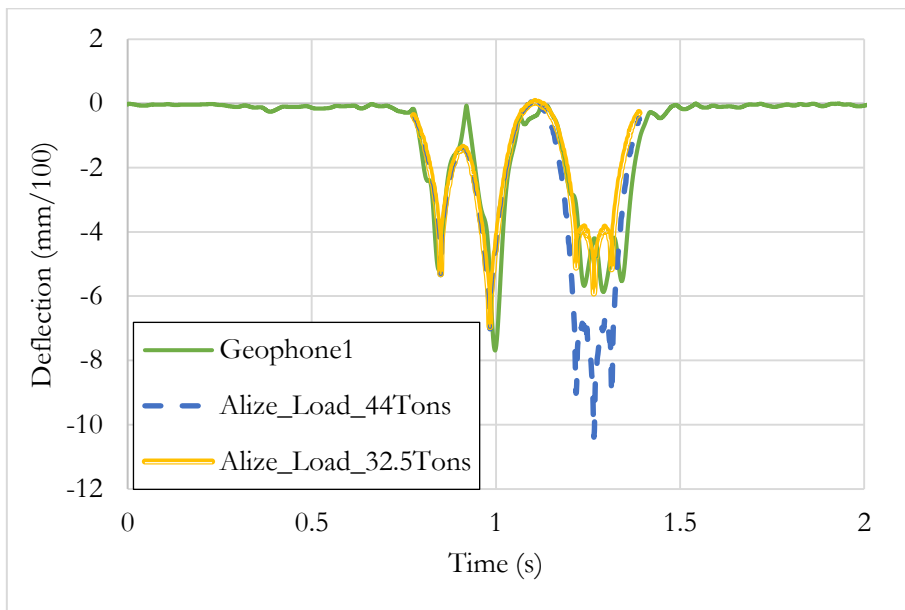


Figure D-6. Comparison of the deflection obtained with the representative signal of April 2016 (25/04/2016, 15h24min10s, 27m/s and 20°C) and the simulation with Alize with truck loaded at 32.5 tons and with the adjusted axles spacing

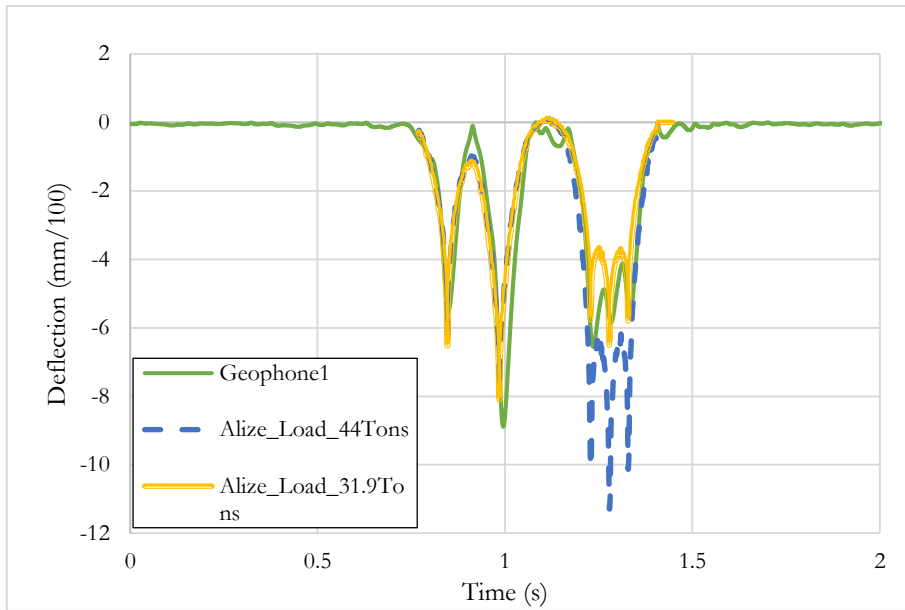


Figure D-7. Comparison of the deflection obtained with the representative signal of May 2016 (21/05/2016, 18h38min25s, 26m/s and 29°C) and the simulation with Alize with truck loaded at 32.5 tons and with the adjusted axles spacing

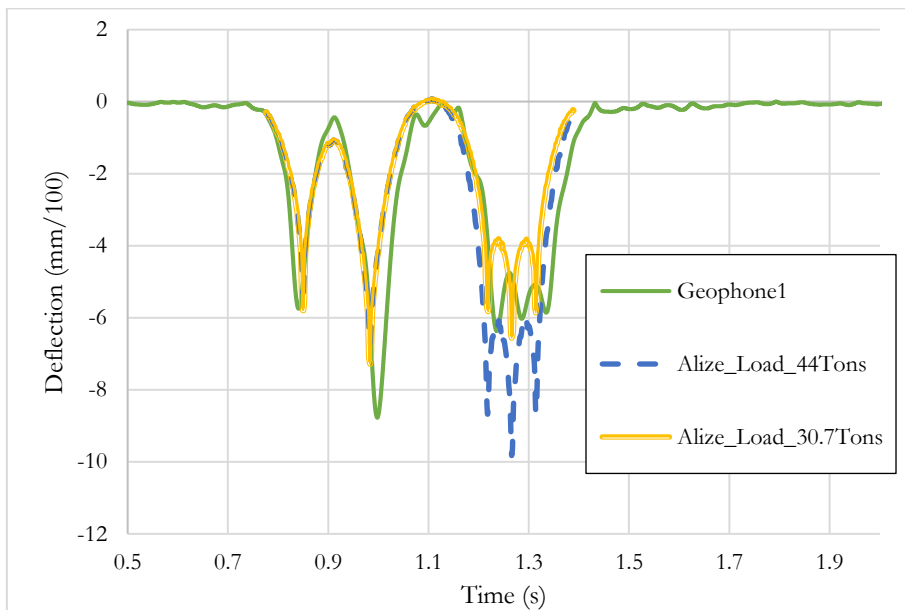


Figure D-8. Comparison of the deflection obtained with the representative signal of June 2016 (26/06/2016, 23h37min23s, 27m/s and 25°C) and the simulation with Alize with truck loaded at 32.5 tons and with the adjusted axles spacing

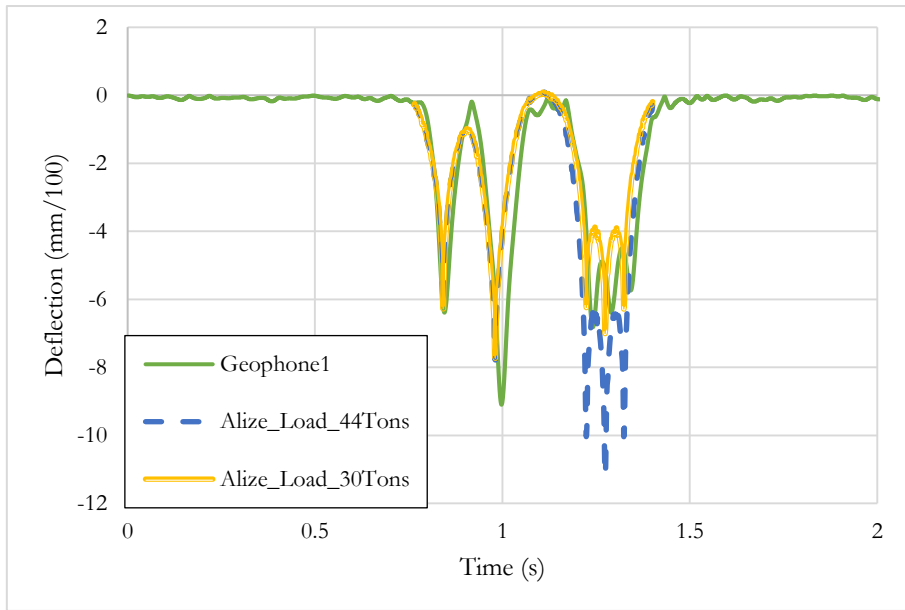


Figure D-9. Comparison of the deflection obtained with the representative signal of July 2016 (20/07/2016,6h28min32s,27m/s and 30°C) and the simulation with Alize with truck loaded at 32.5 tons and with the adjusted axles spacing

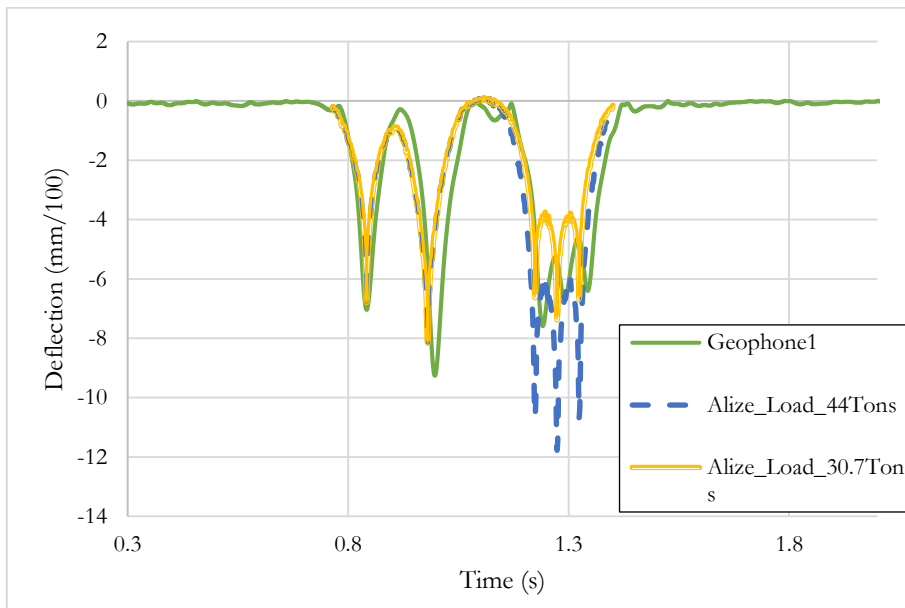


Figure D-10. Comparison of the deflection obtained with the representative signal of August 2016 (28/08/2016, 17h52min10s, 26m/s and 33°C) and the simulation with Alize with truck loaded at 32.5 tons and with the adjusted axles spacing

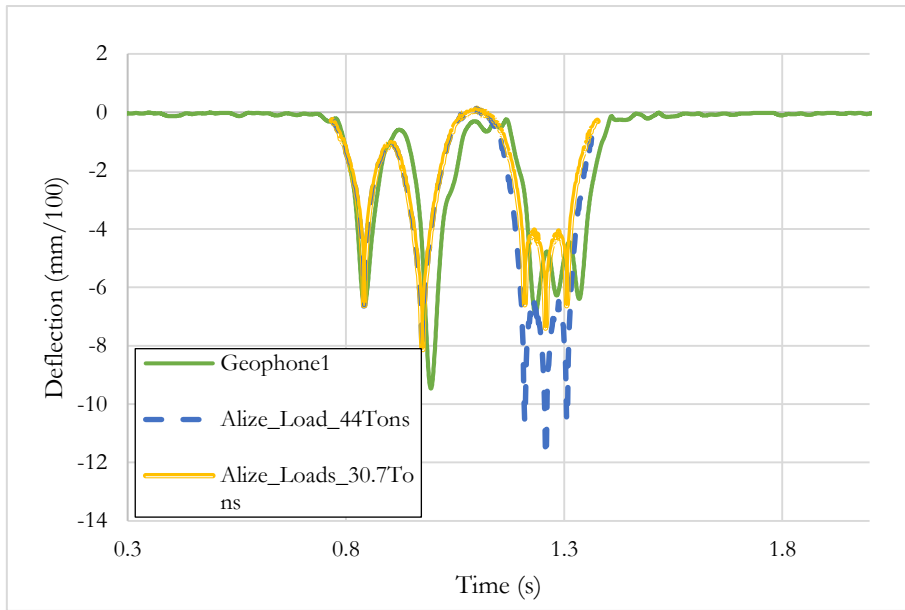


Figure D-11. Comparison of the deflection obtained with the representative signal of September 2016 (04/09/2016, 19h1min26s, 27m/s and 23°C) and the simulation with Alize with truck loaded at 32.5 tons and with the adjusted axles spacing

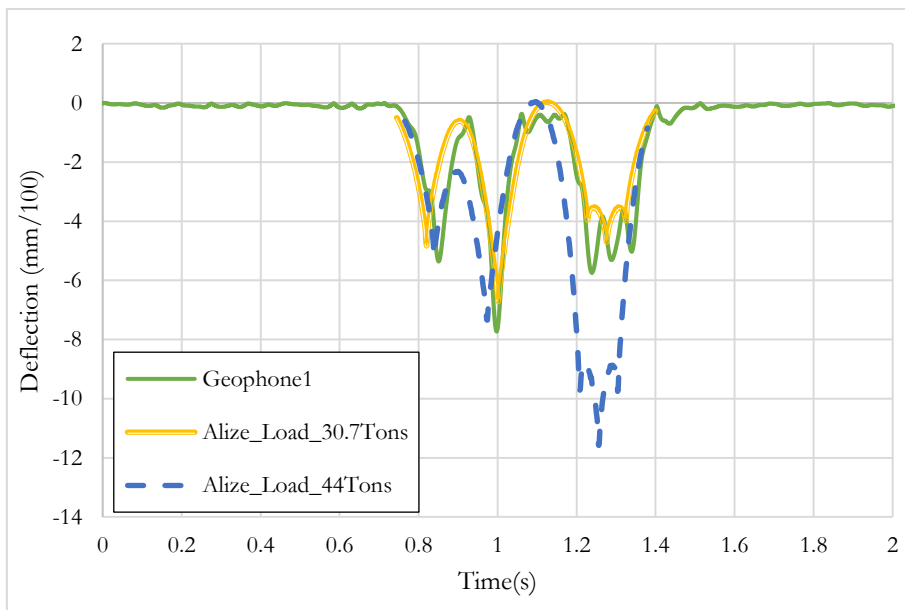


Figure D-12. Comparison of the deflection obtained with the representative signal of October 2016 (08/10/2016, 15h27min54s, 27m/s and 18°C) and the simulation with Alize with truck loaded at 32.5 tons and with the adjusted axles spacing

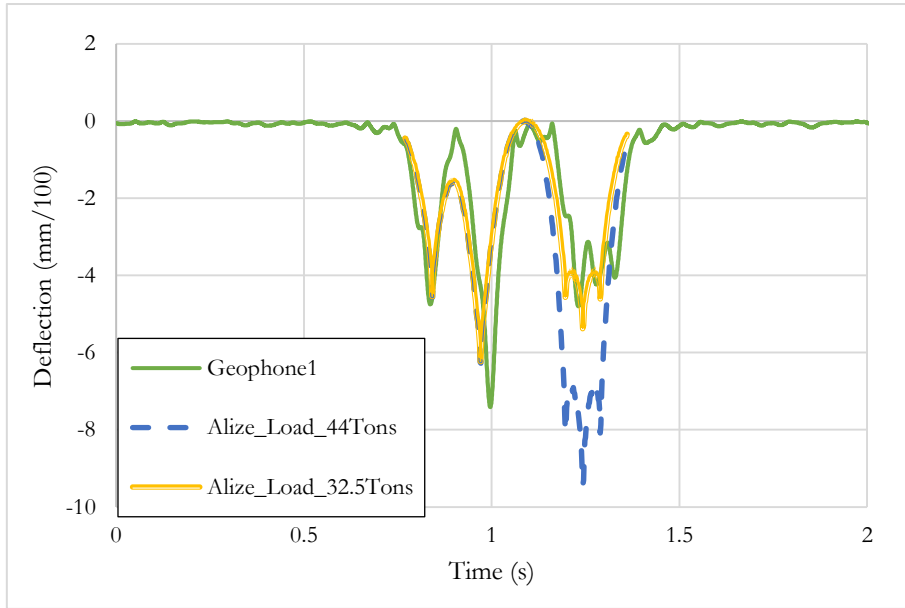


Figure D-13. Comparison of the deflection obtained with the representative signal of November 2016 (20/11/2016,13h15min18s, 28m/s and 13°C) and the simulation with Alize with truck loaded at 32.5 tons and with the adjusted axles spacing

**Titre :** Wirelessbox- Système de surveillance routière multifonctionnel

**Mots clés :** Géophone, Accéléromètre, Traitement de données, Chaussées, Instrumentation, Surveillance à distance

**Résumé :**

**Résumé :** L'instrumentation des chaussées est l'une des méthodes les plus efficaces pour surveiller l'état des chaussées. L'objectif de cette thèse est de développer un système multifonctionnel pour la surveillance des chaussées. Ce système est basé sur la mesure des déflexions de la chaussée, à l'aide de géophones ou d'accéléromètres, et des températures de chaussée. La déflexion est un indicateur clé de la réponse structurelle des chaussées, car elle caractérise la rigidité globale de la chaussée et peut être utilisée pour recalculer les modules de couche de chaussée. Différents géophones et accéléromètres ont été sélectionnés et testés en laboratoire d'abord puis au banc d'essai accéléré des chaussées, pour évaluer leur réponse, sous des charges représentatives des conditions de terrain. Ces tests ont permis de comprendre l'influence de différents paramètres, tels que la vitesse de chargement, la position de la charge et la température sur la réponse du capteur.

Des méthodes de rétrocalcul des modules de couche de chaussée à l'aide des bassins de déflexion mesurés ont également été développées. Pour approfondir l'applicabilité de ces capteurs sur une route réelle à fort trafic, ces capteurs ont été installés sur un site autoroutier français, et connectés à un système d'acquisition de données sans fil. A partir des données sur une période d'environ 2 ans, l'analyse des variations saisonnières des flèches, en relation avec les variations de température, mais aussi l'identification des types de véhicules, le calcul des vitesses des véhicules et l'estimation des charges des véhicules. Cette étude démontre différentes applications des géophones et des accéléromètres pour l'instrumentation des chaussées, et montre le potentiel offert par les systèmes de télésurveillance pour mieux évaluer le comportement des chaussées.

**Title:** Wirelessbox-Multifunctional Road Monitoring system

**Keywords:** Pavement Engineering, Geophones, Accelerometers, Instrumentation, Remote monitoring

**Abstract:**

Instrumentation of pavements is one of the most effective methods to monitor pavement condition. The objective of this thesis is to develop a multifunctional system for pavement monitoring. This system is based on the measurement of pavement deflections, using geophones or accelerometers, and pavement temperatures. Deflection is a key indicator of the structural response of pavements, as it characterises the global stiffness of the pavement, and can be used to back-calculate pavement layer moduli.

Different geophones and accelerometers have been selected and tested in the laboratory first and then at the accelerated pavement testing facility, to evaluate their response, under loadings representative of the field conditions. These tests helped understand the influence of different parameters, such as loading speed, load position and temperature on the sensor response. Methods of back-calculation of pavement layer moduli using the measured deflection basins were also developed

To further elaborate the applicability of these sensors on a real road under heavy traffic, these sensors were installed on a French motorway site, and connected to a wireless data acquisition system. From the data over a period of about 2 years, the analysis of seasonal variations of deflections, in relation with temperature variations, but also the identification of vehicle types, calculation of vehicle speeds and estimation of vehicle loads. This study demonstrates different applications of geophones and accelerometers for the instrumentation of pavements, and shows the potential offered by remote monitoring systems to better evaluate pavement behaviour.